Macrophage migration inhibitory factor (MIF) but not its homologue D-dopachrome tautomerase (D-DT) promotes fibroblast motility in a CD44/CD74-independent manner

Inaugural dissertation

submitted to the

Faculty of Medicine

in partial fulfilment of the requirements

for the PhD degree of

the Faculties of Veterinary Medicine and Medicine

of the Justus Liebig University Giessen

by

Paweł Szczęśniak

of

Szczecin, Poland

Giessen (2016)

From the Institute of Anatomy and Cell Biology

Director: Prof. Dr. Eveline Baumgart-Vogt

of the Faculty of Medicine of the Justus Liebig University Giessen

First Supervisor and Committee Member: Prof. Dr. Andreas Meinhardt

Second Supervisor and Committee Member: Prof. Dr. Peter Friedhoff

Committee Members: Prof. Dr. Klaus-Dieter Schlüter, Prof. Dr. Tienush Rassaf

Date of Doctoral Defence: 31.10.2016

Table of contents

1. List of abbreviations

Table 1. List of abbreviations.

Abbreviation	Full name
2YT	2X-Yeast extract-tryptone
4-IPP	4-Iodo-6-phenylpyrimidine
A.U.	Arbitrary units
aa	Amino acids
ABCA1	ATP-binding cassette sub-family A member 1
ANOVA	Analysis of variance
AP2	Adaptor protein complex 2
APS	Ammonium peroxodisulfate
ARP2/3	Actin-related protein 2/3 [complex]
ARPC3, 4	Actin-related protein 2/3 complex subunit 3, 4
AS	Ammonium sulphate
ATP	Adenosine triphosphate
birA	Biotin protein ligase A
BMDM	Bone marrow-derived macrophage
CCD	Charge-coupled device
CCL2	C-C motif chemokine 2
ccRCC	Clear cell renal cell carcinoma
CD	Cluster of differentiation
Cdc42	Cell division control protein 42 homolog
CHO	Chinese hamster ovary
CME	Clathrin-mediated endocytosis
COP9	Constitutive photomorphogenesis 9
COS	CV-1 in origin, carrying SV40
COX-2	Cyclooxygenase-2
CPZ	Chlorpromazine
CREB	3’,5’-cyclic adenosine monophosphate-responsive element-binding protein
CSN5	COP9 signalosome subunit 5
CXCL8/12/14	C-X-C motif chemokine ligand 8/12/14
CXCR2/4/7	C-X-C motif chemokine receptor type 2/4/7
DAPI	4’,6-Diamidino-2-phenylindole
D-DT	D-Dopachrome tautomerase
D-DTL	D-Dopachrome tautomerase-like
DMEM	Dulbecco’s modified Eagle’s medium

DMSO	Dimethyl sulfoxide
DTT	Dithiothreitol
DYN	Dynasore
E. coli	*Escherichia coli*
EC	Enzyme Commission
ECL	Enhanced chemiluminescence
ECM	Extracellular matrix
EDTA	2,2’,2’’,2’’’-(Ethane-1,2-diyldinitrilo)tetraacetic acid
EGF	Epidermal growth factor
EGFP	Enhanced green fluorescent protein
EGFR	Epidermal growth factor receptor
EGTA	Ethylene glycol-bis(2-aminoethylether)-N,N,N’,N’-tetraacetic acid
Ena/VASP	Protein enabled homolog/vasodilator-stimulated phosphoprotein
ERK1/2	Extracellular signal-regulated kinase 1/2
ERM	Ezrin-radixin-moesin (family)
EtOH	Ethanol
F	Focus
F-actin	Filamentous actin
FCS	Foetal calf serum
FIL	Filipin
For	Forward primer
FPLC/HPLC	Fast protein/high-performance liquid chromatography
fps	Frames per second
g	G-force (gravitational force)
G-actin	Globular actin
GAP	GTPase-activating protein
GDP	Guanosine 5’-diphosphate
GEF	Guanine nucleotide exchange factor
GFP	Green fluorescent protein
GILZ	Glucocorticoid-induced leucine zipper
GPCR	G-protein coupled receptor
GR	Glucocorticoid receptor
GST	Glutathione *S*-transferase
GTP	Guanosine 5’-triphosphate
HA	Hyaluronic acid
HCC	Hepatocellular carcinoma
HCl	Hydrochloric acid
hD-DT	Human D-DT

HED	2-Hydroxyethyldisulfide
HEK293	Human embryonic kidney 293 cells
HIF-1α	Hypoxia-inducible factor-1α
hMIF	Human MIF
HPP	*p*-Hydroxyphenylpyruvate
HRP	Horseradish peroxidase
IB	Immunoblot
IF	Intermediate filament
IGF-I	Insulin-like growth factor I
IgG	Immunoglobulin G
IL	Interleukin
IP	Immunoprecipitation
IPTG	Isopropyl-β-D-thiogalactopyranoside
ISO-1	(*S*,*R*)-3-(4-Hydroxyphenyl)-4,5-dihydro-5-isoxazole acetic acid
JAB1	Jun activation domain-binding protein 1
LAS	Lysis and F-actin-stabilising [buffer]
LB	Lysogeny broth
MAPK	Mitogen-activated protein kinase
MCP-1	Monocyte chemotactic protein 1
mD-DT	Murine D-DT
MDSC	Myeloid-derived suppressor cell
MEF	Mouse embryonic fibroblast
MHC	Major histocompatibility complex
MIF	Macrophage migration inhibitory factor
MIP	MIF- and D-DT-interacting protein
miRNA	MicroRNA
MLCK	Myosin light chain kinase
MMP	Matrix metalloproteinase
MT	Microtubule
NaOH	Sodium hydroxide
NDPK	Nucleoside diphosphate kinase
NET	Neutrophil extracellular trap
NF-κB	Nuclear factor of kappa light polypeptide gene enhancer in B cells
NYS	Nystatin
OD_{600}	Optical density at 600 nm
Opti-MEM	Optimal minimal essential medium
$p27^{Kip1}$	p27/kinesin-related protein 1
PBMC	Peripheral blood mononuclear cell

PBS or DPBS	Phosphate-buffered saline (or Dulbecco's phosphate-buffered saline)
PCR	Polymerase chain reaction
PDGF	Platelet-derived growth factor
PDGF-BB	Platelet-derived growth factor chain BB
pH	Power of hydrogen (or negative log of the hydrogen ion concentration)
PMSF	Phenylmethyl sulfonyl fluoride
PtK1	Female rat-kangaroo kidney epithelial [cell]
RA	Rheumatoid arthritis
Rac1	Ras-related C3 botulinum toxin substrate 1
Rev	Reverse primer
RhoA	Ras homolog gene family, member A
RhoGDI	Rho GDP-dissociation inhibitor
RNAi	RNA interference
ROS	Reactive oxygen species
rpm	Revolutions per minute
SDF-1	Stromal cell-derived factor 1
SDS	Sodium dodecyl sulphate
SDS-PAGE	Sodium dodecyl sulphate-polyacrylamide gel electrophoresis
siRNA	short interfering RNA
SOB	Super optimal broth
SOC	Super optimal broth with catabolite repression
STAT5	Signal transducer and activator of transcription 5
TAE	Tris base, acetic acid, EDTA
TBST	Tris-buffered saline/Tween-20
TCA	Trichloroacetic acid
TEMED	*N*,*N*,*N'*,*N'*-Tetramethylethylenediamine
TEV	Tobacco etch virus
TFB	Transformation buffer
T_H	T helper [cell]
THP-1	Human monocytic leukaemia cell line
TIFF	Tagged Image File Format
TNF-α	Tumour necrosis factor alpha
VEGF	Vascular endothelial growth factor
VSMC	Vascular smooth muscle cell
WAVE	WASP (Wiskott-Aldrich syndrome protein)-family verprolin-homologous protein

2. Introduction

This thesis focuses on cell motility and two paralogous cytokines, macrophage migration inhibitory factor (MIF) and D-dopachrome tautomase (D-DT). MIF's eponymous function was first demonstrated when it was shown to inhibit random migration of peritoneal macrophages in the delayed-type hypersensitivity reaction (Bloom and Bennett, 1966). In the next decades, it turned out to mediate a number of processes in healthy as well as diseased cells and tissues. The essential role of MIF in a number of inflammatory conditions such as wound healing (Gilliver *et al.*, 2011) or acute respiratory distress syndrome (ARDS) (Donnelly *et al.*, 1997; Lai *et al.*, 2003) is well documented.

Depending on its tissue of origin, MIF may act as a stress-induced hormone and cytokine (Bernhagen *et al.*, 1993), chemokine (Bernhagen *et al.*, 2007), tumour promoter (Mitchell, 2004; Bucala and Donnelly, 2007; Du *et al.*, 2012), tumour suppressor (Tarnowski *et al.*, 2010), redox modulator (Koga *et al.*, 2011), inducer of epithelial-to-mesenchymal transition (Funamizu *et al.*, 2012), pro-angiogenic factor (Ren *et al.*, 2003), pro-proliferative factor (Ohta *et al.*, 2012), and pro-survival agent (Mitchell *et al.*, 2002). Particularly, as a modulator of cell motility, it plays a differential role in wound healing (Gilliver *et al.*, 2011), chemotaxis and invasion. D-DT is a structural and functional homologue of MIF that likely arose due to MIF gene duplication (Kamir *et al.*, 2008). Similar to MIF, D-DT binds CD74 and upregulates mitogen-activated protein kinase (MAPK)/extracellular signal-regulated kinase 1/2 (ERK1/2), a pathway responsible for mitogen-mediated transduction of signalling from the extracellular environment, via CD74 as well as G-protein coupled receptors (GPCRs), through a cascade of cytoplasmic kinases to the nucleus where it activates target genes including cyclin D1 (Merk *et al.*, 2011). In A549 adenocarcinoma cells, MIF/D-DT promote two pro-angiogenic factors – C-X-C motif chemokine ligand 8 (CXCL8)/interleukin-8 (IL-8) and vascular endothelial growth factor (VEGF) (Coleman *et al.*, 2008). Moreover, MIF/D-DT regulate the migration of human clear cell renal cell carcinoma (ccRCC) cells (Pasupuleti *et al.*, 2014). Clinically, D-DT and *S*-nitros(yl)ated MIF are cardioprotective (Luedike *et al.*, 2012; Qi *et al.*, 2014) and serve as markers of sepsis severity (Merk *et al.*, 2011).

2.1. MIF/D-DT play a role in immunity and inflammation

The immune system endows us with protection against viruses, parasites and bacteria by means of non-specific innate immunity (section 2.1.1) and antibody-based adaptive immunity (section 2.1.2).

2.1.1. Innate immunity

Innate immunity is triggered within a matter of minutes and hours after an encounter of a variety of extracellular compounds known as danger-associated molecular patterns (DAMPs) – DNA, RNA, or adenosine triphosphate (ATP) – and pathogen-associated molecular patterns (PAMPs) – foreign DNA or RNA, endotoxin, or CpG motifs.

A key part of innate immunity is the release of neutrophil extracellular traps (NETs) – composed of neutrophil-derived DNA and histones, neutrophil elastase, and cathepsin G – in order to encapsulate and digest large bacteria and fungi through a specialised cell death phenomenon known as NETosis (Branzk *et al.*, 2014). Via MAPK and reactive oxygen species (ROS), MIF promotes NET release upon infection with *Pseudomonas aeruginosa* (Dwyer *et al.*, 2014). In the context of cystic fibrosis, prolonged MIF-triggered NETosis aggravates the disease (Dwyer *et al.*, 2014), a finding supported by the fact that $MIF^{-/-}$ mice exhibit better *P. aeruginosa* clearance than their WT littermates (Bozza *et al.*, 1999).

There are a number of cell types associated with innate immunity: certain subsets of T cells, eosinophils and basophiles, dendritic cells, mast cells, monocytes/macrophages, and neutrophils. MIF was shown to: (*a*) promote eosinophil accumulation via C-X-C motif chemokine receptor 4 (CXCR4) (de Souza *et al.*, 2015); (*b*) enhance mast cell recruitment via signal transducer and activator of transcription 5 (STAT5) and possibly CXCR4 (Põlajeva *et al.*, 2014); (*c*) promote chemotaxis and cause a subsequent arrest of monocytes/macrophages (Bernhagen *et al.*, 2007); (*e*) affect lung neutrophil recruitment (Rajasekaran *et al.*, 2014); and (*f*) induce chemotaxis of interstitial monocytes and neutrophils in sterile inflammation (Stark *et al.*, 2013).

Although MIF is not known to be directly involved in danger or pathogen recognition, its key function seems to be the induction of the expression of tumour necrosis factor (TNF)-

α, interleukins, and cyclooxygenase-2 (COX-2) (Xin *et al.*, 2010) in macrophages. Indeed, the basis of the resolution of acute, early inflammation is that macrophages phagocytose foreign material and secrete cytokines. Overall, one report suggested that MIF is an early modulator of inflammation rather than a pro-inflammatory cytokine (Kudrin *et al.*, 2006).

2.1.2. Adaptive immunity

The adaptive immune system is comprised of B and T cells that generate antibodies against foreign peptides and proteins over the course of a few days. MIF-dependent chemotaxis is essential for the migration of circulating B and T cells (adaptive immunity) but also neutrophils and monocytes/macrophages (innate immunity) (Bernhagen *et al.*, 2007; Klasen *et al.*, 2014; Alampour-Rajabi *et al.*, 2015) (section 2.6). Both B and T cells are regulated by many factors including regulatory B and T (B_{reg} and T_{reg}) cells.

The T cell-mediated responses are further modulated by type 1 (T_H1) and type 2 (T_H2) T helper (Th) cells. Briefly, T_H1 are associated with pro-inflammatory, cell-mediated responses, and T_H2 with anti-inflammatory, humoral responses. MIF is known to promote T_H1-mediated immunity after cardiovascular surgery and may contribute to multiple organ dysfunction syndrome (de Mendonça-Filho *et al.*, 2006; Larson and Horak, 2006). T_H2 cells can also release MIF (Bacher *et al.*, 1996).

In concert with other cytokines, MIF is known to be responsible for the following chain of inflammation-potentiating events in monocytes/macrophages and fibroblasts: activation of ERK1/2 by phosphorylation, activation of cytosolic phospholipase A_2 ($cPLA_2$) and COX-2, and the production of prostaglandins (Xin *et al.*, 2010).

Therapeutically, such inflammation may be treated with immunosuppressants such as glucocorticosteroids, and MIF is involved at this stage as well.

Binding of glucocorticosteroids to their cytoplasmic glucocorticoid receptor (GR) elicits (*a*) inhibition of $cPLA_2$ as well as (*b*) GR translocation to the nucleus to (*c*) trigger anti-inflammatory gene expression including mitogen-activated protein kinase phosphatase-1 (MKP-1). At the same time, glucocorticoid-induced leucine zipper (GILZ) facilitates the expression of MKP-1. Overall, ERK1/2 dephosphorylation by MKP-1 and the GC-mediated

inhibition of $cPLA_2$ diminishes immune responses as well as the synthesis of prostaglandins. One of the most prominent features of MIF is that it counteracts the anti-inflammatory action of glucocorticosteroids (Alourfi *et al.*, 2005) by: (*a*) upregulating ERK1/2 phosphorylation which leads to COX-2 activation, as well as (*b*) inhibiting GILZ in a mitogen-activated protein kinase phosphatase-1 (MKP-1)-dependent manner (Roger *et al.*, 2005; Fan *et al.*, 2014). One example of an autoimmune disorder treated with glucocorticosteroids is chronic joint inflammation known as rheumatoid arthritis (RA). In RA, prolonged MIF exposure is known to exacerbate the symptoms, as it overrides the glucocorticosteroid effect.

In summary, MIF is important in human immunity by keeping the homeostasis of tissues by inhibiting the anti-inflammatory responses of glucocorticoids, thereby potentiating the inflammation to fight the disease. Nonetheless prolonged inflammation aggravates tissue damage, so that the development of novel MIF inhibitors such as MIF DNA vaccines is much needed (section 2.5).

2.2. MIF/D-DT: gene and protein

Human *MIF* and *D-DT* genes are located at chromosome 22q11.23 and are conserved across a broad range of species including humans, rodents, bacteria, parasitic nematodes (Qu *et al.*, 2014), plants (Panstruga *et al.*, 2015), and others (Fingerle-Rowson *et al.*, 2003). Following cleavage of the first methionine, the first amino acid in the mature full-length MIF (and D-DT) protein is Pro-2 encoded by the triplet CCT for *MIF* and CCG for *D-DT* (Figure 1A-B). Conserved among species, Pro-2 is required for MIF/D-DT isomerase/tautomerase enzymatic activities (section 2.4) (Bendrat *et al.*, 1997; Nishihira *et al.*, 1998).

MIF and *D-DT* genes both contain three exons and two introns (Calandra and Roger, 2003; Merk *et al.*, 2012). Within their promoters various transcription factor-binding elements can be found including: (*a*) NF-κB (for *MIF*); (*b*) 3',5'-cyclic adenosine monophosphate-responsive element-binding protein (CREB) (for both *MIF* and *D-DT*), and (*c*) hypoxia-responsive elements (HREs) (for both *MIF* and *D-DT*) (Pasupuleti *et al.*, 2014). Upon

oxygen depletion, hypoxia-inducible factor-1α (HIF-1α) potently induces *MIF* expression which is further promoted by concomitant hypoxia-driven CREB degradation (Baugh *et al.*, 2006).

Two gene promoter polymorphisms for *MIF* are documented in a number of autoimmune diseases and cancer: a single-nucleotide polymorphism (SNP) -173 G>C (guanine-to-cytosine) (rs755622) and a short tandem repeat (STR) -794 $CAAT_{5-8}$ (5-8 repeats of cytosine-adenine-thymine-thymine) (rs5844572) (Grieb *et al.*, 2010). Their identification helps to improve disease risk assessment by validating MIF as a biomarker.

At the protein level human MIF is a 12.5-kDa single-chain polypeptide composed of 114 amino acids whereas human D-DT (12.7 kDa) is 118-amino-acid in length. MIF and D-DT monomers contain two α-helices and six β-sheets (Figure 1A-B). Deletions and substitutions of select MIF residues were a basis for much research on MIF's enzymatic activities and secondary structure in the past (section 2.5). Δ4 MIF (deletion of the first four amino acids at the N-terminus: Pro-2, Met-3, Phe-4 and Ile-5) exhibits an increase in random coil structure.

In solution as well as in tissues, MIF monomers are capable of forming higher oligomers including trimers. An MIF homotrimer – which possesses a negatively-charged channel, akin to a barrel – exerts most if not all of its physiological effects (Fan *et al.*, 2013). An Asn-110 substitution (N110C) results in an artificially locked MIF trimer (Ouertatani-Sakouhi *et al.*, 2010; Reidy *et al.*, 2013). Leu-46 was reported to play a role in the maintenance of the secondary/tertiary structure of MIF (El-Turk *et al.*, 2012).

An ELR motif, composed of Glu (E), which be substituted for Asp (D) by a conserved exchange, and Arg (R), is necessary for chemokine-chemokine receptor interactions. In MIF there is no genuine ELR motif but there is a *pseudo (E)LR* motif composed of Arg-12 (R) and Asp-45 (D) (Figure 1A). Physiologically, this *pseudo (E)LR* motif is responsible for the interaction between MIF and one of its receptors, CXCR2 (Weber *et al.*, 2008). Such an ELR or *pseudo (E)LR* motif is absent from human and murine D-DT (Figure 1B).

MIF has a Cys-Xaa-Xaa-Cys (CXXC)-based thiol-protein oxidoreductase activity (Figure 1A). In case of MIF, the CXXC motif is a Cys-57-Ala-Leu-Cys-60 (CALC) motif. The two cysteines within CALC are indispensable for enzymatic activity. Out of the three conserved cysteines (Cys-57, -60 and -81) in MIF across species, D-DT retains only one (Cys-57) (Figure 1A and B), which is insufficient for D-DT to catalyse oxidoreduction. Physiologically, *S*-nitros(yl)ation of Cys-81 increases the oxidoreductase activity and is cardioprotective by decreasing apoptosis (Luedike *et al.*, 2012).

O-linked β-N-acetylglucosamine (*O*-GlcNAc) modifies MIF at Ser-112/Thr-113. *O*-GlcNAc-MIF binds epidermal growth factor receptor (EGFR) and has implications in tumour invasion (Zheng *et al.*, 2015).

MIF may be putatively cleaved by kallikrein-related peptidases (Shahinian *et al.*, 2014). In a mass spectrometry-based proteomics screen two other putative post-translational modifications of MIF were identified: cysteinylation and glycation (Sherma *et al.*, 2014). An oxidised form of MIF exists in tumour tissues (Thiele *et al.*, 2015b) and is essential for triggering glomerulonephritis (Thiele *et al.*, 2015a).

Based on a study with a series of MIF-derived synthetic peptide fragments, the region spanning MIF amino acids 50-65 (MIF_{50-65}) (Figure 1A) was described as physiologically-relevant because it was capable of mediating most of full-length MIF's biological functions including redox (CALC motif), pro-proliferative, and glucocorticoid overriding activities (Nguyen *et al.*, 2003). Taken together, it appears that all the many post-translational modifications of MIF generate a variety of MIF molecules which might be tissue-, cell-, and disease-specific.

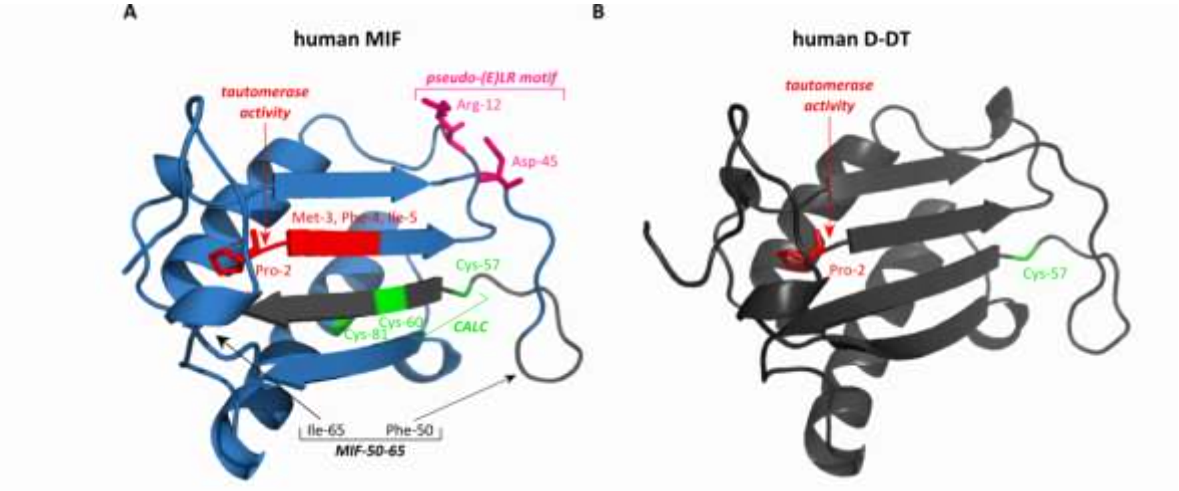

Figure 1. MIF/D-DT monomers share similarities in their primary and secondary structures. (**A and B**) MIF/D-DT crystal structures are shown as false colour-coded ribbons (made with PyMOL) and based on data deposited under Protein Database identifiers 1MIF and 1DPT, respectively. The amino acid sequence identity between human MIF and human D-DT is 37% based on Blocks Substitution Matrix 62 (BLOSUM62). For clarity only some of the identical amino acids are shown (Pro-2, Cys-57). Each MIF/D-DT monomer is composed of two α-helices and six β-sheets. (**A**) The first four amino acids of the N-terminus (Pro-2, Met-3, Phe-4 and Ile-5) in MIF (red) are deleted in the MIF Δ4 mutant (Materials and Methods). Pro-2 (red, stick structure) is required for the tautomerase activity. Arg-12 and Asp-45 (magenta, stick structures) form a *pseudo-(E)LR* motif responsible for the MIF-CXCR2 interaction. MIF's CALC (Cys-Ala-Leu-Cys) oxidoreductase motif contains three cysteines (Cys-57, -60, and -81). Cys-60 is mutated to Ser in the oxidoreductase-null MIF mutant (Materials and Methods). The MIF_{50-65} polypeptide is marked in black. (**B**) Pro-2 (red) and Cys-57 (green) of D-DT are conserved in both proteins.

2.3. MIF/D-DT are distributed among various tissue

At the cellular level MIF can be nuclear, cytoplasmic, or secreted. Though MIF localises to the nucleus (Pyle, 2003), a nuclear localisation signal is missing from its sequence, and its nuclear function remains undetermined. Within the cytoplasm, MIF localises to the cell periphery (Kleemann *et al.*, 2000a; Filip *et al.*, 2009) where it complexes with Jun activation domain-binding protein 1 (JAB1)/COP9 signalosome complex subunit 5 (CSN5). Current knowledge holds that JAB1 and MIF bind and mutually inhibit one another. On the one hand JAB1 binds MIF, inhibits its secretion, and as such inhibits secreted MIF-mediated AKT phosphorylation in human HEK293 cells (Lue *et al.*, 2007). On the other hand, MIF binds and inhibits JAB1 leading to $p27^{Kip1}$ stabilisation and fibroblast growth arrest (Kleemann *et al.*, 2000a). JAB1 regulates both transient and sustained ERK1/2 activation by MIF (Lue *et al.*, 2006). In HCT116 human adenocarcinoma cells, a ternary

complex composed of MIF, JAB1 and HIF-1α plays a role in stabilising the latter (No *et al.*, 2015). D-DT has also been recently described to bind JAB1 (Merk *et al.*, 2011).

Although MIF and D-DT lack a cleavable N-terminal or internal secretion signal, MIF is secreted in a non-classical manner by binding to the Golgi complex-associated protein p115 (Eickhoff *et al.*, 2001; Flieger *et al.*, 2003; Merk *et al.*, 2009). In LPS-stimulated monocytes, MIF co-localises with the Golgi-associated protein p115 in the cytoplasm as well as at the Golgi, and both are secreted as a complex, but competition binding assays do not exclude the possibility that additional proteins are present within such a complex (Merk *et al.*, 2009).

Because MIF does not enter the endoplasmic reticulum and Golgi apparatus (Merk *et al.*, 2009) it cannot be N-glycosylated. On the other hand, since *O*-glycosylation takes place in the MIF-containing nucleus and cytoplasm, a secreted *O*-GlcNAcylated MIF species have been described in human cells (Zheng *et al.*, 2015). Zheng *et al.* identified two enzymes – *O*-GlcNAc transferase and *O*-GlcNAcase – as mediating this post-translational modification. How secreted MIF can acquire *O*-linked glycosylation within the cytoplasm *in vivo*, and whether O-glycosylated MIF specifically affects cell migration or invasion, remains currently unknown.

In human monocytic leukaemia THP-1 cells, the export of MIF is mediated by a 12-transmembrane anion transporter known as ATP-binding cassette sub-family A member 1 (ATP-binding cassette transporter 1, ABCA1) based on a report using ABCA1 inhibitors glyburide and probenecid (Flieger *et al.*, 2003). However, in human renal cell carcinoma RCC4 cells shRNA-mediated knockdown of ABCA1 did not impair radiation-induced MIF secretion (Gupta *et al.*, 2016), suggesting MIF secretion pathways vary between cell types.

MIF is constitutively expressed and is believed to be released into the extracellular milieu upon stimulation with various substances including endotoxin. However, human foreskin fibroblasts produce MIF *de novo* upon human cytomegalovirus infection (Bacher *et al.*, 2002). In quiescent NIH 3T3 – used by many laboratories including ours to study the physiology of MIF – adhesion to fibronectin triggers MIF release and subsequent cyclin D1 expression and DNA synthesis (Liao *et al.*, 2003).

MIF and D-DT are ubiquitously produced by resident as well as circulating cells. The sources of MIF include the hypothalamic-pituitary-adrenal axis (Fingerle-Rowson and Bucala, 2001), activated monocytes/macrophages, T cells, platelets (Strüßmann *et al.*, 2013), B cells (Rocklin *et al.*, 1974), eosinophils (Rossi *et al.*, 1998), epithelium (Lan *et al.*, 2000; Rice *et al.*, 2003), endothelium (Hu *et al.*, 2015), Leydig cells (Meinhardt *et al.*, 1996) and Sertoli cells after Leydig cell depletion (Meinhardt *et al.*, 2000), fibroblasts (Selvi *et al.*, 2003), and a plethora of others (Fingerle-Rowson and Bucala, 2001). A number of immortalised fibroblast-like cell lines produce and secrete MIF – high levels of intracellular MIF are found in NIH 3T3 of murine origin (Mitchell *et al.*, 1999) and low levels of intracellular MIF are found in the M6 clone of CV-1 cells derived from Green African monkey kidney fibroblasts – COS-7/M6 (Figure 22A). Upon secretion, MIF is found in saliva (de Souza *et al.*, 2014), serum (Sobierajski *et al.*, 2013), synovial fluid (Onodera *et al.*, 1999), urine (Hong *et al.*, 2012), follicular fluid (Wada *et al.*, 1999), and testicular interstitial fluid (Meinhardt *et al.*, 1998) in a concentration range between 0.1-150 ng/ml.

2.4. MIF/D-DT have enzymatic activities

As mentioned earlier, MIF/D-DT catalyse the isomerisation (a reaction of one substrate yielding one product) and tautomerisation (a keto/enol conversion) of various compounds. Additionally MIF catalyses an oxidoreduction (a disulphide reduction). All of these reactions may play a role in signal transduction including redox signalling.

As L-dopachrome isomerase/tautomerase (EC 5.3.3.12), MIF catalyses *in vitro* the following reaction: L-dopachrome ↔ 5,6-dihydroxyindole-2-carboxylate (Rosengren *et al.*, 1996). D-DT catalyses the tautomerisation of the non-naturally occurring D-dopachrome (D-dopachrome ↔ 5,6-dihydroxyindole + CO_2). As this reaction is accompanied by a simultaneous decarboxylation, D-DT is additionally referred to as a D-dopachrome decarboxylase (EC 4.1.1.84) (Rosengren *et al.*, 1996). As phenylpyruvate tautomerase (EC 5.3.2.1) (for MIF) and phenylpyruvate tautomerase II (for D-DT), the two catalyse the conversion of keto-phenylpyruvate to enol-phenylpyruvate (a typical *in vitro* substrate is *p*-hydroxyphenylpyruvate (HPP)) (Lubetsky *et al.*, 1999).

As protein-thiol oxidoreductase, MIF catalyses the reduction of both insulin as well as 2-hydroxyethyldisulfide (HED) by glutathione (Kleemann *et al.*, 1998; Nguyen *et al.*, 2003).

Two bacterial homologues of MIF/D-DT, 4-oxalocrotonate tautomerase and 5-carboxymethyl-2-hydroxy-muconate isomerase retain their Pro-2-mediated eponymous enzymatic activities important in catabolic processes (Burks *et al.*, 2010). Although MIF and D-DT retain Pro-2 and thus the tautomerase activity, this ancient feature may no longer be necessary in metazoans. Some authors attribute it to redox signalling regulation since MIF-deficient cardiac fibroblasts have fewer ROS (Koga *et al.*, 2011). However, an endogenous substrate of MIF/D-DT is yet to be described, and Pro-2 appears to be critical for the maintenance of the secondary/tertiary structure rather than the enzymatic action *per se* (Fingerle-Rowson *et al.*, 2009).

2.5. MIF inhibition is clinically relevant

Despite an incomplete understanding of the physiological role of the enzymatic activities of MIF, the inhibition of MIF by small-molecule agonists (Xu *et al.*, 2013) and neutralising antibodies has a viable therapeutic potential. In animal models of sepsis, neutralising antibodies – which bind the extracellular (serum) MIF pool only – alleviated disease symptoms and increased survival in mice (Calandra *et al.*, 2000).

Neutralising MIF secreted by bone marrow-derived macrophages (BMDM) is an effective strategy to inhibit germ cell tumour (teratoma) formation after stem cell transplantation (Wang *et al.*, 2012). A monoclonal antibody against the oxidised form of MIF was documented to be beneficial in tumour targeting (Thiele *et al.*, 2015b) and alleviated kidney infection (Thiele *et al.*, 2015a). Antibodies that bind to MIF epitopes aa 50-68 and aa 86-102 seem to be most effective in alleviating sepsis (Kerschbaumer *et al.*, 2012). A new fully-humanised antibody that specifically targets the tautomerase activity was described, and may be used to diminish inflammatory responses (Tarasuk *et al.*, 2014).

Pancreatic ductal adenocarcinomas secrete MIF-rich exosomes which contribute to pre-metastatic niche formation, that can be prevented by MIF lentiviral knockdown (Costa-Silva *et al.*, 2015). In tumour biology, MIF and CD74 levels correlate positively with the

severity of cancer (Grieb *et al.*, 2014), and genetic depletion of either MIF or CD44/CD74 reduces tumourigenic potential of ccRCCs (Du *et al.*, 2012).

In a phase I clinical trial on cancer patients vaccinated with lethally irradiated, autologous tumour cells, the patients successfully developed autoantibodies against pro-angiogenic factors such as angiopoietin-1 and -2, leading to prolonged survival by impairing tumour vascularisation (Schoenfeld *et al.*, 2010). Remarkably, MIF autoantibodies were detected after combined vaccination with (*a*) inactivated tumour cells and (*b*) a neutralising antibody against cytotoxic T lymphocyte-associated antigen-4 in five patients, including one stage IV melanoma patient who survived more than 50 months, and one advanced ovarian carcinoma patient. Thus MIF autoantibody generation is a natural reaction to protect the body from tumour-induced inflammation.

In contrast, since MIF stimulates rhabdomyosarcoma cell adhesion, recombinant MIF administration or MIF gene therapy rather than MIF inhibition would appear to be therapeutically beneficial in treating this cancer (Tarnowski *et al.*, 2010).

Out of the many small-molecule pharmacological inhibitors, (*S,R*)-3-(4-hydroxyphenyl)-4,5-dihydro-5-isoxazole acetic acid (ISO-1) (Al-Abed *et al.*, 2005; Al-Abed and VanPatten, 2011) and 4-iodo-6-phenylpyrimidine (4-IPP) (Winner *et al.*, 2008) are most widely used. They are membrane-permeable, inhibit the secretion of MIF, and – in the case of 4-IPP but not ISO-1 – covalently bind Pro-2 in MIF and D-DT to form 6-PP-adducts (Rajasekaran *et al.*, 2014). 4-IPP is more potent than ISO-1 in inhibiting MIF's tautomerase activity (Schulte, 2011) as well as A549 adenocarcinoma cell motility and anchorage-independent growth (Winner *et al.*, 2008). Moreover, 4-IPP decreases active Ras-related C3 botulinum toxin substrate 1 (Rac1) (section 2.7.4) in A549 cells (Winner *et al.*, 2008).

As much as neutralising antibodies, *in vitro* and *in vivo* inhibition of MIF´s tautomerase activity by ISO-1 and 4-IPP and their derivatives has been reported to diminish many MIF-stimulated responses and alleviate sepsis. The physiological relevance of MIF's tautomerase activity was studied in a knock-in mouse in which the N-terminal Pro-2-coding codon CCT within the endogenous *Mif* locus was mutated into a glycine-coding

GGC by homologous recombination (Fingerle-Rowson *et al.*, 2009). This model revealed: (*a*) that tautomerase-null MIF P2G binds to its receptor, the invariant chain of the major histocompatibility complex (MHC) class II (CD74 or Ii), but with a lower affinity than MIF WT, (*b*) that MIF P2G binds JAB1, and (*c*) that the phenotype of $Mif^{P2G/P2G}$ mice in terms of growth control and tumour induction is intermediate between $Mif^{+/+}$ and $Mif^{-/-}$ mice. This indicates that the intrinsic tautomerase activity of MIF is dispensable for its cellular functions in mice, suggesting Pro-2 is rather important for protein-protein interactions.

To delineate which amino acid(s) might be involved in MIF-mediated enzymatic activity, an array of mutants was used in the past.

Tautomerase-inactive MIF P2F (Pro-2-to-Phe substitution) and nearly completely tautomerase-inactive MIF P2S (Pro-2-to-Ser substitution) retain their capacity to inhibit chemotaxis and random migration of peripheral blood mononuclear cells (PBMCs) (Hermanowski-Vosatka *et al.*, 1999). The P2S mutant can also override glucocorticoid-driven TNF-α release from monocytes (Bendrat *et al.*, 1997). Due to the different physicochemical properties of amino acids, the enzymatic activity of point mutants varies depending on which amino acid replaces P2. While MIF P2F is enzymatically fully inactive, P2S is active but to a lesser extent than WT (Hermanowski-Vosatka *et al.*, 1999; Stamps *et al.*, 2000). MIF C60S (Cys-60-Ser substitution) but not P2A (Pro-2-to-Ala substitution) tautomerises HPP (Kleemann *et al.*, 2000b). While insulin reduction is the same for MIF WT, MIF P2A, and MIF Δ4, in a hydroxyethyl disulphide transhydrogenase assay (whereby MIF catalyses the reduction of hydroxyethyl disulphide by glutathione) MIF P2A is only half-active and MIF Δ4 is completely inactive.

Beyond neutralising antibodies and tautomerase activity inhibitors, two other MIF inhibition strategies were described – one involving protein-protein interactions and the other one involving DNA vaccines.

Heat-shock protein 90 (HSP90) protects its clients such as MIF from degradation, and inhibition of HSP90 ATPase activity by tanespimycin proved successful in destabilising MIF (Schulz *et al.*, 2012; Schulz and Moll, 2014). Furthermore, C-terminus of gremlin-1, a bone

morphogenic protein antagonist, inhibits MIF-induced monocyte chemotaxis (Beck *et al.*, 2016). From a pre-clinical standpoint, two proteins have the potential to abrogate MIF-induced damage: (*a*) secreted ribosomal protein S19 (RPS19) protects mice against renal dysfunction in a model of anti-glomerular basement membrane glomerulonephritis by inhibiting MIF-CD74 binding (Lv *et al.*, 2013), and (*b*) knockdown of p115 in human multiple myeloma cells decreases proliferation and induces apoptosis by inhibiting MIF secretion (Jin and Dai, 2016). In sum, HSP90, gremlin-1, RPS19 and p115 have the potential to be exploited in designing alternative MIF inhibition strategies.

Because of the limitations of anti-MIF antibodies in treating RA – high titres and repeated injections are necessary – a MIF cDNA-containing tetanus toxoid DNA vaccine was developed and tested in mice to help to resolve chronic inflammation in RA (Onodera *et al.*, 2007). Such a vaccine successfully inhibited the development of spontaneous autoimmune arthritis.

Overall, there exist a few distinct modes of MIF inhibition, most notably including (*a*) neutralising antibodies (block extracellular/serum MIF), (*b*) cell-permeable tautomerase-activity inhibitors (block intracellular and extracellular MIF), and RPS19-based inhibition of secreted MIF. In the case of cancer, either MIF inhibition or MIF supplementation might be therapeutically useful, while under inflammatory conditions, where high MIF levels potentiate immune responses, only inhibition appears to have a positive outcome on survival.

2.6. MIF/D-DT mediate their actions via cell receptors

Many cell-surface molecules have been described to bind extracellular MIF and either facilitate its uptake (thioredoxin, CD74) or transduce an MIF signal (EGFR, CD44, CD74, and GPCRs – CXCR2, CXCR4 and CXCR7). D-DT is known to require CD74 for signal transduction. Major endocytic pathways and the essential role of CD74-mediated endocytosis are mentioned within section 2.6.2.

2.6.1. MIF binds thioredoxin and EGFR

Surface-bound thioredoxin helps to internalise MIF in immortalised T-cell and macrophage lines (Son *et al.*, 2009) but the role of this interaction in cell motility has yet to be identified.

Furthermore, *O*-GlcNAcylated MIF inhibits epidermal growth factor (EGF)-induced invasion by binding and inactivating EGFR in U87 human glioblastoma cells (Zheng *et al.*, 2015). *O*-GlcNAcylation-deficient MIF does not alter ERK1/2 or AKT signalling (Zheng *et al.*, 2015). As high levels of *O*-GlcNAcylated MIF are found in U87 but not in human monocytic leukaemia THP-1 cells or BV2 mouse microglia cells (Zheng *et al.*, 2015), the production of *O*-GlcNAcylated MIF is rather cell-specific.

2.6.2. CD74 is a primary MIF receptor and mediates MIF's endocytosis in fibroblasts

Based on evidence from a THP-1-derived cDNA library expressed in COS-7 cells, CD74 was classified a receptor for extracellular MIF (Leng *et al.*, 2003). CD74 was originally considered to be incapable of propagating intracellular signalling without a co-receptor. Nevertheless, CD74 does undergo intramembrane proteolysis. and further signalling can be elicited by a CD74-intracellular domain (CD74-ICD) which translocates to the nucleus to activate NF-κB (Becker-Herman *et al.*, 2005). Notably, CD74 downregulates dendritic cell migration to facilitate the uptake of antigens which has a physiological significance in terms of efficient innate immunity responses (Faure-André *et al.*, 2008). CD74 resides in the endoplasmic reticulum and is involved in antigen presentation as it shields the MHC class II α/β heterodimers from binding autoantigens (Riberdy *et al.*, 1992). A small percentage of CD74 molecules (5%) can be trafficked to the plasma membrane and acts independent of MHC (Pantouris *et al.*, 2015).

In a number of human cells – mostly fibroblasts (Figure 3A-D) but also cancer cells, dendritic cells, monocytes, and B cells (Figure 3A-B) – MIF binds and mediates its actions through plasma membrane-bound CD74.

CD74 and CD44 – a proteoglycan and the major receptor for hyaluronic acid (HA) and fibronectin (Zöller, 2011) – form a complex and mediate the MIF signal via Src tyrosine kinase (Shi *et al.*, 2006). Src associates with the cytoplasmic tail (last C-terminal 67 amino

acids) of CD44 (Figure 3C). Once MIF is bound to CD74 and has recruited the cytoplasmic tail-deficient $CD44^{\Delta 67}$ molecule, the effects of MIF on ERK1/2 phosphorylation are abrogated (Figure 3C) (Shi *et al.*, 2006).

While these effects are transduced by MIF acting as a ligand that is binding to its receptors CD74/CD44 and eliciting downstream cytoplasmic signalling, MIF can also be taken up by endocytosis that is facilitated by CD74. Generally, cellular uptake of cargo involves endocytic entry by (*a*) receptor- and clathrin-mediated endocytosis (CME), (*b*) clathrin- and caveolin-independent endocytosis, or (*c*) caveolin- and lipid-raft-dependent endocytosis (non-CME) (Figure 2) (Johannes *et al.*, 2015). In CME and non-CME a nascent vesicle may be cleaved off the membrane by dynamin (Wieffer *et al.*, 2009). Caveolin-rich vesicles are known as caveolar vesicles and can dynamically dock and fuse with either caveosomes or early endosomes (Pelkmans, 2005).

Once a vesicle enters the intracellular space, a variety of ligand-, receptor-, and context-specific events may occur: (*a*) endosomal escape of the cargo into the cytoplasm; (*b*) generation of a stable vesicle that elicits endosomal signalling (Figure 3D); (*c*) a fusion of a caveolar vesicle with caveosomes or early endosomes; (*d*) a fusion of an endosome with a lysosome and subsequent cargo degradation, (*e*) cargo recycling from a vesicle back to the plasma membrane, or (*e*) cargo exocytosis (Figure 2) (Pelkmans, 2005).

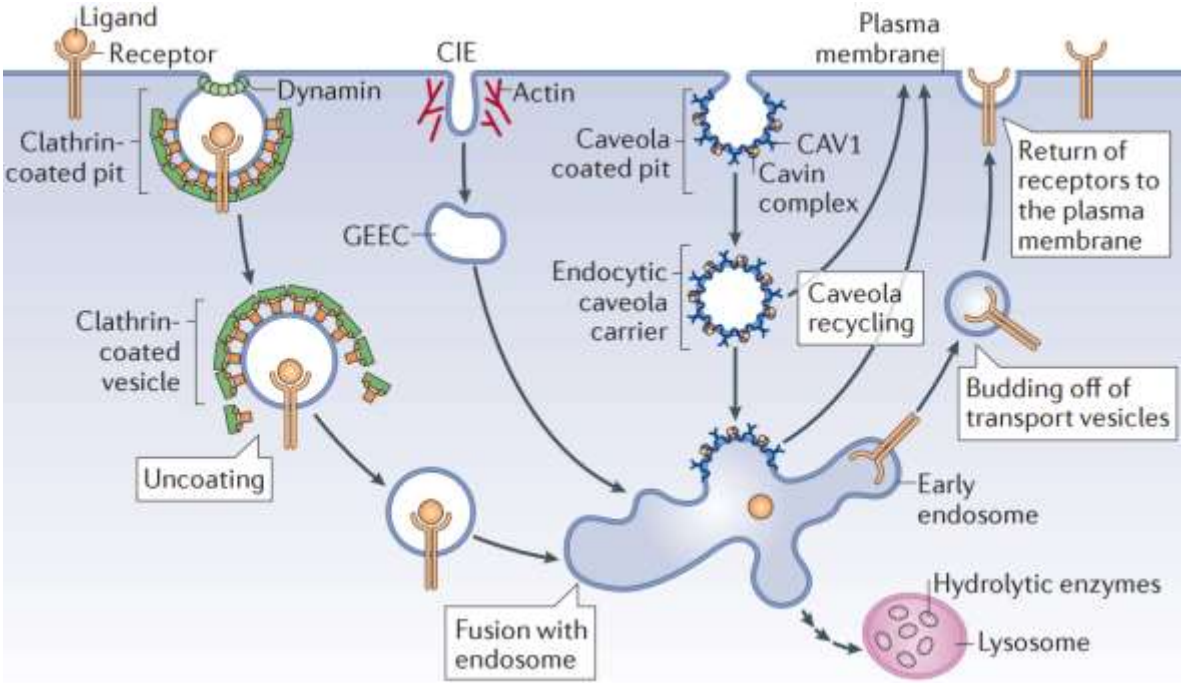

Figure 2. Endocytic trafficking. While clathrin chains form pits made up of hexagonal and pentagonal clathrin-rings, dynamin enables the scission of a budding vesicle. Bacteria and viruses (not shown) as well as multiple ligands such as proteins or small molecules enter mammalian cells through clathrin-/dynamin- and receptor-mediated endocytosis (*first from top left*), tubular clathrin-independent endocytosis (CIE; *second from top left*), or caveolin-1- and dynamin- (dynamin not depicted)-mediated endocytosis (*third from top left*). Not shown is caveolin-independent but lipid raft-dependent endocytosis. The internalised cargo fuses with an endosome and either undergoes lysosomal degradation (*bottom right*) or recycling (*top right*). Not depicted is that cargo may escape the endosomal compartment into the cytosol and act cytoplasmatically. Chlorpromazine (clathrin-mediated endocytosis inhibitor), dynasore (dynamin inhibitor, i.e. both clathrin-dependent and clathrin-independent endocytosis inhibitor), nystatin and filipin (caveolae/lipid raft-mediated endocytosis inhibitors) were used in this thesis. Adapted from (Johannes *et al.*, 2015). **Abbreviations**: **CAV1**, caveolin 1; **CIE**, clathrin-independent endocytosis; **GEEC**, GPI (glycosylphosphatidylinositol)-anchored protein-enriched early endosomal compartments.

Extracellular MIF can be endocytosed in a CD74-dependent manner, remain associated with the CD74 molecule within an endosome and elicit endosomal signalling via the receptors and second messengers (Figure 3D) (Xie *et al.*, 2011). MIF endocytosis appears to be dependent on clathrin, dynamin, β-arrestin (which has a Src activity) (Xie *et al.*, 2011), and on CD74 and CXCR4 (Schwartz *et al.*, 2012), and to be independent of caveolin in HEK293 cells (Schwartz *et al.*, 2012).

Long-term (24 h) MIF endosomal signalling triggers a sustained activation of ERK1/2 and cyclin D1 (Xie *et al.*, 2011). However, long-term stimulation with MIF does not affect cell

motility of WT nor MIF$^{-/-}$ mouse embryonic fibroblasts (MEFs) (Figure 3B) (Dewor *et al.*, 2007). In contrast, presumably shortly after MIF binds CD74/CD44, a rapid and transient activation of ERK1/2 (30 min – 2 h) occurs (Figure 3D) (Xie *et al.*, 2011). This may result in a calcium influx and subsequent upregulation of motility of WT and MIF$^{-/-}$ MEFs (Figure 3B) (Dewor *et al.*, 2007).

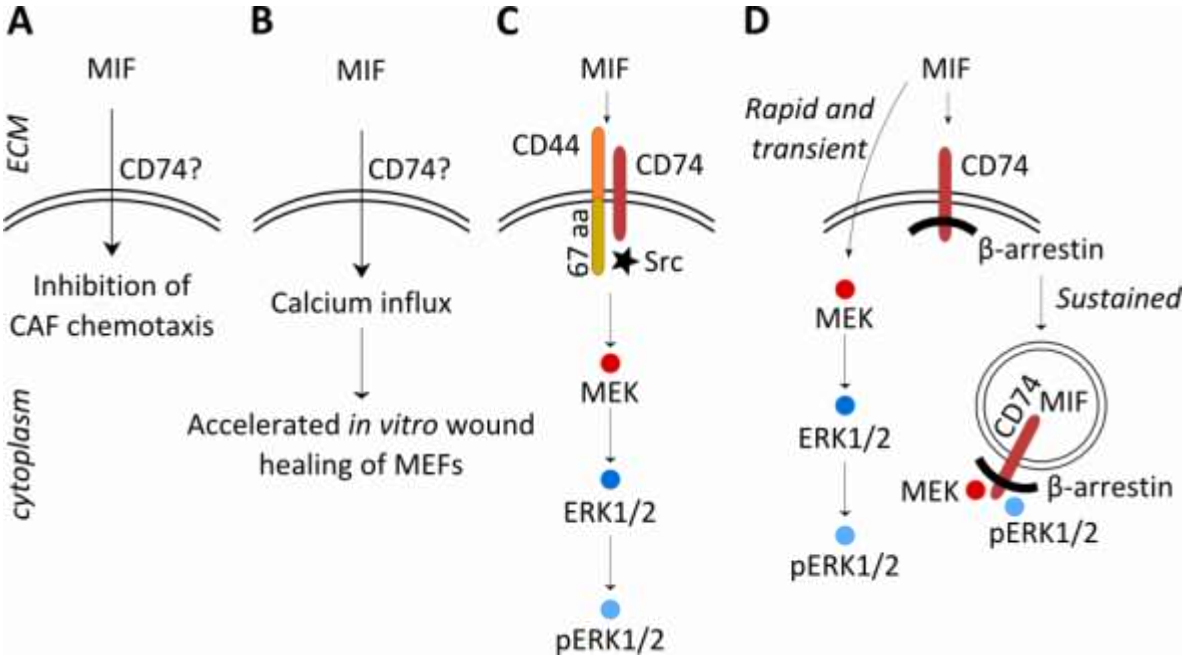

Figure 3. MIF modulates the motility of fibroblasts typically through CD74/CD44. (**A-D**) Schematic representation of the modes of action of MIF. (**A**) Via an unknown mechanism, rhabdomyosarcoma-derived MIF inhibits the chemotaxis of CAFs. (**B**) Short-term (2 h) but not long-term (24 h) stimulation with MIF triggers calcium influx and accelerated wound healing of primary mouse embryonic fibroblasts (MEFs). The role of CD74 in this process remains unknown. (**C**) In CD44^{+}/CD74^{+} COS-7/M6 cells MIF stimulates EKR1/2 phosphorylation which confers resistance against apoptosis specifically through its receptors CD44/CD74 and Src. (**D**) In RAW 264.7 macrophages as well as in COS-7 fibroblasts MIF is internalised in a CD74- and β-arrestin-dependent manner (**D**, *right*) and elicits endosomal signalling which leads to sustained ERK1/2 activation and downstream gene activation including *cyclin D1* (not depicted). Whether CD44/CD74 are required for MIF-triggered rapid and transient ERK1/2 activation remains unknown (**D**, *left*). **Abbreviations: CAFs**, cancer-associated fibroblasts; **ECM**, extracellular matrix; **MEF**, mouse embryonic fibroblast; **MEK**, mitogen-activated protein kinase (MAPK)/ERK kinase; **p**, phosphorylated.

2.6.3. MIF acts via CXCR2, CXCR4 and CXCR4 in immunocompetent cells

Circulating cells exhibit an amoeboid type of motility characterised by GPCR-mediated formation of a glycoprotein-rich uropod (Vicente-Manzanares and Sánchez-Madrid, 2004; Thelen and Stein, 2008; Sánchez-Madrid and Serrador, 2009). In circulating cells, MIF engages GPCRs – CXCR2, CXCR4 and CXCR7 – to elicit downstream signalling. Yet these receptors have their own cognate ligands: (*a*) IL-8 binds CXCR2 (also called CD182 or IL-8R B); (*b*) CXCL12/stromal cell-derived factor 1 (SDF-1), CXCL14, extracellular ubiquitin, and human immunodeficiency virus-1 (co-receptor with CD4) bind CXCR4 (CD184); and (*c*) CXCL11 and CXCL12 (SDF-1) bind CXCR7 (Tillmann *et al.*, 2013).

GPCRs are involved in signal transduction pathways for light, odours and neurotransmitters across species, and many of them are directly implicated in cancer metastasis (Roussos *et al.*, 2011; Wu *et al.*, 2012). The entire GPCR signalling unit consists of three components: a seven-transmembrane cell surface GPCR, a trimeric cytoplasmic αβγ G protein, and an effector. Once a GPCR is activated by an extracellular ligand, the G_{α} and $G_{\beta\gamma}$ subunits dissociate, and G_{α} elicits further signalling via an effector such as adenylyl cyclase, phospholipases, phosphodiesterases, or ion channels (Wu *et al.*, 2012).

An excellent physiological example of how GPCRs contribute to migration was demonstrated in zebrafish (*Danio rerio*). In its development, a group of approx. 200 epithelial cells known as the posterior lateral line primordium self-generates a gradient of Cxcl12/Sdf-1 to guide its migration along the embryo until it reaches the tip of its tail (Friedl and Gilmour, 2009). Cxcr7 is expressed at the rear end of the primordium and acts as a molecular sink to locally abrogate Sdf-1 signalling. At the front, Sdf-1 guides the migration of the primordium via Cxcr4 as there is more Cxcr4 than Cxcr7 (Donà *et al.*, 2013; Venkiteswaran *et al.*, 2013). Physiologically, such an elaborate mechanism ensures proper direction of motility and positioning of inner organs during development of zebrafish. MIF is a neutrophin in zebrafish (Shen *et al.*, 2012), but its role in cell motility of the developing or adult organism is unknown at present.

In human T cells, MIF activates AKT through a heterodimer composed of CD74 and CXCR4 (Schwartz *et al.*, 2009). MIF acts via CXCR4 and triggers the arrest of human neutrophils

(which are endogenously $CD74^{-/-}$) and primary human effector T cells (Figure 4A and C) (Bernhagen *et al.*, 2007). Upon MIF binding to CXCR2/CD74, it elicits chemotaxis followed by the arrest of PBMC-derived monocytes (Figure 4B) (Bernhagen *et al.*, 2007) as well as chemotaxis of natural killer T cells (Hsieh *et al.*, 2014).

B cell chemotaxis is triggered by MIF by two distinct ERK1/2- and 70-kDa zeta-chain associated protein-dependent mechanisms: via CXCR4/CD74 followed by calcium influx and actin polymerisation, and via CXCR7 (Figure 4D) (Klasen *et al.*, 2014; Alampour-Rajabi *et al.*, 2015).

MIF promotes adhesion of rhabdomyosarcoma cells via CXCR4 and CXCR7. Additionally, in the microenvironment of a rhabdomyosarcoma, MIF inhibits the recruitment of CAFs through an unknown mechanism (Figure 3A) (Tarnowski *et al.*, 2010). MIF and SDF-1 cooperate through CXCR4 to promote migration of metastatic colon cancer cells (Shin *et al.*, 2012). As a clinically-relevant illustration, hypoxia-stimulated MIF expression mediates chemotaxis of $CD11b^{+}/Gr\text{-}1^{+}$ myeloid cells – also known as myeloid-derived suppressor cells (MDSCs) – in a CD74/CXCR2/CXCR4-dependent manner (Zhu *et al.*, 2014). MIF mediates MDSC migration and may contribute to lung metastasis (Simpson and Cross, 2013; Kitamura *et al.*, 2015). Moreover, tumour-derived MIF increases the number of immune-suppressive MDSCs and contributes to tumour growth and metastasis (Simpson *et al.*, 2012).

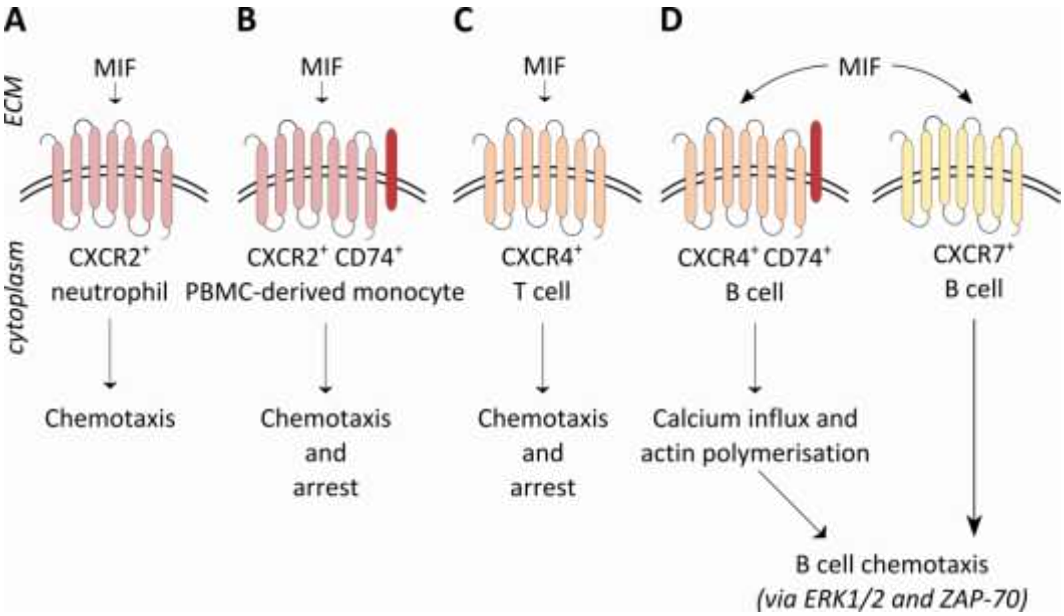

Figure 4. MIF modulates motility of mononuclear immunocompetent cells by acting on CXCR2/4/7. (**A-D**) Schematic representation of the mode of action of MIF. (**A**) MIF triggers neutrophil chemotaxis via CXCR2, (**B**) monocyte chemotaxis/arrest via CXCR2/CD74, and (**C**) T-cell chemotaxis/arrest via CXCR4. (**B-C**) Under flow conditions *in vivo*, endothelium-immobilised MIF attracts monocytes and T cells (chemotaxis) and causes their arrest at the arterial wall. (**D**) MIF promotes B cell chemotaxis via CXCR4/CD74 or CXCR7, calcium influx, actin polymerisation, ERK1/2 phosphorylation, and ZAP-70. **Abbreviations**: **CXCR**, C-X-C motif chemokine receptor; **ZAP-70**, 70-kDa zeta-chain associated protein.

2.7. MIF/D-DT influence cytoskeletal dynamics and migration

Cell migration is essential in health and disease. It primarily relies on dynamic rearrangements of the cellular cytoskeleton including microtubules (MTs), actin filaments, septins (Mostowy and Cossart, 2012; Shindo and Wallingford, 2014), and intermediate filaments (IFs) (Chung *et al.*, 2013). The following paragraphs provide an overview on MIF-dependent regulation of MTs (section 2.7.1) and actin (section 2.7.2-2.7.4) in the context of cell motility since little or no experimental evidence exists for MIF-mediated regulation of septins or IFs. The chapter describes further the link between MIF and adhesion (section 2.7.5) and motility (2.7.6).

2.7.1. MIF causes microtubule rearrangements

Responsible for intracellular transport and chromosome partitioning during cell division, MTs – composed of α- and β-tubulin dimers – are known to cooperate with actin filaments

to drive cell migration. In fibroblasts, MT polymerisation drives Rac1 and lamellipodial protrusion (Waterman-Storer *et al.*, 1999). In Chinese hamster ovary cells, MTs are dispensable for cell motility but govern the directionality of cell migration (Ganguly *et al.*, 2012). *In vitro*, chemotaxis of human monocytes/macrophages is typically inhibited by MIF (Lind *et al.*, 1999). MIF triggers excessive MT polymerisation thereby inhibiting macrophage migration (McCarthy *et al.*, 1979).

Under flow conditions, chemokines immobilised on the endothelium trigger rapid integrin activation leading to the arrest of a rolling leukocyte (Laudanna and Alon, 2006). In atherosclerosis, MIF immobilised on the endothelium of the arterial wall is now recognised as a chemoattractant as well as an arrest molecule for PBMC-derived monocytes and T cells (Figure 4) (Bernhagen *et al.*, 2007). In fact, syndecan-1 is one of the proteoglycans that bind MIF on the surface of epithelial cells to directly contribute to MIF-mediated motility (Pasqualon *et al.*, 2016), but the interaction between MIF and endothelium were not assessed there.

However, only a few follow-up studies addressed this putative MIF-MT axis. First, MIF promotes MT formation in human myocardial (atrial) trabeculae but motility remained uncharacterised (Preau *et al.*, 2013). In a different study human cytomegalovirus was shown to hijack the host immune responses of human monocyte-derived macrophages, as evidenced by a variety of methods including treatments with MIF-depleted supernatants. Upon infection, the virus triggers MIF secretion, thereby causing a loss of (*a*) podosomes, (*b*) ruffling lamellipodia and (*c*) the conical tail. Finally this leads to a complete rearrangement of actin, tubulin, and IF (vimentin) networks into dense and rigid assemblies. Ultimately, virus-induced MIF inhibits chemokine-induced but not random motility of macrophages (Frascaroli *et al.*, 2009). In a third study of human monocytic U-937 cells, MIF causes a cyclic activation and deactivation of Rho GTPases (DiCosmo-Ponticello *et al.*, 2014). Although this leads to migration inhibition as assessed by an agarose microdroplet assay, the status of the MT and actin networks remains unevaluated (DiCosmo-Ponticello *et al.*, 2014). Lastly, MIF inhibition by 4-IPP disrupts microtubule networks in $CD74^{+}$ human thyroid cancer TCP-1 cells and leads to a mitotic catastrophe

(Varinelli *et al.*, 2015), suggesting that MIF inhibition overcomes the cancer's resistance to apoptosis.

Interestingly, $p27^{Kip1}$ – described as an MIF-dependent fibroblasts cell-cycle inhibitor – associates in neurons with MTs to promote MT polymerisation *in vitro* and *in vivo* and hence neurite outgrowth (Godin *et al.*, 2012). However, the relation between MIF, $p27^{Kip1}$ and microtubules in fibroblasts remains unknown.

Taken together, recombinant MIF as well as MIF's tautomerase inhibition by 4-IPP disrupts the microtubular network. Excessive recombinant MIF (*a*) downregulates chemotaxis of monocytes by perturbing their MTs and (*b*) causes human myocardial contractile dysfunction by promoting excessive MT polymerisation. Similarly, MIF's inhibition leads to disrupted MTs, suggesting that (*a*) under normal conditions MIF levels ought to be low and (*b*) MIF's inhibition in a disease state is beneficial.

2.7.2. Cell migration depends on actin cytoskeleton

Cytoplasmic actin exists in the form of globular actin (G-actin) that can dimerise into helical filamentous actin (F-actin; also known as axial bundles or stress fibres) in human and rodent cells. Only recently it became clear that also the nucleus is equipped with a dynamic and polymeric actin network that is modulating the serum response (Vartiainen *et al.*, 2007; Baarlink *et al.*, 2013). In the cytoplasm, actin orchestrates a myriad of processes including cell division (Heng and Koh, 2010), muscle contraction, and cell migration. Six highly homologous actin isoforms exist ($\alpha_{skeletal}$-, $\alpha_{cardiac}$-, α_{muscle}-, β_{cyto}-, γ_{cyto}-, and γ_{smooth}-actin) in different cell types (Perrin and Ervasti, 2010) but β-actin specifically drives cell motility in MEFs and T cells (Bunnell *et al.*, 2011).

In the lamellipodial form of cell migration, actin filaments are severed at the cell rear (trailing) end of a migrating cell by actin depolymerising actors such as destrin or cofilin. Inhibition of these factors by phosphorylation may lead to accumulation of F-actin within the cytoplasm. At the same time actomyosin contractions facilitate the retraction of the cell rear end. While at this site focal adhesions are disassembled, new focal adhesions are built at the cell forward end (Ridley *et al.*, 2003). New actin filaments are assembled at the leading edge where the actin-related protein 2/3 (ARP2/3) complex – a 7-subunit actin-

binding protein complex – is mediating actin branching at a fixed angle of 70° (Robinson *et al.*, 2001). An existing filament is elongated by addition of new actin monomers. The barbed (plus) end of such a filament can be capped by capping proteins, which inhibit further elongation. Such a mechanism ensures that the filaments are kept short, thereby allowing for new filament generation which ultimately steers motility (Mejillano *et al.*, 2004). The verprolin, cofilin, acidic (VCA) domain of WASP (Wiskott-Aldrich syndrome protein)-family verprolin-homologous proteins (WAVE) activates the ARP2/3 complex (Rotty *et al.*, 2013). The VCA domain is sufficient to activate actin assembly *in vitro*.

Actin-rich filopodia, pseudopodia and invadopodia are specialised cell protrusions in which formins are responsible for actin elongation in form of parallel bundles, in contrast to the ARP2/3-mediated branched actin network (Faix and Grosse, 2006). Aside from the ARP2/3 complex and formins, Ena/VASP proteins also mediate actin elongation by competitively antagonising capping proteins (Krause *et al.*, 2003; Rotty *et al.*, 2015).

In either case the net movement forward of a cell is achieved by an actin build-up at the cell front and actin severing at the rear cell end. At the morphological level single-cell motility is defined as either amoeboidal or mesenchymal. Prominent F-actin stress fibres and the presence of lamellipodia and filopodia can be attributed to mesenchymal cell migration. Contrariwise, cells that are migrating in an amoeboid fashion are faster and lack F-actin stress fibres (Welch, 2015). When more than one cell is considered, collective-cell motility, that is rather characteristic of transformed cells such as cancer-derived cells, is either cluster- or strand-like (Friedl and Alexander, 2011). Two cell motility assays based on these features were employed in this work: a chemokinesis assay, to assess random single-cell motility, and a wound healing (scratch) assay to assess collective-cell motility.

2.7.3. MIF causes actin cytoskeleton rearrangements

Although MIF/D-DT do not bind actin directly, actin cytoskeleton-associated proteins such as destrin, cofilin, and myosin light chain kinase (MLCK) were described experimentally in the context of MIF. In human umbilical vein endothelial cells for example, cholinergic agonists increased not only MIF but also destrin. While this is the only study which identifies both proteins as part of one signalling network, the authors assessed this MIF-

destrin relationship within the non-neuronal acetylcholine system but not in the context of cell migration (Zhang *et al.*, 2014).

A link between MIF and actin polymerisation has been established based on F-actin rhodamine-phalloidin immunostaining and F-actin quantification by flow cytometry. While $MIF^{-/-}$ as well as $CD74^{-/-}$ BMDMs exhibit fewer C-C motif chemokine 2 (CCL2)/monocyte chemotactic protein 1 (MCP-1)-induced stress fibres (Fan *et al.*, 2011), recombinant MIF induces calcium influx and F-actin accumulation in B cells (Klasen *et al.*, 2014). Notably, MIF also triggers metastatic colorectal cancer cell chemotaxis by increasing the F-actin content through phosphorylation of cofilin at Ser-3 (Hu *et al.*, 2015). One study from 2005 identified the actomyosin-associated protein myosin light chain kinase (MLCK) as an interactor of cytoplasmic MIF in endothelial cells (Wadgaonkar *et al.*, 2005), and co-localised both proteins along F-actin stress fibres which was enhanced by thrombin. While MLCK activates the contractile machinery of endothelial cells, the precise role of MIF in contractility, let alone F-actin assembly, remained uncharacterised.

In a mass spectrometry-based proteomics study of pseudopodia isolated from chemotaxis-stimulated cells, MIF was found predominantly in pseudopodia but not the cell body (Lin *et al.*, 2004). However, another study did not corroborate that finding (Ito *et al.*, 2012). In addition, MIF localises near peripheral plasma membrane – reminiscent of a leading edge – of HeLa cells (Kleemann *et al.*, 2000a) as well as NIH 3T3 (Filip *et al.*, 2009).

Overall, MIF has been found to be associated with a few actin-associated proteins, or to be localized at the leading edge of migrating cells, but these relationships were never fully investigated in the context of cell migration. This thesis provides some experimental evidence for the MIF-actin cytoskeleton axis based on actin assembly assays and F-actin staining with phalloidin.

2.7.4. MIF influences Rho GTPases

Crucial for cell migration are Rho GTPases which exist in two states: an active GTP-bound and an inactive GDP-associated state (Figure 5A). Guanine nucleotide exchange factors (GEFs) activate Rho GTPases by mediating the exchange of GDP into GTP. Conversely, GTPase-activating proteins (GAPs) deactivate Rho GTPases by hydrolysis and release of an

inorganic phosphate (P_i). Within the cytoplasm, Rho GDP-dissociation inhibitors (RhoGDI) binds and sequesters Rho GTPases from the plasma membrane to keep them in an inactive cytoplasmic form. This mechanism serves two purposes: it protects Rho GTPases from degradation and prevents the GDP-to-GTP exchange. In other words, a Rho GTPase is in an inactive state when either bound to the membrane or to RhoGDI (Figure 5A) (Heasman and Ridley, 2008; Garcia-Mata *et al.*, 2011).

A

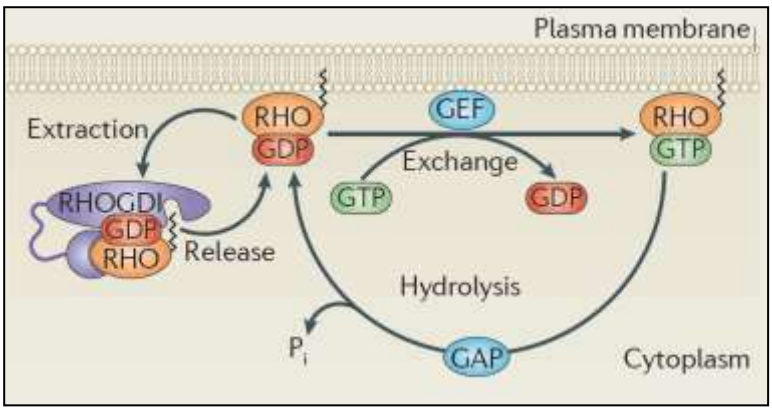

B

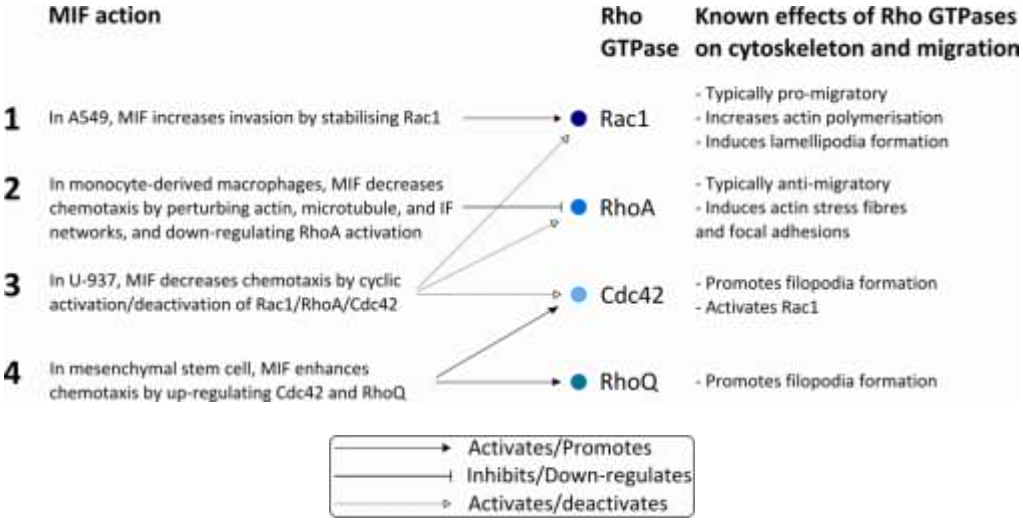

Figure 5. Rho GTPases cycle between an active and inactive state. (**A**) Cytoplasmic Rho proteins – most notably Rac1, RhoA, Cdc42 and RhoQ – cycle between an inactive, GDP-bound state, and an active, plasma membrane/GTP-bound state. RhoGDI prevents Rho degradation by sequestering them from the membrane. Adapted from (Garcia-Mata *et al.*, 2011). (**B**) MIF affects Rho GTPases in a cell-type dependent manner (**1-4**) (see text for explanation). **Abbreviations**: **IF**, intermediate filaments.

Three main Rho GTPases were described in quiescent NIH 3T3 (Hall, 1998): (*a*) Rac1 is best-known to promote cell motility via increasing actin polymerisation in membrane ruffles and inducing lamellipodia (leading edges) by activating WAVE (Ridley *et al.*, 1992; Eden *et al.*, 2002); (*b*) Ras homolog gene family, member A (RhoA) contributes to the formation of actin stress fibres and focal adhesions (Ridley and Hall, 1992; Rottner and Stradal, 2011); and (*c*) cell division control protein 42 homolog (Cdc42) stimulates filopodia formation but also activates Rac and therefore contributes to the formation of lamellipodia. Although cell type-dependent, Rac1 is typically associated with pro-migratory and RhoA with anti-migratory phenotypes (Rottner and Stradal, 2011).

Abundant in serum, lysophosphatidic acid induces characteristic RhoA-dependent stress fibres. On the other hand insulin or platelet-derived growth factor (PDGF) stimulate typical Rac1-mediated cortical actin accumulation, lamellipodia and ruffles/filopodia (Hall, 1998). Starvation produces a characteristic cortical actin rim around the periphery of a cell. It reduces the number of stress fibres, results in fewer organised actin filaments, and ultimately slows down motility. The migration of starved cells can be rescued by re-addition of either full serum or a single growth factor such as EGF.

In collective cell motility, Rac is enriched in leader but not follower cells (Yamaguchi *et al.*, 2015). In single-cell motility, differential Rac levels determine the migratory capacity of cells. Too low and too high Rac levels immobilise cells but a moderate Rac level promotes motility. In fact, a moderate reduction of Rac can stimulate chemotaxis. Over-reactive Rac is inhibitory due to over-accumulation of actin at the cell rim (Pankov *et al.*, 2005).

While MIF promotes RhoA to drive cyclin D1 expression and proliferation of MEFs and NIH 3T3 cells (Swant *et al.*, 2005), it decreases RhoA in monocyte-derived macrophages (Frascaroli *et al.*, 2009). Similar to reduced actin polymerisation (section 2.6.3), CCL2-induced RhoA activity was reduced in $MIF^{-/-}$ BMDMs as compared to WT (Fan *et al.*, 2011). In A549 adenocarcinoma cells, MIF stabilises Rac1 in caveolin-1-rich lipid rafts – cholesterol-rich plasma-membrane domains which serve as 'signalling platforms' – and upregulates motility (Figure 5B) (Rendon *et al.*, 2007). In one report MIF was found within the proteome of focal adhesions of human foreskin fibroblasts, and defined as one of Rac1

activators leading to dendritic actin treadmilling (Kuo *et al.*, 2011). Nonetheless, the exact mechanisms are yet to be elucidated (Lawson and Burridge, 2014).

MIF promotes human bone marrow-derived mesenchymal stromal cell (fibroblast-like, interstitial stem cells) chemotaxis via $G\alpha_i$ protein-coupled receptor CXCR4 through upregulation of Cdc42 and then RhoQ (Figure 5B) (Lourenco *et al.*, 2015). In contrast, MIF inhibits chemokinesis of iliac crest bone marrow-derived mesenchymal stem cells, but the mechanism remains poorly understood (Fischer-Valuck *et al.*, 2009; Barrilleaux *et al.*, 2010). Only one study systematically addressed the role of MIF in Rho GTPase activation in human monocytic U-937 cells where it caused Rac deactivation, RhoA activation, and Cdc42 cyclic activation/deactivation, eventually leading to motility inhibition, finally providing compelling evidence for the eponymous function of MIF (DiCosmo-Ponticello *et al.*, 2014).

In summary, MIF regulates the actin cytoskeleton in a highly cell-dependent manner via the activation/deactivation of Rho GTPases (Figure 5B).

2.7.5. MIF alters cell adhesion and plays a role in wound healing

Integrins are a family of transmembrane receptors that mediate cell adhesion by either linking two neighbouring cells (cell-cell interaction) or the cytoskeleton with the extracellular matrix (ECM) (cell-ECM interaction). MIF upregulates $\alpha_v\beta_3$ integrin in human chondrosarcoma cells (Lee *et al.*, 2011). Concurrently, the levels of integrins in $MIF^{-/-}$ endometrium are downregulated (Rakhila *et al.*, 2014). The fact that the E-cadherin interactome contains MIF points to a role in cell adhesion by means of protein-protein interactions (Guo *et al.*, 2014). Additionally, MIF stimulates rhabdomyosarcoma adhesion leading to a diminished tumour spreading (Tarnowski *et al.*, 2010). Aside from the cytoplasmic phenomena which largely rely on protein-protein interactions, cell migration involves ECM degradation and rearrangements. MIF is known to promote the expression of matrix metalloproteinases (MMPs) and thus directly contributes to invasion of cancer cells (Pakozdi *et al.*, 2006). Wound healing (multicellular migration) also involves many simultaneous events including dynamic ECM rearrangements. However, wound healing is distinct from single-cell migration as it maintains intact cell-cell junctions. In fact, MIF

exhibits opposing roles in wound healing; on the one hand it promotes fibroblast proliferation and migration thus enhancing wound healing but on the other it may impair healing by upregulating MMP-2 (Pakozdi *et al.*, 2006) or MMP-9 (Li *et al.*, 2004).

2.7.6. Summary

Overall, there were many attempts to elucidate the molecular pathways that MIF utilises to influence cell migration. The research in the field of circulating cells points to the fact that MIF promotes motility via GPCRs (CXCR2, CXCR4 and CXCR7). Other studies attribute upregulation of cell motility by MIF to steady-state Rac1 levels in A549 adenocarcinoma cells (Rendon *et al.*, 2007) or inhibition of cell motility by MIF to cyclic Rac1/RhoA/Cdc42 activation/deactivation in human monocytic U-937 cells (DiCosmo-Ponticello *et al.*, 2014). In mesenchymal stromal cells, MIF upregulates Cdc42 and RhoQ (Lourenco *et al.*, 2015). Calcium signalling (Dewor *et al.*, 2007) and subsequent calcium influx and ERK1/2 phosphorylation mediates MIF-induced motility in fibroblasts. It is well established that calcium, a danger signal released after wounding, drives actin polymerisation and wound resealing via Rho GEFs and Rho GTPases (Cordeiro and Jacinto, 2013).

In vitro, MIF enhances U373 human glioblastoma cell chemotaxis in an ERK1/2-dependent and CD74-independent manner (Piette *et al.*, 2009). In hepatocellular carcinoma cells (HCC), MIF drives angiogenesis and migration by promoting IL-8 (Ren *et al.*, 2003). Conversely, in a human neuroblastoma cell line, MIF inhibition decreases IL-8 levels, reduces cell growth and chemotaxis, and inhibits metastasis to lung and liver *in vivo* (Ren *et al.*, 2006). In A549 adenocarcinoma cells, MIF promotes invasion and anchorage-independent growth, and the inhibition of MIF's tautomerase activity by ISO-1 or a knockdown of MIF attenuates these effects (Rendon *et al.*, 2007).

Short-term (30 min – 2 h) but not long-term (24 h) MIF exposure accelerates MEF wound healing (Dewor *et al.*, 2007). This might be attributed to a rapid and transient MAPK/ERK1/2 activation (Xie *et al.*, 2011) or calcium signalling (Dewor *et al.*, 2007). In vascular smooth muscle cells (VSMCs), short-term (6.5 h) MIF treatment enhanced PDGF-BB-mediated chemotaxis; long-term (24 h) treatment reduced the stimulatory effect of PDGF but retained the effect of PDGF-BB (Schrans-Stassen *et al.*, 2005).

The clinical relevance of fibroblast migration is best exemplified by fibroblast-guided collective invasion of squamous cell carcinoma cells (Gaggioli *et al.*, 2007). Because carcinoma cells cannot degrade ECM, migrating fibroblasts create tracks in an integrin- and protease-dependent manner which supports invasion of carcinoma cells. While the role of MIF in fibroblast-guided invasion is yet to be elucidated, it is important to study the biology of MIF in migrating fibroblasts in order to complement the vast body of evidence that already exists for MIF in cancer and circulating cells.

The intertwined signalling pathways show the complexity of MIF's action on motility and leaves room for future experiments not only in the field of protein-protein interaction but also in cell-to-cell crosstalk.

2.8. The MIF/D-DT interactome – the starting point

The MIF/D-DT interactome in fibroblasts has been determined (Cayli *et al.*, 2009; Filip *et al.*, 2009; unpublished results). To that end four stable NIH 3T3 murine fibroblast cell lines had been generated: one expressing biotin protein ligase A (birA) only and three more cell lines co-expressing birA in combination with human MIF, human D-DT, and murine D-DT, all fused to a biotin linker and a tobacco etch virus (TEV) protease cleavage site.

Following *in vivo* biotinylation of MIF/D-DT fusion proteins, MIF/D-DT-interacting proteins (MIPs) were pulled down on streptavidin-agarose beads. After a TEV protease-mediated release of MIPs from the biotin-streptavidin-agarose resin, proteins were separated by SDS-PAGE. Individual lanes were sliced, digested with trypsin, and subjected to mass spectrometric analysis to determine the *m/z* ratio of the resulting peptides. These peptides were mapped *in silico* against a MASCOT library of all theoretical proteins (a catalogue of all known open-reading frames) in order to create a list of candidate MIPs. Ultimately a repertoire of actin cytoskeleton-associated proteins was identified as putative interactors of MIF and D-DT (Table 2). These results sparked an interest in delineating the role of cytoplasmic MIF/D-DT in modulating motility of fibroblasts. Specific interest was placed on addressing the question whether known MIF/D-DT receptors are required for modulating the motility of fibroblasts.

Table 2. List of putative MIF/D-DT-binding partners.

Name of putative MIF/D-DT interactors	UniProt identifier
ARPC3 (ARP2/3 complex subunit 3; or p21-ARC)	human: O15145
ARPC4 (ARP2/3 complex subunit 4; or p20-ARC)	human: P59998
CAPZA1 (F-actin-capping protein subunit α-1)	human: P52907
CAPZB (F-actin-capping protein subunit β	human: P47756
Destrin (actin-depolymerising factor or ADF)	human: P60981
Moesin (membrane-organizing extension spike protein), member of the ERM (ezrin-radixin-moesin) family	human: P26038
NDPKB (nucleoside diphosphate kinase B; also: NM23-H2 or NME2)	human: P22392
RhoGDI1 or RhoGDIα (Rho GDP-dissociation inhibitor 1 or α)	human: P52565
TPM4 (tropomyosin α-4 chain)	human: P67936

Only proteins associated with the actin cytoskeleton and motility are shown. RhoGDI was identified within the MIF but not D-DT interactome. Protein identification by mass spectrometry was performed in collaboration with Dr. Henning Urlaub and is partially published elsewhere (Filip *et al.*, 2009). Data originate from affinity-tag protein purification of biotinylated MIF from stable cell lines generated by Suada Fröhlich, Tamara Henke and Dr. Jörg Klug.

3. Purpose of the study

MIF/D-DT exhibit their biological effects extra- and intracellularly. While cytosolic MIF promotes cell cycle progression by interacting with JAB1, secreted MIF activates secondary messenger signalling by binding CD44/CD74. MIF/D-DT have emerged as crucial regulators of cell motility based on evidence from studies using recombinant MIF supplementation, genetic depletion, and overexpression. Whereas MIF inhibits cancer-associated fibroblast chemotaxis, it promotes mouse embryonic fibroblast wound healing. Since prior studies on motility did not systematically evaluate the status of the endogenous receptors, it remains unknown whether or not the effects of MIF were receptor-dependent. Moreover, the extent of the contribution of D-DT was lacking. Mechanistically, the MIF/D-DT-actin cytoskeleton axis was never broadly addressed.

This thesis aims to elucidate the mechanisms of action of MIF/D-DT on motility, building on two previous studies (Shi *et al.*, 2006; Dewor *et al.*, 2007). The specific questions were:

- ***Are the MIF receptors CD44 and CD74 essential for the action of MIF/D-DT on cell migration?*** Here fibroblasts deficient in MIF/D-DT receptors CD44 and CD74 were used to establish stable cell lines expressing CD44, CD74 and their combination.
- ***Are native MIF, tautomerase-null and oxidoreductase-null MIF mutants, and D-DT capable of influencing fibroblast chemokinesis* in vitro*?***
- ***If exogenous MIF/D-DT are capable of influencing fibroblast motility, what is the contribution of endogenous MIF to the observed effect?*** This question is addressed by employing siRNA-mediated *MIF* knockdown in WT and $CD44^+/CD74^+$ COS-7/M6 cells.
- ***Are exogenous MIF/D-DT endocytosed and released from the endosomal compartment in order to be able to act cytoplasmically?*** This question is addressed by employing specific inhibitors of clathrin- and non-clathrin-mediated endocytosis.
- ***Does MIF affect actin dynamics in cell extracts and living cells?*** To define the role of MIF/D-DT in affecting actin polymerisation, a series of actin assays was employed: actin assembly assays that measure the rate of actin polymerisation; and F-actin staining with phalloidin.

4. Materials and methods

4.1. Materials

Table 3. List of equipment.

Name	Supplier or origin
Agarose gel electrophoresis system PerfectBlue	peqlab, Erlangen
Bacterial shaker Certomat® *IS*	B. Braun Biotech International, Melsungen
Benchtop centrifuges Labofuge® 400/400R	Thermo Fisher Scientific, Waltham MA, USA
Cryo freezing container *Mr. Frosty™*	Nalgene®, a brand of Thermo Fisher Scientific, Waltham MA, USA
Electrophoresis Power Supply E143	Consort, Turnhout, Belgium
Fluorescence microscope Axioplan 2 Imaging with AxioCam	Carl Zeiss, Oberkochen
FPLC/HPLC system: Monitor UPC-900; Pump P-900; Fraction collector Frac-920; columns: Sephacryl™ S-100 HiPrep™ 16/60 High Resolution size-exclusion chromatography; Resource™ S and Mono S™ 5/50 GL (cation exchangers); Mono Q™ 5/50 GL (anion exchanger) (ÄKTAbasic)	GE Healthcare
Haemocytometer Neubauer – improved	LO, Laboroptik, Lancing, UK
High-speed Centrifuge Sorvall® RC-5C with Fiberlite F14 and SS34 rotors	Sorvall, a brand of Thermo Fisher Scientific, Waltham MA, USA
Incubators (for bacterial and mammalian cells)	Binder, Tuttlingen
Inverted microscope CKX41 with Olympus C-7070 camera	Olympus Optical, Hamburg
Inverted microscope system Eclipse *Ti* with CCD camera Clara	Nikon, Düsseldorf and Andor Technology Ltd., Belfast, UK
Laminar-flow hood class II BDK-S 1800	BDK, Sonnenbühl
Liquid nitrogen container ARPEGE 170	Air Liquide Deutschland GmbH, Düsseldorf
Microcentrifuge Pico 21	Heraeus®, a brand of Thermo Fisher Scientific, Waltham MA, USA
Orbital shaker (3017)	GFL Gesellschaft für Labortechnik, Burgwedel
pH-meter 766 Calimatic®	Knick, Berlin
Power Supply PowerEase 500	Invitrogen
Spectrofluorophotometer RF-5301PC	Shimadzu, Kyoto, Japan
Spectrophotometer NanoDrop™ 2000	NanoDrop, a brand of Thermo Fisher Scientific, Waltham MA, USA
Spectrophotometer Ultrospec 2011 *pro*	GE Healthcare
Stuart tube rotator SB3	Barloworld Scientific Ltd, Stone, Staffordshire, UK
Thermocycler PCR Primus 96 Advanced® Gradient	peqlab, Erlangen
Thermocycler PTC-200	MJ Research, now a brand of Bio-Rad, Munich
Thermoshaker PCMT	Grant Instruments, Shepreth, Cambridgeshire, UK
Thermoshaker TS-100	peqlab, Erlangen

Trans-Blot® Semi-Dry Electrophoretic Transfer Cell	Bio-Rad, Munich
Ultracentrifuge Ultra Pro 80 with T-865 rotor	Sorvall, a brand of Thermo Fisher Scientific, Waltham MA, USA
Ultrasonic bath Sonorex Super	Bandelin, Berlin
UV transilluminator 312 nm / INTAS Gel Jet Imager	Intas Science Imaging Instruments, Göttingen
Vertical electrophoresis chamber (*Slab-Gel-Kammer*)	von Keuz Labortechnik, Reiskirchen

Table 4. List of consumables.

Name	**Supplier or origin**
Centrifugation bucket (high-speed, 250 ml)	Nalgene, Langenselbold
Chemiluminescence film Amersham Hyperfilm™	GE Healthcare
Chromatography paper Whatman™	GE Healthcare
Cryogenic vials	Nalgene, Langenselbold
Filtropur syringe filter, 0.2-µm pore size	Sarstedt, Nümbrecht
Glass Pasteur pipettes	VWR International, Darmstadt
Glass Superfrost™ slides (to mount coverslips)	R. Langenbrinck, Emmendingen
High-speed centrifugation tubes (15, 50 ml falcons)	Sarstedt, Nümbrecht
Microcentrifuge tubes (0.5, 1.5 and 2.0 ml)	Sarstedt, Nümbrecht; Eppendorf, Hamburg
MµltiFlex Round Tips	Sorenson, BioScience, Salt Lake City, UT, USA
Nitrocellulose membrane Amersham™ Hybond™-ECL	GE Healthcare
Petri dishes (92x16 cm) for bacterial culture	Sarstedt, Nümbrecht
Pipette tips (10, 20 and 200 µl, 1 ml)	Sarstedt, Nümbrecht
Pipette tips (5 ml epT.I.P.S.)	Eppendorf, Hamburg
Polystyrene cuvettes 10x4x45 mm	Sarstedt, Nümbrecht
Round coverslips (11 mm diameter)	R. Langenbrinck, Emmendingen
Serological pipettes (5 ml, 10 ml, 25 ml)	Greiner Bio-One, Frickenhausen
Snap cap tubes (15 ml)	Thermo Fisher Scientific, Waltham MA, USA
Spectra/Por® Biotech Grade cellulose ester dialysis tubing with a 5-kDa molecular weight cut-off	Spectrum Laboratories, Rancho Dominguez, CA, USA
Syringes (1 ml, 5 ml, 10 ml, 20 ml)	B. Braun, Melsungen
Tissue-culture 75-cm^2 flask (T75)	Sarstedt, Nümbrecht
Tissue-culture multi-well plates (12- and 24-well)	BD Labware, Fanklin Lakes, NJ, USA
Tissue-culture multi-well plates (6- and 96-well)	Sarstedt, Nümbrecht
Tissue-culture Petri dishes (Ø35 mm, 6 cm, 10 cm)	Sarstedt, Nümbrecht
µ-Slide 8-well ibiTreat	ibidi, Planegg/Martinsried

Table 5. List of reagents employed in cell culture and molecular biology experiments.

Name	**Supplier or origin**
(*S,R*)-3-(4-Hydroxyphenyl)-4,5-dihydro-5-isoxazole acetic acid (ISO-1)	Merck, Darmstadt
1,4-Dithiothreitol (DTT)	Roche, Mannheim
1,4-Piperazinediethanesulfonic acid (PIPES)	Sigma-Aldrich, Steinheim

2-(N-Morpholino)ethanesulfonic acid (MES)	Serva Electrophresis, Heidelberg
3,8-Diamino-5-ethyl-6-phenylphenanthridinium bromide (ethidium bromide)	Carl-Roth, Karlsruhe
3',3'',5',5''-Tetrabromophenolsulfophthalein sodium salt (bromophenol blue)	Sigma-Aldrich, Steinheim
4-(2-Hydroxyethyl)-1-piperazineethanesulfonic acid (HEPES)	Carl-Roth, Karlsruhe
4-Iodo-6-phenylpyrimidine (4-IPP)	Sigma-Aldrich, Steinheim
5X siRNA resuspension buffer	Dharmacon/GE Healthcare
6-Aminocaproic acid ($C_6H_{13}NO_2$)	Carl-Roth, Karlsruhe
Acetic acid (CH_3COOH) (100% or 17.5 M)	Merck, Darmstadt
Acrylamide (Rotiphorese® Gel 30 (37, 5:1))	Carl-Roth, Karlsruhe
Adenosine triphosphate (ATP)	Sigma-Aldrich, Steinheim
Agarose (electrophoresis grade)	Invitrogen
Ammonium persulfate (APS)	Sigma-Aldrich, Steinheim
Ammonium sulphate (AS)	Carl-Roth, Karlsruhe
Ampicillin (ampicillin sodium salt)	Sigma-Aldrich, Steinheim
Bacto™ agar	Becton, Dickinson and Co., Sparks, MD, USA
Bacto™ yeast extract	Becton, Dickinson and Co., Sparks, MD, USA
BglII	Promega, Mannheim
Blue/Orange 6X loading dye	Promega, Mannheim
Bovine serum albumin (BSA, Fraction V, 60 kDa)	Carl-Roth, Karlsruhe
Bovine serum albumin (BSA, Fraction V, 67 kDa)	Serva Electrophoresis, Heidelberg
Calcium chloride ($CaCl_2$)	Merck, Darmstadt
Chloroform (100%)	Merck, Darmstadt
Chlorpromazine (CPZ)	Sigma-Aldrich, Steinheim
Collagen type I from calf skin	Sigma-Aldrich, Steinheim
Coomassie Brilliant Blue G-250 (PageBlue™ Protein Staining Solution)	Fermentas, Vilnus, Lithuania
Creatine phosphate	Sigma-Aldrich, Steinheim
Dimethyl sulfoxide (DMSO) (≥99.5%, BioScience-Grade)	Carl-Roth, Karlsruhe
Di-potassium hydrogen phosphate (K_2HPO_4)	Merck, Darmstadt
Disodium hydrogen phosphate (Na_2HPO_4)	Merck, Darmstadt
DNaseI (from bovine pancrease, grade II)	Boehringer, Mannheim; Roche
Dulbecco's phosphate-buffered saline (DPBS), without calcium and magnesium	PAA, Pasching, Austria/Cölbe, Marburg-Biedenkopf; Life Technologies, Darmstadt
Dulbecco's modified Eagle's medium (DMEM) GlutaMAX™, high glucose (4.5 g/l)	Life Technologies, Darmstadt
Dulbecco's modified Eagle's medium (DMEM), high glucose (4.5 g/l), L-glutamine	PAA, Pasching, Austria/Cölbe, Marburg-Biedenkopf
Dynasore (DYN)	Sigma-Aldrich, Steinheim
Ethanol (CH_3CH_2OH)	J.T.Baker (now VWR), Darmstadt
Ethylene glycol-bis(2-aminoethylether)-N,N,N',N'-tetraacetic acid (EGTA)	Carl-Roth, Karlsruhe
Ethylenediaminetetraacetic acid (EDTA)	Carl-Roth, Karlsruhe

Filipin III from *Streptomyces filipinensis*	Sigma-Aldrich, Steinheim
Foetal calf serum (FCS)	PAA, Pasching, Austria/Cölbe, Marburg-Biedenkopf; Life Technologies, Darmstadt
G418 sulfate (geneticin)	Calbiochem/Merck, Darmstadt
GIBCO® Zeocin™ selection reagent	Invitrogen
Glycerol	Merck, Darmstadt
Glycine	Carl-Roth, Karlsruhe
Hexammine cobalt(III) chloride ($[Co(NH_3)_6]Cl_3$)	Sigma-Aldrich, Steinheim
High-mass DNA ladder	Invitrogen
Hydrochloric acid (HCl)	Merck, Darmstadt
Hydrogen peroxide (H_2O_2)	Merck, Darmstadt
IGEPAL® CA-630 (previously known as NP-40)	Sigma-Aldrich, Steinheim
Immersion liquid type F (refractive index 1.518)	Leica Microsystems CMS, Wetzlar
Isopropanol ($(CH_3)_2CHOH$, 2-propanol)	Sigma-Aldrich, Steinheim
Isopropyl-β-D-thiogalactopyranoside (IPTG)	Carl-Roth, Karlsruhe
L-3,4-Dihydroxyphenylalanine methyl ester hydrochloride (L-dopa methyl ester)	Sigma-Aldrich, Steinheim
Lipofectamine™ 2000 Reagent	Invitrogen
Luminol sodium salt	Sigma-Aldrich, Steinheim
Lysozyme from chicken egg white (EC 3.2.1.17)	Sigma-Aldrich, Steinheim
Magnesium chloride ($MgCl_2$)	Sigma-Aldrich, Steinheim
Magnesium sulphate ($MgSO_4$)	Sigma-Aldrich, Steinheim
Manganese(II) chloride dihydrate ($MnCl_2 \cdot H_2O$)	Merck, Darmstadt
Methanol (CH_3OH)	Sigma-Aldrich, Steinheim
Milk powder, blotting grade	Carl-Roth, Karlsruhe
N,N,N',N'-Tetramethylethylenediamine (TEMED)	Carl-Roth, Karlsruhe
Nystatin (NYS)	Sigma-Aldrich, Steinheim
Opti-MEM® GlutaMAX™	Invitrogen
PageRuler™ pre-stained protein ladder	Fermentas/Thermo Scientific, Vilnus, Lithuania
Paraformaldehyde	Fluka/Sigma-Aldrich, Steinheim
p-coumaric acid	Sigma-Aldrich, Steinheim
Penicillin (10,000 units/ml) and streptomycin (10,000 µg/ml)	Pasching, Austria/Cölbe, Marburg-Biedenkopf; Thermo Scientific/Life Technologies, Darmstadt
Phenylmethyl sulfonyl fluoride (PMSF)	Carl-Roth, Karlsruhe
Ponceau S	Carl-Roth, Karlsruhe
Potassium chloride (KCl)	Merck, Darmstadt
Potassium dihydrogen phosphate (KH_2PO_4)	Merck, Darmstadt
ProLong® gold antifade mountant with DAPI	Thermo Scientific/Life Technologies, Darmstadt
Protease inhibitor cocktail (cat. no. P8340)	Sigma-Aldrich, Steinheim
Rabbit skeletal muscle α-actin (10% pyrene-labelled)	Hypermol, Bielefeld
Sodium chloride (NaCl)	Carl-Roth, Karlsruhe
Sodium deoxycholate	Sigma-Aldrich, Steinheim
Sodium dihydrogen phosphate monohydrate ($NaH_2PO_4 \cdot H_2O$)	Merck, Darmstadt
Sodium dodecyl sulphate (SDS)	Carl-Roth, Karlsruhe

Sodium fluoride (NaF)	Sigma-Aldrich, Steinheim
Sodium hydroxide (NaOH)	Merck, Darmstadt
Sodium orthovandate (Na_3VO_4)	Sigma-Aldrich, Steinheim
Sodium periodate ($NaIO_4$)	Merck, Darmstadt
Sulfosalicylic acid	Sigma-Aldrich, Steinheim
SuperSignal® West Pico Chemiluminescence Substrate (Luminol/Enhancer and Stable Peroxide)	Thermo Scientific/Life Technologies, Darmstadt
Texas Red®-X-conjugated phalloidin	Invitrogen
Trichloroacetic acid (TCA)	Carl-Roth, Karlsruhe
Tris-(hydroxymethyl aminomethane) (Tris)	Carl-Roth, Karlsruhe
Triton® X-100	Sigma-Aldrich, Steinheim
Trypsin-EDTA (0.25%), phenol red	GIBCO™, Life Technologies, Darmstadt
Tween-20	Sigma-Aldrich, Steinheim; Carl-Roth, Karlsruhe
Yeast extract	Sifin, Berlin
β-Mercaptoethanol	Sigma-Aldrich, Steinheim

Table 6. List of recombinant proteins.

Name	**Origin**
Recombinant GST-tagged VCA (GST-VCA) (1 mg/ml)	Robert Grosse lab, Marburg
Recombinant human epidermal growth factor (EGF)	Sigma-Aldrich, Steinheim
Recombinant human insulin-like growth factor (IGF)-I (7.6 kDa; 1 mg/ml in PBS)	R&D Systems, Wiesbaden (Małgorzata Wygrecka lab)
Recombinant human macrophage migration inhibitory factor (MIF): MIF WT/buffer P (13.08.2010), MIF C60S/20 mM phosphate buffer (01.11.2005), MIF P2A/PBS (01.11.2005), and MIF Δ4/PBS (17.11.2005)	*Laboratory stock* (Ana-Maria Filip, Suada Fröhlich, and Jörg Klug)
Recombinant human MIF, human and mouse D-dopachrome tautomerase (D-DT)	*This thesis*

Table 7. List of bacterial strains.

Name	**Origin**
E. coli BL21 (DE3) (B F^- *dcm ompT hsdS*(r_B^- m_B^-) *gal* λ(DE3))	*Laboratory stock*
Subcloning Efficiency™ *E. coli* DH5α™ competent cells (*fhu*A2 Δ(*arg*F-*lac*Z)U169 *pho*A *gln*V44 Φ80 Δ(*lac*Z)M15 *gyr*A96 *rec*A1 *rel*A1 *end*A1 *thi*-1 *hsd*R17)	Thermo Fisher Scientific

Table 8. List of mammalian cell lines.

Name	Origin
COS-7 (African green monkey kidney) fibroblasts	*Laboratory stock*
COS-7/M6 (COS-7 clone M6)	Kindly provided by the Richard Bucala lab, Yale
COS-7/M6 $CD44^+$	*This thesis,* stable cell line
COS-7/M6 $CD44^+/CD74^+$	*This thesis,* stable cell line
COS-7/M6 $CD44\Delta67^+$	*This thesis,* stable cell line
COS-7/M6 $CD44\Delta67^+/CD74^+$	*This thesis,* stable cell line
COS-7/M6 $CD74^+$	*This thesis,* stable cell line
HEK293 (human embryonic kidney) fibroblasts	*Laboratory stock*

Table 9. List of primary antibodies.

Name	Catalogue number; manufacturer or supplier	Dilution; blocking solution; electro-transfer time
Anti-CD74 (FL-296) (rabbit pc)	sc-20082, Santa Cruz	1:500; 5% milk; 60 min
Anti-MIF (83) (rabbit pc)	Meinhardt lab, JLU Giessen	1:20,000; 5% milk; 80 min
Anti-mouse CD44 (Hermes-3) (mouse mc)	Margot Zöller, Heidelberg	1:500; 5% milk; 90 min
Anti-β-actin antibody (AC-15) (ascites fluid)	A5441, Sigma-Aldrich	1:5,000; 5% milk
Purified mouse anti-human CD74 (mouse mc) (IgG2a)	555538, BD Pharmingen	1:500; 5% milk; 60 min
Rabbit anti-phospho-p44/42 MAPK (ERK1/2) (Thr-202/Tyr-204 and Thr-185/Tyr-187) (rabbit pc)	9101S, Cell Signaling	1:1,000; 5% BSA; 35 min
Rabbit anti-total p44/42 MAPK (ERK1/2) (rabbit pc)	9102, Cell Signaling	1:1,000; 5% BSA; 35 min

Table 10. List of secondary antibodies.

Name	Catalogue number; manufacturer or supplier	Dilution; blocking solution
Goat anti-rabbit HRP-conjugated secondary antibody	55676, MP Cappel; and 12-348, Merck	1:10,000; 5% milk or BSA
Sheep anti-mouse HRP-conjugated secondary antibody	A5906, Sigma-Aldrich	1:10,000; 5% milk or BSA

Table 11. List of primers.

Primer name	Sequence (5'→3')	Length [bp]	T_m [° C]	Amplicon size [bp]	Features recognised by primers; ID
β-actin-For	ATGGTGGGTATGGGTCAGAA	20	60.0	232	β-actin; AB004047.1
β-actin-Rev	GGGTCATCTTTTCACGGTTG	20	60.3		
CD74-For1	ACGCTCCACCGAAAGAGTC	19	60.4	194	His-tag and V5 epitope; NM_004355.3
CD74-Rev1	CGTAGAATCGAGACCGAGGA	20	60.3		
CD44FL-For3	CTCCAGTGAAAGGAGCAGCA	20	59.9	146	Exon 5-exon 6; NM_001001391.1
CD44FL-Rev3	TGGGGTGGAATGTGTCTTGG	20	59.8		
CD74-For2	CCATGGAGACCATAGACTGGA	21	59.9	99	Exon 5-exon 6; NM_004355.3
CD74-Rev2	CGTCAGTGGGCTTTTGCT	18	59.9		

Primer synthesis was carried out by Invitrogen.

Table 12. List of DNA constructs and their maps.

Name	Origin	Antibiotic resistance
pTracer™-SV40-CD44H	Richard Bucala lab, Yale (Shi *et al.*, 2006)	Zeocin
pTracer™-SV40-CD44Δ67	Richard Bucala lab, Yale (Shi *et al.*, 2006)	Zeocin
pcDNA™3.1/V5-His TOPO®-CD74	Richard Bucala lab, Yale (Shi *et al.*, 2006)	Ampicillin
pET-11b-WT hMIF	Jürgen Bernhagen lab, Aachen (Bernhagen *et al.*, 1994)	Ampicillin
pET-22b(+)-WT hD-DT	Richard Bucala lab, Yale (Merk *et al.*, 2011)	Ampicillin
pET-22b(+)-WT mD-DT	Richard Bucala lab, Yale (Merk *et al.*, 2011)	Ampicillin

1. pTracer™-SV40 (Thermo Scientific)

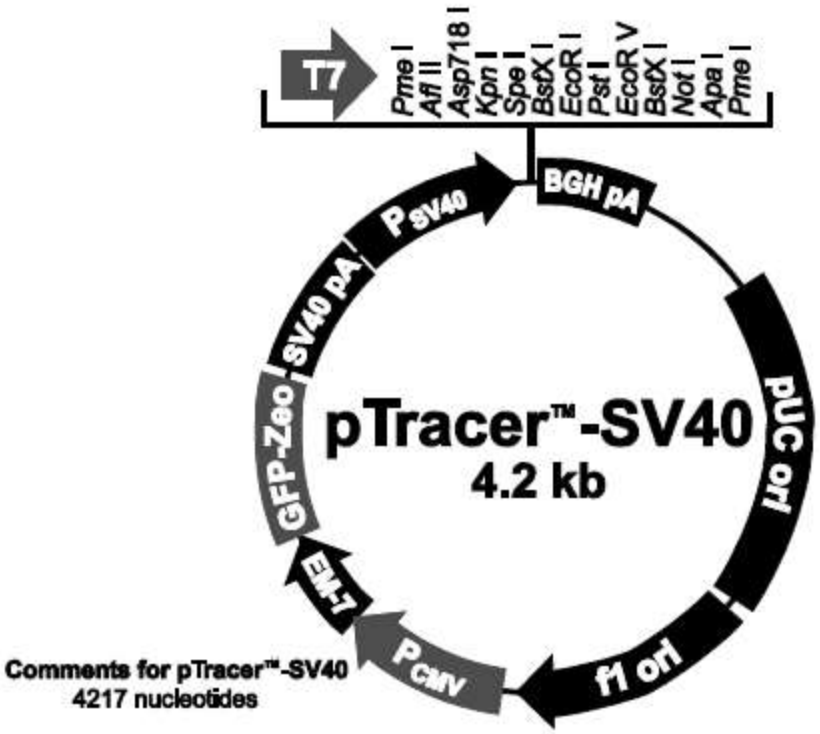

Comments for pTracer™-SV40
4217 nucleotides

SV40 promoter: bases 10-356
T7 promoter: bases 401-420
Multiple Cloning Site: bases 439-548
BGH reverse priming site: bases 560-577
BGH polyadenylation signal: bases 560-773
pUC origin: bases 812-1537
f1 origin: bases 1780-2290
CMV promoter: bases 2304-2930
EM-7 promoter: bases 2931-2997
GFP-Zeocin™ ORF: bases 2998-4074
GFP ORF bases: 2998-3702
Zeocin™ resistance gene ORF bases: 3703-4074
SV40 polyadenylation signal: bases 4082-4217

2. pcDNA™3.1/V5-His TOPO® (Thermo Scientific)

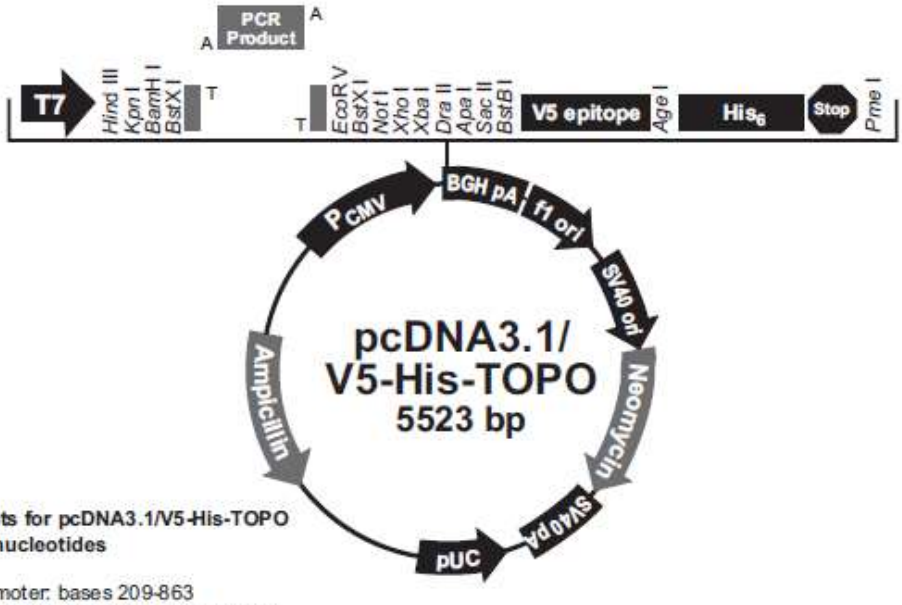

Comments for pcDNA3.1/V5-His-TOPO
5523 nucleotides

CMV promoter: bases 209-863
T7 promoter/priming site: bases 863-882
Multiple cloning site: bases 902-1019
TOPO® Cloning site: 953-954
V5 epitope: bases 1020-1061
Polyhistidine tag: bases 1071-1088
BGH reverse priming site: bases 1111-1128
BGH polyadenylation signal: bases 1110-1324
f1 origin of replication: bases 1387-1800
SV40 promoter and origin: bases 1865-2190
Neomycin resistance gene: bases 2226-3020
SV40 polyadenylation signal: bases 3039-3277
pUC origin: bases 3709-4382
Ampicillin resistance gene: bases 4527-5387

3. pET-11b (Agilent)

T7 promoter with *lac* operator 1–43
ribosome binding site 74–80
Nde I cloning site 86–91
T7 gene 10 leader 89–121
BamH I cloning site 124–129
T7 terminator 198–244
ampicillin resistance (*bla*) ORF 656–1513
pBR322 origin 1664–2331
***lacI*q repressor ORF** 4211–5167

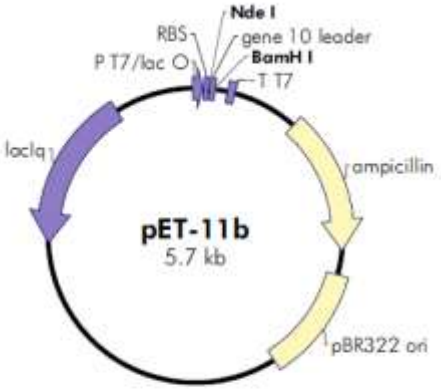

pET-11b Cloning Site Region
sequence shown (74–130)

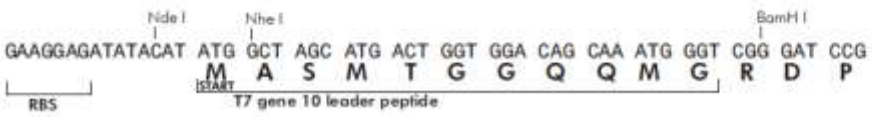

4. pET-22b(+) (Novagen)

pET-22b(+) sequence landmarks	
T7 promoter	361-377
T7 transcription start	360
pelB coding sequence	224-289
Multiple cloning sites	
(*Nco* I - *Xho* I)	158-225
His•Tag coding sequence	140-157
T7 terminator	26-72
lacI coding sequence	764-1843
pBR322 origin	3277
bla coding sequence	4038-4895
f1 origin	5027-5482

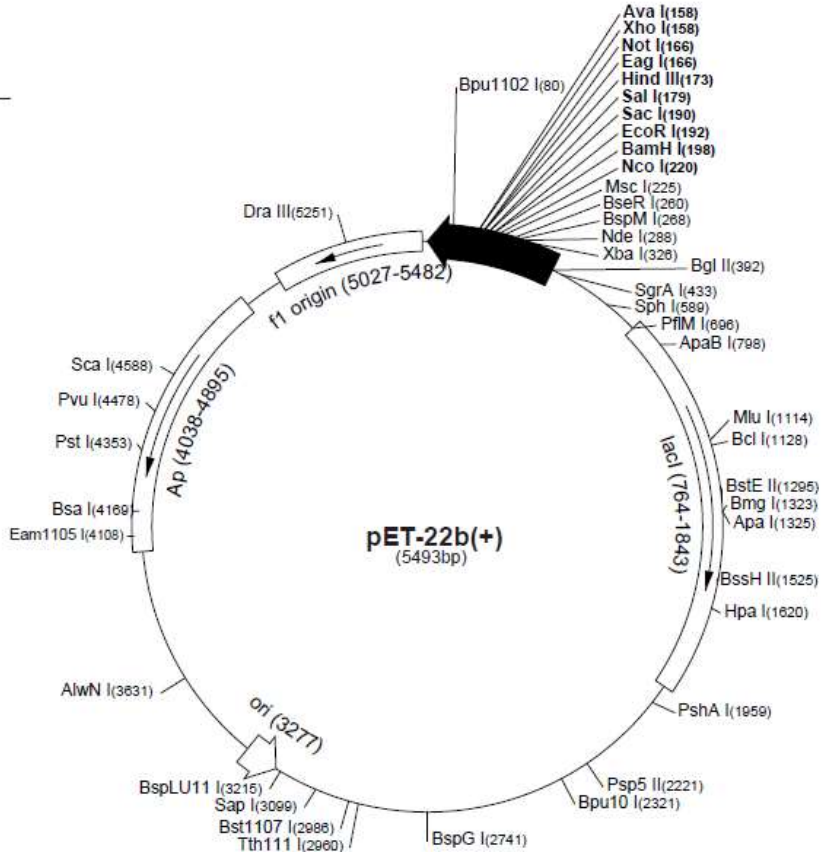

Table 13. List of short interfering RNAs (siRNAs).

Name	Sequence (5' to 3')
ON-TARGET*plus* MIF #1	Sense: GGGUCUAC**AUC**AACUAUUAUU Antisense: P–UAAUAGUUGAUGUAGACCCUU
ON-TARGET*plus* MIF #2	Sense: GCGCAGAA**CCG**CUCCUACAUU Antisense: P–UGUAGGAGCGGUUCUGCGCUU
ON-TARGET*plus* MIF C911 #1	Sense: GGGUCUAC**UAG**AACUAUUAUU Antisense: P–UAAUAGUUCUAGUAGACCCUU
ON-TARGET*plus* MIF C911 #2	Sense: GCGCAGAA**GGC**CUCCUACAUU Antisense: P–UGUAGGAGGCCUUCUGCGCUU

All siRNAs (10 nmol each) were custom-synthesised by Dharmacon/GE Healthcare. Base pairs 9 to 11 (complementary in C911 #1 and 2 to MIF #1 and2, respectively – are highlighted.

4.2. Methods

4.2.1. Biochemistry

4.2.1.1. Preparation of nucleic acids

DNA midi-preps were prepared according to manufacturer's instructions (NucleoBond® Xtra Midi, Macherey-Nagel, Düren) and stored at –20°C. RNA was prepared with the peqGOLD Total RNA Kit (peqlab, Erlangen) and stored at –80°C.

4.2.1.2. Determination of protein and nucleic acid concentrations

Protein concentrations were determined with the Bradford assay (Bradford, 1976) using the Bradford assay reagent (BioRad, Munich). Nucleic acid (DNA or RNA) concentrations were determined with a NanoDrop™ 2000 spectrophotometer using the NanoDrop software (version 1.4.2).

4.2.1.3. RNA reverse transcription and PCR

2 µg of RNA from WT and stable COS-7/M6 cell lines were combined with 0.5 µg oligo dT primer (all reagents were from Promega, Mannheim) per 1 µg RNA and heated up to 70 °C for 5 min. Following the Promega protocol, the total volume of this reaction was always smaller or equal to 15 µl (in water), because each starting RNA preparation had a different concentration. Next, the RNA-oligo dT primer mix was combined with 5 µl 5X reaction buffer, 1.25 µl each deoxynucleotide (dNTP, i.e. dATP, dCTP, dGTP and dTTP, each 10 mM), 0.625 µl (25 units) recombinant RNasin® ribonuclease inhibitor (stock: 40 u/µl), 1 µl (200 units) Moloney murine leukemia virus reverse transcriptase (200 u/µl), and water up to 25 µl. Following an incubation at 42 °C for 1 h in a PCR thermal cycler, the reaction was stopped at 72 °C for 15 min. 1 µl of freshly-prepared cDNA was used in the subsequent PCR.

Next, a PCR mix was combined in 0.5-ml microcentrifuge tubes on ice (Table 14).

Table 14. Components of PCR mix.

Component	Volume	Final concentration
5X Green GoTaq® reaction buffer containing 7.5 mM $MgCl_2$	10 µl	1X buffer and 1.5 mM $MgCl_2$
dNTPs (each 10 mM)	1 µl	0.2 mM
Forward primer (10 pmol)	0.5 µl	0.1 pmol
Reverse primer (10 pmol)	0.5 µl	0.1 pmol
cDNA generated as described above	1 µl	-
GoTaq® DNA polymerase	0.25 µl (1.25 units)	-
Water	Fill up to 50 µl	-

The tubes were placed within a PCR thermal cycler. All steps of the PCR were performed with lid heating (100 °C). The template cDNA was denatured at 95 °C for 2 minutes. Then 25 cycles of denaturation (95 °C) for 30 sec, annealing (53.7 °C for actin, 60 °C for CD74, and 66.3 °C for CD44FL) for 1 min, and extension (72 °C) for 1 min/kb were performed. The final extension was carried out at 72 °C for 5 minutes, and the PCR reactions were cooled down to 4 °C until retrieved for agarose electrophoresis.

4.2.1.4. Agarose gel electrophoresis

For a standard agarose gel, 1.2 % (w/v) agarose were dissolved in 100 ml TAE buffer (40 mM Tris base, 1 mM EDTA pH 8.0, 20 mM acetic acid) in an Erlenmeyer flask by boiling for 1-5 min at maximum power in a microwave oven. Once agarose had dissolved completely, the flask was cooled down under cold tap water for 2 min. Following drop-wise addition of ethidium bromide (2-3 drops for a small 7x8 cm and 4-5 drops for a large 15x15 cm gel), the agarose solution was poured into the gel holder mounted within the adjustable casting chamber, and the gelation of the agarose gel was allowed for approx. 30 min. 5 µl of the PCR samples were loaded into the wells together with a suitable DNA size marker and electrophoresed for 30 min at constant 110 V. If the PCR mix or DNA size marker did not include already a dye, the samples were complemented with 6X Blue/Orange loading dye (0.4% orange G, 0.03% bromophenol blue, 0.03% xylene cyanol FF, 15% Ficoll® 400, 10 mM Tris-HCl (pH 7.5) and 50 mM EDTA (pH 8.0), Promega) so that the final concentration was 1X. After electrophoresis the gel was placed on a 312

nm UV transilluminator and documented with an INTAS Gel Jet Imager running INTAS GDS Software (version 3.2816.01.2009).

4.2.1.5.Sodium dodecyl sulphate-polyacrylamide gel electrophoresis (SDS-PAGE)

Two glass plates and 1-mm spacers were assembled on a temporary holder. To cast the resolving gel the following components were combined (Table 15):

Table 15. Components of the resolving gel.

Component	**Gel percentage**			**Unit**
	7.5%	**12.5%**	**15%**	
Water	4.895	3.225	2.395	ml
1.5 M Tris-HCl pH 8.8	2.5	2.5	2.5	ml
20% (w/v) SDS	50	50	50	µl
Acrylamide (30%)	2.5	4.17	5	ml
10% (w/v) APS	50	50	50	µl
TEMED	5	5	5	µl
Total volume (2 gels)	**10**			**ml**

The polymerisation of each polyacrylamide gel was catalysed by APS and TEMED. The solution was immediately poured into the space between the two glass plates, overlaid with 100% isopropanol, and set aside to polymerise for 30 min at room temperature. Following isopropanol removal, a stacking gel solution containing 4% acrylamide (Table 16) was combined and poured over the resolving gel.

Table 16. Components of the stacking gel.

Component	**Gel percentage: 4%**	**Unit**
Water	3.025	ml
0.5 M Tris-HCl pH 6.8	1.25	ml
20% (w/v) SDS	25	µl
Acrylamide (30%)	0.65	ml
10% (w/v) APS	25	µl
TEMED	5	µl
Total volume (2 gels)	**5**	**ml**

As earlier, APS and TEMED were added shortly before casting the gel. A multi-well comb was inserted momentarily between the spacers, and the gel was set aside to polymerise for 15-20 min at room temperature.

Finally, the gels were mounted within the electrophoresis apparatus, creating an inner as well as outer chamber. The running buffer (25 mM Tris base, 192 mM glycine, 0.1% (w/v) SDS, no pH adjustment) was poured into both chambers. The comb was carefully removed and the wells thoroughly rinsed with running buffer.

Protein samples (either chromatography fractions or cell culture-derived, see sections below) were dissolved in an SDS-PAGE sample loading dye (50 mM Tris-HCl pH 6.8, 2% (w/v) SDS, 10% (v/v) glycerol, 0.002% (w/v) bromophenol blue, 200 mM DTT), boiled for 5 min, and immediately applied to the wells.

During electrophoresis through the stacking gel, the conditions were 80-90 V until the proteins reached the resolving gel. Within the resolving gel, the voltage was increased to 120-140 V, and the electrophoresis continued until the bromophenol blue dye migrated out of the gel.

4.2.1.6. Immunoblotting

Following SDS-PAGE, proteins were transferred in transfer buffer (25 mM Tris-HCl pH 8.3, 192 mM glycine, 20% (v/v) methanol) from the polyacrylamide gel onto nitrocellulose membranes using a semi-dry electroblotter (Trans-Blot® Semi-Dry Electrophoretic Transfer Cell). Briefly, four sheets of chromatography paper (Whatman™) were immersed in the transfer buffer and placed on the anode, followed by the buffer-soaked membrane, the SDS-acrylamide gel, and additional four sheets of chromatography paper. The cathode was placed back on the stack, and proteins were transferred at 1 mA/cm^2. To validate protein transfer, the membranes were stained in Ponceau S solution (0.2% (w/v) Ponceau S, 3% (v/v) trichloroacetic acid (TCA), 3% (w/v) sulfosalicylic acid) for 5 min, scanned, and destained with TBST (15 mM Tris-HCl pH 7.6, 137 mM NaCl, 1% (v/v) Tween-20). Membranes were blocked with freshly-made 5% (w/v) non-fat dry milk or BSA in TBST for 1 h on an orbital shaker. The blocking solution was discarded and a new primary antibody-

containing milk solution was added to the membranes and kept overnight at 4 °C with shaking (for dilutions see Table 9). Following washing with TBST for 3 x 5 min, the membranes were incubated for 1 h at room temperature with shaking in either 5% (w/v) non-fat dry milk or BSA supplemented with secondary antibodies (Table 10). Secondary antibodies were conjugated to horseradish peroxidase which catalyses the oxidation of luminol to chemiluminescent 3-aminophthalate.

Following the incubation with secondary antibodies, the membranes were washed with TBST for 3 x 10 min, placed within the Fusion development chamber (Vilber Lourmat, Eberhardzell), and covered entirely with the ECL substrate. To create an ECL substrate (Haan and Behrmann, 2007), 1 ml solution A (0.1 M Tris-HCl pH 8.6, 0.25 mg/ml luminol), 0.3 µl 30% (v/v) H_2O_2, and 100 µl solution B (1.1 mg/ml *p*-coumaric acid ((E)-3-(4-hydroxyphenyl)-2-propenoic acid) in DMSO) were combined 1 min before image recording. The ECL signal was detected using the FusionCapt Advance software (Vilber Lourmat, Eberhardzell).

Immunoblots against phosphorylated proteins were performed in essentially the same manner with the following exceptions. The blocking solution (5% BSA instead of 5% (w/v) non-fat dry milk in TBST) contained 50 mM NaF and Na_3VO_4, and the primary and secondary antibodies were dissolved in 5% BSA/TBST/50 mM NaF to inhibit phosphatases.

To re-probe with new antibodies, the membranes were incubated in stripping buffer (62 mM Tris-HCl pH 6.8, 0.5% (w/v) SDS, 0.8% (v/v) β-mercaptoethanol) for 5 min in a water bath at 65 °C, and then washed with TBST in order to quantitatively remove β-mercaptoethanol (approx. 1 h). The stripping procedure – time, temperature, and stripping buffer composition – has been standardised in our laboratory (Zhang, 2015) such that an ECL exposure after stripping does not yield a detectable signal.

4.2.2. Bacterial cell culture

Bacterial media were prepared as follows: LB (10 g/l tryptone, 5 g/l yeast extract (the supplier were switched from Sifin to Becton, Dickinson and Co.), 10 g/l NaCl); 2YT (16 g/l tryptone, 10 g/l yeast extract, 5 g/l NaCl); SOB (20 g/l tryptone, 5 g/l yeast extract, 0.5 g/l

NaCl; 833 µl of 3 M KCl to a final of 2.5 mM; 10 mM $MgCl_2$ and 10 mM $MgSO_4$); and SOC (SOB supplemented 20 mM glucose). All media – without prior pH adjustment – were autoclaved and stored at 4 °C. Glucose (SOC) was added after autoclaving. For LB/agar plates, 15 g/l agar was added to LB, sterilised by autoclaving, and allowed to cool down to approx. 50 °C before the addition of antibiotics. The LB-agar mixture was poured into Petri dishes and allowed to harden at room temperature. LB/agar plates were dried at 37 °C overnight and stored at 4 °C until use.

4.2.2.1. Inoculation from a glycerol stock, propagation from a single-colony

Bacterial cells were stored in microcentrifuge tubes at – 80 °C and were retrieved from a glycerol stock and kept on ice when necessary. A sterile inoculation loop was submerged into the tube with partially-thawed cells and the bacteria were streaked out on an LB/agar plate. For overnight cultures a single colony was picked with a sterile pipette tip, and the tip was put into a 13 ml snap cap tube containing 3-5 ml LB and incubated in an orbital shaker at 37°C overnight.

4.2.2.2. Preparation of competent bacterial cells and transformation

Chemically-competent *Escherichia coli (E. coli)* cells were prepared according to a simplified Hanahan protocol (Hanahan, 1983) and transformed with plasmid DNA encoding the gene/protein of interest – human MIF, mouse D-DT (mD-DT) or human D-DT (hD-DT). For overnight cultures a colony of *E. coli* DH5α (for plasmid DNA mini-preps) or *E. coli* BL21 (DE3) (for protein overexpression) was picked and inoculated into 3 ml SOB medium and grown overnight at 37 °C.

100 µl of the overnight culture were transferred into 30 ml SOB in a 500 ml Erlenmeyer flask. The optical density at 600 nm (OD_{600}) was checked regularly. At OD_{600} = 0.45-0.55, the culture was transferred into a 50 ml conical tube and put on ice for 10-15 min. The cells were pelleted by centrifugation at 2,500 rpm for 12 min at 4 °C. The supernatant was discarded, and the pellet resuspended in 10 ml transformation buffer (TFB) (10 mM K-MES pH 6.2, 100 mM KCl, 45 mM $MnCl_2$, 10 mM $CaCl_2$, 3 mM $[Co(NH_3)_6]Cl_3$, filter-sterilised and stored at 4 °C). After 10-15 min on ice, the cells were centrifuged again at 2,500 rpm for 12 min at 4 °C, the supernatant was discarded, and the pellet resuspended in 2.4 ml TFB.

The following compounds were added to the bacteria sequentially, the suspension was mixed, and the tubes were incubated on ice for the indicated time: DMSO (84 µl, 5 min); 1 M DTT (84 µl, 10 min); DMSO (84 µl, 5 min). The competent cell suspension was split into 200 µl aliquots in 1.5 ml microcentrifuge tubes and either used directly or snap-frozen in liquid nitrogen and stored at – 80 °C.

For transformation 1-5 µl plasmid DNA (100-300 ng) was added to 200 µl competent cell suspension. After incubation on ice for 30 min, the cells were heat-shocked for 45 sec at 42 °C and immediately transferred onto ice for 1-2 min. 800 µl SOC medium was added, and the microcentrifuge tubes were securely mounted in a bacterial shaker and incubated for 1 h at 37 °C with shaking for establishing antibiotic resistance. 200 µl bacterial suspension were streaked out on an ampicillin-containing agar plate. The plate was dried for 30 min at room temperature and incubated at 37 °C overnight.

4.2.2.3. Glycerol stocks

As needed, 1 ml overnight culture of wild type as well as transformed bacteria were combined with glycerol to a final concentration of 25% (v/v) and stored at – 80 °C.

4.2.3. Purification of recombinant MIF/D-DT from *E. coli*

4.2.3.1. Cell lysis

In order to produce wild-type recombinant proteins, fresh competent *E. coli* BL21 (DE3) were transformed (section 4.2.2.2) with an expression plasmid encoding either human MIF, human D-DT (hD-DT) or mouse D-DT (mD-DT) (Table 12), and plated on LB/ampicillin plates. 200 ml 2YT/ampicillin was inoculated with 200 µl of an overnight culture and incubated with shaking at 37°C. 1 ml of the bacterial culture was periodically transferred from the flask into a cuvette, and the OD_{600} was measured. At OD_{600} = 0.5, protein expression was induced by adding 40 µl 0.25 M IPTG (0.5 mM final). After shaking for another 3 h at 37°C the flask was put on ice for 5 min. The culture was centrifuged at 4,500 rpm for 15 min in a Fiberlite F14 rotor at 4 °C, the supernatant discarded and the pellet weighed (a 200-ml culture should yield a pellet of approx. 1 g). The pellet was resuspended in 3 ml of freshly-made *resuspension buffer I* (50 mM Tris-HCl pH 8.0, 1 mM EDTA, 100 mM NaCl) per gram of pellet. The suspension was transferred into a 50 ml high-

speed centrifugation tube (www.laborgeraete-beranek.de) for the Sorvall SS34 rotor. Per gram pellet 4 µl 100 mM PMSF and 80 µl lysozyme (10 mg/ml) were added. After incubation on a rotating platform at room temperature for 20 min, 4 mg Na-deoxycholate were added per gram pellet. The bacterial lysate was then placed at 37°C with occasional careful mixing until the solution became viscous (approx. 30 min). Next, 20 µl DNase I (1 mg/ml) was added per gram pellet, and the lysate was incubated at room temperature for 30 min until it was no longer viscous. The lysate was cleared by centrifugation at 11,000 rpm in a SS34 rotor at 4°C for 15-30 min.

The lysate was dialysed at room temperature using a 16 mm flat width Spectra/Por CE membrane with a MWCO of 5,000 (from www.spectrumlabs.com) against PBS (87.6 g NaCl, 22.8 g K_2HPO_4, 6.8 g KH_2PO_4, pH 7.4, water up to 1 l) supplemented with 1 mM DTT. In 2 hour intervals the dialysis buffer was replaced with fresh buffer twice, and the last dialysis step continued overnight. The next morning the dialysate was centrifuged in a SS34 rotor at 11,000 rpm and 4°C for 30 min. At this point, the purification protocols for MIF and D-DT diverged.

4.2.3.2. Purification of human MIF

The MIF-containing dialysate was recovered and proteins were precipitated by adding drop-wise 3.33 ml saturated ammonium sulphate (AS) solution per 5 ml dialysate (40% AS saturation) for 30 min on ice. A saturated AS solution is obtained by dissolving 80 g AS in 100 ml deionised water (approx. 4.1 M) with gentle heating (60 °C). The solution is cooled down to room temperature, adjusted to pH 7.0 with concentrated NH_4OH, 0.45 µm filtered and stored at 4°C. The precipitate was collected by centrifugation at 11,000 rpm in a Sorvall SS34 rotor at 4°C for 30 min. The pellet was set aside and remaining proteins were precipitated from the supernatant by increasing AS saturation to 60%. If start volume was 5 ml, 2.5 ml saturated AS solution was added to the 8.33 ml of the 40% solution. After 30 min on ice the precipitate was again collected by centrifugation at 11,000 rpm in a Sorvall SS34 rotor at 4°C for 30 min. The supernatant was set aside for analysis by SDS-PAGE, and the 60% AS pellet (if starting with a 200-ml bacterial culture)

was dissolved in 1 ml buffer P (20 mM HEPES pH 7.9, 5 mM EDTA, 200 mM NaCl, 1 mM DTT) and transferred to an Eppendorf tube.

The dissolved protein solution was cleared by centrifugation for 10 min at maximum speed in a microcentrifuge at 4 °C.

The protein concentration was determined (section 4.2.1.2), and 1 ml (up to 25 mg) was applied to a 16/60 HiPrep S-100 gel filtration column operated manually by an ÄKTA Basic HPLC system (GE Healthcare) using buffer P without PMSF as solvent (flow 0,4 ml/min, fraction size 2 ml). The major protein peak representing the recombinant protein eluted at approx. 58 ml.

The peak fractions (2-3 fractions) were combined, and the protein concentration was measured again. Using a 10-ml superloop and buffer P as solvent the combined peak fractions (approx. 4-6 ml) were passed over a 1-ml Resource™ S column screwed on top of a 1-ml Mono Q™ column operated again manually by an ÄKTA Basic HPLC system. The flow-through, containing MIF, was collected in one tube by manual fractionation and stored at 4 °C.

All samples that were set aside at critical preparation steps during the whole procedure were analysed by SDS-PAGE followed by Coomassie staining with either commercially-available Coomassie Brilliant Blue G-250 staining solution (Fermentas) or a staining solution made according to Sedmak and Grossberg (2% H_3PO_4, 10% $(NH_4)SO_4$, 20% methanol, 0.1% Coomassie Brilliant Blue G-250) (Sedmak and Grossberg, 1977).

4.2.3.3. Endotoxin removal

The next day the protein concentration of the flow-through was determined. The NaCl concentration was adjusted to 0.5 M and the protein sample was applied to a Detoxi-Gel™ AffinityPak Prepacked Column (Thermo Scientific, Pierce Biotechnology, Rockford, IL, USA) according to the manufacturer's instructions. Briefly, the column was conditioned with 1% (w/v) sodium deoxycholate, MilliQ water, and Ampuwa water. Then, the protein solution was applied, and the flow-through was collected in Eppendorf tubes for protein concentration measurement and long-term storage.

4.2.3.4. Purification of D-DTs

The purification of mD-DT and hD-DT was similar to the purification of hMIF (section 4.2.3.2) with the following exceptions. In the AS precipitation step mD-DT precipitated already at 40% AS saturation whereas hD-DT precipitated at 60% AS saturation like MIF. Following size-exclusion chromatography combined fractions were passed over Mono S™/Mono Q™ instead of Resource™ S™/Mono Q™, and 20 mM phosphate buffer pH 7.0 (12.2 ml of 1 M Na_2HPO_4, 7.8 ml 1 M NaH_2PO_4 in a total of 1 l) was used as solvent. Both D-DTs, identical to MIF, did not bind to the combined anion/cation exchangers, and eluted in the flow-through that was collected manually, aliquoted, and snap-frozen in liquid nitrogen for long-term storage at – 80 °C.

4.2.3.5. Confirmation of MIF and D-DT protein identity – mass spectrometry

The identity of all purified proteins was verified by matrix-assisted laser desorption/ionisation time-of-flight (MALDI-TOF) mass spectrometry (Protein Analytics, Institute for Biochemistry, JLU, Günter Lochnit lab). Briefly, recombinant proteins were separated on a polyacrylamide gel, bands were cut out, digested with trypsin and LysC (MIF only), and subjected to MS (see results below, points 1-3). In each result there is a box containing the expected amino acid sequence, and each peptide identified by MS is represented by one or more black boxes (e.g. for hMIF the box spans IGGAQNRSYSK), revealing the identity of each recombinant protein sequence verified over large parts of the primary amino acid sequence. Taken together, the multiple sequence alignments (below, point 4) show that the species identity could be confirmed for all proteins.

1. Human MIF

hMIF

Intensity Coverage:	79.3 % (48176 cnts)	Sequence Coverage MS:	9.6%
Sequence Coverage MS/MS:	0.0%	pI (isoelectric point):	9.1

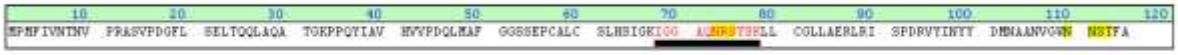

Display Parameter:

Sequence Name:	hMIF	MH+ (mono):	1.0
MH+ (avg):	1.0	Threshold (a.i.):	0.0
Tolerance (Da):	0.5	Number of Peaks:	28

Peaklist:

Peak	Mass	Intensity	Peak	Mass	Intensity
1	801.4	408.2	2	832.3	206.9
3	878.8	151.7	4	906.9	274.8
5	934.9	148.2	6	964.5	265.9
7	995.5	122.6	8	1010.5	107.5
9	1051.5	662.7	10	1067.5	116.4
11	1109.5	113.6	12	1135.6	107.7
13	1162.6	279.7	14	1166.3	278.6
15	1180.6	48176.4	16	1182.6	6187.6
17	1202.6	822.4	18	1207.6	81.0
19	1237.7	299.8	20	1276.6	615.4
21	1316.7	801.9	22	1365.6	127.6
23	1645.8	83.8	24	1702.8	52.8
25	1978.0	213.7	26	1992.0	36.0
27	4291.5	9.1	28	4306.7	3.2

2. Human D-DT

hD-DT

Intensity Coverage:	80.4 % (40294 cnts)	Sequence Coverage MS:	78.8%
Sequence Coverage MS/MS:	0.0%	pI (isoelectric point):	7.8

Display Parameter:

Sequence Name:	hD-DT	MH+ (mono):	1.0
MH+ (avg):	1.0	Threshold (a.i.):	0.0
Tolerance (Da):	0.5	Number of Peaks:	22

Peaklist:

Peak	Mass	Intensity	Peak	Mass	Intensity
1	833.4	259.1	2	881.4	2727.2
3	883.4	547.8	4	886.4	260.5
5	897.5	673.1	6	901.4	16251.5
7	1074.6	3172.1	8	1156.6	955.4
9	1230.7	1610.8	10	1351.7	4497.7
11	1450.7	10401.9	12	1499.8	5223.9
13	1507.7	368.0	14	1511.8	1076.1
15	1513.8	895.7	16	1556.8	1065.9
17	2390.2	3.9	18	2535.1	11.0
19	2719.2	68.4	20	3188.5	10.6
21	3856.9	45.1	22	3873.0	8.1

3. Murine D-DT

Chain A, D-Dopachrome Tautomerase (D-Dt) MACROPHAGE MIGRATION INHIBITORY Factor 2 (Mif2) Complexed With Inhibitor 4-Ipp
gi|308387818

Intensity Coverage:	90.7 % (57745 cnts)	Sequence Coverage MS:	96.6%
Sequence Coverage MS/MS:	0.0%	pI (isoelectric point):	6.1

Display Parameter:

Sequence Name:	Chain A, D-Dopachrome Tautomerase (D-Dt) MACROPHAGE MIGRATION INHIBITORY Factor 2 (Mif2) Complexed		
MH+ (mono):	1.0	MH+ (avg):	1.0
Threshold (a.i.):	0.0	Tolerance (Da):	0.5
Number of Peaks:	27		

Peaklist:

Peak	Mass	Intensity	Peak	Mass	Intensity
1	848.5	125.8	2	854.4	128.3
3	869.5	9627.3	4	896.5	2564.8
5	912.5	498.4	6	924.4	7665.3
7	981.5	124.2	8	1004.5	242.9
9	1230.6	110.8	10	1286.7	132.6
11	1335.7	5530.3	12	1417.7	103.7
13	1450.6	113.2	14	1465.6	11809.8
15	1472.7	6421.7	16	1484.7	1797.4
17	1529.8	1784.9	18	1616.8	148.4
19	1642.8	1078.3	20	1659.8	3265.4
21	1673.8	6025.2	22	1675.9	1574.8
23	1691.9	467.6	24	2368.1	16.1
25	2425.1	2294.7	26	2439.3	11.2
27	2482.3	17.8			

4. CLUSTAL O(1.2.1) multiple sequence alignments

Selected peptides found by MS that were not identical between human and murine are highlighted:

- Human MIF

```
sp|P14174|MIF_HUMAN      MPMFIVNTNVPRASVPDGFLSELTQQLAQATGKPPQYIAVHVVPDQLMAFGGSSEPCALC
sp|P34884|MIF_MOUSE      MPMFIVNTNVPRASVPEGFLSELTQQLAQATGKPAQYIAVHVVPDQLMTFSGTNDPCALC
                         ****************:***************** *************:*.*:.:*****

sp|P14174|MIF_HUMAN      SLHSIGKIGGAQNRSYSKLLCGLLAERLRISPDRVYINYYDMNAANVGWNNSTFA
sp|P34884|MIF_MOUSE      SLHSIGKIGGAQNRNYSKLLCGLLSDRLHISPDRVYINYYDMNAANVGWNGSTFA
                         **************.*********::**:********************** ****
```

- Human D-DT

```
sp|P30046|DOPD_HUMAN      MPFLELDTNLPANRVPAGLEKRLCAAAASILGKPADRVNVTVRPGLAMALSGSTEPCAQL
sp|O35215|DOPD_MOUSE      MPFVELETNLPASRIPAGLENRLCAATATILDKPEDRVSVTIRPGMTLLMNKSTEPCAHL
                          ***:**:*****.*:*****:*****:*:** ** ***.**:***::: :. ******:*

sp|P30046|DOPD_HUMAN      SISSIGVVGTAEDNRSHSAHFFEFLTKELALGQDRILIRFFPLESWQIGKIGTVMTFL
sp|O35215|DOPD_MOUSE      LVSSIGVVGTAEQNRTHSASFFKFLTEELSLDQDRIVIRFFPLEAWQIGKKGTVMTFL
                           :**********:**:*** **:***:**:* ****:*******:***** *******
```

- Murine D-DT

```
sp|P30046|DOPD_HUMAN      MPFLELDTNLPANRVPAGLEKRLCAAAASILGKPADRVNVTVRPGLAMALSGSTEPCAQL
sp|O35215|DOPD_MOUSE      MPFVELETNLPASRIPAGLENRLCAATATILDKPEDRVSVTIRPGMTLLMNKSTEPCAHL
                          ***:**:*****.*:*****:*****:*:** ** ***.**:***::: :. ******:*

sp|P30046|DOPD_HUMAN      SISSIGVVGTAEDNRSHSAHFFEFLTKELALGQDRILIRFFPLESWQIGKIGTVMTFL
sp|O35215|DOPD_MOUSE      LVSSIGVVGTAEQNRTHSASFFKFLTEELSLDQDRIVIRFFPLEAWQIGKKGTVMTFL
                           :**********:**:*** **:***:**:* ****:*******:***** *******
```

4.2.3.6. Crystal structures of MIF and D-DT in PyMOL

Based on X-ray-derived atom coordinates, three-dimensional structures of MIF (1MIF) (Sun *et al.*, 1996) and D-DT (1DPT) (Sugimoto *et al.*, 1999) were visualised by the PyMOL Molecular Graphics System (Version 1.7.4 Schrödinger, LLC.) on a transparent background. False colour-coding was employed to show residues responsible for distinct biological functions. Select amino acids were shown as sticks (i.e. the side chains were visible in full) whereas most of the structure is shown as a ribbon presentation (i.e. α-helices and β-sheets).

4.2.4. Mammalian cell culture

4.2.4.1. Passaging, freezing, and thawing of mammalian cells

WT and stable COS-7/M6 cell lines were cultured in GlutaMAX™ high-glucose DMEM supplemented with 10% (v/v) FCS (heat-inactivated at 56 °C for 30 min) and 100 units/ml penicillin and 100 µg/ml streptomycin (1:100 dilution of stock). COS-7/M6 single-transfectant stable cell lines were cultured in DMEM supplemented with antibiotics at 500 µg/ml: for $CD44^+$, zeocin (diluted from the ready-to-use stock solution of 100 mg/ml); for $CD44\Delta67^+$, zeocin; for $CD74^+$, geneticin (diluted from the stock of 100 mg/ml in 100 mM HEPES pH 7.3). COS-7/M6 double-transfectant stable cell lines were cultured in DMEM with both zeocin and geneticin (250 µg/ml each): $CD44^+$-$CD74^+$ or $CD44\Delta67^+$-$CD74^+$-double-expressing cells.

Cell passaging was performed according to the American Type Culture Collection guidelines for all cell types under investigation. Having inspected a flask or dish under a phase-contrast microscope, cells were washed once with PBS and 1 ml of the releasing solution (0.1 mM trypsin, 0.9 mM EDTA, Invitrogen) per a T75 flask/10-cm dish was used

to dislodge adherent cells from the substrate. To facilitate the detachment, the tissue culture vessel was kept in the incubator at 37 °C for 1-2 min. To stop the reaction, serum-containing DMEM was added to a total of 10 ml. In a new vessel, 11 ml of fresh medium was combined with a fraction of the trypsin-DMEM cell suspension such that the surface of a T75 flask was entirely covered. This fraction determined by cell counting with a haemocytometer. The cells were returned to an incubator with a humidified atmosphere consisting of 5% carbon dioxide (CO_2) at a constant temperature of 37 °C. Routine maintenance of cells involved passaging for up to 20-30 passages, after which the cells were discarded and cells with a lower-passage number were retrieved from the liquid nitrogen storage.

Cryopreservation of mammalian cells was carried out in liquid phase nitrogen. Cells grown to 80% confluency in T75 flasks were washed with PBS, trypsinised and centrifuged for 6 min at 600*g*. Following resuspension in 0.5 ml DMEM/10% (v/v) FCS without antibiotics, cells were transferred to a cryogenic vial and 0.5 ml of pre-chilled DMSO-containing freezing medium (DMEM/10% (v/v) FCS/20% (v/v) DMSO) was added. Tubes were gently inverted several times and kept in a Nalgene® Mr. Frosty™ Cryo 1 °C freezing container overnight at – 80 °C. The next day the tubes were placed in a designated area within the liquid nitrogen container.

In order to retrieve cells from liquid nitrogen, cells were warmed up in a water bath at 37 °C, transferred immediately to 10 ml pre-warmed medium, centrifuged for 6 min at 600*g* to remove DMSO, and transferred to a T75 flask. This way cells quickly reached confluency, so that passaging was required the next day. It was only after the second passage that functional assays were performed.

4.2.4.2. Generation of stable cell lines

To create stable COS-7/M6 cell lines, the following steps were undertaken. WT cells were grown in 6-cm dishes to 50% confluency. To determine the concentration of antibiotics for selection of clones, DMEM was supplemented with either zeocin, geneticin or both at a final concentration of 0, 100, 250, 500, 750 and 1000 µg/ml. For single antibiotics 500

µg/ml and for a combination of the two 250 µg/ml of each were eventually chosen as the lowest and yet 100% cytotoxic concentrations.

For transfection, WT COS-7/M6 were seeded at 50% confluency on 6-cm dishes. Lipofectamine 2000 (6.25 µl) and Opti-MEM (500 µl) were combined and incubated at room temperature for 5 min. Next 2 µg of BglII-linearised plasmid DNA was mixed with Opti-MEM (500 µl), added to the Lipofectamine-Opti-MEM mixture and incubated for 15 min at room temperature. The culture medium was aspirated and replaced by the new Lipofectamine-DNA-Opti-MEM-containing medium. After 6 h, the medium was replaced by FCS-free DMEM. After 2 days, cells were grown in new medium with FCS, and zeocin/geneticin were introduced to begin selection. The targeted linearisation step prior to transfection ensured that a full-length coding sequence was introduced into the genome of COS-7/M6 cells.

4.2.4.3. Cell lysis

To isolate cytoplasmic proteins, cells were grown to 80% confluency, washed with pre-warmed PBS, and lysed in a standard lysis buffer containing 1% (v/v) IGEPAL® CA-630, 150 mM NaCl, 50 mM Tris-HCl pH 8.0, protease inhibitor cocktail (1:100), and 1 mM PMSF. After centrifugation at 13,000*g* for 10 min at 4 °C, the supernatant was carefully removed and protein concentration determined.

4.2.4.4. Wound healing (scratch) assay in multi-well plates and µ-Slides: phase-contrast microscopy

Wound healing assays were performed as described previously (Liang *et al.*, 2007). The desired tissue culture vessels were coated with collagen type I (stock: 0.1% w/v in 0.1 M acetic acid, sterilised in chloroform according to manufacturer's instructions) at 8 µg/cm^2 for several hours at 37 °C.

The cells were seeded at 100% confluency in either (*a*) 1-cm^2 µ-Slides or (*b*) multi-well plates. A gap was created in the monolayer with a p10 (µ-Slide) or p200 (multi-well plate) pipette tip.

Serving as a positive control, epidermal growth factor (EGF) was supplied as a 100 µg/ml stock in water (Sigma).

The establishment of a wound healing assay in a µ-Slide was challenging due to its small size and a high risk of cell detachment, but eventually a seeding density of 50,000 cells per well in a total volume of 300 µl with collagen type I coating were chosen as most optimal conditions. Because these experiments yielded ambiguous results, wound healing assays were next performed in multi-well plates based on the same set of principles established for wound healing in µ-Slides. Cells were cultured in DMEM/10% (v/v) FCS. When being 90%-100% confluent, cells were trypsinised, centrifuged, resuspended in DMEM/1% (v/v) FCS and seeded so as to reach confluency within 6 h in a well of a 24-well plate. Following a wound with a p200 pipette tip, cells were allowed to migrate for 1-2 days. Images were acquired manually under a phase-contrast microscope (at a 4X magnification) 3, 6, 9, 24 and 48 h post wounding. Surface area was measured with ImageJ (version 1.49i, US National Institutes of Health, Bethesda, MD, USA, http://imagej.nih.gov/ij/, 1997-2014). For data analysis, only cell velocity was reported.

4.2.4.5. Chemokinesis (random single-cell motility) assay in µ-Slides: phase-contrast microscopy

Chemokinesis (random single-cell motility) assays allowed for single-cell tracking. Cells were seeded at 20% confluency (13,000 cells/well/cm^2) and allowed to adhere for 6 h in order to measure cell velocity (calculated as velocity = accumulated distance/time) (µm/min).

To set up a time-lapse chemokinesis experiment with COS-7/M6 cells at the Nikon Eclipse *Ti* microscope, the live-cell imaging chamber was mounted onto the motorised stage. To maintain a humidified atmosphere, water was poured into the outer basin of the chamber and maintained at 37 °C. The NIS-Elements software was initiated and 10 fields of view per one treatment were chosen under the 20X objective (200X final magnification; 1 px = 0.46 µm). A µ-Slide was carefully mounted in the chamber and data was acquired for at least 3.5 h with 30-min intervals. Following acquisition, data were saved as an ".nd" file, and each image stack (i.e. video) was then exported in the NIS-Elements software as an

".avi" file. Using the *Manual Tracking* plug-in of ImageJ, approx. 100 cells were selected and their trajectories were tracked and saved. Using the *Chemotaxis Tool* plug-in, the velocity was calculated based on cell trajectories.

For chemokinesis assays, a boxplot representing all measured velocities was shown. Boxplots were composed of: (*a*) a box extending from the 25th to 75th percentile (i.e. half of all data points); (*b*) a line in the middle of the box representing the median and a plus sign representing the mean; (*c*) whiskers encompassing the 10th-90th percentiles (i.e. 80% of all data points); and (*d*) outliers depicted as individual dots (i.e. 10% of all data points form the 0th-10th percentile and 10% of all data points from the 90th-100th percentile). In the case of individual data points, the mean ± interquartile range (25%-75% percentiles) was shown.

In total, approx. 100 cells were chosen per condition (one well in one µ-Slide). Final figures represent therefore approx. 300 cells from three unique wells in three separate µ-Slides, each representing a different cell passage (n = 3). A similar approach was employed elsewhere (Kuriyama *et al.*, 2014).

Following data analysis from all the experiments, figures were generated and statistical analyses were performed in GraphPad Prism (version 5.04 for Windows, GraphPad Prism software, San Diego, CA, USA, www.graphpad.com).

4.2.4.6. siRNA-mediated knockdown of endogenous MIF in COS-7/M6 cells

Dharmacon (GE Healthcare) offers a SMART pool composed of four human MIF-specific siRNAs (L-HUMAN-XX-0005) that have been selected by a proprietary SMART–selection™ design algorithm and guarantees high efficiency silencing. However, the knockdown was performed in COS-7/M6 cells that had been derived from the African green monkey (*Chlorocebus*) which is closely related to man (Gluzman, 1981).

The MIF protein sequences from both species are identical, and both mRNAs differ in only eight nucleotides within the open reading frame. Dharmacon confidentially provided the human siRNA nucleotide sequences so that they could be tested for identity with the *Chlorocebus* sequence. Based on this comparison two sequences from the human MIF

SMART pool were selected for knockdown of the *Chlorocebus* MIF mRNA (Table 13). The specificity of these siRNAs was enhanced by a patented modification pattern to reduce off-target effects called ON-TARGET plus.

In the past control siRNAs with a scrambled, i.e. randomly shuffled, sequence of the gene-specific siRNA had been routinely used for identifying potential off-target effects. Although it has been pointed out that scrambled siRNAs are not optimal controls, a validated alternative was introduced only in 2012 (Buehler *et al.*, 2012). They introduced the C911 controls that eliminate on-target effects while retaining the same off-target effects of the gene-specific siRNA by maintaining its guide and passenger strand seed sequences (bases 2-8 and bases 12-17 respectively). C911 controls have the same sequence as the gene-specific siRNA except that bases 9 through 11 are the complement of the original siRNA (Table 13). Therefore C911 controls allow effective experimental discrimination between true and false positive knockdown effects (Chung *et al.*, 2014).

Both siRNA preparation and siRNA-mediated knockdown were carried out according to the manufacturer's instructions. Briefly, 10 nmol of each lyophilised siRNA (Table 13) were resuspended in 0.5 ml to a final concentration of 20 µM in 1X resuspension buffer (60 mM KCl, 6 mM HEPES pH 7.5, 0.2 mM $MgCl_2$) diluted from a 5X stock (Dharmacon) resuspension buffer using RNase-free DEPC-treated water. siRNAs were further diluted 1:4 in 1X resuspension buffer before setting up the transfection reactions (final concentration 5 µM). The day before transfection, COS-7/M6 cells were seeded in four wells of a 6-well plate at 50,000 cells/well:

- Well no. 1: non-treated cells.
- Well no. 2: cells transfected with MIF siRNA #1 + #2.
- Well no. 3: cells transfected with MIF siRNA C911 #1 + #2.
- Well no. 4: mock-transfected cells (OptiMEM + Lipofectamine, no siRNA).

The next day, medium was exchanged for the transfection medium that was set up in the following manner.

In one tube 2.5 µl of each siRNA #1 and #2 (5 µM, either specific or C911 control) were combined with 15 µl of 1X resuspension buffer and 180 µl OptiMEM to a final volume of 200 µl. For the mock transfection, 200 µl OptiMEM were used. Overall there were three individual microcentrifuge tubes at this stage, one for experimental siRNA, one for the C911 control, and the last one for the mock reaction.

In a separate tube 4 µl Lipofectamine 2000 were combined with 196 µl OptiMEM to a final volume of 200 µl per individual transfection. This reaction was assembled in one microcentrifuge tube and was scaled up according to the total number of reactions intended.

After a 5-min incubation at room temperature, 200 µl of diluted Lipofectamine were added to the tube containing the siRNAs, and incubated for additional 20 min at room temperature. Complete medium (1.6 ml, DMEM/10% (v/v) FCS) was added at last to each transfection reaction yielding a total volume of 2 ml (final concentration of both siRNAs together 12.5 nM).

Cell culture medium in a well was exchanged for the transfection medium for 6 h. Subsequently the transfection medium was aspirated, and replaced by DMEM/10% (v/v) FCS cell culture medium without washing.

In test experiments to establish transfection conditions, after 3 days cells were lysed and cytoplasmic proteins were extracted to perform an immunoblot against MIF (section 4.2.1.6).

On the morning of a live-cell imaging experiment (66 h after transfection), cells were trypsinised, counted, seeded in µ-Slides (section 4.2.4.5), and incubated for another 6 h. As one µ-Slide has eight wells, each cell line (i.e. WT and $CD44^+/CD74^+$ COS-7/M6) was assayed individually on a single µ-Slide in the following manner. Commencing with four transfection conditions in four wells of each 6-well plate – (*a*) non-siRNA-treated, (*b*) MIF siRNA #1 + #2, (*c*) MIF siRNA C911 #1 + #2, and (*d*) mock-transfected – cells were seeded in such a way that two wells in an 8-well µ-Slide contained cells from (*a*), two from (*b*), two from (*c*), and finally two from (*d*). This allowed for a simultaneous comparison of cell

motility under non-MIF and MIF-stimulated conditions. To that end three days (72 h) after transfection, medium was exchanged for medium containing 0.5% (v/v) FCS with or without MIF, and time-lapse data acquisition followed as described before (section 4.2.4.5).

4.2.4.7. Actin staining with phalloidin: static distribution of actin

WT COS-7/M6 cells were seeded at 20,000 cells/cm^2 on round coverslips in a 12-well plate, allowed to adhere overnight, and treated with the compounds of interest. All the subsequent steps were performed at room temperature. The cells were fixed with 4% paraformaldehyde in PBS for 10 min, washed twice with PBS, permeabilised with 0.1% (v/v) Triton™ X-100 in PBS for 3-5 min, washed again twice in PBS, blocked with 1% (w/v) BSA for 30 min, and stained with Texas Red®-X-conjugated phalloidin (1:500 in PBS/1% (w/v) BSA) in the dark for 30 min. Following washing, the coverslips were removed from the 12-well plate, air-dried, overlaid with 4',6-diamidino-2-phenylindole (DAPI)-containing mounting medium, placed on a glass slide sample side-down, and dried overnight in the dark. This procedure is based on the 'Actin Staining Protocol' provided by the manufacturer of Texas Red®-X phalloidin (Invitrogen).

To visualise and document Texas Red®-X-conjugated phalloidin-stained actin in COS-7/M6 cells, the Axioplan 2 imaging microscope with AxioVisio 4.8.2 SP2 software were used. First the microscope and then the mercury light source were initiated. A glass slide with coverslips was mounted onto the microscope stage. Each coverslip was brushed with mineral oil and the 63X objective was initiated (630X final magnification). To take an overlay photograph of the nucleus and actin, two channels were activated within the *Mehrdimensionale Bildaufnahme* (multidimensional acquisition) panel: "3" for DAPI and "6" for Texas Red®-X. The illumination time was approx. 70-100 ms for the latter and 100-300 ms for the former. Images were saved as a TIFF file (1300 px x 1030 px/138,84 µm x 110 µm). The excitation/emission wavelengths of 596 nm/615 nm (for Texas Red®-X phalloidin) and 358 nm/461 nm (for DAPI) were used. For data analysis, ImageJ was used to enhance the contrast in order to better visualise all cytoplasmic actin structures. The

cells were categorised based on the unique characteristics of their actin cytoskeleton. More than 100 cells were quantified for each MIF and boiled MIF samples.

4.2.5. Cell-free assays/Spectrophotometric assays

4.2.5.1. Tautomerase activity assay

The tautomerase activity of recombinant and endogenous MIF was determined using L-dopachrome methyl ester as substrate in a spectrophotometric assay in a spectrophotometer (Filip et al, 2009).

Freshly-made 200 µl solution of 4 mM L-3,4-dihydroxyphenylalanine methyl ester was combined with 200 µl freshly-made solution of 8 mM sodium periodate and incubated for 3 min at room temperature in a microcentrifuge tube protected from light. Next, the substrate solution was combined with either 400 µl PBS to determine the background substrate decay or with 1 µM MIF or D-DT in 400 µl PBS to determine intrinsic MIF/D-DT tautomerase activities.

The SWIFT II programme was initiated to measure the kinetics of each reaction. The settings were adjusted in *Open View* > *Parameters*. To monitor the reaction kinetics at 475 nm, the options were adjusted to: (*a*) time units: mm:ss or sec; (*b*) duration: 10 min; (*c*) period: 0:00:02 (i.e. 2 sec); (*d*) number of assays: 1; (*e*) serial mode; (*f*) wavelength: 475.0 nm. Next, *Run* > *Method* was selected. After a short calibration step, two windows appeared: one ('load cell changer') with a list of all available cuvette positions ('cell 1 to cell 8') and another one with the real-time values of the absorbance, slope (A/min), duration, next reading, and sample name. Before commencing the measurement with *OK*, an empty cuvette filled with air was inserted in the Ultrospec 2011 *pro* UV/visible spectrophotometer in position 1 (or cell 1). When the 3-min incubation was over, the substrate (400 µl) was transferred from the microcentrifuge tube to the cuvette, and a plastic inoculating loop was placed into the cuvette. The remaining 400 µl PBS with or without protein was transferred to the cuvette and mixed as quickly as possible. The loop was taken out of the cuvette and the lid of the spectrophotometer was closed. As soon as possible, *OK* was pressed to begin measurement. The data were saved by exporting to an Excel file via *File* > *Export*.

4.2.5.2. Pyrene-actin assembly assay

Human embryonic kidney 293 (HEK293) cells were washed twice with ice-cold PBS and harvested in a lysis buffer (section 4.2.4.3) in the minimal possible volume (approx. 600 µl per T75, with several used at a given time) in order to maximise the end protein concentration. After 15 min on ice in a microcentrifuge tube, the lysates were centrifuged at 13,000*g* at 4 °C for 20 min, and immediately dialysed against XB buffer (10 mM HEPES pH 7.7, 100 mM KCl, 2 mM $MgCl_2$, 0.1 mM $CaCl_2$, 5 mM EGTA, 1 mM DTT) at 4 °C (two buffer exchanges during the day, then the third buffer exchange for an overnight dialysis). Combined always in the following order, the final reaction volume of 100 µl consisted of: (*1*) XB buffer, up to 100 µl (see composition above); (*2*) 10 µl energy regenerating mix (150 mM creatine phosphate, 20 mM ATP, 2 mM EGTA, 20 mM $MgCl_2$); (*3*) 700 µg total HEK293 cell extract as source of the ARP2/3 (63 µl when a stock of 11 mg/ml HEK293 extract was used); (*4*) 10 µg (2.6 µM) GST-VCA to activate the ARP2/3 complex (10 µl when a stock of 1 mg/ml GST-VCA was used); (*5*) 1 µM MIF/D-DT or the same volume of the corresponding buffer (MIF or buffer P – 3.1 µl; D-DT or 20 mM sodium phosphate buffer pH 7.0 – 7.4 µl); and (*6*) 10 µl pyrene-labelled G-actin (final concentration 2 µM, 10% labelled).

Immediately after the addition of pyrene-actin the reaction was mixed by pipetting up and down, and transferred into a black-walled quartz cuvette. Pyrene-actin fluorescence was measured at 10-second intervals for 10 minutes at 407 nm with excitation at 365 nm using a RF-5301PC spectrofluorophotometer (Shimadzu, Kyoto, Japan). Data were saved using the Panorama Fluorescence (version 2.1.16.0) software (Shimadzu, Kyoto, Japan/LabCognition Analytical Software, Cologne) and exported as a text file. To normalise, fluorescence at time zero (the first out of 60 measurements is defined as '10 sec' and the last one is defined as '600 sec') was set to zero by subtracting the initial value (in arbitrary units) from all measurements.

The rate of actin assembly was calculated by determining the slope of each curve at 50% polymerisation using the linear regression-based function *=slope()* in Excel 2010 (Microsoft Corporation, Redmond, WA, USA). The slope was measured for all data points within the log phase by performing a linear regression on seven data points – three data

points below and three data points above the point of interest. The maximal value was regarded as the slope at 50% polymerisation.

4.2.6. Statistical analysis

R (R Project, Vienna, Austria) and GraphPad Prism version 5.04 for Windows, GraphPad Prism software (San Diego, CA, USA, www.graphpad.com) were used to: (*a*) assess normality of data by generating q-q plots; and (*b*) calculate statistical significance using the following tests: Student's *t*-test for two samples of normal distribution (for experiments where triplicates were performed); Mann-Whitney U-test for two samples of non-normal distribution (for experiments where triplicates were performed); and Kruskal-Wallis one-way ANOVA with Dunn's multiple comparison test as a post test (significance level set to $\alpha = 0.05$) for a group of more than 3 samples with non-Gaussian distribution (i.e. non-parametric) (for chemokinesis experiments).

4.2.6.1. Assessment of normality of chemokinesis data

To determine if chemokinesis datasets came from a Gaussian (normal) distribution, q-q plots were generated in R. Data input in R was performed using the concatenate option:

```
(FCS10 <- c( 0.51, 0.09, 0.08, 0.09))
```

where **FCS10** was the name of a dataset corresponding to 10% (v/v) FCS-containing control, **<-c** was the concatenate function, and the numerical values (**0.51** and so forth) were velocities in µm/min).

Normal q-q plots with reference lines were generated using the **qqnorm** and **qqline** functions (*below*). In a typical q-q plot, sample quantiles fall on the Y axis and theoretical quantiles fall on the X axis. If the reference line (*below*) crosses all or almost all data points, the data are considered to be normally distributed. If this is the case it would be justified to use statistical tests which assume normality in order to calculate statistical significance. Otherwise, if a q-q plot does not reveal normality, it indicates that data do not originate from an ideal Gaussian distribution. In such a case tests which do not assume normality would rather be employed.

Often present in motility assays, outlier points skew the distribution and thus the overall dataset is not of a Gaussian distribution. As shown by the q-q plot analysis (*below*), none of the chemokinesis datasets were normally distributed. Therefore a Kruskal-Wallis ANOVA was used to determine statistical significance.

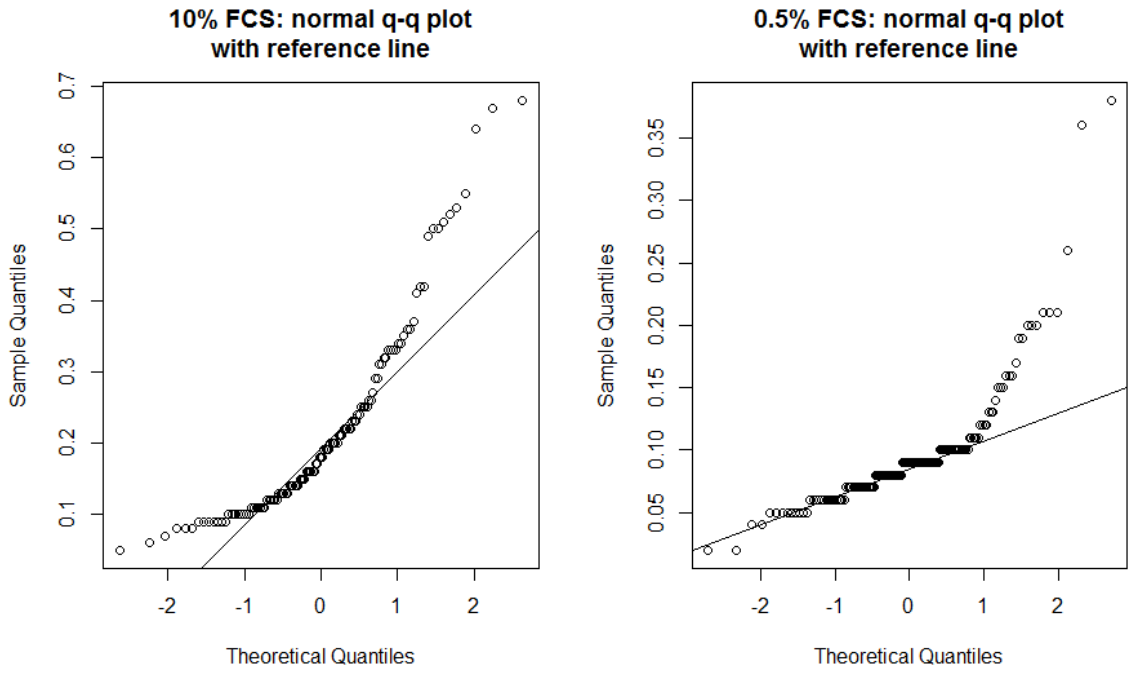

4.2.7. Genetic safety

Documentation on genetically modified bacterial or mammalian cells – i.e. date of generation, storage location, and date of disposal by autoclaving – was maintained according to university regulations. Sterilisation of material derived from or contaminated with transformed bacteria or transfected mammalian cells was performed by autoclaving (*Betriebsanweisung* UGI 67).

5. Results

5.1. Bacterial expression and purification of recombinant MIF and D-DT

To study MIF/D-DT in cell and cell-free assays, recombinant proteins were generated. Overexpression of human MIF and human D-DT (hD-DT) and mouse D-DT (mD-DT) was carried out in protease-deficient BL21 (DE3) *E. coli*. Bacteria were grown in 2YT medium overnight and a fraction of the overnight culture was used to inoculate a large-volume of 2YT for the preparative small-scale protein production. The levels of overexpressed proteins were monitored on Coomassie-stained SDS-polyacrylamide gels (Figure 6). Before induction of protein expression, there was no appreciable band at 12.5 kDa indicative of human recombinant MIF (Figure 6A, lane 1 vs 4). Upon induction of protein expression at OD_{600} = 0.5 with 0.5 mM IPTG (Figure 6A, lane 2-4), cells were allowed to grow for 3 h and then lysed (Figure 6A, lane 3-5).

Prior to the chromatographic purification, cell lysates were dialysed against PBS/1 mM DTT (Figure 6A, lane 6), and precipitated with 40% (Figure 6A, lane 7) and 60% ammonium sulphate (AS) (Figure 6A, lane 8-9; Figure 6B, lane 1). AS-precipitated proteins were first passed onto a size-exclusion column (Figure 6B, lane 2), and then anion and cation exchangers (Figure 6B, lane 3). While MIF was captured by these exchangers and then eluted in a high-salt gradient (Figure 6, lane 3), D-DTs were found in the flow-through of the exchangers (data not shown). The purity of the endotoxin-free proteins was monitored through a Coomassie-stained polyacrylamide gel (Figure 6B, lane 5; Figure 7). The identity of the protein sequences was determined by mass spectrometry (section 4.2.3.5), and the yield was 7.5 mg total protein from 200 ml of *E. coli* culture, similar to the first MIF purification report (1 mg/50 ml of *E. coli* culture) (Bernhagen *et al.*, 1994).

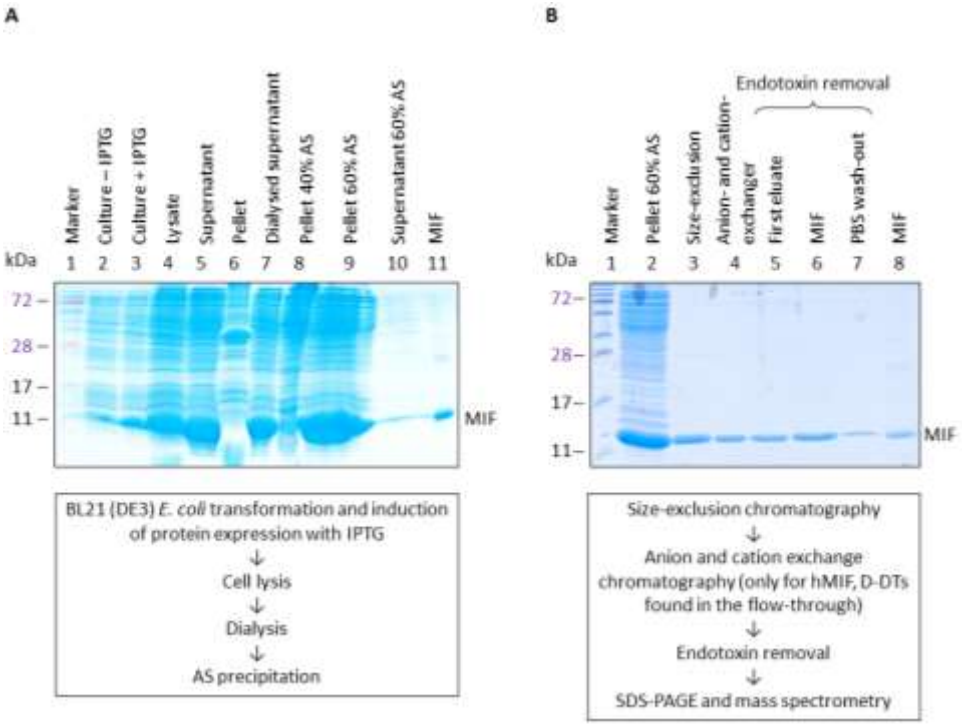

Figure 6. Purification of human MIF from bacteria. (**A and B**) Coomassie-stained polyacrylamide gels (*top*) with protein samples collected after each purification step (*schematics below*). Each fraction (a pellet resuspended in SDS loading dye, a supernatant, or a post-chromatography sample/pooled samples) is abbreviated as such for clarity. Sample in lane 9 in **A** is the same as in lane 2 in **B**. Recombinant hMIF served as a size control (**A**, lane 11; **B**, lane 8). (**A**) Plasmid DNA encoding hMIF was overexpressed in *E. coli* BL21 (DE3) and protein expression was induced with IPTG (lane 2-3). Following cell lysis (lane 4-6), the lysate was dialysed against PBS/1 mM DTT (lane 7) and the proteins were precipitated with AS (lane 8-10). (**B**) Precipitated proteins were subjected to size-exclusion chromatography (lane 3) and anion- and cation-exchange chromatography (lane 4) using an FPLC/HPLC system. Endotoxin was removed by passing the purified protein over columns with immobilised polymyxin B which has affinity towards endotoxin (lane 5-7). **Abbreviations**: **AS**, ammonium sulfate; **DTT**, dithiothreitol; **FPLC/HPLC**, fast protein/high-performance liquid chromatography; **IPTG**, isopropyl-β-D-thiogalactopyranoside.

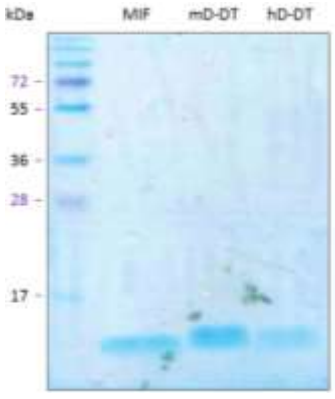

Figure 7. Analysis of purified recombinant MIF and D-DTs. Purified proteins (MIF, 12. 5kDa; mD-DT, 13.1 kDa; and hD-DT, 12.7 kDa) were resolved on a 15% polyacrylamide gel and stained with Coomassie.

5.2. MIF but not D-DTs has a high tautomerase activity

MIF and D-DT catalyse the tautomerisation of non-naturally occurring L-dopachrome (Rosengren *et al.*, 1996; Filip *et al.*, 2009). While a genuine, endogenous substrate for MIF/D-DT in metazoans is yet to be identified, the inhibition of MIF's tautomerase activity has been shown to be therapeutically beneficial in murine models of sepsis (Al-Abed *et al.*, 2005) and human cell-culture models of gallbladder cancer invasion (Subbannayya *et al.*, 2015). Hence tautomerase assays were employed to verify whether recombinant MIF/D-DT used in cell-culture experiments were biologically active. A robust enzymatic activity of MIF/D-DT in solution would suggest they are properly folded.

To verify that MIF remains stable and active in cell-culture medium, and to exclude the possibility that an FCS- or cell-derived component binds and inactivates it, WT COS-7/M6 cells were seeded in multi-well plates in DMEM supplemented with 10 nM, 100 nM, and 1 µM MIF, with or without MIF's tautomerase inhibitors (*S,R*)-3-(4-hydroxyphenyl)-4,5-dihydro-5-isoxazole acetic acid (ISO-1) and 4-iodo-6-phenylpyrimidine (4-IPP) and their solvent, DMSO. The next day, 1 ml of MIF-containing supernatant was used in a tautomerase activity assay in which L-dopachrome methyl ester is tautomerised into 5,6-dihydroxy-1-H-indole-2-carboxylic acid methyl ester over the course of 600 sec at room temperature. Noteworthily, the tautomerase activity of MIF-containing supernatants may be lower than if MIF was dissolved in DMEM/10% (v/v) FCS only, due to the fact that some MIF molecules might have been endocytosed by the cells or stay immobilised on their surface.

The substrate and the MIF-containing supernatant were mixed in a cuvette placed directly within the spectrophotometer. The reaction started immediately and a kinetics recording was initiated as soon as the lid of the spectrophotometer was closed (Figure 8).

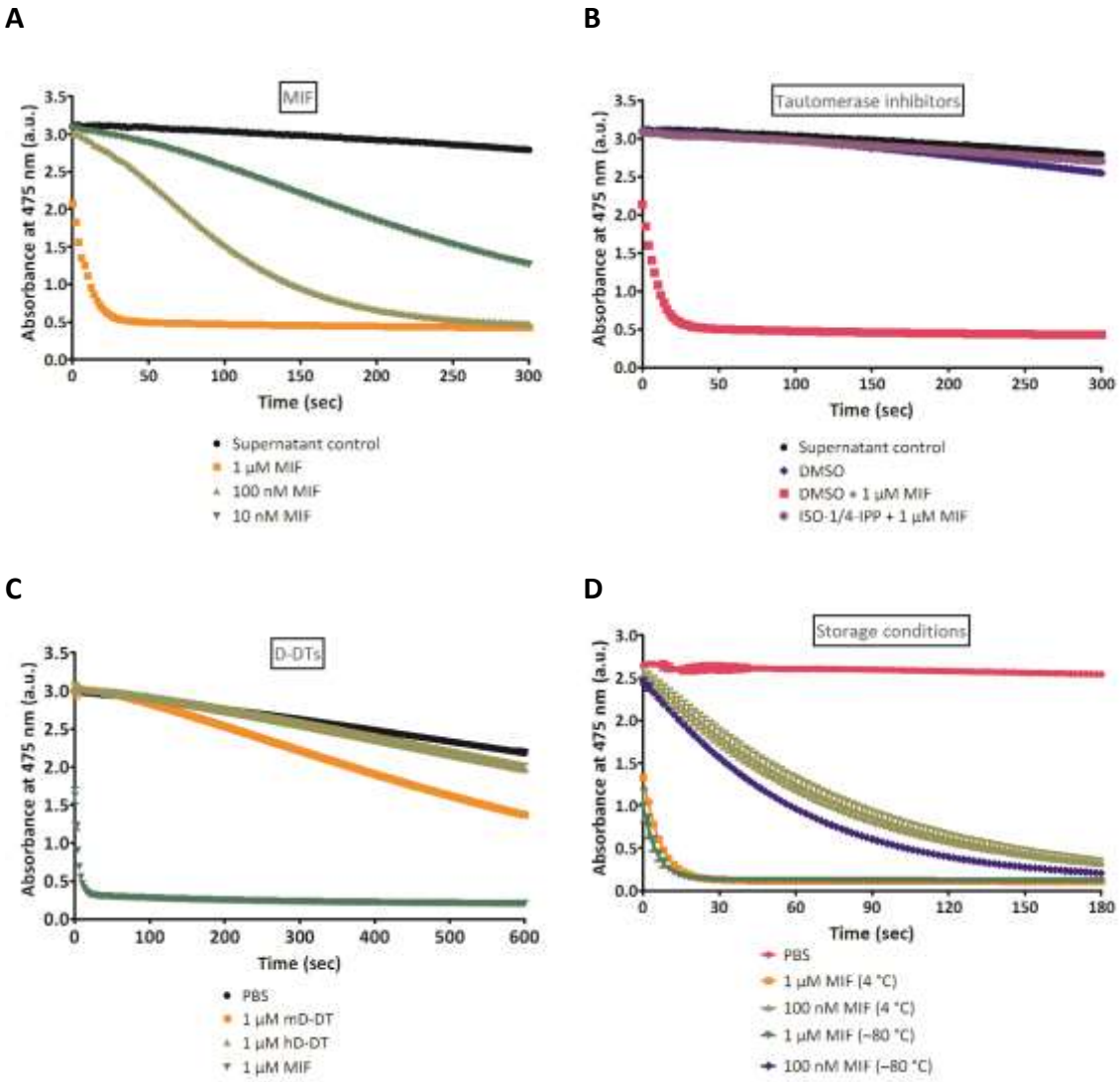

Figure 8. MIF but not D-DT tautomerises L-dopachrome methyl ester in a dose-dependent manner. Original kinetics traces of absorbance are shown over the course of (**C**) 600 sec (full-time experiment), (**A-B**) 300 sec and (**D**) 180 sec (shorter scale for better data visualisation). (**A-B**) Supernatants of COS-7/M6 cells were supplemented with increasing concentrations of MIF. The next day, 1 ml of supernatant was used for a spectrophotometric measurement of absorbance at 475 nm. MIF tautomerised L-dopachrome methyl ester into 5,6-dihydroxy-1-H-indole-2-carboxylic acid methyl ester. The graphs represent one (single) replicate (in order to avoid the use of too much recombinant protein in cell culture medium). (**A**) MIF tautomerises L-dopachrome methyl ester in a dose-dependent manner. (**B**) The tautomerisation reaction is sensitive to the inhibition of MIF's tautomerase activity by ISO-1 and 4-IPP. (**C**) Recombinant MIF, mD-DT and hD-DT were assayed for their tautomerase activity. The graph represents triplicate values of absorbance ± standard deviation. (**D**) Two samples of MIF, one stored at 4 °C and the other at – 80 °C, were assayed side-by-side for their tautomerase activity. The graph represents duplicate values of absorbance ± standard deviation. **Abbreviations**: **4-IPP**, 4-iodo-6-phenylpyrimidine; **ISO-1**, (*S,R*)-3-(4-hydroxyphenyl)-4,5-dihydro-5-isoxazole acetic acid.

Within the initial few seconds, 1 µM MIF tautomerised 50% of the substrate (Figure 8A). Moreover, 100 nM and 10 nM MIF tautomerise 50% of the substrate within 100 sec and 250 sec, respectively (based on raw absorbance data) (Figure 8A). While DMSO (solvent for ISO-1 and 4-IPP) did not affect the reaction, a combination of 50 µM ISO-1 and 50 µM 4-IPP abrogated the MIF-mediated tautomerase activity (Figure 8B).

Recombinant mD-DT exhibited a modest tautomerase activity since it tautomerised only 50% of the substrate at the end of the 600-sec experiment (Figure 8C). On the other hand, hD-DT had no measurable tautomerase activity (Figure 8C).

To complement results obtained with MIF incubated in cell-culture medium for 24 h (Figure 8A), purified MIF – stored either at 4 °C for a few months or directly retrieved from storage at – 80 °C – was used in PBS in the same tautomerase assay. One µM and 100 nM MIF tautomerised 50% of the substrate in a few seconds and approx. 40 sec, respectively (Figure 8D). Importantly, freezing did not negatively affect MIF's tautomerase activity. On the contrary, the tautomerase activity of the frozen protein was slightly higher (Figure 8D). For the following experiments (sections 5.3-5.4) MIF was stored at 4 °C.

Taken together, MIF is a stable protein as it exhibits its tautomerase activity in an ISO-1/4-IPP-sensitive manner both in cell-culture medium and in PBS, virtually irrespective of storage conditions. mD-DT has a modest whereas hD-DT has no tautomerase activity towards L-dopachrome methyl ester. In the subsequent experiments on cell migration, biologically active MIF was used for 3.5 h in DMEM since no detrimental effect on its activity could be expected.

5.3. The role of MIF receptors in cell motility

5.3.1. Generation of stable COS-7/M6 cell lines expressing CD44 and CD74

To address the questions if (*a*) MIF receptors are required for MIF-mediated motility and if (*b*) endocytosis of MIF mediates this effect, MIF receptor-negative WT COS-7/M6 cells (Shi *et al.*, 2006) were chosen to generate stable cell lines expressing the receptors. WT COS-7 cells are parental to WT COS-7/M6 cells but express CD44 i.e. they are $CD44^{+}/CD74^{-}$ (Shi *et al.*, 2006). WT COS-7/M6 cells do not express CD44/CD74 as shown in this thesis and elsewhere (Shi *et al.*, 2006).

The pTracer-CD44, pTracer-CD44$^{\Delta 67}$, and pcDNA-CD74 receptor-expression constructs also contained antibiotic-resistance genes – zeocin, zeocin, and geneticin, respectively. Moreover, CD74 protein was fused to a V5 epitope and His-tag. CD44 and CD44$^{\Delta 67}$ were not tagged but the zeocin-resistance gene within the backbone of each plasmid was fused with enhanced green fluorescence protein (EGFP) (section 4.1: Table 12 and maps).

Cells were seeded on 6-cm dishes, transfected with BglII-linearised pTracer or pcDNA constructs, and allowed to grow for a few weeks with decreasing antibiotic concentrations. Well-defined foci (5-6) were picked with trypsin-soaked paper filter disks and allowed to grow further in 6-well plates. The levels of CD44 and CD74 gene expression and protein production were assessed by PCR (Figure 9) and immunoblotting (Figure 10), respectively.

Using PCR primers (Table 11) amplifying non-tagged CD74 mRNA, CD74 mRNA was detected in one CD74^{+}, CD44^{+}/CD74^{+} and CD44$^{\Delta 67+}$/CD74^{+} clone, respectively, and in RAW264.7 macrophages (positive control) (Figure 9A). mRNA fragment specifically encoding V5 and His-tag was detected in two out of three CD74^{+} foci and in both CD44^{+}/CD74^{+} and CD44$^{\Delta 67+}$/CD74^{+} clones but not in the other ones (Figure 9B). While the presence of the V5 epitope and His-tag mRNA was useful in a PCR validation of CD74^{+} clones, the tags were not used in later experiments. Primers amplifying the V5 epitope and His-tag mRNA of CD74 show four positive clones (Figure 9B) but when compared to the non-tagged regions of CD74 amplicons, CD74^{+} F1 has a lower CD74 expression, reflecting differential primer efficiency. CD44 mRNA was detected in all CD44^{+} stable lines and in HeLa cells (positive control) (Figure 9C-D). Lowly-expressed CD44 mRNA was also found in parental, CD44-negative cells (Figure 9C-D). β-actin mRNA was detected in all mRNA preparations (loading control) (Figure 9E).

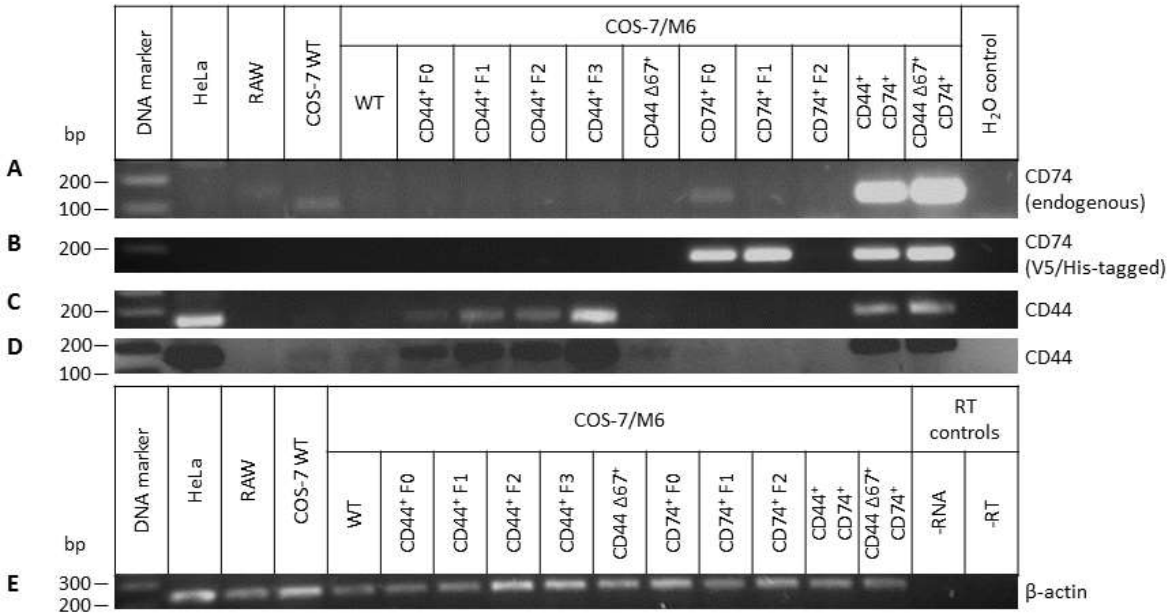

Figure 9. PCR analyses of stable COS-7/M6 cell lines expressing MIF receptors. RNA from indicated cells was isolated, reverse-transcribed, and specific gene fragments were amplified. Specific mRNA regions were amplified under conditions described in Materials and Methods with cognate primers, and resolved on 1.2% agarose gels. DNA was stained with ethidium bromide. (**A-D**) HeLa mRNA was used as a positive control for CD44 and RAW264.7 mRNA for CD74. (**A**) A 99-bp amplicon of exon 5 and 6 of the non-tagged CD74 mRNA. (**B**) A 194-bp non-intron-spanning amplicon of V5- and His-tag-encoding CD74 mRNA. (**C**) A 146-bp amplicon between exon 5 and 6 of the CD44 mRNA (encoding all variable v1-v10 splice variants). (**D**) An inversed and contrast-enhanced gel image of (**C**) is shown to better visualise low-intensity endogenous CD44 mRNA bands. (**E**) A 232-bp amplicon of β-actin mRNA.

CD74 was found in one out of three $CD74^+$ foci and in both $CD44^+/CD74^+$ and $CD44^{\Delta67+}/CD74^+$ clones (Figure 10B). β-actin was used as loading control (Figure 10C). Multiple antibodies were tested in CD44 immunoblots: (*a*) monoclonal antibody 23-32 (Margot Zöller); (*b*) Hermes-1 (Margot Zöller); (*c*) Hermes-3 (Margot Zöller), and (*d*) Santa Cruz sc-7297 (Shi *et al.*, 2006). Only Hermes-3 recognised CD44 (Figure 10A). CD44 protein was found in all $CD44^+$ lines. Faint, non-specific CD44 protein bands were also detected in CD44-negative cells upon closer inspection of the blots (Figure 10A). As $CD44^{\Delta67+}$ has a lower molecular weight than full-length CD44, a corresponding shift in size was observed for the single-transfectant (Figure 10A, lane $CD44^{\Delta67+}$) but not the double-transfectant (Figure 10A, lane $CD44^{\Delta67+}/CD74^+$), possibly due to differential protein processing.

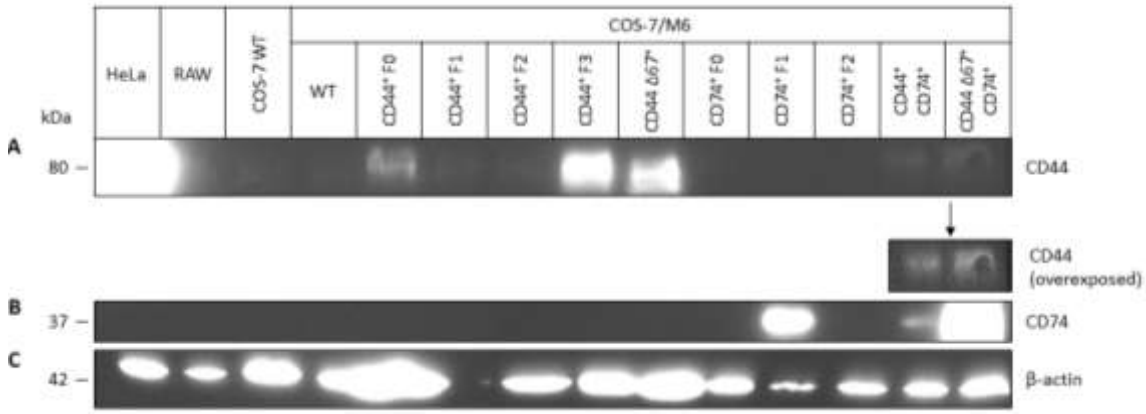

Figure 10. Immunoblot analysis of stable COS-7/M6 cell lines expressing MIF receptors. Protein lysates were resolved on two polyacrylamide gels, and transferred onto nitrocellulose membranes. The membranes were probed with antibodies against (**A**) CD44 (full-length as well as truncated $CD44^{\Delta67}$) (Hermes-3), (**B**) CD74 (FL-296), and (**C**) β-actin, then washed, and probed with HRP-conjugated secondary antibodies. After washing, the HRP signal was detected using ECL. HeLa and RAW264.7 whole protein extracts were used as positive controls for CD44 and CD74, respectively. COS-7 is COS-7/M6's parental cell line. Insert in **A** depicts the chemiluminescence signal with increased contrast to better visualise low levels of CD44.

To summarise, Table 17 lists all generated cell lines and the patterns of CD44 and CD74 gene and protein expression.

Table 17. Levels of mRNA expression and protein production in WT and stable COS-7/M6 cells.

COS-7/M6 cell line	**CD44**		**CD74**	
	mRNA	**Protein**	**mRNA**	**Protein**
WT	–/+	–/+	–	–
$CD44^{+}$ F0	+++	+	–	–
$CD44^{+}$ F1	+++	–	–	–
$CD44^{+}$ F2	+++	–	–	–
$CD44^{+}$ F3	+++	++	–	–
$CD44^{\Delta 67+}$	–/+	+	–	–
$CD74^{+}$ F0	–/+	–	++	–
$CD74^{+}$ F1	–/+	–	+	++
$CD74^{+}$ F2	–/+	–	–	–
$CD44^{+}/CD74^{+}$	+++	+	+++	+
$CD44^{\Delta 67+}/CD74^{+}$	+++	+	+++	+++

Abbreviations and signs: F, focus; **–** lack of mRNA/protein; **–/+** background; **+, ++ and +++** slight to strong mRNA/protein.

The pTracer construct encoding CD44 protein contained EGFP protein-coding DNA fused to the zeocin-resistance DNA (section 4.1: Table 12 and maps). Because EGFP was not fused to the insert (CD44), the EGFP signal marks the stability of transfection and not the cellular localisation of CD44 (Figure 11). The levels of EGFP were visualised by fluorescence microscopy in WT and $CD44^+/CD74^+$ COS-7/M6 cells. Whereas there was no measurable EGFP signal in WT cells (Figure 11C), almost every cell was EGFP-positive in $CD44^+/CD74^+$ COS-7/M6 cells (Figure 11D). For the duration of image acquisition, the phenol red-containing DMEM was exchanged for PBS to avoid phenol red-derived autofluorescence.

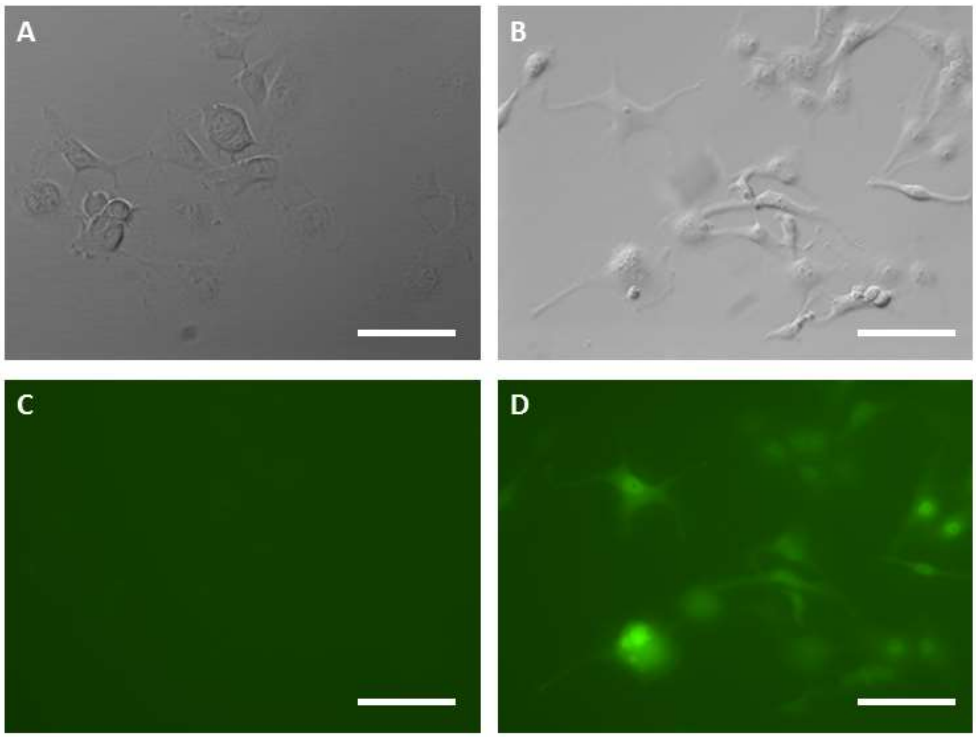

Figure 11. EGFP levels in WT and $CD44^+/CD74^+$ COS-7/M6 cells visualised by fluorescence microscopy. (**A and C**) WT and (**B and D**) $CD44^+/CD74^+$ COS-7/M6 cells were seeded in tissue-culture flasks and grown to 50% confluency. Medium was exchanged for PBS to avoid autofluorescence, and the cells were observed under phase-contrast (**A and B**) and with the EGFP channel (**C and D**) for 50 sec. The bar is 100 µm.

Considering that MIF triggers extracellular signal-regulated kinase 1/2 (ERK1/2) phosphorylation via CD74 and CD44/CD74, the functionality of the introduced receptors was evaluated. Therefore the levels of total as well as phosphorylated ERK1/2 were evaluated by immunoblotting with antibodies recognising (*a*) total ERK1/2 (Figure 12B, D, F) and (*b*) Thr-202/Tyr-204- and Thr-185/Tyr-187phosphorylated ERK1/2 (Figure 12A, C, E) in MIF-treated cell lysates. MIF upregulated ERK1/2 phosphorylation in MIF receptor-positive $CD74^+$ COS-7/M6 and $CD44^+/CD74^+$ COS-7/M6 cells after a 30-minute stimulation but not in MIF receptor-negative WT COS-7/M6 cells (Figure 12, MIF 30 min vs. boiled MIF). This result validates the observations from the original investigation on COS-7/M6 cells (Shi *et al.*, 2006). In sum, MIF stimulation enhances the ratio of phosphorylated-to-total ERK1/2 when compared to heat-inactivated MIF treatment, showing the functionality of the receptors ($CD74^+$ and CD44+/$CD74^+$) (Figure 12G).

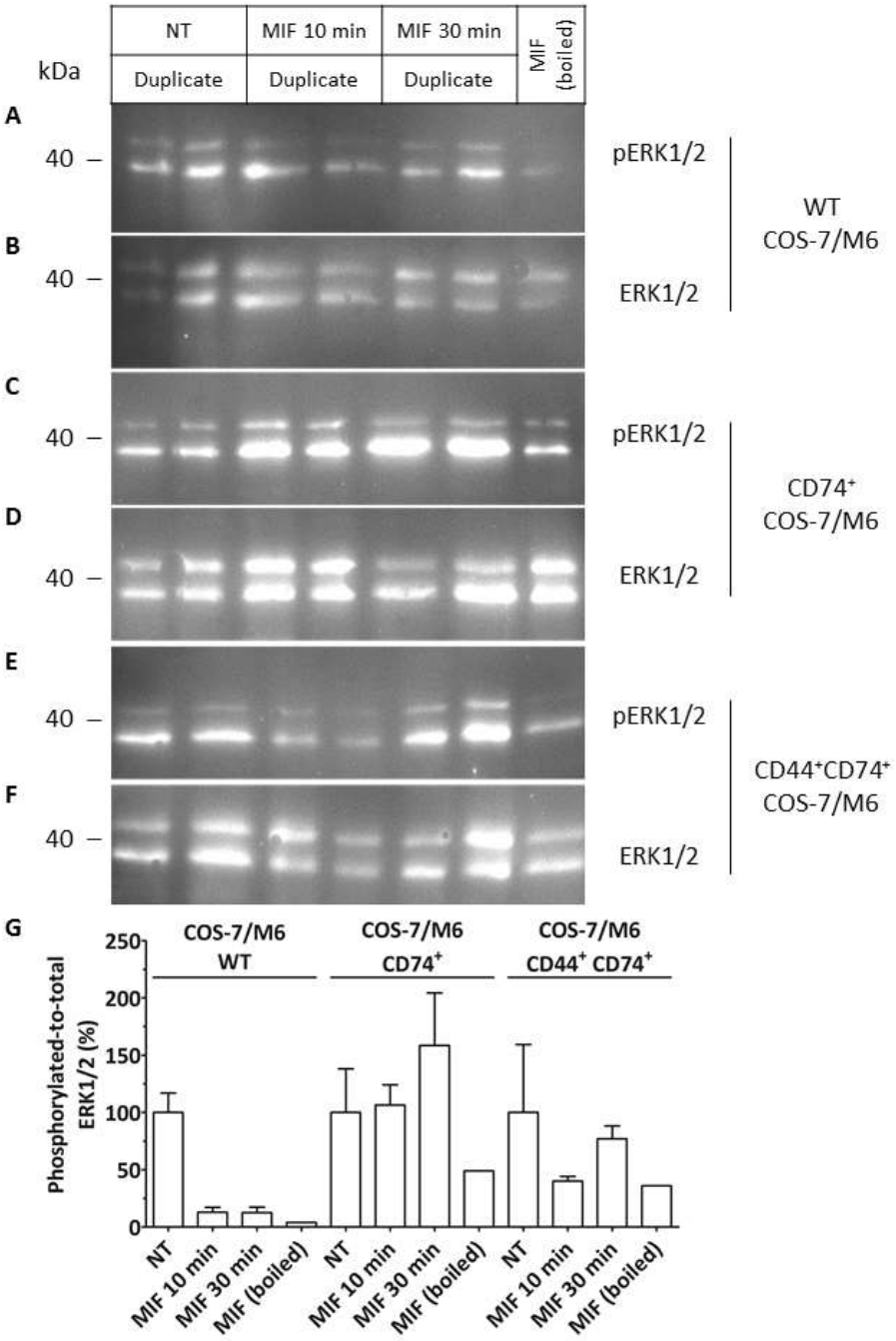

Figure 12. Analysis of MIF-mediated ERK1/2 phosphorylation in COS-7/M6 cells. Immunoblot analyses of (**A, C, E**) phosphorylated and (**B, D, F**) total ERK1/2 in lysates from MIF-treated WT, CD74$^+$, and CD44$^+$/CD74$^+$ COS-7/M6 cells. Proteins (15 µg) were resolved on one large-scale polyacrylamide gel and transferred onto a nitrocellulose membrane. The membrane was blocked in 5% BSA, probed with antibodies against phosphorylated ERK1/2, washed, and probed with HRP-conjugated secondary antibodies. After washing, the HRP signal was detected using ECL. The membrane was stripped (section 4.2.1.6) and re-probed against total ERK1/2. All ECL images were slightly contrast-enhanced using the FusionCapt Advance software to better visualise lowly-expressed protein bands. For clarity the ECL images were cropped to show ERK1/2 bands only. (**G**) Quantification of pERK1/2-to-totalERK1/2. Pixel values (area under peak in ImageJ) for each lower band were normalised towards NT (100%). Error bars are derived from duplicates (NT, MIF 10 min, MIF 30 min).

5.3.2. Wound healing (scratch) assays are not suitable to study COS-7/M6 cell motility

Wound healing (scratch) assays were initially chosen to address the role of MIF receptors in cell motility. In each assay, cells are seeded on a collagen-coated surface and allowed to attach such that they form a confluent monolayer. Cells are seeded in µ-Slides (ibidi), a microscopy-compatible chamber allowing to study cell behaviour under eight distinct conditions at a time. Next, a wound (scratch) is created with a pipette tip, and cell migration is monitored over time either in an automated time-lapse fashion (live-cell imaging in a humidified chamber) or by taking individual photographs (cells are manually taken out of the incubator, observed, and returned to the incubator) at a known position within the wound (section 4.2.4.4).

First, experiments were performed on monolayers of cells seeded in 35-mm dishes. To measure the expected wound width and wound closure time, three different pipette tips were used to create a wound (width ± SEM; time to close): p10 (187 ± 32 µm; 2.9 h); p200 (312 ± 38 µm; 15.3 h); and p1000 (430 ± 39 µm; only 90% closed overnight). Because a 300-µm wide wound can be easily observed under a 200X magnification, and the acquisition time of 15-20 h (overnight) is best to identify differences between stimulations, the p200 tip was chosen as optimal to create a wound in a monolayer grown in a µ-Slide.

However, within µ-Slides all pipette tips (p10, p200) removed many more cells than the width of the tip. Unlike in 35-mm dishes, the two cell fronts were not fully visible on µ-Slides in the field of view (20X objective; 200X total magnification). Visibility of the two cell fronts was required to determine cell motility as well as wound closure (Figure 13 depicts a rare example of two cell fronts visible within one field of view). Taken together, the wound width could not be controlled in a reproducible manner.

Furthermore, because of the confluency of the monolayers, the cells were frequently washed off at the edges of each well, causing stress to the remaining cells and leaving behind not enough cells for analysis. Cells which did remain attached to the well often rounded up – a phenomenon indicative of cell death upon stress. As data acquisition was limited to the duration of the overnight time-lapse experiment, it was challenging to

measure when the wound closed up entirely. Because the width of each wound always differed considerably, some gaps never closed. To be more precise, the two cell fronts more than 500-700 µm apart would never meet even after 2-3 days of observation whereas the two cell fronts 200-300 µm apart would close the gap in a few hours (Figure 14C).

As the two cell fronts approach one another, a cellular bridge would be formed between two fronts by some fast-moving cells (Figure 13) (Green *et al.*, 2004). Only then the remaining cells would close up the wound. A similar phenomenon was observed with COS-7/M6 cells, making it difficult to unambiguously measure cell velocity across the wound edge.

Even though wound healing assays provide easy imaging and relatively simple analysis, the abovementioned challenges prevented proper data analysis. A major disadvantage was that collagen appeared to be removed mechanically from the surface once a wound was made. Sometimes only one cell front migrated to close the wound while the other would not, possibly due to the removal of the substrate. Overall, data analysis was considerably hindered by these problems.

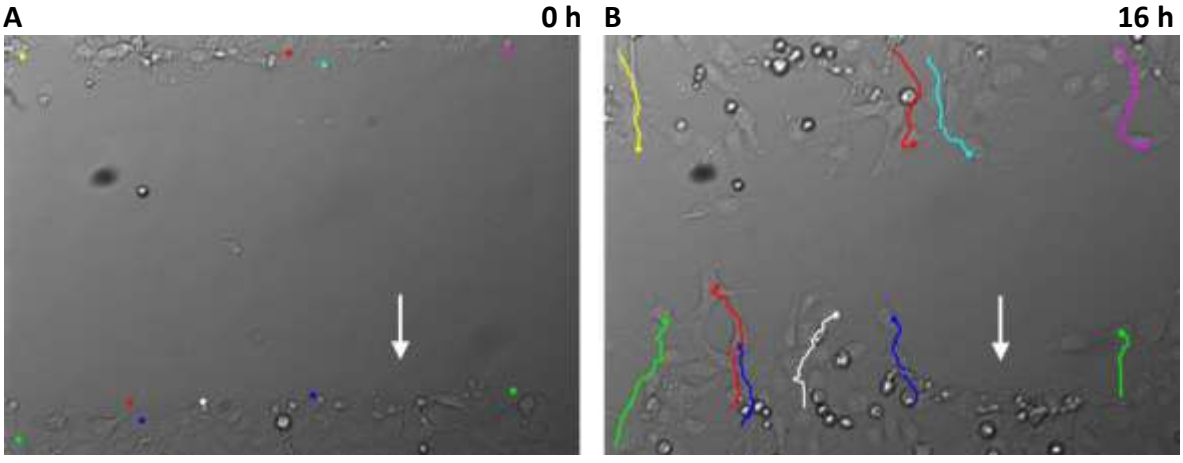

Figure 13. The pattern of WT COS-7/M6 cell migration in wound healing (scratch) assays. Cells were seeded at 100% confluency (**A**) and imaged under a phase-contrast microscope for 16 h (**B**). Some cells did not migrate over the course of the experiment (white arrows, **A** vs. **B**) possibly because they were too confluent or undergoing cell death (**B**, round cells). Motile cells were tracked (dots in **A** representing the initial coordinates of unique cells) over time (trajectories in colour, **B**). However, the migration was often halted at a certain stage, possibly because of the removal of the substrate.

For these reasons, wound healing assays were next performed in multi-well plates over the course of 9 h. One advantage over µ-Slides was that the cells were no longer washed out, probably due to a larger surface area (9.62 cm^2 vs. 1 cm^2). Still the wound was never of the same width even when the lid of a multi-well plate was used as a ruler to help to move the tip across a monolayer of cells in a straight way. Because larger wounds failed to close up, a normalisation step to the narrowest wound was included in the final assessment of wound closure (Figure 14). Instead of calculating cell velocity, total wound surface area was measured in pixels and then converted to μm^2 and normalised to the smallest wound. This normalisation step involved calculating the difference between the narrowest wound and all the other ones, and that difference was subtracted from all wound surface areas. The final data are reported as % of control (Figure 14A-B).

Similar to experiments with µ-Slides, a great variability of wound widths was noted within multi-well plates even when using a single tip for all wounds. For example, four wounds created with a p10 tip had the following widths (in thousand pixels): 662; 864; 639; and 754 such that the difference between the narrowest and widest wound was approx. 30%. As a result, cells encompassing a narrow gap closed it up in a matter of few hours whereas wide wounds did not close within 9 h (Figure 14C). Recombinant epidermal growth factor (EGF) and insulin-like growth factor (IGF)-I (100 ng/ml each, Figure 14) were tested as positive controls, but none of them consistently showed upregulation of cell motility. Recombinant MIF/D-DT (100 ng/ml) failed to alter cell motility regardless of MIF receptor status (Figure 14). The two graphs in Figure 14 represent one out of three replicates; each replicate greatly differed from one another in the response to the growth factors – once non-treated (NT) cells were the fastest in closing the wound in a matter of 6-9 h, another time NT cells were the slowest.

Double-transfected $CD44^+/CD74^+$ COS-7/M6 cells were much slower than WT COS-/M6 cells, possibly due to the fact that CD44 mediates strong cell-cell adhesion, particularly important during multi-cellular mode of migration (Figure 14A-B).

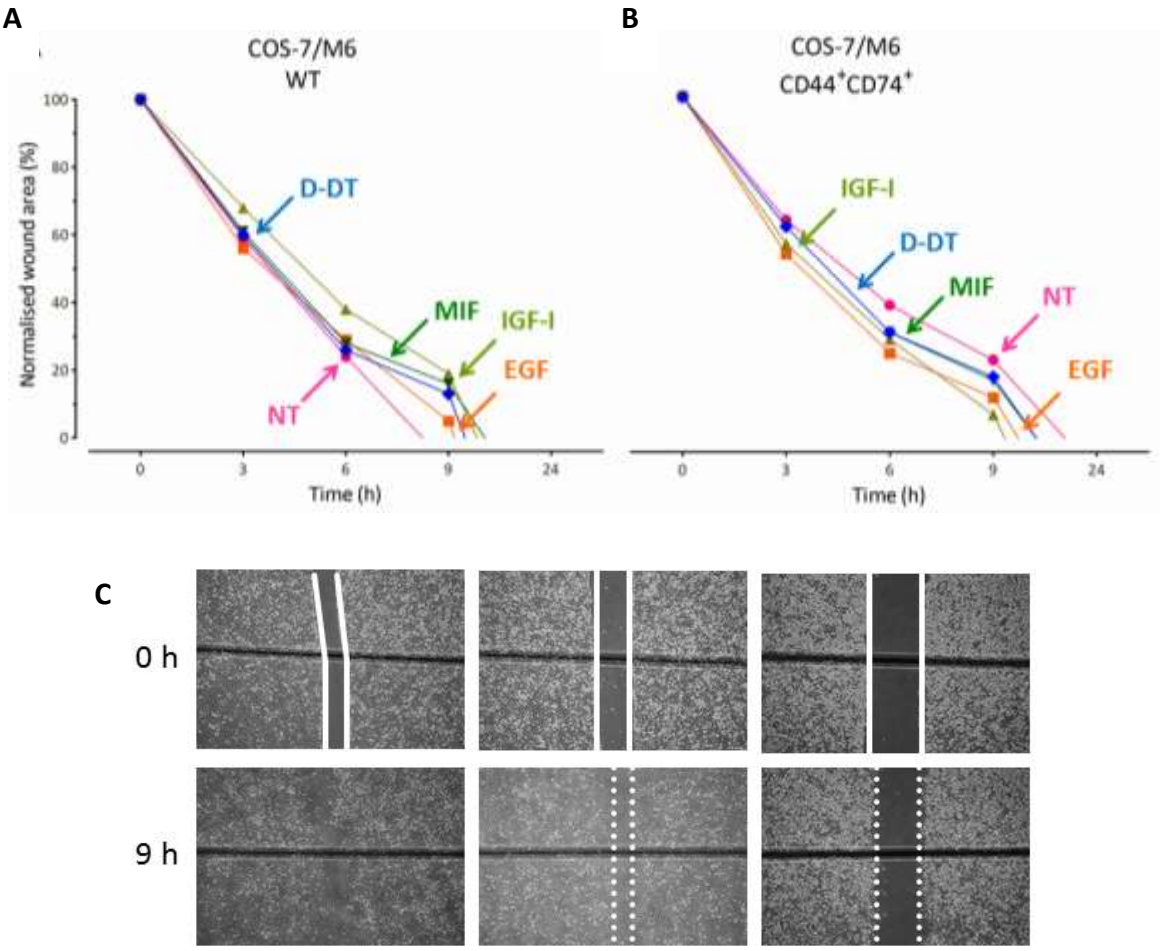

Figure 14. Analysis of COS-7/M6 wound healing in multi-well plates. (**A**) WT and (**B**) $CD44^+/CD74^+$ COS-7/M6 cells were seeded at 100% confluency and allowed to adhere. Upon medium exchange from 10% to 0.5% (v/v) FCS supplemented with indicated recombinant proteins, the first photograph was taken (time 0 h). A photograph of the wound was taken at indicated times (0,3, 6, 9, and 24 h). Wound area was normalised to the narrowest wound due to the varying wound widths (**C**). Experiments were repeated three times for each cell line (n = 3). (**C**) An example of a 9-h time point (40X magnification): a narrow wound (*left*) closed entirely; an intermediate-size wound closed by half (*middle*); cells within a wide wound (*right*) did not migrate. The line across each photograph (left-right) was made with a scalpel on the bottom of each plate to be able to take the photograph always at the same position.

Taken together, the wound healing assays were inconclusive. First, the positive controls – recombinant growth factors – failed to induce cell motility to an extent that has been published before (Knapek *et al.*, 2010). Second, subsequent chemokinesis experiments showed that EGF is indeed a robust and reproducible inducer of fibroblast motility. Only

one wound-healing result was reproducible: WT COS-7/M6 cells exhibited much faster migration than $CD44^+/CD74^+$ COS-7/M6 cells.

5.3.3. COS-7/M6 chemokinesis (random single-cell motility)

5.3.3.1. Chemokinesis assays are suitable to study motility of COS-7/M6 cells

In search for a reproducible motility assay, chemokinesis (random single-cell motility) assays were tested. Briefly, cells were seeded at a low confluency in µ-Slides, allowed to attach for a few hours, and stimulated with recombinant MIF/D-DT/EGF with or without endocytosis inhibitors or MIF's tautomerase inhibitors. Images were taken at 30-min intervals over 3.5 h and data of cell trajectories were expressed as velocities (section 4.2.4.5).

Preliminary chemokinesis experiments were performed in order to estimate the effects of recombinant proteins on fibroblast motility, and to verify the normality of velocity data, using a variety of cell lines:

- WT COS-7 cells,
- WT COS-7/M6 cells,
- stable $CD44^+$ COS-7/M6 cells, and
- stable $CD44^+/CD74^+$ COS-7/M6 cells.

Recombinant proteins were added in serum-reduced medium to diminish the amount of endogenous growth factors influencing motility.

All above-mentioned cell lines significantly responded to 100 ng/ml EGF as a stimulator of motility. All but $CD44^+$ COS-7/M6 cells were observed to respond to 100 ng/ml MIF. Ten percent (v/v) FCS was used (*a*) to examine cell morphology and (*b*) to estimate what maximal cell velocity can be expected under standard conditions. Under DMEM/10% (v/v) FCS, no abnormalities in cell morphology were found using phase-contrast microscopy, suggesting that the cells stayed healthy throughout the experiment. Furthermore, it was established that endocytosis and tautomerase inhibitors were to be used 1 h before the addition of the recombinant proteins instead of simultaneously with them (data not shown).

At the same time, the normality of chemokinesis data was assessed. The visual distribution of velocity data resembled a non-Gaussian distribution. This was further confirmed by q-q plots (R Project) (section 4.2.6.1).

All chemokinesis experiments that follow were performed in triplicate such that cells from three subsequent passages were seeded in three distinct µ-Slides on different days. All data were analysed by Kruskal-Walllis one-way analysis of variance (ANOVA) with Dunn's multiple comparison test as a post test (significance level set to $\alpha = 0.05$).

In these assays, recombinant proteins (EGF, MIF, MIF mutants, D-DT) and an array of pharmacological inhibitors (endocytosis and tautomerase activity inhibitors) were tested for their capacity to alter basal and MIF-induced cell migration (Figures 15-22). Following cell attachment, the medium was exchanged from DMEM/10% (v/v) FCS to DMEM/0.5% (v/v) FCS, and supplemented with recombinant proteins. In line with the preliminary experiments, pharmacological inhibitors of endocytosis and MIF's tautomerase activity were added 1 h prior to the supplementation with recombinant proteins, and the cells were live-imaged for 3.5 h (section 4.2.4.5).

5.3.3.2. MIF but not D-DT upregulates chemokinesis independent of CD44/CD74

Previous experiments established to what extent MIF and EGF stimulate motility in a reproducible manner. Therefore recombinant MIF, D-DT, a combination of MIF and D-DT, and their heat-inactivated counterparts were used at 200 ng/ml in three independent experiments to verify how both members of the MIF family alter chemokinesis (Alampour-Rajabi *et al.*, 2015) (Figure 15). Such a side-by-side comparison of MIF/D-DT receptor-negative and -positive COS-7/M6 cells allowed to address the question if MIF/D-DT receptors CD44/CD74 are required for MIF-mediated upregulation of fibroblast chemokinesis.

The data distribution in Figure 15 is depicted as a boxplot (25th-75th percentile) with whiskers (10th-90th percentile), the arithmetic mean (a plus sign), and the median (a line in the middle of the box). Such a representation allows to appreciate the fact that some cells are virtually non-motile (outliers shown as dots below the boxplots within the 0.00-

0.05 µm/min range) whereas another population is highly motile (outliers shown as dots above the boxplots, from 0.50 µm/min) (Figure 15).

Recombinant EGF (200 ng/ml, same as MIF/D-DT) served as a *bona fide* stimulator of cell motility (Figure 15). In $CD44^+/CD74^+$ COS-7/M6 cells, MIF and EGF stimulated motility to the same extent (Figure 15B and Appendix 1), whereas in WT COS-7/M6 cells MIF stimulated motility to a lesser extent than EGF (Figure 15A and Appendix 1).

MIF enhanced WT COS-7/M6 chemokinesis in a significant way (Figure 15A) when compared to the non-treated control as well as when compared to its heat-inactivated control (Figure 15A). The combination of MIF/D-DT upregulated motility of both cell lines as compared to the non-treated cells (Figure 15A-B); as compared to heat-inactivated MIF/D-DT, it was only significant in $CD44^+/CD74^+$ COS-7/M6 cells.

While recombinant human MIF promoted COS-7/M6 cell motility independent of the MIF receptor status (Figure 15A), recombinant human D-DT promoted only $CD44^+/CD74^+$ COS-7/M6 cell motility (Figure 15B). Heat-inactivated proteins (MIF, D-DT, and MIF/D-DT) did not induce motility in either cell line (Figure 15). While there was a non-significant trend towards D-DT induced chemokinesis in WT COS-7/M6 cells as compared to non-treated cells (Figure 15A), heat-inactivated D-DT vs. D-DT was insignificant (Figure 15A).

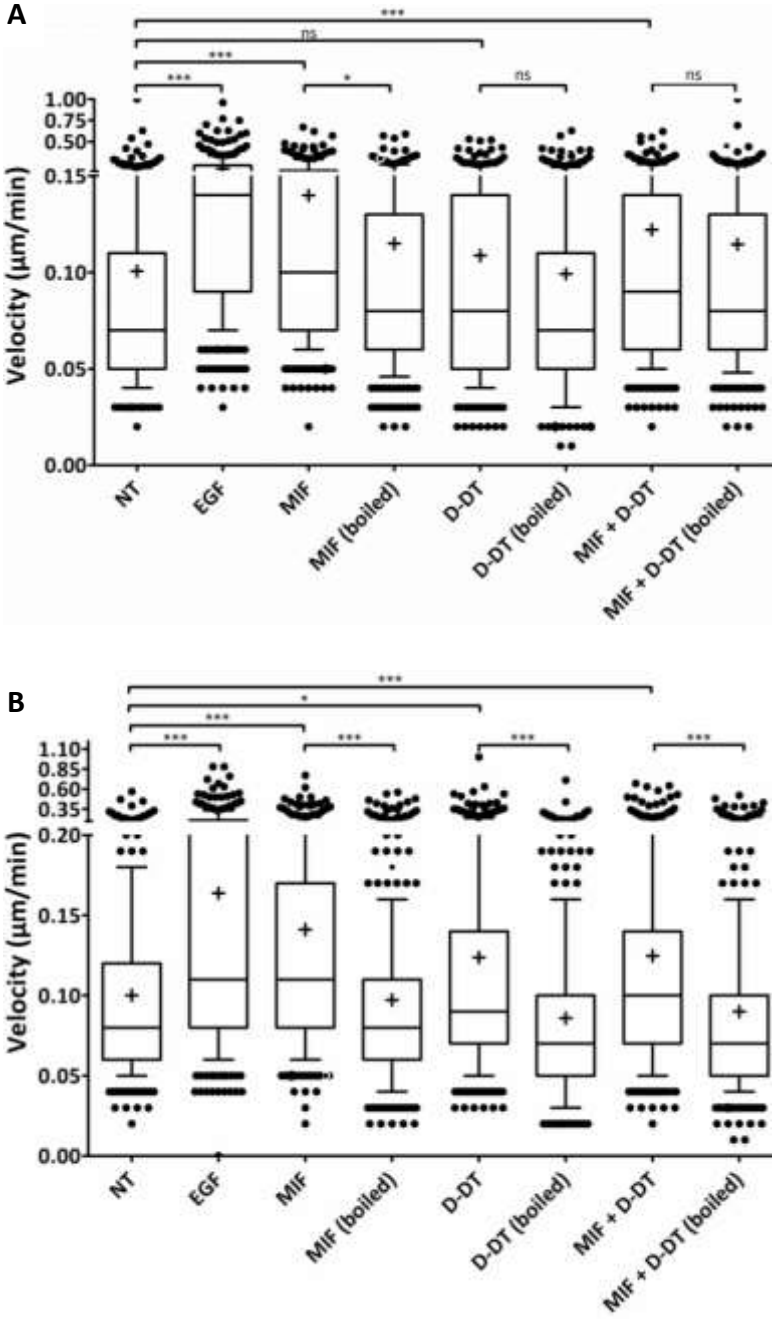

Figure 15. MIF upregulates chemokinesis independent of MIF receptors whereas D-DT requires the presence of receptors. MIF and D-DT were added at 200 ng/ml hereafter. EGF (100 ng/ml) was used as a positive control. (**A**) WT and (**B**) $CD44^+/CD74^+$ COS-7/M6 cells were seeded at 13,000 cell/cm^2 in eight-well µ-Slides and allowed to attach in 10% (v/v) FCS-containing DMEM. Subsequently medium was exchanged for 0.5% (v/v) FCS/DMEM with or without the compounds of interest. The µ-Slide was mounted in a live-cell imaging chamber (humidified atmosphere, 37 °C, 5% CO_2) at a Nikon *Ti* microscope stage and time-lapse phase-contrast microscopy was performed over the course of 3.5 h with 30-min intervals. Velocity data from three independent wells (replicates) (approx. 300 cells from 30 fields of view) were pooled from each experimental round, and a Kruskal-Walllis one-way analysis of variance (ANOVA) was performed. Data are shown as boxplots composed of a box (25th-75th percentile), a plus sign (arithmetic mean), a line in the middle of the box (median), whiskers (10th-90th percentile), and dots (outliers). **Significance levels**: **ns**, non-significant ($p > 0.05$); *, $p \leq 0.05$; **, $p \leq 0.01$; ***, $p \leq 0.001$.

5.3.3.3.ISO-1 and 4-IPP abrogate MIF-triggered chemokinesis of WT COS-7/M6 cells

Knowing that the inhibition of MIF's enzymatic activity may interfere with MIF-mediated migration and invasion, specific inhibitors of MIF's tautomerase activity, ISO-1 and 4-IPP, were used at maximal non-toxic concentrations established elsewhere (Winner *et al.*, 2008). But ISO-1 and 4-IPP inhibited MIF-induced cell motility only to a minimal extent (Figure 16A-B, MIF + DMSO vs. MIF + ISO-1 and MIF + DMSO vs. MIF + 4-IPP) because their solvent, DMSO, had a strong inhibitory effect on its own (Figure 16 and Appendix 1). However, ISO-1 appeared to inhibit MIF-driven chemokinesis in WT COS-7/M6 cells (Figure 16A) and 4-IPP – in $CD44^+/CD74^+$ COS-7/M6 cells (Figure 16B).

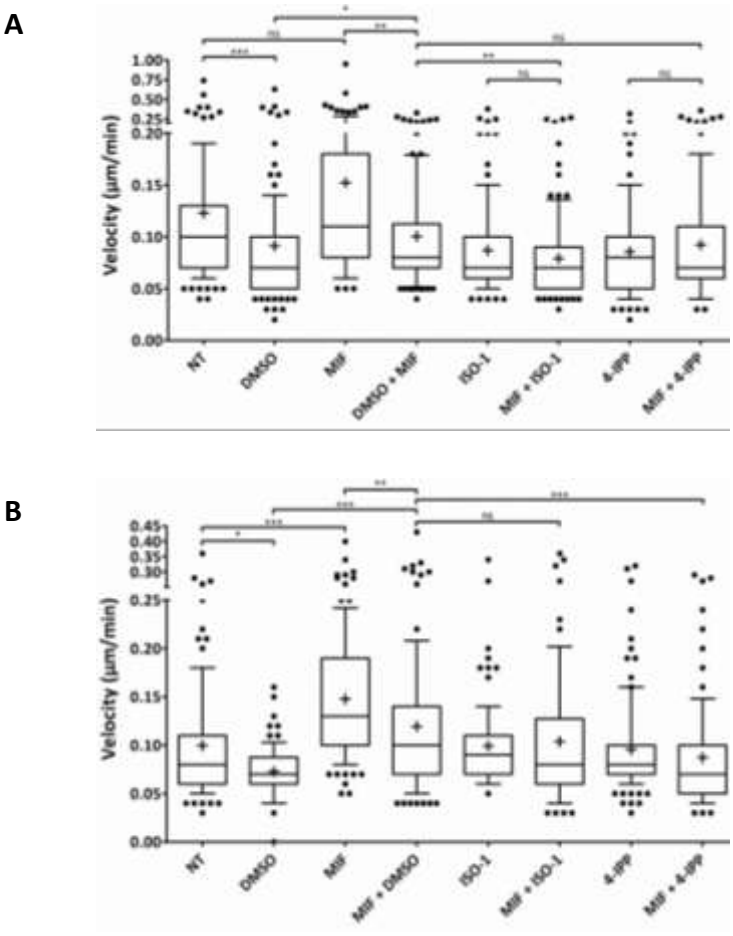

Figure 16. ISO-1 and 4-IPP dissolved in DMSO moderately inhibit MIF-triggered chemokinesis due to the inhibitory effect of DMSO. ISO-1 and 4-IPP were added at 100 µM. DMSO was at 0.5% (v/v) not only in DMSO-only but also ISO-1- and 4-IPP-containing wells. (**A**) WT and (**B**) $CD44^+/CD74^+$ COS-7/M6 cells were seeded in µ-Slides and imaged as described in Figure 15, with one exception: the data represents only one replicate. **Abbreviations**: **4-IPP**, 4-iodo-6-phenylpyrimidine; **ISO-1**, (*S,R*)-3-(4-hydroxyphenyl)-4,5-dihydro-5-isoxazole acetic acid (ISO-1). **Significance levels**: **ns**, non-significant ($p > 0.05$); *, $p \leq 0.05$; **, $p \leq 0.01$; ***, $p \leq 0.001$.

Prompted by the fact that DMSO exhibited an inhibitory effect on chemokinesis on its own, ethanol was tested as an alternative solvent for MIF's tautomerase inhibitors ISO-1 and 4-IPP. Because D-DT did not exhibit a measurable tautomerase activity (Figure 8C), only one cell line – WT COS-7/M6 – that was MIF-responsive but not D-DT-responsive was used here. Since ethanol altered neither basal nor MIF-induced chemokinesis, it was considered an appropriate solvent (Figure 17 and Appendix 1). Ultimately both ethanol-dissolved ISO-1 and 4-IPP abrogated MIF-stimulated motility of WT COS-7/M6 cells, leading to non-stimulated levels (Figure 17).

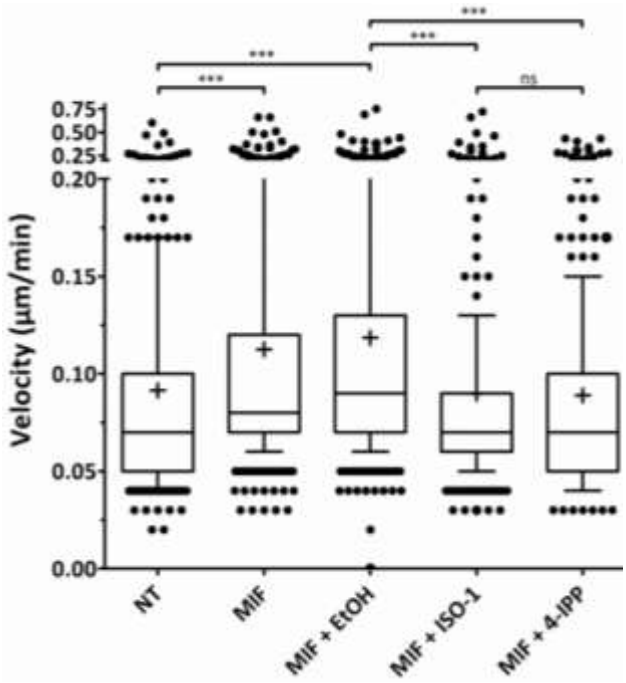

Figure 17. ISO-1 and 4-IPP dissolved in ethanol abrogate MIF-triggered chemokinesis of WT COS-7/M6 cells. ISO-1 and 4-IPP were added at 100 or 50 µM, respectively. Ethanol concentration was 0.1% (v/v) in treatments no. 3-5 (from left to right). The cells were seeded in µ-Slides, imaged, and analysed as described in Figure 15. Velocity data from three independent wells (replicates) (approx. 300 cells from 30 fields of view) were pooled from each experimental round, and a Kruskal-Walllis one-way analysis of variance (ANOVA) was performed. **Abbreviations**: **4-IPP**, 4-iodo-6-phenylpyrimidine; **EtOH**, ethanol; **ISO-1**, (*S,R*)-3-(4-hydroxyphenyl)-4,5-dihydro-5-isoxazole acetic acid (ISO-1). **Significance levels**: **ns**, non-significant ($p > 0.05$); *****, $p \leq 0.05$; ******, $p \leq 0.01$; *******, $p \leq 0.001$.

5.3.3.4. Full-length WT but not tautomerase-null MIF upregulates chemokinesis

To complement the result obtained with pharmacological MIF's tautomerase inhibitors, recombinant tautomerase-null MIF mutants – MIF P2A (Pro-2-to-Ala substitution) and Δ4 (deletion of the first four amino acids of the N-terminus) were employed. They both acted as dominant-negative proteins as they did not alter the motility of WT COS-7/M6 cells (Figure 18 and Appendix 1).

Taken together, the use of MIF's tautomerase inhibitors as well as tautomerase-null MIF mutants show that tautomerase activity is required for chemokinesis.

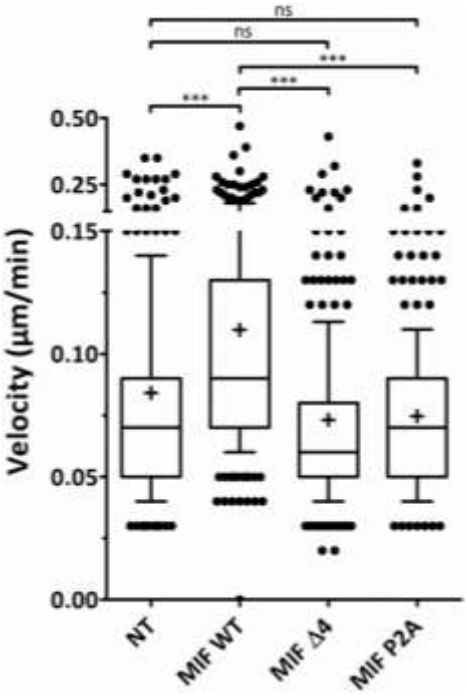

Figure 18. Full-length WT but not tautomerase-null MIF upregulates chemokinesis. WT COS-7/M6 cells were seeded in µ-Slides, imaged, and analysed as described in Figure 15. Velocity data from three independent wells (replicates) (approx. 300 cells from 30 fields of view) were pooled from each experimental round, and a Kruskal-Walllis one-way analysis of variance (ANOVA) was performed. **Abbreviations**: **P2A**, Pro-2-to-Ala substitution; **Δ4**, deletion of the first four amino acids of the N-terminus. **Significance levels**: **ns**, non-significant ($p > 0.05$); *, $p \leq 0.05$; **, $p \leq 0.01$; ***, $p \leq 0.001$.

5.3.3.5. Oxidoreductase-null MIF C60S is defective in upregulation of WT COS-7/M6 chemokinesis

To find out if MIF's oxidoreductase activity is also required to alter WT COS-7/M6 cell chemokinesis, oxidoreductase-null MIF C60S (Cys-60-to-Ser substitution) was used. Here, a few changes were incorporated into the protocol as compared to other experiments.

Recombinant MIF C60S is known to localise to inclusion bodies during bacterial expression (Kleemann *et al.*, 1998). Likewise, MIF C60S – particularly a highly concentrated stock thereof – tends to precipitate after thawing. Therefore MIF C60S – believed to have a concentration of 350 ng/µl following protein purification – was first centrifuged at the highest speed, the supernatant was transferred to a new microcentrifuge tube, and kept at room temperature. The protein concentration was measured on a semi-quantitative basis with an immunoblot using MIF WT as standard and estimated to be 23 ng/µl. Ultimately this approach ensured that the motility assays were performed with a fully reconstituted protein in solution. To that end, WT COS-7/M6 cells were seeded in one µ-Slide instead of three consecutive µ-Slides as in all other experiments. Three wells contained non-treated cells, three wells contained MIF C60S-treated cells, and two wells contained MIF WT-treated cells. Such an approach ensured that the appropriate protein amount (200 ng/ml) of soluble MIF C60S (Figure 19A) was added to all wells.

MIF C60S only slightly increased chemokinesis (Figure 19A and Appendix 1) but the significance level is merely below the threshold of 0.05. This result is corroborated by other experiments (Figure 19B) in which a stock of MIF C60S with a lower concentration (nominal protein concentration of 45 ng/µl following protein purification, and 11.7-17.8 ng/µl when measured on two spectrophotometers after thawing) did not alter chemokinesis at a final concentration of 200 ng/ml in a significant way (Figure 19B, *low*), and neither did MIF C60S re-solubilised at 37 °C (the protein was kept in a cell-culture incubator until it was fully re-solubilised) or on ice (the protein was kept on ice until it was fully re-solubilised) (Figure 19B, *37 °C* and *ice*). Overall, oxidoreductase-null MIF C60S is defective in upregulation of WT COS-7/M6 chemokinesis.

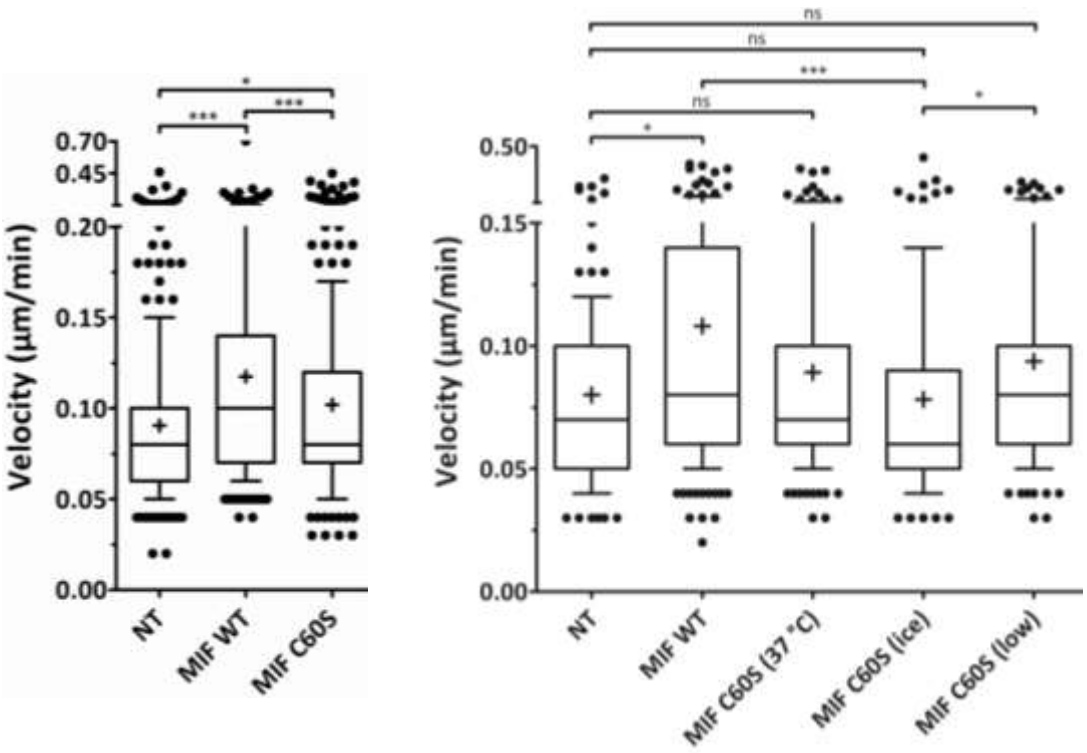

Figure 19. Oxidoreductase-null MIF C60S is defective in upregulating WT COS-7/M6 chemokinesis. (**A-B**) The cells were seeded in µ-Slides, treated with 200 ng/ml MIF WT or C60S, imaged, and analysed as described in Figure 15. (**A**) The concentration of MIF C60S was estimated by immunoblot, with MIF WT as reference. (**B**) The concentration of MIF C60S was determined (section 4.2.1.2) after re-solubilisation at given conditions (see text for details of re-solubilisation). Here one experimental round was performed – in one µ-Slide there were two (for NT) and three wells (for recombinant proteins) to ensure that the appropriate protein amount was added to the cells. **Significance levels**: **ns**, non-significant ($p > 0.05$); *****, $p \leq 0.05$; ******, $p \leq 0.01$; *******, $p \leq 0.001$.

5.3.3.6. MIF-triggered chemokinesis appears to rely on lipid raft/caveolae- and not clathrin-mediated endocytosis

Extracellular cargo – including growth factors and cytokines – is known to be internalised by a plethora of mechanisms (Figure 2 and Wieffer *et al.*, 2009):

- receptor-independent endocytosis,
- receptor-dependent endocytosis (Figure 3D for MIF),
- clathrin-mediated endocytosis (CME),
- non-clathrin-mediated endocytosis (non-CME, or caveloae-dependent),
- non-clathrin-mediated (non-CME) and caveloae-independent but lipid raft-dependent endocytosis.

MIF has been hitherto described to be endocytosed in MEFs (Schwartz *et al.*, 2012) as well as in RAW264.7 macrophages (Xie *et al.*, 2011) in a clathrin- and CD74-dependent but caveolae-independent manner, although no data exist on MIF internalisation in fibroblasts.

Given that MIF does not require its receptors to stimulate motility of MIF receptor-negative COS-7/M6 cells (Figure 15), the hypothesis was tested that MIF endocytosis – specifically non-CME endocytosis – contributes to the observed effects. Once released from a vesicle via the so-called endosomal escape mechanism, internalised MIF could potentially act within the cytoplasm in order to alter motility.

Prior to the assessment of the effect of endocytosis inhibition on MIF-mediated chemokinesis, titration of four pharmacological inhibitors was performed. COS-7/M6 cells were grown to 50% confluency and treated with inhibitors at a wide range of concentrations (Table 18). The toxic dose was defined as the concentration that led to the detachment of all cells upon stimulation with each inhibitor, and was assessed under a phase-contrast microscope for up to 3.5 h (Table 18). In fact, 100% cell detachment was observed within the first 10-30 minutes. Concentrations chosen for the assays closely resemble the concentrations used in earlier studies (Table 18).

Table 18. **Evaluation endocytosis inhibitor cell toxicity.**

	Chlorpromazine (CPZ)	Dynasore (DYN)	Nystatin (NYS)	Filipin (FIL)
Stock	50 mM in water	10 mM in DMSO	5.4 mM in DMSO	7.6 mM in DMSO
Inhibitor target	CME	CME and non-CME	Non-CME	Non-CME
Tested doses	100 pM; 1; 10; 100 nM; 1; 10; 50 µM	0.1; 1; 10; 15; 50 µM	0.108; 1.08; 10.8; 27; 54 and 108 µM	0.03; 0.06; 0.15; 0.3; 0.75; 1.5; 3; 7.5 µM
Toxic dose(s)	50 µM	No detachment observed	54 and 108 µM	3 and 7.5 µM
Dose used	10 µM	50 µM	27 µM	1.5 µM
Previously used doses (reference)	14 µM for MIF in RAW294.7 cells (Xie *et al.*, 2011); 50 µM (Schwartz *et al.*, 2012)	80 µM (IC_{50} = 15 µM) for transferrin in COS-7 cells (Kirchhausen *et al.*, 2008); 80 µM for MIF in HEK293 cells (Schwartz *et al.*, 2012)	54 µM for MIF in HEK293 cells (Schwartz *et al.*, 2012)	5 µM for MIF in RAW294.7 cells (Xie *et al.*, 2011); 7.7 µM for MIF in HEK293 cells (Schwartz *et al.*, 2012)

At toxic dose(s) all WT COS-7/M6 cells detached in 10-30 minutes. **Abbreviations**: **CME**, clathrin-mediated endocytosis.

The mechanism of action varies between the four drugs (Macia *et al.*, 2006; Ivanov, 2008). Chlorpromazine is known to inhibit clathrin-mediated endocytosis (CME) by lowering clathrin and adaptor protein complex 2 (AP2) levels at the cell surface. Dynasore (DYN) binds dynamin and therefore inhibits both clathrin-mediated endocytosis (CME) and non-CME (caveolae-mediated endocytosis). Nystatin (NYS) and filipin (FIL) are believed to inhibit non-CME by sequestering cholesterol from lipid rafts (Macia *et al.*, 2006; Ivanov, 2008).

For chemokinesis experiments with endocytosis inhibitors, WT and $CD44^+/CD74^+$ COS-7/M6 cells were prepared as earlier (Figure 15), with the following exception. Medium was changed from DMEM/10% (v/v) FCS to DMEM/0.5% (v/v) FCS supplemented with endocytosis inhibitors, and the cells were returned to the incubator for 1 h. Without a second medium exchange, MIF was added to appropriate wells to a final concentration of 200 ng/ml, and the cells were imaged for 3.5 h (Figure 15).

While chlorpromazine and dynasore did not alter MIF-mediated motility of WT COS-7/M6 cells (Figure 20A), MIF-triggered chemokinesis was abrogated upon inhibition of lipid raft/caveolae-dependent endocytosis by nystatin (Figure 20A). In contrast, dynasore and nystatin but not chlorpromazine inhibited MIF-mediated motility of $CD44^+/CD74^+$ COS-7/M6 cells (Figure 20B), implicating the receptor- and dynamin-mediated internalisation in transducing MIF's actions on motility in receptor-positive cells. Dynamin in WT COS-7/M6 cells was not required for MIF-mediated upregulation of chemokinesis (Figure 20A). Taken together, MIF appears to exploit non-CME in upregulating chemokinesis in receptor-negative cells, and non-CME and dynamin in receptor-positive cells.

On the other hand, D-DT upregulates chemokinesis of $CD44^+/CD74^+$ COS-7/M6 cells under basal conditions (Figure 20C) but never under endocytosis inhibition. Because D-DT does not promote WT COS-7/M6 cell migration (Figure 15A), this implies that at least one receptor-dependent endocytic pathway is essential for mediating D-DT's effect.

Unlike the relatively well-established endocytosis inhibitors chlorpromazine and dynasore (section 6.3.2 of the Discussion provides a critical analysis), nystatin is known to not only perturb cellular uptake but also permeabilise cell membranes, making it an attractive compound to study ion transport across a variety of cell barriers such as lung epithelium or vascular endothelium. As shown in Figure 20, nystatin (*a*) somewhat diminishes the basal motility of all cells under starvation and (*b*) seems to abrogate MIF-driven increase in chemokinesis. Because it is likely that nystatin simply permeabilised the COS-7/M6 fibroblasts under investigation, an alternative inhibitor of endocytosis, filipin, was tested (Figure 20C, for D-DT, and Figure 21 for MIF).

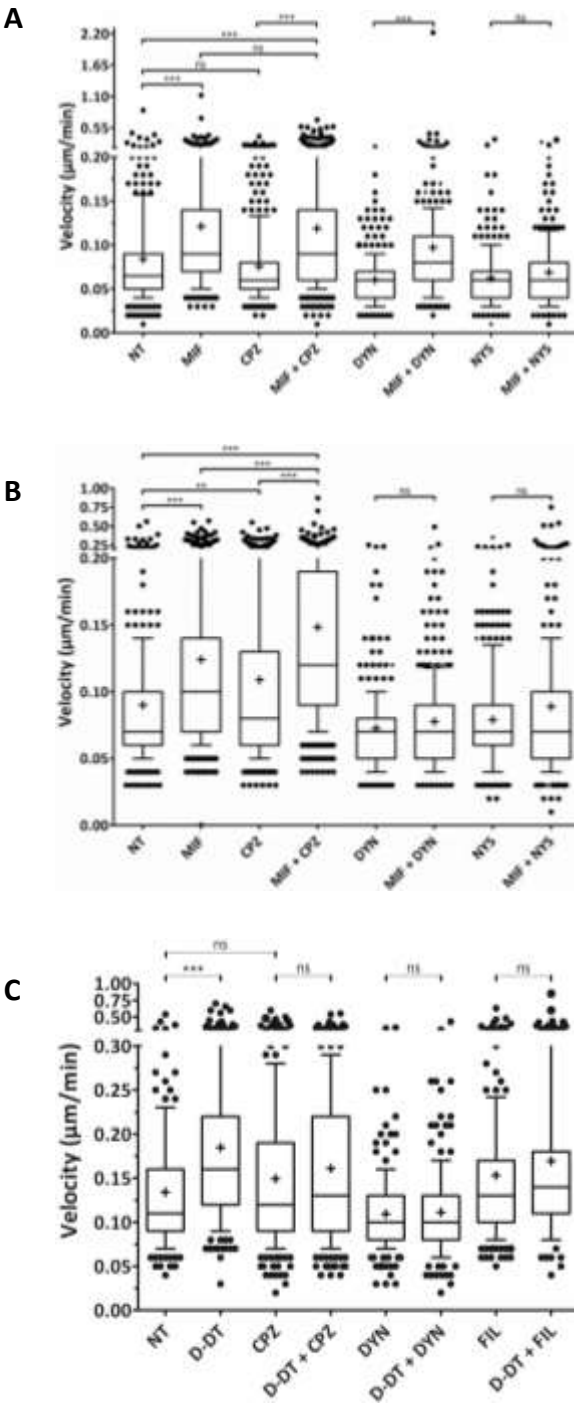

Figure 20. MIF-triggered chemokinesis appears to rely on lipid raft/caveolae- and not clathrin-mediated endocytosis. Functional dynamin in $CD44^+/CD74^+$ COS-7/M6 cells is required for MIF-mediated upregulation of chemokinesis, whereas D-DT only upregulates chemokinesis when at least one endocytic pathway is active. CPZ was added at 10 µM, DYN at 50 µM, FIL at 1.5 µM, and NYS at 27 µM, 1 h before the addition of MIF/D-DT. (**A**) WT and (**B-C**) $CD44^+/CD74^+$ COS-7/M6 cells were seeded in µ-Slides and imaged as described in Figure 15. Velocity data from three independent wells (replicates) (approx. 300 cells from 30 fields of view) were pooled from each experimental round, and a Kruskal-Walllis one-way analysis of variance (ANOVA) was performed. **Abbreviations**: **CPZ**, chlorpromazine; **DYN**, dynasore; **FIL**, filipin; **NYS**, nystatin. **Significance levels**: **ns**, non-significant ($p > 0.05$); *, $p \leq 0.05$; **, $p \leq 0.01$; ***, $p \leq 0.001$.

Finally, filipin – known to sequester cholesterol from lipid rafts and inhibit endocytosis similar to nystatin without its inhibitory effect on migration – abrogated MIF-induced chemokinesis of WT and $CD44^+/CD74^+$ COS-7/M6 cells (Figure 21A and B), providing additional evidence in support that MIF-induced fibroblast chemokinesis depends on lipid raft/caveolae assembly rather than CME.

A **B**

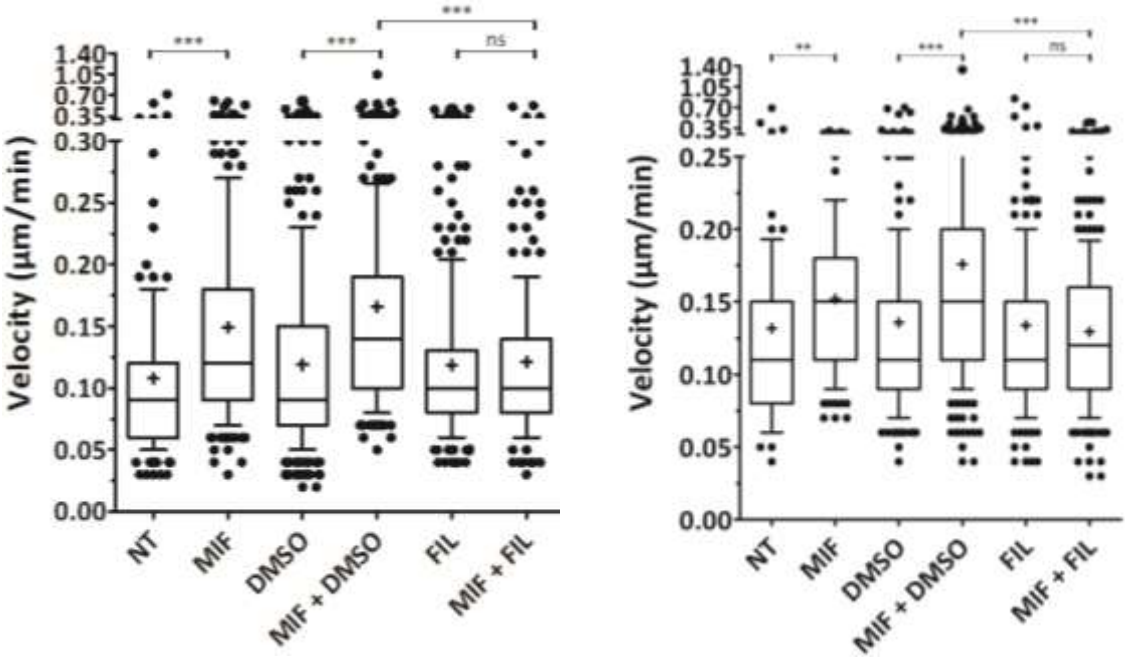

Figure 21. MIF-triggered WT and $CD44^+/CD74^+$ COS-7/M6 chemokinesis appears to rely on lipid raft/caveolae-dependent endocytosis. Filipin was added at 1.5 µM; DMSO was present in all DMSO- and FIL-containing wells at 0.02% (v/v). (**A**) WT and (**B**) $CD44^+/CD74^+$ COS-7/M6 cells were seeded in µ-Slides and imaged as described in Figure 15 with the same exception as in Figure 20 (i.e. 1-h pre-treatment with DMSO/FIL). Velocity data from three independent wells (replicates) (approx. 300 cells from 30 fields of view) were pooled from each experimental round (two for NT and MIF), and a Kruskal-Walllis one-way analysis of variance (ANOVA) was performed. **Abbreviations**: **FIL**, filipin. **Significance levels**: **ns**, non-significant ($p > 0.05$); *, $p \leq 0.05$; **, $p \leq 0.01$; ***, $p \leq 0.001$.

5.3.3.7. Endogenous MIF contributes to upregulation of chemokinesis by exogenous MIF in CD44+/CD74+ but not WT COS-7/M6 cells

As WT and $CD44^+/CD74^+$ COS-7/M6 cells express appreciable amounts of endogenous MIF (Figure 22A, lane 10), its contribution to chemokinesis induced by exogenous MIF is unclear. Therefore endogenous MIF was ablated using a knockdown strategy. Two individual *MIF* gene-specific short interfering RNAs (siRNAs) (Table 13) efficiently blocked MIF production in both cell lines three days after transfection (Figure 22A, lanes 2-3 and 5-6). The cognate C911 controls (Buehler *et al.*, 2012) did not affect expression levels (Figure 22A, lanes 4, 7 and 9). When both specific siRNAs were combined MIF production was abrogated to background levels (Figure 22, lane 8, upper panel). Interestingly, the levels of endogenous MIF in $CD44^+/CD74^+$ COS-7/M6 cells was lower than in WT cells. Hence, the knockdown led to undetectable MIF levels (Figure 22A, lane 8, lower panel).

Having proven that ablation of endogenous MIF is efficient, chemokinesis was again induced with exogenous MIF three days after transfection (Figure 22B-C, Appendix 1). The velocity was not significantly affected by the transfection procedure in $CD44^+/CD74^+$ cells, but was indeed affected in WT COS-7/M6 cells (Figure 22B, NT vs. C911 siRNA). The velocity was not significantly affected by the knockdown of MIF in COS-7/M6 cells but was indeed affected in $CD44^+/CD74^+$ COS-7/M6 cells (Figure 22C, NT vs. MIF siRNA and NT vs. C911 siRNA). The addition of exogenous MIF to untreated cells (WT and $CD44^+/CD74^+$ COS-7/M6) induced chemokinesis as shown before (Figure 16 and 22B-C). Because there was no significant change in upregulation of chemokinesis neither after knockdown of MIF nor after transfection of the C911 control siRNAs, it appears that endogenous MIF does not contribute to chemokinesis induced by exogenous MIF, at least not in WT COS-7/M6 cells (for a more detailed interpretation, see Discussion, section 6.3.2.2).

A

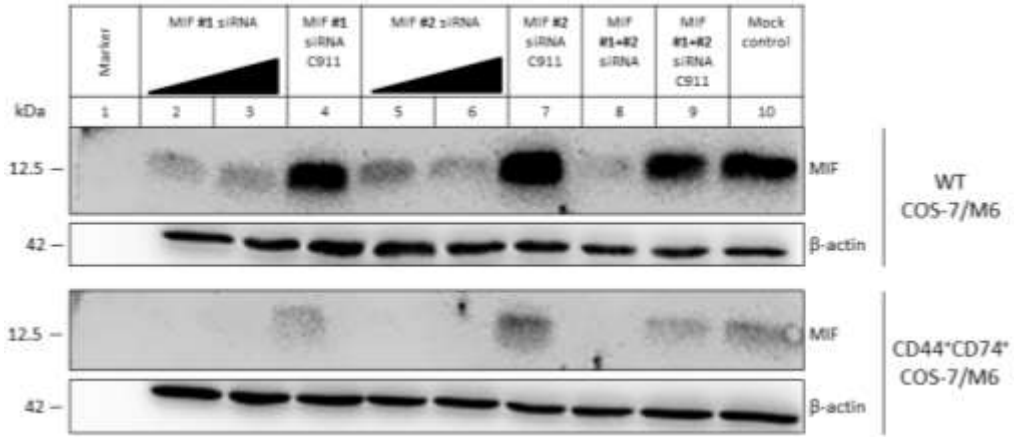

B **C**

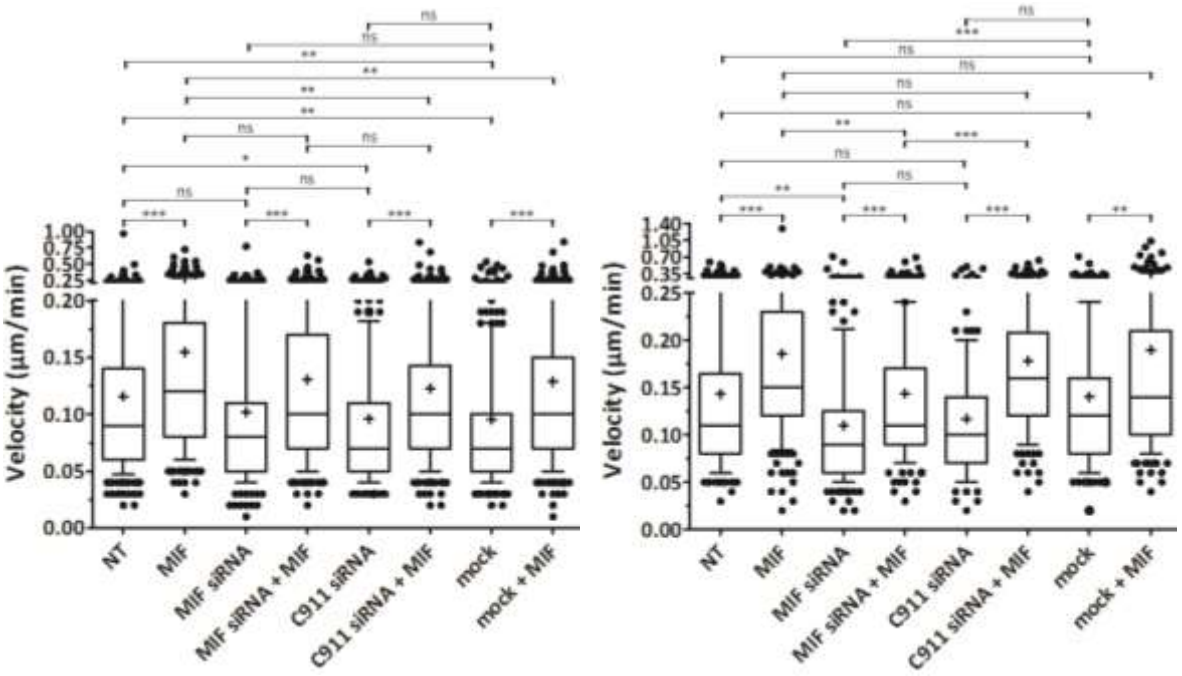

Figure 22. Endogenous MIF contributes to upregulation of chemokinesis by exogenous MIF in CD44+/CD74+ but not WT COS-7/M6 cells. (**A**) MIF Immunoblot proves MIF knockdown in WT COS-7/M6 cells (*top panel*) and $CD44^+/CD74^+$ COS-7/M6 cells (*bottom panel*). β-actin was used as loading control. (**B**) WT and (**C**) $CD44^+/CD74^+$ COS-7/M6 cells were seeded in µ-Slides and imaged as described in Figure 15, with the following exception. Cells were transfected in 6-well plates with MIF siRNA #1 and #2 and allowed to grow for 2.5 days. On the morning of the third transfection day (66 h after transfection), cells were split and seeded in µ-Slides for the remaining time (6 h) to a total of 72 h post-transfection. Velocity data (**B-C**) from three independent wells (replicates) (approx. 300 cells from 30 fields of view) were pooled from each experimental round, and a Kruskal-Walllis one-way analysis of variance (ANOVA) was performed. **Significance levels**: **ns**, non-significant ($p > 0.05$); *, $p \leq 0.05$; **, $p \leq 0.01$; ***, $p \leq 0.001$.

5.4. MIF/D-DT and actin cytoskeleton

5.4.1. The MIF/D-DT interactomes include many actin cytoskeleton-associated proteins

Fibroblasts play a key role in ECM maintenance, wound healing, and cancer-associated angiogenesis (Kalluri and Zeisberg, 2006). As fibroblasts secrete ECM components in order to facilitate healing, cells ensure proper spatiotemporal regulation of migration and proliferation of fibroblasts upon wounding and inflammation. MIF has been implicated in this process as it promotes wound closure of MEFs (Dewor *et al.*, 2007). Clinically, stromal fibroblasts steer the collective invasion of carcinoma cells in an integrin- and protease-dependent fashion (Gaggioli *et al.*, 2007), suggesting that fibroblasts are attractive therapy targets.

The abovementioned characterisation of COS-7/M6 fibroblasts and the effect of MIF and D-DT on their motility expand our knowledge of the biology of fibroblasts with a focus on their receptors. NIH 3T3 fibroblasts, which do not express CD74 but do express CD44, serve as a useful tool to study fibroblast behaviour, and specifically the cytoplasmic roles for MIF and D-DT.

The MIF/D-DT interactome defined in NIH 3T3 fibroblasts helps to delineate the mechanism of action of cytoplasmic MIF in cell motility (Table 2). We aimed to focus on the MIF-ARP2/3 axis by subsequently performing actin stainings as well as ARP2/3-driven *in vitro* actin assembly assays.

The actin-related protein 2/3 (ARP2/3) complex binds to existing actin filaments and initiates actin branching at a fixed angle of 70° (Robinson *et al.*, 2001). Two out of seven of ARP2/3 subunits putatively interact with both MIF and D-DT. As actin filaments extend towards the direction of cell movement, their elongation can be inhibited by capping proteins of which two – CAPZA1 and CAPZB – were also found to interact with MIF/D-DT.

Destrin (actin-depolymerising factor or ADF), a protein involved in the eponymous actin depolymerisation and another MIF/D-DT interactor, mediates the fast turnover of actin filaments. Tropomyosin, implicated in muscle contraction and actin stabilisation, antagonises ADFs and slows down the turnover of actin (Bugyi *et al.*, 2010). This suggests

that MIF/D-DT may fine tune cytoplasmic actin dynamics in terms of actin filament elongation and/or depolymerisation and therefore contribute to cell migration.

Furthermore, MIF but not D-DT interacts with Rho GDP-dissociation inhibitor (RhoGDI) which binds and sequesters Rho GTPases such as Rac1/RhoA/Cdc42 from the plasma membrane to keep them in an inactive cytoplasmic form. Since MIF is known to interfere with Rho GTPase activation (Figure 5, Table 19), its interaction with RhoGDI would provide a novel explanation to the observed effects of MIF on Rac1/RhoA/Cdc42.

On the other hand, MIF/D-DT interact with (*a*) nucleoside diphosphate kinase proteins (NDPKs) which in turn interact with many cytoskeletal proteins and the cell adhesion machinery (Snider *et al.*, 2015), and (*b*) moesin, a protein bridging the cytoskeleton and plasma membrane. As such, the MIF/D-DT-NDPK/moesin axis could be explored on the basis of not only cell migration but also cell adhesion and membrane dynamics.

5.4.2. MIF induces F-actin stress fibre formation in WT COS-7/M6 cells

Intrigued by the two observations that MIF upregulates the migration of MIF receptor-negative COS-7/M6 cells, and that the receptor-negative NIH 3T3-derived MIF interactome contains various actin cytoskeleton-related proteins, actin staining was performed to assess the status of the actin cytoskeleton before and after stimulation with recombinant MIF.

WT COS-7/M6 cells were seeded on coverslips in multi-well plates and allowed to adhere overnight (section 4.2.4.7). Next, medium containing 10% (v/v) FCS was exchanged for medium with 0.5% (v/v) FCS supplemented with MIF or heat-inactivated MIF. Following fixation and permeabilisation, cells were stained with Texas Red®-conjugated phalloidin, a fungal toxin that binds filamentous actin, and imaged under a fluorescence microscope (Figure 23A-C). Under starvation, MIF but not heat-inactivated MIF promoted actin stress fibre formation (Figure 23D). Three times more cells were stress fibre-positive under MIF stimulation as compared to non-treated as well as heat-inactivated controls (Figure 23D). Concomitantly, the number of cells with a prominent cortical rim decreased under MIF treatment, while the abundance of dividing or multinucleated cells remained virtually unchanged (Figure 23D).

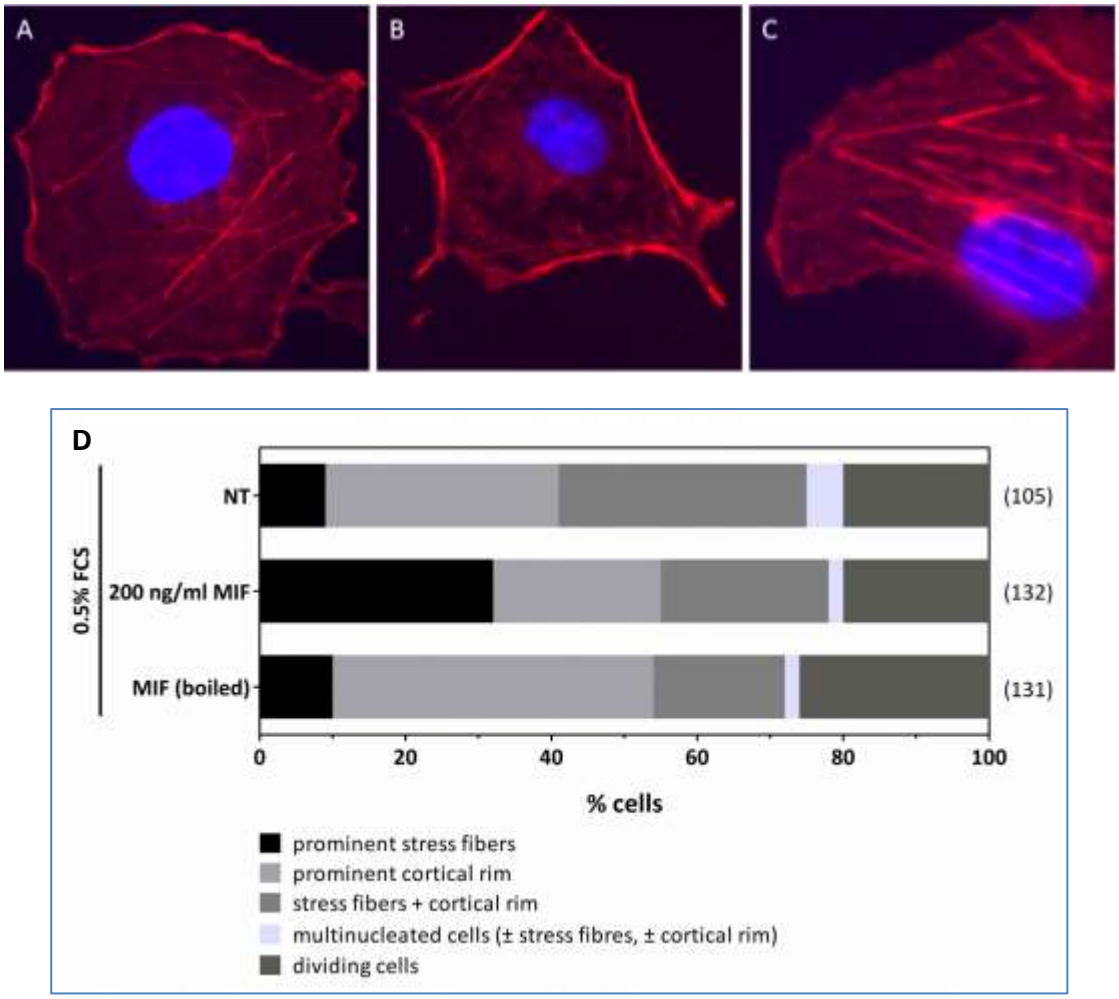

Figure 23. MIF induces F-actin stress fibre formation in WT COS-7/M6 cells. Cells were seeded at 40,000 cell/cm^2 on coverslips in a 12-well plate, allowed to adhere overnight, and treated with native or heat-inactivated MIF for 3.5 h. The cells were fixed in 4% paraformaldehyde, permeabilised in 0.1% Triton™ X-100, blocked in 1% BSA, and stained with Texas Red®-conjugated phalloidin (1:500) in the darkness for 30 min. Following washing, the coverslips were overlaid with DAPI-containing mounting medium, and put upside down on a glass slide. The next day the cells were visualised using a fluorescence microscope under 630X magnification (oil objective). The excitation/emission wavelengths were 596 nm/615 nm (for Texas Red®-phalloidin) and 358 nm/461 nm (for DAPI). (**A-C**) Representative images of phalloidin-stained actin. (**A**) A cell positive for both actin stress fibres and a cortical rim. (**B**) A cell with a prominent cortical rim but with no or few stress fibres. (**C**) A cell with prominent actin stress fibres but no cortical rim. (**D**) More than 360 cells were categorised based on the unique characteristics of their actin cytoskeleton. The number of unique cells used for each treatment assessment is shown in parenthesis (right). The data in graph **D** is representative of one out of three experiments. **Abbreviations**: **BSA**, bovine serum albumin; **DAPI**, 4',6-diamidino-2-phenylindole; **FCS**, foetal calf serum; **NT**, non-treated.

5.4.3. MIF but not D-DT slows down the rate of actin assembly in actin assembly assays

In order to test if MIF can directly affect the actin assembly, *in vitro* pyrene-actin assembly assays were performed. Actin polymerisation from globular to filamentous actin requires a number of factors. A branched actin network is built *in vitro* as well as *in vivo* through a seven-subunit actin-related protein 2/3 (ARP2/3) complex. ARP2/3 is activated by VCA domain present within WASP (Wiskott-Aldrich syndrome protein)-family verprolin-homologous protein (WAVE). In *in vitro* reconstituted assays, total cell extracts from HeLa, NIH 3T3 or HEK2393 can be used as sources of ARP2/3 (Baarlink *et al.*, 2013). Typically the first stage of actin assembly is the so-called lag phase when nucleation takes place (Figure 24A-D) (Harris and Higgs, 2006). Actin elongation occurs during the second stage – known as the log phase. Purified GST-tagged VCA is sufficient to induce actin assembly which results in a prominent change in the fluorescence curve from a linear to a sigmoidal shape (Figure 24A, actin+ARP2/3 vs. actin+ARP2/3+VCA).

While MIF, mD-DT and hD-DT did not modify the rate of VCA-triggered actin assembly in a fully reconstituted system with the seven-subunit ARP2/3 complex (Jan Faix lab, Hannover) (Figure 24A-C), MIF reduced the rate of VCA-induced actin assembly by 60% when a total HEK293 cell extract was used as a source of the ARP2/3 complex (Robert Grosse lab, Marburg) (not shown, pilot experiment performed by Haicui Wang PhD).

An additional set of experiments involving HEK293 total cell extracts was performed later with appropriate buffer controls. MIF but not D-DT decreased the rate of cell extract-driven actin assembly as compared to respective buffer controls (buffer P for MIF and 20 mM phosphate buffer pH 7.0 for D-DT), likely due to protein-protein interactions between MIF and unknown components of the cell extract (Figure 24D).

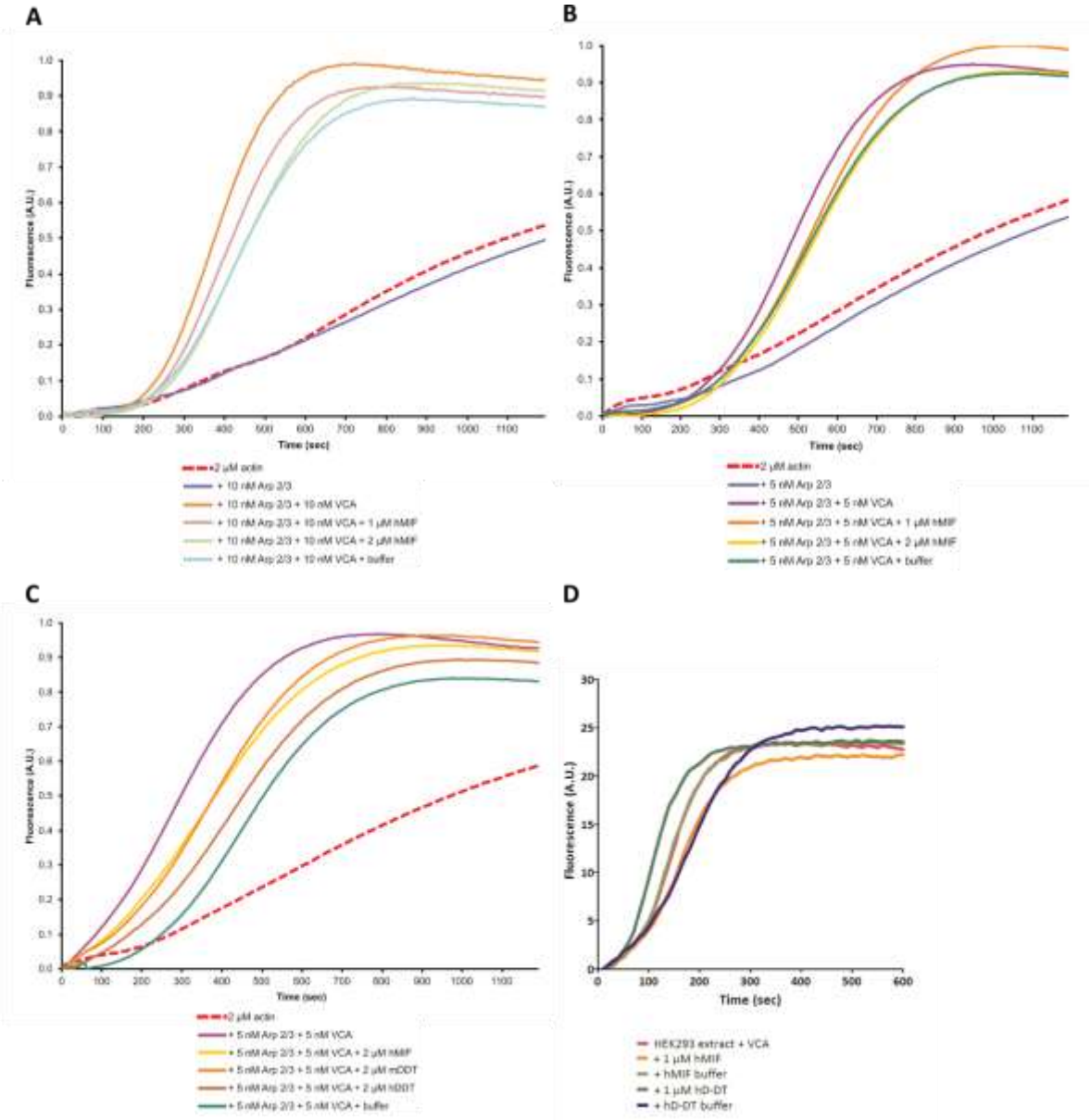

Figure 24. The differential influence of MIF on the rate of actin assembly *in vitro*. To measure the rate of actin assembly, non-fluorescent pyrene-labelled G-actin was combined with either (**A-C**) purified ARP2/3 or (**D**) the ARP2/3-containing total HEK293 cell extract, with or without recombinant proteins. In both assays, the formation of filamentous actin was induced with recombinant VCA domain. Fluorescence of filamentous pyrene-actin was monitored at 407 nm with excitation at 365 nm in a (**A-C**) 200-µl or (**D**) 100-µl reaction volume, using a spectrofluorophotometer. Original fluorescence traces over time are shown (**A-C**, 20 min; **D**, 10 min). Each experiment in A-C was performed once (Jan Faix lab, Hannover). Experiments in D are representative of one experiment and were consistently reproduced overall three or more times. **Abbreviations**: **ARP2/3**, actin-related protein 2/3 complex; **A.U.**, arbitrary units; **VCA**, verprolin, cofilin, acidic domain.

6. Discussion

Initially described as a factor inhibiting monocyte/macrophage random migration, MIF has emerged as a pleiotropic cytokine, chemokine and hormone. It is implicated in migration and invasion of cancer and non-cancer cells and orchestrates cell migration of a variety of immortalised and primary cells (Table 19). Much research is dedicated to MIF-mediated cell arrest of circulatory T cells, monocytes/macrophages, and neutrophils. Such cell arrest under flow conditions is primarily mediated by endothelium-immobilised MIF that is binding to C-X-C motif chemokine receptor type 2/4/7 (CXCR2, 4 and 7) on mononuclear immunocompetent cells (see Introduction, Figure 4), and plays a role in inflammation. Aside from circulating cells, resident cells such as fibroblasts (stromal mesenchymal cells) serve an equally important role in resolving inflammation, wound healing and scarring. Nevertheless, the mode of action of MIF on fibroblasts received much less attention (Table 19). First, although migration was assessed in cancer-associated fibroblasts and mouse embryonic fibroblasts (MEFs), the presence of MIF receptors – CD44, CD74 and others – was not (see Introduction, Figure 3A-B). Second, when MIF receptors CD44 and CD74 were identified and studied in other cellular models – COS-7/M6 and RAW264.7 cells – the migration remained unassessed (see Introduction, Figure 3C-D).

Aside from the actions of extracellular MIF on its receptors, many intertwined cytoplasmic signalling pathways are modulated by MIF. MIF acts in a pro-migratory manner on cancer and B cells via Rho GTPase Rac1, calcium influx, and actin polymerisation, and anti-migratory on monocytes via a cyclic activation/deactivation of Rho GTPases (Table 19). However, how secreted or cytosolic MIF mechanistically influences Rho GTPases is unknown.

D-DT, a structural and functional homologue of MIF, was initially characterised in the context of apoptosis and anchorage-independent growth (Brock *et al.*, 2014). Despite the fact that MIF/D-DT increased cell migration of clear cell renal cell carcinoma (ccRCC) (Pasupuleti *et al.*, 2014), the role of D-DT in migration remains poorly understood.

Table 19. MIF affects migration via the cytoskeleton and Rho GTPases – summary.

Cell phenomenon	Actions of MIF	Cell type	Reference
Actin polymerisation	Upregulates	B cell	(Klasen *et al.*, 2014)
Actin polymerisation	Downregulates (because of MIF knockout)	$MIF^{-/-}$ monocyte/macrophage	(Fan *et al.*, 2011)
Actin polymerisation	Upregulates (via phospho-cofilin)	Colorectal cancer	(Hu *et al.*, 2015)
Actin, microtubule, and IF network / Rho activation	Perturbs / downregulates (hence downregulates chemotaxis)	Monocyte	(Frascaroli *et al.*, 2009)
Chemokinesis	Downregulates	Mesenchymal stem cell	(Fischer-Valuck *et al.*, 2009; Barrilleaux *et al.*, 2010)
Chemokinesis	Upregulates	COS-7/M6	***This thesis***
Chemotaxis	Upregulates (via CXCRs and CD74)	Monocyte/macrophage, neutrophil, T cell	(Bernhagen *et al.*, 2007)
Chemotaxis	Downregulates	CAF	(Tarnowski *et al.*, 2010)
Chemotaxis	Upregulates	Glioblastoma	(Piette *et al.*, 2009)
Chemotaxis	Upregulates	MDSC	(Simpson *et al.*, 2012)
Chemotaxis	Upregulates (only PDGF-BB-induced chemotaxis)	VSMC	(Schrans-Stassen *et al.*, 2005)
Co-localisation with stress fibres	MIF and MLCK co-localise (motility was not assessed)	Endothelium	(Wadgaonkar *et al.*, 2005)
IL-8 production	Upregulates	HCC	(Ren *et al.*, 2003)
Integrin expression	Upregulates	Chondrosarcoma	(Lee *et al.*, 2011)
Integrin expression	Downregulates (because of MIF knockout)	$MIF^{-/-}$ endometrium	(Rakhila *et al.*, 2014)
Microtubule polymerisation	Upregulates	Monocyte/macrophage, myocardial trabeculae	(McCarthy *et al.*, 1979; Preau *et al.*, 2013)
Rac1 stabilisation in lipid rafts	Upregulates	A549	(Rendon *et al.*, 2007)
Rac1/RhoA/Cdc42 (de)activation	Activates/deactivates (hence downregulates chemotaxis)	Monocyte/macrophage	(DiCosmo-Ponticello *et al.*, 2014)
RhoA activation	Upregulates (increases growth but does not affect motility)	MEF, NIH 3T3	(Swant *et al.*, 2005)
RhoQ and Cdc42	Upregulates (hence upregulates chemotaxis)	Mesenchymal stem cell	(Lourenco *et al.*, 2015)
Wound healing	Upregulates	MEF	(Dewor *et al.*, 2007)
Wound healing	Downregulates (because of MIF knockout)	Skin of $MIF^{-/-}$ mice	(Ashcroft *et al.*, 2003)

Abbreviations: **BMDM**, bone marrow-derived macrophage; **CAF**, cancer-associated fibroblast; **Cdc42**, cell division control protein 42 homolog; **CXCR**, C-X-C motif chemokine receptor; **HCC**, hepatocellular carcinoma; **IF**, intermediate filament; **IL-8**, interleukin-8; **MEF**, mouse embryonic fibroblast; **MDSC**, myeloid-derived suppressor cell; **MLCK**, myosin light chain kinase; **PDGF-BB**, platelet-derived growth factor chain BB; **Rac1**, Ras-related C3 botulinum toxin substrate 1; **RhoA**, Ras homolog gene family, member A; **VSMC**, vascular smooth muscle cell.

6.1. Protein purification

Recombinant non-tagged MIF and D-DT were purified from *E. coli* BL21 (DE3). One caveat in the field of MIF research is the use of bacterially-produced MIF that is tagged (Chen *et al.*, 2015). The interpretation of data could be hindered if a tag causes polypeptide misfolding or a steric hindrance, potentially leading to perturbed biological functions. Since a non-tagged MIF molecule was used throughout here, no biological interference can be attributed to a tag.

Because *E. coli*-produced proteins lack post-translational modifications which may be essential for certain biological functions, MIF was tested for its biological activity. MIF appears to exert its effects as a trimer based on an elegant study involving a locked MIF trimer N110C (Fan *et al.*, 2013), and its tautomerase catalytic site resides in a cleft between two MIF monomers. Therefore the tautomerase assay allowed for determination that the recombinant protein was: (*a*) biologically active with respect to its enzymatic (tautomerase) activity and (*b*) it formed a trimer in solution. MIF was active not only in PBS but also in cell-culture medium after the addition to cultured cells for 24 h. Furthermore MIF storage at 4 °C (for a few months) or – 80 °C (also for a few months, snap-frozen immediately after its production) did not significantly change its tautomerase activity, showing its stability under different conditions.

6.2. MIF/D-DT interactome and random cell motility assays

Fibroblasts play a pivotal role in health and disease. During wound healing, fibroblasts become reversibly activated and secrete ECM components such as collagen (Kalluri and Zeisberg, 2006). In cancer, cancer-associated fibroblasts (CAFs) secret matrix metalloproteinases (MMPs), monocyte chemotactic protein 1 (MCP-1) and a variety of oncogenic factors (Kalluri and Zeisberg, 2006). Hence fibroblast-like NIH 3T3 and COS-7/M6 cells were chosen as convenient model cells in order to study the relationship between MIF, MIF receptors, actin cytoskeleton, and cell motility.

As fibroblast-like NIH 3T3 and COS-7/M6 cells do not express the entire repertoire of MIF receptors, they were deemed appropriate to study the physiology of MIF and its novel homologue D-DT in this thesis. Importantly, both do not produce the principal MIF/D-DT

receptor CD74 (Fernandez-Cuesta *et al.*, 2014). On the other hand, CD44 and CXCR4 may be found in minute amounts in NIH 3T3 (Okabe *et al.*, 2005; Tzircotis *et al.*, 2006; Yamada *et al.*, 2015) and COS-7/M6 cells (section 5.3.1).

The rationale of this study is based on two questions. First, since MIF is both an extra- and intracellular protein, are the receptors essential for MIF-mediated motility? Knowing that (*a*) MIF classically affects cell motility via its receptors but also that (*b*) MIF has multiple intracellular binding protein partners, attention was directed at a model of receptor-negative COS-7/M6 cells. Second, a mass spectrometry-based proteomics screen in NIH 3T3 cells for interactors of cytosolic MIF and D-DTs (Cayli *et al.*, 2009; Filip *et al.*, 2009; and unpublished data) revealed many actin-associated molecules including ARP2/3 and RhoGDI to be putative MIF/D-DT interactors. This raised the question if intracellular MIF mediates cell motility?

To examine whether MIF requires its receptors for mediating motility, COS-7/M6 cells were chosen as a model of MIF receptor-deficient cells (Shi *et al.*, 2006). Stable cell lines expressing CD44 and CD74 were generated to define the contribution of these two MIF receptors to MIF-mediated motility.

6.2.1. Wound healing (scratch) assays

A wound healing (scratch) assay is a cost-effective method that provides insight into collective cell motility characteristic of e.g. cancer cells. Collective migration in such a two-dimensional setup is reminiscent of the capacity of a cancer cell to explore the environment within the metastatic cascade.

Such collective-cell motility assays were performed in collagen-coated µ-Slides and multi-well plates. The use of ECM was recommended by the original publication describing the method (Liang *et al.*, 2007), based on the observation that the ECM components promote integrin-dependent cell motility hence would promote the overall motility of cells on tissue-culture vessels (Friedl, 2004). However, those assays proved challenging because prototypical inducers of motility such as insulin-like growth factor (IGF)-I and epidermal growth factor (EGF) did not upregulate motility of the investigated cells.

Similar to cancer cells, wound healing assays measure polarised, microtubule (MT)-dependent cell motility (Goulimari *et al.*, 2005). Velocity (or distance) of single cells might be measured but because of the formation of cellular bridges (Green *et al.*, 2004), some cells are always much faster than others. In time-lapse microscopy images were acquired overnight but a typical wound would close only in 1-2 days. Often one cell front did not migrate or migrated slowly and appeared to be stuck after approximately one hour, which was indicative of a disrupted ECM substrate. One approach to circumvent the observed problem of varying wound widths would be to use cell-culture inserts of a defined 500-µm width (ibidi) or circular cell seeding stoppers (Oris™ Cell Migration Assays, Platypus Technologies) in order to ensure consistency in wound creation. It would also provide an environment without a physical damage inflicted by the wounding.

In search for an alternative and more reliable technique to test migration, chemokinesis (random single-cell motility) assays were employed.

6.2.2. Chemokinesis (random cell motility) assays

6.2.2.1. Chemokinesis assays are suitable to study motility of COS-7/M6 cells

Another convenient method to study motility is a chemokinesis (random motility) assay as it allows for single-cell investigations without the need for physical wounding of a monolayer. During preliminary chemokinesis data collection, 10% (v/v) FCS-containing DMEM was used as a reference to monitor the cells over the time of the experiment. Cell death or lack of proper cell morphology would have been indicative of non-physiological conditions such as altered osmolality, pH, temperature or CO_2 concentration within the µ-Slide (Cole, 2014). None of these phenomena were observed under 10% or 0.5% (v/v) FCS in chemokinesis assays. In contrast, aberrant cell morphology was often noted during wound healing assays that likely arose due to physical wounding with a pipette tip.

Although MIF-mediated chemotaxis was studied in many reports, one caveat of chemotaxis assays is the maintenance of a stable gradient over the course of an experiment. The approach employed in this thesis creates an extracellular milieu with a uniform distribution of MIF/D-DT. As such, their direct effect on random motility of single cells was measured. Adherent fibroblasts – such as COS-7/M6 cells – have an intrinsic

capacity to migrate during healing *in vivo*. In contrast, MIF-driven chemotaxis of mononuclear immunocompetent cells such as monocytes/macrophages, neutrophils and T cells were often tested in Transwell® chambers where cells are seeded on inserts and allowed to migrate through 3- or 5-µm pores (Bernhagen *et al.*, 2007). Such a strategy mimics the ECM/endothelium environment through which these circulating cells normally migrate (see Introduction, Figure 4).

Moreover, chemotaxis assays measure the bulk motility of a heterogeneous population of cells. Contrary to that, an assay measuring single-cell chemokinesis permits a real-time observation of how individual cells behave under stimulation with MIF or D-DT. In sum, one can observe that some cells remain immotile throughout the experiment while some are strong responders, indicating the heterogeneity of cells and highlighting the importance of single-cell experimentation. It would be tempting to hypothesise that strong MIF-responders are positive for a yet-unknown MIF receptor or can better internalise MIF.

MIF-mediated chemokinesis assays used in this thesis were performed with fibroblasts seeded at low confluency on cell-culture slides. The duration of each fibroblast chemokinesis assay (3.5 h) used here was similar to that in chemotaxis assays with circulating cells (3-6 h) and sufficient to monitor short-term (up to an hour) as well as long-term effects of a treatment (3.5 h) but was not exceedingly long (12-24 h). The first study on MIF and migration by Dewor *et al.* also concluded that short-term but not long-term stimulation with MIF was necessary for MIF-mediated upregulation of motility in wound healing assays with WT MEFs and $MIF^{-/-}$ MEFs (Dewor *et al.*, 2007). PDGF-BB stimulated – bot not basal – chemotaxis of vascular smooth muscle cells (VSMCs) was also more pronounced upon short-term (6.5 h) stimulation with MIF (Schrans-Stassen *et al.*, 2005).

6.2.2.2. Endogenous MIF contributes to upregulation of chemokinesis by exogenous MIF in CD44+/CD74+ but not WT COS-7/M6 cells

In order to validate chemokinesis assays with COS-7/M6 cells, EGF was successfully used as a positive control for cell motility. Next, MIF was shown to be a similar potent inducer of motility of both WT and $CD44^+/CD74^+$ COS-7/M6 cells.

In a set of following experiments with WT and $CD44^+/CD74^+$ COS-7/M6 cells, siRNA-mediated MIF knockdown was employed to test the hypotheses that (*a*) MIF knockdown diminishes cell motility and (*b*) both endogenous and exogenous MIF additively upregulate cell motility. Because velocity values measured under a combination of starvation and transient siRNA/mock transection oscillate within a narrow range of 0.10 and 0.12 µm/min (Figure 22), the following interpretation is presented cautiously.

In theory, endogenous MIF could influence the actin machinery to drive motility via (*a*) an intracrine effect (intracellular MIF produced by the same cell acts cytoplasmically), (*b*) a paracrine effect (MIF secreted by a neighbouring cell is taken up by a different cell), or (*c*) an autocrine effect (MIF is secreted and taken up by the same cell). In a scenario outlined in (*a*), cytoplasmic MIF only would drive cell motility. In scenarios (*b*) and (*c*), MIF-driven motility can be either receptor-mediated (likely accompanied by subsequent calcium influx and ERK1/2 activation) or endocytosis-mediated with subsequent cytoplasmic action (likely via actin cytoskeleton). In either case, knockdown of endogenous MIF with specific siRNAs ought to diminish motility when compared to a non-specific siRNA control.

In $CD44^+/CD74^+$ COS-7/M6 cells, knockdown of MIF indeed resulted in a significant downregulation of motility as compared to basal motility of non-treated cells. However, it is non-significant as compared to the C911 siRNA controls, implying that the observed effect in receptor-positive cells is related to an effect exerted by the siRNA transfection. In WT COS-7 cells, MIF knockdown does not downregulate motility in a significant way as compared to non-treated cells. Additionally, the velocity of WT COS-7 cells under MIF knockdown is the same as that of cells treated with C911 siRNA control (with or without exogenous MIF). Overall, if only the velocities of siRNA-treated cells were to be compared, there is no observable effect of endogenous MIF on migration in either cell line.

However, a comparison between velocity values of siRNA-treated and mock-transfected cells could shed light on whether Lipoectamine-mediated transfection affects basal cell migration. Again, it is worth mentioning that the values measured in chemokinesis assays oscillate within a relatively narrow range. The velocities of WT COS-7/M6 cells (*a*) under MIF depletion versus the velocity of mock-transfected cells and (*b*) the velocity of control siRNA-transfected cells versus mock-transfected cells are non-significant, suggesting that the transfection does not affect basal velocity of receptor-negative cells. Surprisingly, in receptor-positive COS-7/M6 cells, the velocity of MIF-depleted cells is significantly lower than that of mock-transfected cells; the velocity of control siRNA-treated cells and that of mock-transfected cells is non-significant. As mentioned above, this phenomenon is not related to the presence of siRNAs because there is no significant difference between the velocity of control siRNA-transfected cells versus that of mock-transfected cells. This suggests that it is not the transfection procedure, but the specific downregulation of MIF that diminishes motility of receptor-positive cells. Overall, given that the differences in velocity values are so small, it is concluded that endogenous MIF knockdown does not diminish cell motility of either cell line. MIF knockdown has been reported to significantly impair wound healing of ccRCCs (7% wound surface area open with control GFP siRNA versus 33% wound surface area open upon MIF knockdown, overnight) (Pasupuleti *et al.*, 2014) and somewhat reduce wound healing of $MIF^{-/-}$ MEFs (15 arbitrary units for WT MEFs versus 10 arbitrary units for $MIF^{-/-}$ MEFs, after 24 h) (Dewor *et al.*, 2007). While those experiments were performed over longer periods of time, the chemokinesis assays employed here lasted 3.5 h.

Next it was asked whether the contributions of endogenous and exogenous MIF are additive and tested by comparing the velocities of cells with or without MIF knockdown but stimulated with recombinant MIF. MIF-stimulated migration of MIF-depleted WT COS-7/M6 cells was the same as that of MIF-stimulated MIF-positive cells, implying that there is no underlying positive effect of endogenous MIF on migration of receptor-negative cells. Remarkably, in receptor-positive cells, only within the siRNA-background, a comparison between velocity values draws a different conclusion. The velocity of cells

transfected with control C911 siRNA and stimulated with MIF (i.e. positive for both endogenous and exogenous MIF) is significantly higher than that of MIF-depleted cells stimulated with exogenous MIF (i.e. positive for exogenous MIF only). This implies that the effect of both MIF populations is additive in receptor-positive cells, but not in receptor-negative cells.

Taken together, (*a*) MIF knockdown does not significantly lower cell velocity in either cell line tested over the course of 3.5 h but (*b*) cell velocity of receptor-positive/MIF-depleted cells is significantly increased by exogenous MIF and reaches the velocity observed in MIF-stimulated MIF-positive cells, likely due to the fact that CD44/CD74 are present and trigger classical MIF responses via Src kinase and ERK1/2. This suggests that the CD44/CD74-dependent mechanism is somewhat stronger than the other, unknown one, which triggers motility of WT COS-7/M6 cells.

6.2.2.3. COS-7/M6 fibroblasts respond differentially to native and enzyme-null MIF mutants as well as D-DT

At a molecular level, MIF's tautomerase activity has been implicated in mediating MIF's actions including cell motility, and is a druggable target in a variety of disorders (Al-Abed and VanPatten, 2011; O'Reilly *et al.*, 2016). In experimental disease management, the use of tautomerase-null recombinant proteins as well as specific tautomerase inhibitors ISO-1 and 4-IPP has been proven successful, suggesting that the enzymatic activity of MIF is essential (Al-Abed and VanPatten, 2011; Varinelli *et al.*, 2015). Although a genuine physiological substrate for MIF/D-DT is yet to be defined, the active site of MIF has been well characterised. In a trimer, there are three active sites composed of hydrophobic amino acids. Specifically, the nucleophilic N-terminal proline (the first amino acid after methionine cleavage) acts as a catalytic base, and its deletion renders MIF enzymatically-inactive, impairs the MIF-CD74 interaction, and intracellular MIF protein-protein interactions (O'Reilly *et al.*, 2016). A recent study developed a range of amino acid insertions within the active site to further delineate the role of the N-terminus in MIF-mediated accumulation of neutrophils in the lung (Pantouris *et al.*, 2015). A proline-to-methionine (P2M) MIF mutant exhibited the same neutrophil accumulation activity as MIF WT, ΔP2, and M3A. However, it was not the catalytic pocket of MIF but rather the

residues surrounding it that were involved in the MIF-CD74 interaction (Pantouris *et al.*, 2015). Here tautomerase-null mutants (MIF P2A and Δ4) did not enhance motility of WT COS-7/M6 cells, hence the tautomerase activity of MIF is required for MIF-mediated upregulation of random two-dimensional motility of fibroblasts. Furthermore, due to the fact that D-DT exhibits a much lower tautomerase activity than MIF, the impact of D-DT's tautomerase activity on migration was not assessed here.

One interpretation is that the stimulatory effect of MIF on migration is dependent on its intrinsic tautomerase activity, conserved across species including man and rodents (Merk *et al.*, 2011), bacteria (Burks *et al.*, 2010) and parasites (Qu *et al.*, 2014). As an alternative explanation, the lack of four initial amino acids or a Pro-2 substitution may perturb the MIF-protein interaction network or MIF trimer formation (Fingerle-Rowson *et al.*, 2009), resulting in a dominant-negative effect. Similar questions were partially investigated in a study using N-terminal MIF truncations (P2A, Δ4, Δ5, Δ6, Δ7, Δ8, Δ10, where Δn indicates how many amino acids (n) were deleted from the N-terminus of MIF) (Kleemann *et al.*, 2000b). Based on far-ultraviolet circular dichroism spectroscopy, the secondary structure of MIF and its mutants was assessed. While the conformation of all MIF mutants closely resembled that of native MIF (WT), the structure of Δ4 MIF was characterised by more random coil structure (Kleemann *et al.*, 2000b). Moreover, MIF P2F (Pro-2-to-Phe substitution) and MIF P2S (Pro-2-to-Ser substitution) with no or very low tautomerase activity, respectively, inhibit (*a*) MCP-1-induced chemotaxis and (*b*) non-induced, random migration of peripheral blood mononuclear cells (PBMCs) similarly to MIF WT (Hermanowski-Vosatka *et al.*, 1999). Interestingly, PBMCs investigated by Hermanowski-Vosatka *et al.* were composed of 70-90% monocytes and 10-30% B lymphocytes, but the status of MIF receptors such as CD74 remained uncharacterised. Hence, it appears that tautomerase activity is not required for MCP-1-induced chemotaxis and random migration of PBMCs. In contrast to MIF WT, MIF P2A – a mutant slightly different than the abovementioned 2PF and P2S – did not induce motility of WT COS-7/M6 fibroblasts investigated here. While monocytes and fibroblasts may differentially respond to the same stimulus, this result also suggests that each MIF mutant protein may exhibit a

different tertiary and quaternary structure and hence distinct modes of action. Next to tautomerase-null mutant proteins, specific pharmacological inhibitors of MIF's tautomerase activity, ISO-1 and 4-IPP were used. Both ISO-1 and 4-IPP inhibited MIF-induced motility of WT COS-7/M6 cells. In summary, as tautomerase-null MIF mutants as well as pharmacological tautomerase inhibitors abolish MIF's stimulatory effect on chemokinesis of WT COS-7/M6 fibroblasts, the tautomerase activity itself seems to be required for the observed effects.

Because the oxidoreductase-null MIF mutant C60S increased motility to a much lesser extent than MIF WT, the oxidoreductase activity might be partially required for MIF-triggered upregulation of motility. Interestingly, nucleoside diphosphate kinase A (NDPKA, also known as NM23-H1 or NME1) interacts with MIF and this interaction is mediated by Cys-60 of MIF (Jung *et al.*, 2008). Consequently, NDPKA-MIF interaction abrogates MIF-induced proliferation of quiescent NIH 3T3 cells and MIF-induced ERK1/2 activation (Jung *et al.*, 2008). The facts that (*a*) NDPKB is a negative regulator of MIF via a redox reaction mediated by Cys-60 (Jung *et al.*, 2008), (*b*) its closely related paralogue NDPKB (NM23-H2 or NME2) was found within the MIF/D-DT interactome (see Introduction, Table 2), and (*c*) MIF C60S does not upregulate chemokinesis of WT COS-7/M6 cells to the same extent as MIF WT, suggest that MIF-induced upregulation of chemokinesis might be mediated by an interaction with a member of the NDPK family.

The C60S substitution results in poor solubility as compared to native MIF (Kleemann *et al.*, 1998; Ouertatani-Sakouhi *et al.*, 2010) but does not affect the tertiary structure (Kleemann *et al.*, 1999). To unambiguously show that the CALC (Cys-Ala-Leu-Cys)-based oxidoreductase activity is required for MIF's upregulation of chemokinesis, a substitution of both cysteines (resulting in a double mutant C57S/C60S) would be advantageous. Nonetheless, MIF C57S/C60S could not be tested in enzymatic assays due to solubility problems (Kleemann *et al.*, 1998). Alternatively, a pharmacological inhibitor of MIF's oxidoreductase activity would be valuable to complement the tautomerase-activity inhibitors ISO-1 and 4-IPP.

In an attempt to better characterise the MIF family of proteins, D-DT was tested for its effect on random motility of WT and $CD44^+/CD74^+$ COS-7/M6 cells. Only MIF but not D-DT enhanced random motility of WT COS-7/M6 cells. Moreover, MIF alone, D-DT alone, and both together enhanced motility of $CD44^+/CD74^+$ COS-7/M6 cells. These results provide here first experimental evidence that MIF receptors CD44/CD74 are essential for D-DT-mediated chemokinesis but dispensable for MIF. It is remarkable since MIF and D-DT have hitherto been described as acting synergistically in a variety of disease models and signalling pathways. Both MIF and D-DT (*a*) are upregulated in human sepsis and ovarian cancer patients (Merk *et al.*, 2011), (*b*) inhibit p53 in human lung cancer cell lines (Brock *et al.*, 2014), (*c*) are hypoxia-inducible and (*d*) regulate human clear cell renal cell carcinoma (ccRCC) migration (Pasupuleti *et al.*, 2014). In the last study, D-DT showed a more pronounced pro-tumourigenic effect than MIF (Pasupuleti *et al.*, 2014). Here, conversely, only MIF but not D-DT affected random migration of fibroblasts, adding a novel piece of evidence that MIF and D-DT may act differentially depending on their cellular context. This would be important when considering organ-specific or organism-wide MIF/D-DT inhibition. For instance, Rajesakeran *et al.* suggest that ISO-1 inhibits MIF but not D-DT and 4-IPP inhibits both MIF and D-DT (Rajasekaran *et al.*, 2014). Taken together, it is key to consider the cellular targets of MIF/D-DT and adjust accordingly relevant MIF-alone, D-DT-alone or combined MIF/D-DT inhibition.

6.2.2.4. Endocytosis of MIF via lipid rafts/caveolae may contribute to its action on COS-7/M6 fibroblast motility

In view of the fact that native MIF upregulated motility of MIF receptor-negative COS-7/M6 cells, the question arose whether and how MIF is endocytosed. Most likely, MIF would then either elicit endosomal signalling or undergo endosomal escape. If it undergoes endosomal escape, it could act intracellularly and enhance migration via directly acting on the actin cytoskeleton. Endosomal escape is poorly understood and typically studied in terms of efficient antibody, siRNA, or engineered protein delivery (Li *et al.*, 2015), rather than for endogenous proteins. To that end specific endocytosis inhibitors were used to address this question.

Inhibitors included: (*a*) chlorpromazine which inhibits clathrin-mediated endocytosis (CME) likely due to the loss of clathrin and adaptor protein complex 2 (AP2) from the cell surface; (*b*) dynasore (DYN) which inhibits both clathrin- (CME) and caveolae-mediated endocytosis by inhibiting dynamin GTPase activity; (*c*) nystatin (NYS) which inhibits caveolae-mediated endocytosis by sequestering cholesterol from lipid rafts and redistributing it across the membrane; and (*d*) filipin which also inhibits caveolae-mediated endocytosis by sequestering cholesterol akin to nystatin (Macia et al., 2006; Ivanov, 2008).

All four endocytosis inhibitors were used at non-toxic concentrations of the same order of magnitude as reported elsewhere (Kirchhausen *et al.*, 2008; Xie *et al.*, 2011; Schwartz *et al.*, 2012). However, most previous studies only used a single inhibitor and investigated MEFs, RAW264.7, HeLa and HEK293 cells, but not COS-7/M6 cells, which makes it difficult to compare earlier results with the results shown here.

Even though MIF is known to be endocytosed by MEFs (Schwartz *et al.*, 2012) as well as RAW264.7 macrophages (Xie *et al.*, 2011) via CME, migration was not studied by neither Schwartz *et al*. nor Xie *et al*. Furthermore, Schwartz *et al.* assessed the colocalisation of MIF and Rab7 (late endosome marker) with and without monodansylcadaverine and chlorpromazine in a Rab7GFP overexpression system, potentially inducing overexpression artefacts. Here the inhibition of CME by chlorpromazine did not affect MIF-triggered motility of MIF receptor-negative WT COS-7/M6 cells suggesting a different internalisation pathway. Furthermore, the extent of monodansylcadaverine/chlorpromazine-mediated inhibition of MIF endocytosis was within 20-50%, suggesting non-CME endocytosis might have occurred in parallel (Schwartz *et al.*, 2012).

To interfere with the putative endocytosis of MIF beyond CME, dynasore was used as an inhibitor of dynamin GTPase activity. Interestingly, dynamin is responsible for cargo endocytosis in both CME and non-CME pathways, since both require vesicle scission (von Kleist and Haucke, 2012). In epithelial HeLa cells, MIF endocytosis indeed depends on functional dynamin, as judged by experiments using dynasore (Schwartz *et al.*, 2012). That

result is in line with the observation that $CD44^+/CD74^+$ COS-7/M6 cells rely on functional dynamin to mediate MIF-driven migration. In such a scenario, MIF binds CD44/CD74 on the cell surface, a clathrin-coated pit is formed around the nascent vesicle, the vesicle is ultimately cleaved by dynamin, and MIF can either exert endosomal signalling or undergo endosomal escape (see Introduction, Figure 2 and 3). Admittedly, as Schwartz *et al.* noted, HeLa cells are negative for CD74 but positive for CXCR4, implicating CXCR4-mediated MIF endocytosis as a putative cell entry mechanism. In contrast, MIF upregulates WT COS-7/M6 cell motility upon dynamin inhibition, suggesting MIF is internalised in a non-clathrin and non-dynamin-dependent manner. However, dynasore inhibits fluid-phase endocytosis of dextran – a prototypical endocytic cargo – in dynamin 1, 2 and 3 triple-negative as well as control, dynamin 1, 2 and 3-positive cells (Park *et al.*, 2013). Because of such off-target effects of dynasore, results must be considered with caution. It may be thus concluded that (*a*) dynamin-mediated endocytosis of MIF appears to facilitate MIF-induced upregulation of motility in receptor-positive cells, and (*b*) MIF-mediated motility likely depends on lipid rafts/caveolae and not clathrin and dynamin in receptor-negative cells.

Nystatin – known to sequester cholesterol from lipid rafts and redistribute it uniformly within the plasma membrane – was employed as a model inhibitor of non-CME. In both cell types tested (MIF receptor-positive and -negative), nystatin abrogated the induction of chemokinesis by MIF. Although the status of the MIF receptors was not determined in MEFs obtained for the 2012 endocytosis study (Schwartz *et al.*, 2012), MEFs are presumably positive for both CD44 and CD74 (Shi *et al.*, 2006). However, nystatin – and closely related filipin – did not inhibit endocytosis of MIF by MEFs, despite a trend towards inhibition at time point 60 min (Supplementary Figure 2B in Schwartz *et al.*, 2012). Yet it is noteworthy that nystatin – here used at 25 µg/ml – Is known to permeabilise cell plasma membranes at concentrations four times higher – 100 µg/ml (Schultheiss *et al.*, 2008). Thus it hinders the cells from performing their basic physiological functions such as maintaining ion homeostasis, growth, or migration, hampering a proper analysis of data derived from the MIF/nystatin data. Furthermore, nystatin-mediated inhibition of internalisation of endostatin – an inhibitor of angiogenesis – switches endostatin's uptake

route from lipid raft/caveolae- to clathrin-dependent pathway, suggesting that a much more complex cross-talk between endocytic pathways exists (Chen *et al.*, 2011).

Aware of the limitations of the use of nystatin, additional experiments with filipin – another inhibitor of caveolin- but not clathrin-dependent endocytosis – were performed in WT and $CD44^+/CD74^+$ COS-7/M6 cells. Filipin-mediated inhibitory effect on MIF-stimulated chemokinesis strongly suggests that cholesterol sequestration is indeed responsible for MIF's action, strengthening the conclusion drawn from the MIF/nystatin data. In fact, filipin-treated cells were exposed to a relatively low DMSO concentration of 0.02% (v/v) (Figure 21), twenty-five times less than elsewhere – 0.5% (v/v) (Figure 20).

Overall, results obtained with endocytosis inhibitors indicate that MIF-mediated increase in random cell migration is lipid raft/caveolae-dependent. To address the cytoplasmic route(s) of MIF trafficking, further studies need to be performed. How MIF is endocytosed can be revealed by a double-immunostaining for MIF and endogenous early endosome antigen 1 (EEA1, early endosome marker), Rab5 (early endosome marker), Rab7 (late endosome marker), or caveolin-1 (Wieffer *et al.*, 2009). Localisation of gold nanoparticle-conjugated MIF by using transmission electron microscopy might be useful to confirm the MIF internalisation route.

6.2.2.5. MIF-caveolin/lipid raft axis plays a role in inflammation and migration

Interestingly, MIF was shown to support the assembly of 'signalling platforms' of caveolin-1-rich lipid rafts in less than an hour (Reidy *et al.*, 2013) by enriching caveolin, upregulating extracellular signal-regulated kinase 1/2 (ERK1/2) and interleukin-8 (IL-8), and intensifying inflammation. In a model of epithelial infection, *P. aeruginosa* – known to enter the epithelium in a caveolin-1-dependent fashion – upregulated trimeric MIF in lipid rafts to facilitate its cellular up-take (Reidy *et al.*, 2013). Data derived from this thesis show that lipid raft/caveolae-dependent endocytosis of MIF might mediate MIF's upregulation of WT and $CD44^+/CD74^+$ COS-7/M6 cell chemokinesis. While Reidy *et al.* base their conclusions largely on siRNA-mediated silencing of MIF and caveolin, they do provide evidence that recombinant MIF N101C (almost exclusively a locked trimer) more than MIF WT (more monomeric than trimeric) increases IL-8 synthesis in primary human corneal

epithelial cells. Neither recombinant MIF N101C nor MIF WT were tested for their ability to upregulate caveolin in lipid rafts. Therefore, it is not unlikely that exogenous MIF causes enrichment of caveolin-1 platforms in COS-7/M6 cells and upregulates ERK1/2. If this alternative explanation were correct, MIF could upregulate motility of COS-7/M6 cells without being internalised.

In fact, the study of Shi *et al.* (2006) reported that MIF stimulation of COS-7/M6 cells does not lead to ERK1/2 phosphorylation within 30 min. This result was confirmed in this thesis but MIF still upregulated the chemokinesis of COS-7/M6 cells in assays that lasted 3.5 h. Thus one can speculate that an axis involving MIF and caveolin-1 leads to enhanced motility via signalling cascades other than ERK1/2.

More intriguingly, MIF was shown to stabilise Rac1 – a master regulator of actin cytoskeleton and driver of cell migration (see Introduction, Figure 5) – in caveolin-1-rich lipid rafts and, hence, upregulates invasion of A549 adenocarcinoma cells (Rendon *et al.*, 2007). More specifically, Rendon *et al.* showed that MIF is pro-invasive in A549 adenocarcinoma cells and its inhibition either by siRNA or ISO-1 is a viable therapeutic approach. Mechanistically, evidence was provided that MIF stabilises Rac1 in the plasma membrane and facilitates Rac1 GTP loading and effector binding. That Rac1 from MIF-deficient cells inherently cannot be loaded with GTP points to the fact that Rac1 cannot dissociate from its inhibitor RhoGDI which holds Rho GTPases such as Rac1 in an inactive, GDP-bound state (see Introduction, Figure 5). Moreover, MIF depletion redistributes flotillin-2 and caveolin, two markers of lipid rafts, to non-raft fractions. Taken together these findings suggest that an axis involving MIF-Rac1-caveolae-RhoGDI could explain the observed effects in WT COS-7/M6 fibroblasts. Remarkably, RhoGDI, is not only a putative MIF interactor (see Introduction, Table 2) but also a negative regulator of Rac1 (see Introduction, Figure 5).

Recently, MIF overexpression has been reported to directly induce caveolin-1 phosphorylation, which enables HMGB1 release and subsequent $CD11b^{+}$ cell recruitment in the context of breast cancer metastasis (Lv *et al.*, 2016). This finding is interesting

because $CD11b^+$ cells are innate immunity cells including monocytes/macrophages, providing evidence for a yet another MIF-macrophage signalling pathway.

Combined, all previous studies on the MIF-caveolin axis (Rendon *et al.*, 2007; Reidy *et al.*, 2013; Lv *et al.*, 2016) point to the fact that a MIF-caveolin/lipid raft signalling cascade may be active independent of MIF's classical CD74 receptor.

Alternatively, G-protein coupled receptor (GPCR)-elicited signalling has been implicated in MIF-mediated motility and could help to explain some of the findings of this work. As COS-7/M6 cells are weakly positive for a member of the GPCR family, CXCR4 (Cai *et al.*, 2012), it is possible that MIF-mediated upregulation of chemokinesis is due to downstream CXCR4 signalling. Moreover, CXCR4-mediated endocytosis followed by MIF release into the cytoplasm could explain how MIF is internalised independent of CD44/CD74. In fact, in CD74-negative but CXCR4-positive HEK293 cells, a CXCR4-specific inhibitor AMD3100 inhibits MIF internalisation by 40% (Schwartz *et al.*, 2012). Moreover, CXCR4 resides in lipid rafts in human PC-3 prostate cancer cells (Wong *et al.*, 2014) as well as in human monocytes described in one report (Triantafilou *et al.*, 2002) but not in similarly obtained human PBMCs described elsewhere (Kozak *et al.*, 2002). This line of questioning merits further attention as it would explain why WT COS-7/M6 cells are responsive to MIF.

While D-DT binds CD74, nothing is known about a D-DT-CXCR4 axis. Because D-DT upregulates motility of $CD44^+/CD74^+$ COS-7/M6 but not WT COS-7/M6 cells, it would be unlikely that a receptor such as CXCR4 in WT COS-7/M6 suffices to transduce D-DT-triggered signalling. In fact, D-DT classically engages its two receptors in $CD44^+/CD74^+$ COS-7/M6 cells and transduces the signal downstream. This finding is in line with the *in vitro* actin assembly assays where MIF but not D-DT slowed down the rate of actin assembly (section 6.4).

Taken together, WT but not enzymatically-inactive MIF upregulates motility of fibroblasts independent of its receptors, and possibly due to lipid raft-mediated endocytosis or signalling. Additionally, MIF's structural and functional homologue, D-DT does require its receptors for upregulating motility of fibroblasts, suggesting it uses its orthodox D-DT-

CD74/CD44-Src-ERK1/2 signalling pathway. Mechanistically, the fact that MIF upregulates motility independent of its CD44/CD74 receptors suggests a cytoplasmic rather than an extracellular function, or a presence and action of an unknown receptor. Since the dynamic rearrangements of the actin cytoskeleton are fundamental to driving cell motility, the idea that MIF directly influences actin was further tested.

6.3. Chemokinesis and actin staining upon MIF stimulation

Cells maintained under ordinary culture conditions exhibit a variety of actin structures such as fibres spanning across the cytoplasm, cortical rims around the plasma membrane (Hall, 1998), and nuclear actin playing a role in the serum response (Baarlink *et al.*, 2013). Under starvation, stress fibres disappear whereas cortical rims become more prominent. Conversely, re-introduction of serum or serum components brings back stress fibres. It was hypothesised that MIF may mimic the effects of serum on the fibroblast cytoskeleton.

To observe whether MIF rearranges the actin cytoskeleton, phalloidin stainings of actin stress fibres (filamentous actin) in WT COS-7/M6 cells were employed. MIF rescued the starvation-induced loss of actin stress fibres, as compared to the heat-inactivated protein. This result is in line with the finding that MIF stimulation of B cells leads to actin polymerisation (Klasen *et al.*, 2014) and the fact that $MIF^{-/-}$ bone marrow-derived macrophages (BMDMs) exhibit fewer chemokine-induced stress fibres (Fan *et al.*, 2011) but extends it for the first time to fibroblast-like cells.

Heterogeneity of cells is noticeable not only in the random motility assays but also in actin stainings. In random motility assays, a certain population of cells was observed to remain non-motile with or without stimulus, but a significantly larger amount of cells appeared to be responsive to MIF/D-DT. Same holds true for phalloidin-stained actin cytoskeleton, as some cells appeared to maintain their starvation phenotype (cortical rim) but statistically significantly, more cells exhibited prominent stress fibres. One possible explanation is a local auto- or paracrine effect. Enhanced cell motility as well as prominent stress fibres might be triggered first by MIF/D-DT, and secondarily by other factors such as secreted EGF.

All experiments were performed under reduced-serum conditions (0.5% (v/v) FCS) thus diminishing proliferation and excluding the effect of cell growth. If starving the cells were undesirable, another experimental approach would include the use of mitomycin C to arrest the cell cycle – allowing the cells to stay at 10% (v/v) FCS.

It is worth mentioning that starvation itself can induce morphological changes such as loss of stress fibres in cells. Moreover, starvation upregulates endocytosis (Mueller *et al.*, 2015) and autophagy (Russell *et al.*, 2014). As such, it may facilitate the uptake of membrane proteins/extracellular factors such as recombinant proteins, thus partially contributing to effects observed here. Notably, D-DT and some MIF substitution mutants did not induce chemokinesis in WT COS-7/M6 cells, pointing to the fact that the observed phenomena are stimulus-specific. Were they artefacts, any exogenously added polypeptide such as MIF point-mutant or D-DT would stimulate motility.

6.4. Actin and microtubule assembly

6.4.1. MIF induces F-actin stress fibre formation in WT COS-7/M6 cells

Encouraged by the findings that (*a*) MIF steers WT COS-7/M6 cell chemokinesis independent of CD44/CD74, (*b*) MIF promotes actin stress-fibre formation in the same cells, and (*c*) MIF/D-DT putatively interact with many actin cytoskeleton-associated proteins in NIH 3T3 fibroblasts, the MIF-actin axis was further investigated by two *in vitro* actin assembly assays.

The first assay used fully reconstituted components needed for the actin assembly including monomeric pyrene-actin, purified seven-subunit ARP2/3 complex, and VCA domain as an actin assembly inducer. Hypothesising that MIF/D-DT directly interact with one of the ARP2/3 proteins, MIF/D-DT were tested for their ability to alter the rate of pyrene-actin polymerisation *in vitro*. However, neither MIF nor D-DT influenced actin polymerisation, making it unlikely that a direct MIF-ARP2/3 or MIF-VCA interaction accelerates or slows down the rate of actin assembly occurring *in vivo*. More importantly, when a HEK293 cell extract was used as a source for the ARP2/3 complex instead of purified and reconstituted components of ARP2/3, MIF but not D-DT slowed down the rate of VCA-induced actin assembly. The conclusion of those experiments can be based on

prior research on capping proteins which provides insight into the physiological mechanism of how motility might be promoted while the rate of actin assembly is slowed down. Once a capping protein binds the fast-growing end of an actin filament, it prevents its further out-growth (typically within the lamellipodium, i.e. in the direction of cell movement). While this particular pre-existing actin filament is no longer extended, the remaining available pool of G-actin can be used to build up new actin filaments. Ultimately, the capping of one filament *promotes* the generation of more branching events nearby and thus results in the extension of new filaments within the lamellipodium (Mejillano *et al.*, 2004; Akin and Mullins, 2008; Edwards *et al.*, 2014).

If MIF slowed down the rate of actin assembly by a mechanism akin to that of a capping protein, it eventually could also enhance the build-up of new actin filaments and therefore promote cell motility, as observed in MIF-triggered (*a*) upregulation of COS-7/M6 cell chemokinesis and (*b*) actin polymerisation in the same cells.

This thesis provides a rationale for a new line of questioning in which MIF may function as a chaperone for cytoskeletal proteins. Specifically, monomeric MIF has an exposed hydrophobic face (Israelson *et al.*, 2015) or patch (Sun *et al.*, 1996) which may have affinity towards other proteins and confers a chaperoning role. To illustrate this, MIF was shown to be chaperone for superoxide dismutase 1 (SOD1) in the context of amyotrophic lateral sclerosis as it prevents aggregation of misfolded SOD1 (Israelson *et al.*, 2015). As such, during fast actin turnover at the leading edge of a migrating cell, MIF could help to protect certain cytoskeleton-associated proteins from degradation, resulting in a net movement forward.

6.4.2. Actin and microtubule (MT) assembly

Which cytoskeletal components drive cell motility is cell-specific. In glioblastoma cells it is not actin but MTs that are solely responsible for motility (Panopoulos *et al.*, 2011). Migration of fibroblast and fibroblast-like cells such as COS-7/M6 is actin-dependent but also requires cell polarisation whereby the MT-organising centre is localised between the leading edge and the nucleus. In PtK1 cells, Rac1 coordinates both actin and MTs to drive cell migration (Wittmann *et al.*, 2003).

To broaden our understanding of the mode of action of MIF, a hypothesis could be tested that MIF affects the network of MTs. While MIF promotes excessive MT polymerisation (Frascaroli *et al.*, 2009; Preau *et al.*, 2013), it remains to be determined whether MIF directly modifies MT assembly by performing *in vitro* MT assembly assays. Earlier studies on the MIF-MT axis used crude extracts of MIF derived from guinea pig lymph nodes (McCarthy *et al.*, 1979). Today, not only highly purified, endotoxin-free MIF, but also point mutants such P2A, Δ4 and C60S can be produced, and tested in *in vitro* MT assembly assays.

6.5. Future perspectives

The implications of this work extend into many research areas.

In a screen for a MIF receptor, a cDNA library originating from a human monocytic leukaemia cell line (THP-1) was expressed in COS-7 cells (Leng *et al.*, 2003). While CD74 was identified as a candidate with MIF binding capacity, that study did not identify any other CD44 molecule nor C-X-C receptors on the surface of THP-1 monocytes. In adult T-cell leukemia 2 (ATL-2) cells, thioredoxin was described to be internalised simultaneously with MIF (Son *et al.*, 2009), but the presence of CD74 or CXCRs within that MIF-thioredoxin complex was not evaluated. In U87 human glioblastoma cells, MIF binds EGFR but it is unknown whether a hypothetical CD74/EGFR heterodimer forms as well. In addition, COS-7 cells are marginally positive for CXCR4 (Cai *et al.*, 2012) which might transduce some of MIF's actions. Furthermore, not every study evaluated the status of MIF receptors (see Introduction, Figure 3A-B). All of this fragmentary evidence points to the fact that there exists yet another MIF receptor, or a novel internalisation route.

If MIF upregulates chemokinesis of WT COS-7/M6 cells, this mechanism could involve (*a*) MIF phosphorylating caveolin-1 (Lv *et al.*, 2016) or (*b*) MIF being endocytosed via lipid rafts, possibly via CXCR4 or a yet-unidentified receptor. MIF could be attracted to a lipid raft by its hydrophobic patch in order to bind the plasma membrane, a process similar to that observed elsewhere (Bagnat *et al.*, 2000; Peng *et al.*, 2005). Upon MIF recruitment to the lipid raft, neighbouring rafts could be recruited (*a*) to provide a larger platform for

downstream cytoplasmic signalling but possibly also (*b*) to mediate MIF internalisation (Simons and Toomre, 2000).

Provided exogenous MIF is endocytosed and localises within an endosome, it could either undergo lysosomal degradation or endosomal escape. While cellular trafficking such as endosomal escape has been extensively studied in the context of small-molecule drug delivery, gene/siRNA delivery, and viral infections, not much data and technological advances exist in terms of polypeptide/protein endosomal escape. Only last year has seen a major step forward when aurein 1.2, a 13-residue peptide, has been described to increase non-endosomal protein delivery in mammalian cells (Li *et al.*, 2015). It was found in a screen using superpositively charged GFP (+36 GFP) based on a premise that positively-charged proteins have an intrinsic capacity to be taken up by cells and undergo endosomal escape, effectively evading the proteasomal degradation (Li *et al.*, 2015).

Speculating that MIF has reached the cytosol, MIF could be interacting with a variety of actin cytoskeleton associated proteins. In fact, cytoplasmic MIF localises to the cell periphery in live epithelial HeLa (Kleemann *et al.*, 2000a) and fibroblast-like NIH 3T3 cells (Filip *et al.*, 2009). It also appears to be enriched in the pseudopodial fraction of cells undergoing chemotaxis. After mechanical removal of the cell body, pseudopodia remaining within a 3-µm Transwell® membrane were washed out and MIF was found within the pseudopodial proteome (Lin *et al.*, 2004). However, excimer laser ablation – a technique much more precise than mechanical removal of the cell body – did not corroborate that finding (Ito *et al.*, 2012). Still one could speculate that such a locally-available pool of MIF molecules – either cytoplasmic or recently endocytosed – might be ready to influence the actin network either at the leading edge or within the pseudopodia.

Point or deletion mutants of D-DT would shed more light on the action of D-DT. Further investigation on D-DTL – a D-dopachrome tautomerase-like protein identified within the human proteome (UniPROT ID A6NHG4) – might expand the MIF superfamily. Furthermore, four other *D-DT* genes were recently described (Premzl, 2015). If cells

positive for novel D-DTs could be identified, a question could be asked whether altered physiological levels of novel D-DTs affect cell motility.

While current MIF research community largely focuses on novel MIF/D-DT gene products such as invertebrate MIF orthologues (Furukawa *et al.*, 2016) as well as novel therapeutic approaches in humans (Roger *et al.*, 2016), this thesis emphasises the importance of further delineation of MIF/D-DT signalling axes at a cellular level in fibroblasts. Further identification of novel MIF receptor(s) or internalisation routes could help to better understand the roles of secreted versus intracellular MIF/D-DT.

6.6. Summary of the discussion

Full-length, enzymatically-active MIF promotes cell motility independent of CD44/CD74. This may be due to the fact that it is endocysed in a novel, perhaps a non-receptor mediated way, and thus acts intracellularly. Such an explanation would be in line with the MIF/D-DT interactome data (see Introduction, Table 2) which revealed that MIF/D-DT putatively interact with actin cytoskeleton-related proteins. Alternatively, there might be an unidentified MIF receptor – a GPCR such as CXCR4 or a growth factor receptor such as EGFR – that transduces MIF's downstream signalling in WT COS-7/M6 cells.

Although D-DT is a functional and structural homologue of MIF, the fact that it requires CD44 and CD74 for upregulation of COS-7/M6 cell chemokinesis may stem from the fact that it necessarily needs the classical CD44/CD74-Src-ERK1/2 axis to exhibit its biological effects. In support of this theory, it may be that unlike MIF, D-DT is not endocytosed at all and hence cannot act cytoplasmatically. Such an interpretation is corroborated by the fact that unlike MIF, D-DT did not affect the rate of *in vitro* actin assembly. As an alternative, D-DT may be not as robust as MIF with respect to fibroblast-like cells; in other words, circulating or other resident MIF receptor-negative cells may be highly responsive to D-DT.

While MIF and D-DT were both described to synergistically participate in ccRCC wound healing (Pasupuleti *et al.*, 2014), these cancer cells may exhibit different features than simian fibroblasts. Unlike this thesis, other studies did not address the mode of action of

D-DT on motility of fibroblast-like cells, and certainly more studies are needed to elucidate the role of D-DT in migrating cells.

Fibroblasts are accessory cells that migrate towards the wound and secrete ECM constituents to promote tissue repair. Stromal fibroblasts are known to steer the collective invasion of carcinoma cells – themselves being incapable of invasion – in an integrin- and protease-dependent fashion (Gaggioli *et al.*, 2007), and making them an attractive therapy target and justifying more research on their migratory capacity. MIF promotes the migration of fibroblasts (MEFs) in the migratory phase of wound healing (Dewor *et al.*, 2007). More precisely, short-term but not long-term treatment with MIF stimulates motility of fibroblasts. Conversely, MIF inhibits cancer-associated fibroblast (CAF) in a rhabdomyosarcoma environment (Tarnowski *et al.*, 2010). Based on this thesis, a novel piece of the puzzle is added, as MIF does not require its receptors for upregulation of COS-7/M6 cell motility. It would be clinically relevant to characterise patient-derived CAFs for their CD44/CD74 and CXCRs expression pattern, and subsequently test their responsiveness to MIF/D-DT.

This work builds upon previous studies that showed MIF-mediated upregulation of MEF would healing and extends them by investigating MIF's homologue – D-DT. It also broadens the current knowledge on COS-7/M6 as it seems that receptors are required for D-DT- but not MIF-triggered two-dimensional cell motility (Figure 25).

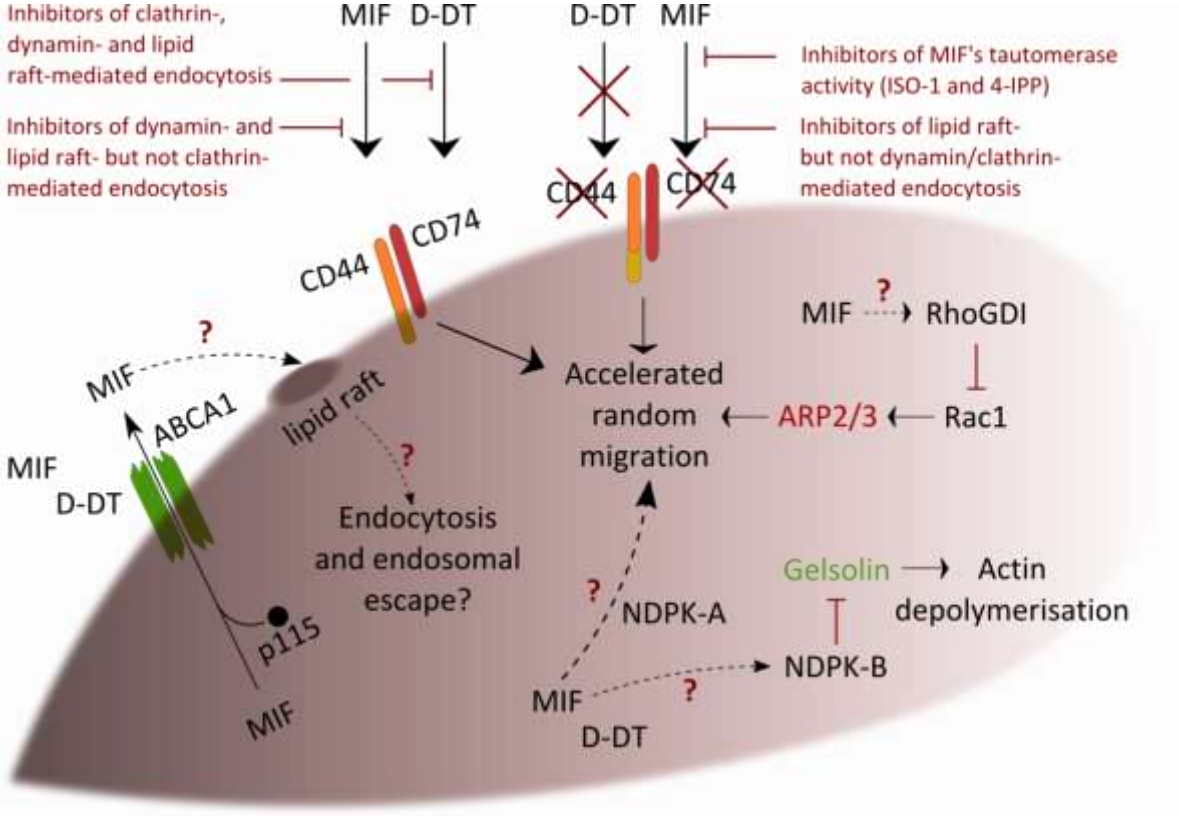

Figure 25. Hypothetical model of how MIF/D-DT affect cell migration based on data from this thesis. MIF but not D-DT facilitates receptor-negative WT COS-7/M6 cell chemokinesis, suggesting either a cytoplasmic role for MIF or lipid raft-mediated signalling. Conversely, D-DT engages CD44/CD74 to upregulate WT COS-7/M6 chemokinesis, consistent with earlier reports (Merk *et al.*, 2011). As not only receptors but also clathrin and dynamin are required for MIF-mediated modulation of intracellular signalling (Schwartz *et al.*, 2009; Xie *et al.*, 2011), inhibitors of clathrin and dynamin abrogated MIF's and D-DT's induction of chemokinesis in receptor-positive cells. In receptor-negative cells only the inhibition of lipid raft-associated endocytosis abolished MIF-induced chemokinesis, again indicative of either a novel MIF internalisation route via lipid rafts and subsequent endosomal escape, the presence of a yet-unidentified MIF receptor, or specific lipid raft/caveolin-mediated signalling. In line with those cell-culture results, MIF but not D-DT decreases the rate of monomeric (globular) actin assembly into filamentous actin in *in vitro* actin assembly assays using HEK293 total cell extracts as ARP2/3 donor, suggesting a novel role for MIF in directly influencing the actin cytoskeletal machinery for driving cell motility.

7. Appendix

Appendix 1. Summary of all chemokinesis results along with the statistical analyses**.**

COS-7/M6 cell line	Stimulation	Median velocity [µm/min]	Mean velocity ± SD (95% CI) [µm/min]	Significance
WT	NT	0.07	0.10 ± 0.09 (0.09, 0.11)	-
$CD44^+/CD74^+$	NT	0.08	0.10 ± 0.07 (0.09, 0.11)	-
WT	EGF (vs. NT)	0.14	0.18 ± 0.14 (0.16, 0.19)	***
$CD44^+/CD74^+$	EGF (vs. NT)	0.11	0.16 ± 0.13 (0.15, 0.18)	***
WT	MIF (vs. NT/boiled MIF)	0.10	0.14 ± 0.11 (0.13, 0.15)	*** / *
$CD44^+/CD74^+$	MIF (vs. NT/boiled MIF)	0.11	0.14 ± 0.09 (0.13, 0.15)	*** / ***
WT	D-DT (vs. NT/boiled D-DT)	0.08	0.11 ± 0.09 (0.10, 0.12)	Ns / Ns
$CD44^+/CD74^+$	D-DT (vs. NT/boiled D-DT)	0.09	0.12 ± 0.10 (0.11, 0.13)	* / ***
WT	Boiled MIF (vs. NT)	0.08	0.12 ± 0.09 (0.10, 0.13)	Ns
$CD44^+/CD74^+$	Boiled MIF (vs. NT)	0.08	0.10 ± 0.08 (0.09, 0.10)	Ns
WT	Boiled D-DT (vs. NT)	0.07	0.10 ± 0.09 (0.09, 0.11)	Ns
$CD44^+/CD74^+$	Boiled D-DT (vs. NT)	0.07	0.09 ± 0.07 (0.08, 0.90)	**
WT	MIF + D-DT (vs. NT)	0.09	0.12 ± 0.09 (0.11, 0.13)	***
$CD44^+/CD74^+$	MIF + D-DT (vs. NT)	0.10	0.12 ± 0.10 (0.12, 0.13)	***
WT	Boiled MIF + boiled D-DT (vs. NT/MIF + D-DT)	0.08	0.11 ± 0.10 (0.10, 0.13)	Ns / Ns
$CD44^+/CD74^+$	Boiled MIF + boiled D-DT (vs. NT/MIF + D-DT)	0.07	0.09 ± 0.07 (0.08, 0.10)	** / ***
WT	NT	0.08	0.09 ± 0.05 (0.09, 0.10)	-
WT	MIF (vs. NT)	0.10	0.12 ± 0.07 (0.11, 0.13)	***
WT	MIF C60S (vs. NT)	0.08	0.10 ± 0.06 (0.10, 0.11)	*
WT	NT	0.07	0.08 ± 0.06 (0.08, 0.91)	-
WT	MIF (vs. NT)	0.09	0.11 ± 0.06 (0.10, 0.12)	***
WT	MIF Δ4 (vs. NT)	0.06	0.07 ± 0.05 (0.07, 0.08)	Ns
WT	MIF P2A (vs. NT)	0.07	0.08 ± 0.04 (0.07, 0.08)	Ns
WT	NT	0.07	0.09 ± 0.07 (0.08, 0.10)	-
WT	MIF + EtOH	0.09	0.12 ± 0.09 (0.11, 0.13)	-
WT	MIF (vs. NT)	0.08	0.11 ± 0.09 (0.10, 0.12)	***
WT	MIF + 4-IPP (vs. MIF + EtOH)	0.07	0.09 ± 0.06 (0.08, 0.10)	***
WT	MIF + ISO-1 (vs. MIF + EtOH)	0.07	0.09 ± 0.08 (0.08, 0.10)	***
WT	NT	0.09	0.12 ± 0.09 (0.10, 0.13)	-
WT	MIF (vs. NT)	0.12	0.16 ± 0.11 (0.14, 0.17)	***
WT	MIF siRNA (vs. NT)	0.08	0.10 ± 0.09 (0.09, 0.11)	Ns
WT	MIF siRNA + MIF (vs. MIF siRNA)	0.10	0.13 ± 0.09 (0.12, 0.14)	***
$CD44^+/CD74^+$	NT	0.11	0.14 ± 0.10 (0.13, 0.16)	-
$CD44^+/CD74^+$	MIF (vs. NT)	0.15	0.19 ± 0.13 (0.17, 0.21)	***
$CD44^+/CD74^+$	MIF siRNA (vs. NT)	0.09	0.11 ± 0.09 (0.10, 0.13)	**
$CD44^+/CD74^+$	MIF siRNA + MIF (vs. MIF siRNA)	0.11	0.14 ± 0.10 (0.13, 0.16)	***

95% CI is the lower and upper 95% CI of the mean. All stimulations with recombinant proteins, MIF's tautomerase activity inhibitors, and ethanol were performed at 0.5% (v/v) FCS. NT denotes 0.5% (v/v) FCS without any exogenous compound. The treatments are statistically compared towards respective NT controls, not an overall mean of all NT values ever generated (colour coding). **Abbreviations**: **CI**, confidence interval; **EtOH**, ethanol; **SD**, standard deviation. **Significance levels**: **ns**, non-significant ($p > 0.05$); *, $p \leq 0.05$; **, $p \leq 0.01$; ***, $p \leq 0.001$.

8. Acknowledgements

Most of all I am indebted to Prof. Andreas Meinhardt for welcoming me in his research group and providing financial and academic support and a positive attitude during my stay, and Dr. Jörg Klug for his day-to-day supervision, discussions, and vast knowledge. I would like to thank all the past and present lab members: Eva, Farhad, Ferial, Jan-Per, Magdalena, Monika, Pia, Pradeep, Suada, Sudhanshu, Tali, Tim and Zhengguo. I would like to especially thank Suada for her technical assistance with recombinant protein preparation within our project on RPS19 and valuable comments on many techniques.

I express my gratitude to Prof. Robert Grosse (Institute for Pharmacology, Faculty of Medicine, Phillips University Marburg) for generously allowing me to carry out a rotation in his group, for data discussions, and supplying multiple materials and techniques. I appreciate the help of Alekya, Andrea, Dominique, Eva, Haicui, Ivana, Javier, Jessica, Katharina, Kathrin, Laura, Marga, Maria, Matthias, Michael, Pilar, Tanja, Vladimir and Ying.

The following collaborators are gratefully acknowledged (Faculty of Medicine, JLU, unless otherwise indicated): Prof. Klaudia Giehl (Molecular Oncology of Solid Tumours) for reagents, project discussions, and assistance with experiments, and Mr Dirk Lohfink for his technical assistance; Prof. Wolfgang Kummer (Institute for Anatomy and Cell Biology) for allowing me to use the Zeiss fluorescence microscope; Prof. Richard Bucala (School of Medicine, Yale University, New Haven, CT, USA) for WT COS-7/M6 cells and bacteria transformed with plasmids encoding CD44s and CD74; Haicui Wang PhD for various reagents and data collection in pilot *in vitro* actin assembly assays; Prof. Dr. Jan Faix and Mr Moritz Winterhoff (Department of Biophysical Chemistry, Hannover Medical School, Hannover) for *in vitro* actin assembly assays, and for their assistance with data analysis; Antje Banning PhD and Prof. Ritva Tikkanen (Institute for Biochemistry) for recombinant EGF; Prof. Małgorzata Wygrecka (Institute for Biochemistry) for recombinant IGF-I; and PD Dr. Mike Althaus (Institute for Animal Physiology, Faculty of Biology and Chemistry, JLU) for thesis editing as well as various reagents and materials. This work was supported by intramural funding from the Faculty of Medicine of the Justus Liebig University Giessen.

9. Summary in English

Macrophage migration inhibitory factor (MIF) and D-dopachrome tautomerase (D-DT) are paralogous pro-inflammatory cytokines. Whereas cytosolic MIF plays a role in cell cycle progression, secreted MIF and D-DT activate second messenger signalling through a CD44/CD74 receptor complex. Using an interactome screen, cytosolic MIF/D-DT were found to interact with many actin cytoskeleton-associated proteins in NIH3T3 fibroblasts suggesting a direct involvement of MIF/D-DT in modulating cell motility, but whether the receptors are indispensable for mediating motility remains elusive. To differentiate between receptor- and non-receptor-mediated events, COS-7/M6 fibroblasts deficient in CD44/CD74 (WT) and stable cell lines expressing CD44 and CD74 were generated. Chemokinesis (random single-cell motility) was assessed in cells stimulated with recombinant MIF/D-DT, mutated forms of MIF, inhibitors of MIF's tautomerase activity, and inhibitors of clathrin- and non-clathrin-dependent endocytosis. Due to low D-DT's tautomerase activity, ISO-1/4-IPP were not tested with D-DT. In the presence of CD44/CD74, both MIF and D-DT stimulated chemokinesis but only MIF enhanced chemokinesis in the absence of receptors. The stimulatory effect of MIF on migration depended on its tautomerase activity and lipid raft/caveolae-mediated – but not clathrin-mediated – endocytosis. To observe a direct effect of MIF and D-DT on actin dynamics, actin polymerization was measured in an *in vitro* actin assembly assay. MIF but not D-DT decreased the rate of F-actin assembly. By decreasing the rate of cell extract-driven actin assembly, MIF phenocopies the function of F-actin capping proteins. Moreover, stimulation with MIF increased the number of prominent F-actin stress fibres in COS-7/M6 WT. Taken together, MIF stimulates fibroblast chemokinesis independent of the status of its cell-surface receptors, likely by directly modulating the actin cytoskeleton. MIF-mediated chemokinesis appears to depend on lipid raft/caveolae-mediated endocytosis. D-DT triggers chemokinesis only in the presence of MIF/D-DT receptors – CD44/CD74 – implying D-DT requires the classical receptor-driven second-messenger transduction pathway.

10. Summary in German (Zusammenfassung auf Deutsch)

Macrophage migration inhibitory factor (MIF) und *D-dopachrome tautomerase* (D-DT) sind paraloge pro-inflammatorische Zytokine. Zytosolisches MIF spielt bei der Progression des Zellzyklus eine Rolle, während sekretiertes MIF und D-DT intrazelluläre Signalkaskaden über eine Aktivierung eines CD44/CD74 Rezeptorkomplexes modulieren können. Mittels Interaktom-Screening in NIH3T3 Fibroblasten wurde gefunden, dass zytosolisches MIF/D-TT mit Zytoskelett-assoziierten Proteinen interagiert. Darauf basierend wurde postuliert, dass MIF/D-DT die Motilität von Zellen moduliert. Ob hier eine Aktivierung der Membranrezeptoren eine Rolle spielt, ist bislang unbekannt. Um zwischen Rezeptor-vermittelten und Rezeptor-unabhängigen Mechanismen zu unterscheiden, wurden CD44/CD74-defiziente COS-7/M6 Fibroblasten (WT) verwendet, sowie Zelllinien erzeugt, welche stabil CD44 und CD74 exprimieren. Chemokinese (*random single-cell motility*) wurde an Zellen untersucht, die mit rekombinantem MIF/D-DT, mutierten Formen von MIF, Inhibitoren der Tautomerase-Aktivität von MIF, sowie Inhibitoren von Clathrin-abhängiger und Clathrin-unabhängiger Endozytose, stimuliert wurden. Aufgrund der geringen D-DT Tautomeraseaktivität, ISO-1/4-IPP wurden nicht mit D-DT getestet. In der Anwesenheit von CD44/CD74 stimulierten sowohl MIF als auch D-DT die Chemokinese, allerdings war nur MIF hierbei in der Lage, in Abwesenheit der Rezeptoren zu stimulieren einen stimulierenden Einfluss auf die Chemokinese auszuüben. Der stimulierende Effekt von MIF basierte auf dessen Tautomerase-Aktivität und wurde durch Lipid raft/Caveolae-abhängige – nicht jedoch Clathrin-abhängige – Endozytose vermittelt. Um einen möglichen direkten Effekt von MIF und D-DT auf die Aktin-Dynamik zu untersuchen, wurde mittels eines Aktin-Assemblierungs-Assays die Aktin-Polymerisation *in vitro* gemessen. MIF, nicht aber D-DT, verminderten die Assemblierungsrate von F-Aktin. Wahrscheinlich beruht dies auf einer *F-Actin Capping Protein*-analogen Funktion von MIF. Darüber hinaus führte die Stimulation mit MIF zu einer erhöhten Anzahl an prominenten F-Aktin Stressfasern in COS-7/M6 (WT) Zellen. Zusammengefasst stimulierte MIF die Chemokinese von Fibroblasten, unabhängig von Membranrezeptoren, über direkte Modulation des Aktin-Zytoskeletts. Die MIF-stimulierte Chemokinese basierte auf Lipid raft/Caveolae-abhängiger Endozytose. Dagegen stimulierte D-DT die Chemokinese nur in Anwesenheit der Membranrezeptoren CD44/CD74, was vermutlich auf einer klassischen Rezeptor- und *second messenger*-vermittelten Signalkaskade beruht.

11. Tabular CV

Der Lebenslauf wurde aus der elektronischen Version der Arbeit entfernt.

12. Declaration of Honour (Ehrenwörtliche Erklärung)

I declare that I have completed this dissertation single-handedly without the unauthorized help of a second party and only with the assistance acknowledged therein. I have appropriately acknowledged and referenced all text passages that are derived literally from or are based on the content of published or unpublished work of others, and all information that relates to verbal communications. I have abided by the principles of good scientific conduct laid down in the charter of the Justus Liebig University of Giessen in carrying out the investigations described in the dissertation.

_____ _____

Place, Date Signature

13. References

Akin, O., and Mullins, R. D. (2008). Capping Protein Increases the Rate of Actin-Based Motility by Promoting Filament Nucleation by the Arp2/3 Complex. Cell *133*, 841–851.

Al-Abed, Y. *et al.* (2005). ISO-1 binding to the tautomerase active site of MIF inhibits its pro-inflammatory activity and increases survival in severe sepsis. J. Biol. Chem. *280*, 36541–36544.

Al-Abed, Y., and VanPatten, S. (2011). MIF as a disease target: ISO-1 as a proof-of-concept therapeutic. Future Med. Chem. *3*, 45–63.

Alampour-Rajabi, S., El Bounkari, O., Rot, A., Muller-Newen, G., Bachelerie, F., Gawaz, M., Weber, C., Schober, A., and Bernhagen, J. (2015). MIF interacts with CXCR7 to promote receptor internalization, ERK1/2 and ZAP-70 signaling, and lymphocyte chemotaxis. FASEB J., 1–15.

Alourfi, Z., Donn, R. P., Stevens, A., Berry, A., McMaster, A., and Ray, D. W. (2005). Glucocorticoids suppress macrophage migration inhibitory factor (MIF) expression in a cell-type-specific manner. J. Mol. Endocrinol. *34*, 583–595.

Ashcroft, G. S., Mills, S. J., Lei, K., Gibbons, L., Jeong, M., Taniguchi, M., Burow, M., Horan, M. a, and Wahl, S. M. (2003). Estrogen modulates cutaneous wound healing by downregulating macrophage migration inhibitory factor. J. Clin. Invest. *111*, 1309–1318.

Baarlink, C., Wang, H., and Grosse, R. (2013). Nuclear actin network assembly by formins regulates the SRF coactivator MAL. Science *340*, 864–867.

Bacher, M., Eickmann, M., Schrader, J., Gemsa, D., and Heiske, A. (2002). Human cytomegalovirus-mediated induction of MIF in fibroblasts. Virology *299*, 32–37.

Bacher, M., Metz, C. N., Calandra, T., Mayer, K., Chesney, J., Lohoff, M., Gemsa, D., Donnelly, T., and Bucala, R. (1996). An essential regulatory role for macrophage migration inhibitory factor in T-cell activation. Proc. Natl. Acad. Sci. *93*, 7849–7854.

Bagnat, M., Keränen, S., Shevchenko, A., Shevchenko, A., and Simons, K. (2000). Lipid rafts function in biosynthetic delivery of proteins to the cell surface in yeast. Proc. Natl. Acad. Sci. U. S. A. *97*, 3254–3259.

Barrilleaux, B. L., Fischer-Valuck, B. W., Gilliam, J. K., Phinney, D. G., and O'Connor, K. C. (2010). Activation of CD74 inhibits migration of human mesenchymal stem cells. In Vitro Cell. Dev. Biol. Anim. *46*, 566–572.

Baugh, J. a., Gantier, M., Li, L., Byrne, A., Buckley, A., and Donnelly, S. C. (2006). Dual regulation of macrophage migration inhibitory factor (MIF) expression in hypoxia by CREB and HIF-1. Biochem. Biophys. Res. Commun. *347*, 895–903.

Beck, S., Simmet, T., Müller, I., Lang, F., and Gawaz, M. (2016). Gremlin-1 C-Terminus Regulates Function of Macrophage Migration Inhibitory Factor (MIF). Cell. Physiol. Biochem. *38*, 801–808.

Becker-Herman, S., Arie, G., Medvedovsky, H., Kerem, A., and Shachar, I. (2005). CD74 is a member of the regulated intramembrane proteolysis-processed protein family. Mol. Biol. Cell *16*, 5061–5069.

Bendrat, K., Al-Abed, Y., Callaway, D. J. E., Peng, T., Calandra, T., Metz, C. N., and Bucala, R. (1997). Biochemical and mutational investigations of the enzymatic activity of macrophage migration inhibitory factor. Biochemistry *36*, 15356–15362.

Bernhagen, J. *et al.* (2007). MIF is a noncognate ligand of CXC chemokine receptors in inflammatory and atherogenic cell recruitment. Nat. Med. *13*, 587–596.

Bernhagen, J., Calandra, T., Mitchell, R. A., Martin, S. B., Tracey, K. J., Voelter, W., Manogue, K. R., Cerami, A., and Bucala, R. (1993). MIF is a pituitary-derived cytokine that potentiates lethal endotoxaemia. Nature *365*, 756–759.

Bernhagen, J., Mitchell, R. A., Calandra, T., Voelter, W., Cerami, A., and Bucala, R. (1994). Purification, bioactivity, and secondary structure analysis of mouse and human macrophage migration inhibitory factor (MIF). Biochemistry *33*, 14144–14155.

Bloom, B. R., and Bennett, B. (1966). Mechanism of a reaction in vitro associated with delayed-type hypersensitivity. Science *153*, 80–82.

Bozza, M., Satoskar, A. R., Lin, G., Lu, B., Humbles, A. A., Gerard, C., and David, J. R. (1999). Targeted Disruption of Migration Inhibitory Factor Gene Reveals Its Critical Role in Sepsis. J. Exp. Med. *189*, 341–346.

Bradford, M. M. (1976). A rapid and sensitive method for the quantitation of microgram quantities of protein utilizing the principle of protein-dye binding. Anal. Biochem. *72*, 248–254.

Branzk, N., Lubojemska, A., Hardison, S. E., Wang, Q., Gutierrez, M. G., Brown, G. D., and Papayannopoulos, V. (2014). Neutrophils sense microbe size and selectively release neutrophil extracellular traps in response to large pathogens. Nat. Immunol. *15*, 1017–1025.

Brock, S. E., Rendon, B. E., Xin, D., Yaddanapudi, K., and Mitchell, R. A. (2014). MIF family members cooperatively inhibit p53 expression and activity. PLoS One *9*, e99795.

Bucala, R., and Donnelly, S. C. (2007). Macrophage Migration Inhibitory Factor: A Probable Link between Inflammation and Cancer. Immunity *26*, 281–285.

Buehler, E., Chen, Y. C., and Martin, S. (2012). C911: A Bench-Level Control for Sequence Specific siRNA Off-Target Effects. PLoS One *7*.

Bugyi, B., Didry, D., and Carlier, M.-F. (2010). How tropomyosin regulates lamellipodial actin-based motility: a combined biochemical and reconstituted motility approach. EMBO J. *29*, 14–26.

Bunnell, T. M., Burbach, B. J., Shimizu, Y., and Ervasti, J. M. (2011). Beta-Actin specifically controls cell growth, migration, and the G-actin pool. Mol. Biol. Cell *22*, 4047–4058.

Burks, E. a., Fleming, C. D., Mesecar, A. D., Whitman, C. P., and Pegan, S. D. (2010). Kinetic and structural characterization of a heterohexamer 4-oxalocrotonate tautomerase from chloroflexus aurantiacus J-10-fl: Implications for functional and structural diversity in the tautomerase superfamily. Biochemistry *49*, 5016–5027.

Cai, C., Rodepeter, F. R., Rossmann, A., Teymoortash, A., Lee, J.-S., Quint, K., DI Fazio, P., Ocker, M., Werner, J. a, and Mandic, R. (2012). SIVmac$_{239}$-Nef down-regulates cell surface expression of CXCR4 in tumor cells and inhibits proliferation, migration and angiogenesis. Anticancer Res. *32*, 2759–2768.

Calandra, T., Echtenacher, B., Roy, D. L., Pugin, J., Metz, C. N., Hültner, L., Heumann, D., Männel, D., Bucala, R., and Glauser, M. P. (2000). Protection from septic shock by neutralization of macrophage migration inhibitory factor. Nat. Med. *6*, 164–170.

Calandra, T., and Roger, T. (2003). Macrophage migration inhibitory factor: a regulator of innate immunity. Nat. Rev. Immunol. *3*, 791–800.

Cayli, S., Klug, J., Chapiro, J., Fröhlich, S., Krasteva, G., Orel, L., and Meinhardt, A. (2009). COP9 signalosome interacts ATP-dependently with p97/valosin-containing protein (VCP) and controls the ubiquitination status of proteins bound to p97/VCP. J. Biol. Chem. *284*, 34944–34953.

Chen, H.-R., Chuang, Y.-C., Chao, C.-H., and Yeh, T.-M. (2015). Macrophage migration inhibitory factor induces vascular leakage via autophagy. Biol. Open *4*, 244–252.

Chen, Y., Wang, S., Lu, X., Zhang, H., Fu, Y., and Luo, Y. (2011). Cholesterol sequestration by nystatin enhances the uptake and activity of endostatin in endothelium via regulating distinct endocytic pathways. Blood *117*, 6392–6403.

Chung, B. M., Rotty, J. D., and Coulombe, P. a. (2013). Networking galore: Intermediate filaments and cell migration. Curr. Opin. Cell Biol. *25*, 600–612.

Chung, H.-Y., Gu, M., Buehler, E., MacDonald, M. R., and Rice, C. M. (2014). Seed sequence-matched controls reveal limitations of small interfering RNA knockdown in functional and structural studies of hepatitis C virus NS5A-MOBKL1B interaction. J. Virol. *88*, 11022–11033.

Cole, R. (2014). Live-cell imaging. Cell Adh. Migr. *8*, 452–459.

Coleman, A. M., Rendon, B. E., Zhao, M., Qian, M., Bucala, R., Xin, D., and Mitchell, R. A. (2008). Cooperative regulation of non-small cell lung carcinoma angiogenic potential by macrophage migration inhibitory factor and its homolog, D-dopachrome tautomerase. J. Immunol. *181*, 2330–2337.

Cordeiro, J. V, and Jacinto, A. (2013). The role of transcription-independent damage signals in the initiation of epithelial wound healing. Nat. Rev. Mol. Cell Biol. *14*, 249–262.

Costa-Silva, B. *et al.* (2015). Pancreatic cancer exosomes initiate pre-metastatic niche formation in the liver. Nat. Cell Biol. *17*, 816–828.

Dewor, M., Steffens, G., Krohn, R., Weber, C., Baron, J., and Bernhagen, J. (2007). Macrophage migration inhibitory factor (MIF) promotes fibroblast migration in scratch-wounded monolayers in vitro. FEBS Lett. *581*, 4734–4742.

DiCosmo-Ponticello, C. J., Hoover, D., Coffman, F. D., Cohen, S., and Cohen, M. C. (2014). MIF inhibits monocytic movement through a non-canonical receptor and disruption of temporal Rho GTPase activities in U-937 cells. Cytokine *69*, 47–55.

Donà, E. *et al.* (2013). Directional tissue migration through a self-generated chemokine gradient. Nature *503*, 285–289.

Donnelly, S. C., Haslett, C., Reid, P. T., Grant, I. S., Wallace, W. a, Metz, C. N., Bruce, L. J., and Bucala, R. (1997). Regulatory role for macrophage migration inhibitory factor in acute respiratory distress syndrome. Nat. Med. *3*, 320–323.

Du, W., Wright, B. M., Li, X., Finke, J., Rini, B. I., Zhou, M., He, H., Lal, P., and Welford, S. M. (2012). Tumor-derived macrophage migration inhibitory factor promotes an autocrine loop that enhances renal cell carcinoma. Oncogene, 1–6.

Dwyer, M., Shan, Q., D'Ortona, S., Maurer, R., Mitchell, R., Olesen, H., Thiel, S., Huebner, J., and Gadjeva, M. (2014). Cystic Fibrosis Sputum DNA Has NETosis Characteristics and Neutrophil Extracellular Trap Release Is Regulated by Macrophage Migration-Inhibitory Factor. J. Innate Immun. *29*, 997–1003.

Eden, S., Rohatgi, R., Podtelejnikov, A. V, Mann, M., and Kirschner, M. W. (2002). Mechanism of regulation of WAVE1-induced actin nucleation by Rac1 and Nck. Nature *418*, 1–4.

Edwards, M., Zwolak, A., Schafer, D. a., Sept, D., Dominguez, R., and Cooper, J. a. (2014). Capping protein regulators fine-tune actin assembly dynamics. Nat. Rev. Mol. Cell Biol. *15*, 677–689.

Eickhoff, R., Wilhelm, B., Renneberg, H., Wennemuth, G., Bacher, M., Linder, D., Bucala, R., Seitz, J., and Meinhardt, A. (2001). Purification and characterization of macrophage migration inhibitory factor as a secretory protein from rat epididymis: evidences for alternative release and transfer to spermatozoa. Mol. Med. *7*, 27–35.

El-Turk, F. *et al.* (2012). Characterization of molecular determinants of the conformational stability of macrophage migration inhibitory factor: leucine 46 hydrophobic pocket. PLoS One *7*, e45024.

Faix, J., and Grosse, R. (2006). Staying in Shape with Formins. Dev. Cell *10*, 693–706.

Fan, C., Rajasekaran, D., Syed, M. A., Leng, L., Loria, J. P., Bhandari, V., Bucala, R., and Lolis, E. J. (2013). MIF intersubunit disulfide mutant antagonist supports activation of CD74 by endogenous MIF trimer at physiologic concentrations. Proc. Natl. Acad. Sci. U. S. A. *110*, 10994–10999.

Fan, H., Hall, P., Santos, L. L., Gregory, J. L., Fingerle-Rowson, G., Bucala, R., Morand, E. F., and Hickey, M. J. (2011). Macrophage migration inhibitory factor and CD74 regulate macrophage chemotactic responses via

MAPK and Rho GTPase. J. Immunol. *186*, 4915–4924.

Fan, H., Kao, W., Yang, Y. H., Gu, R., Harris, J., Fingerle-Rowson, G., Bucala, R., Ngo, D., Beaulieu, E., and Morand, E. F. (2014). Macrophage Migration Inhibitory Factor Inhibits the Antiinflammatory Effects of Glucocorticoids via Glucocorticoid-Induced Leucine Zipper. Arthritis Rheumatol. *66*, 2059–2070.

Faure-André, G. *et al.* (2008). Regulation of dendritic cell migration by CD74, the MHC class II-associated invariant chain. Science *322*, 1705–1710.

Fernandez-Cuesta, L. *et al.* (2014). CD74-NRG1 fusions in lung adenocarcinoma. Cancer Discov. *4*, 415–422.

Filip, A. M. *et al.* (2009). Ribosomal protein S19 interacts with macrophage migration inhibitory factor and attenuates its pro-inflammatory function. J. Biol. Chem. *284*, 7977–7985.

Fingerle-Rowson, G. *et al.* (2009). A tautomerase-null macrophage migration-inhibitory factor (MIF) gene knock-in mouse model reveals that protein interactions and not enzymatic activity mediate MIF-dependent growth regulation. Mol. Cell. Biol. *29*, 1922–1932.

Fingerle-Rowson, G., Petrenko, O., Metz, C. N., Forsthuber, T. G., Mitchell, R., Huss, R., Moll, U., Müller, W., and Bucala, R. (2003). The p53-dependent effects of macrophage migration inhibitory factor revealed by gene targeting. Proc. Natl. Acad. Sci. U. S. A. *100*, 9354–9359.

Fingerle-Rowson, G. R., and Bucala, R. (2001). Neuroendocrine properties of macrophage migration inhibitory factor (MIF). Immunol. Cell Biol. *79*, 368–375.

Fischer-Valuck, B. W., Barrilleaux, B. L., Phinney, D. G., Russell, K. C., Prockop, D. J., and O'Connor, K. C. (2009). Migratory response of mesenchymal stem cells to macrophage migration inhibitory factor and its antagonist as a function of colony-forming efficiency. Biotechnol. Lett. *32*, 19–27.

Flieger, O., Engling, A., Bucala, R., Lue, H., Nickel, W., and Bernhagen, J. (2003). Regulated secretion of macrophage migration inhibitory factor is mediated by a non-classical pathway involving an ABC transporter. FEBS Lett. *551*, 78–86.

Frascaroli, G., Varani, S., Blankenhorn, N., Pretsch, R., Bacher, M., Leng, L., Bucala, R., Landini, M. P., and Mertens, T. (2009). Human Cytomegalovirus Paralyzes Macrophage Motility through Down-Regulation of Chemokine Receptors, Reorganization of the Cytoskeleton, and Release of Macrophage Migration Inhibitory Factor. J. Immunol. *182*, 477–488.

Friedl, P. (2004). Prespecification and plasticity: Shifting mechanisms of cell migration. Curr. Opin. Cell Biol. *16*, 14–23.

Friedl, P., and Alexander, S. (2011). Cancer invasion and the microenvironment: Plasticity and reciprocity. Cell *147*, 992–1009.

Friedl, P., and Gilmour, D. (2009). Collective cell migration in morphogenesis, regeneration and cancer. Nat. Rev. Mol. Cell Biol. *10*, 445–457.

Funamizu, N. *et al.* (2012). Macrophage migration inhibitory factor induces epithelial to mesenchymal transition, enhances tumor aggressiveness and predicts clinical outcome in resected pancreatic ductal adenocarcinoma. Int. J. Cancer.

Furukawa, R., Tamaki, K., and Kaneko, H. (2016). Two macrophage migration inhibitory factors regulate starfish larval immune cell chemotaxis. Immunol. Cell Biol., 1–7.

Gaggioli, C., Hooper, S., Hidalgo-carcedo, C., Grosse, R., and Marshall, J. F. (2007). Fibroblast-led collective invasion of carcinoma cells with differing roles for RhoGTPases in leading and following cells. Nat. Cell Biol. *9*, 1392–1400.

Ganguly, A., Yang, H., Sharma, R., Patel, K. D., and Cabral, F. (2012). The role of microtubules and their dynamics in cell migration. J. Biol. Chem. *287*, 43359–43369.

Garcia-Mata, R., Boulter, E., and Burridge, K. (2011). The “invisible hand”: regulation of RHO GTPases by RHOGDIs. Nat. Rev. Mol. Cell Biol. *12*, 493–504.

Gilliver, S. C., Emmerson, E., Bernhagen, J., and Hardman, M. J. (2011). MIF: A key player in cutaneous biology and wound healing. Exp. Dermatol. *20*, 1–6.

Gluzman, Y. (1981). SV40-transformed simian cells support the replication of early SV40 mutants. Cell *23*, 175–182.

Godin, J. D. *et al.* (2012). P27Kip1 Is a Microtubule-Associated Protein that Promotes Microtubule Polymerization during Neuron Migration. Dev. Cell *23*, 729–744.

Goulimari, P., Kitzing, T. M., Knieling, H., Brandt, D. T., Offermanns, S., and Grosse, R. (2005). G-alpha12/13 is essential for directed cell migration and localized Rho-Dia1 function. J. Biol. Chem. *280*, 42242–42251.

Green, J. A., Stockton, R. a, Johnson, C., and Jacobson, B. S. (2004). 5-lipoxygenase and cyclooxygenase regulate wound closure in NIH/3T3 fibroblast monolayers. Am. J. Physiol. Cell Physiol. *287*, C373–C383.

Grieb, G., Kim, B.-S., Simons, D., Bernhagen, J., and Pallua, N. (2014). MIF and CD74 - suitability as clinical biomarkers. Mini Rev. Med. Chem. *14*, 1125–1131.

Grieb, G., Merk, M., Bernhagen, J., and Bucala, R. (2010). Macrophage migration inhibitory factor (MIF): a promising biomarker. Drug News Perspect. *23*, 257–264.

Guo, Z., Neilson, L. J., Zhong, H., Murray, P. S., Zanivan, S., and Zaidel-bar, R. (2014). E-cadherin interactome complexity and robustness resolved by quantitative proteomics. Sci. Signal. *7*, 1–13.

Gupta, Y., Pasupuleti, V., Du, W., and Welford, S. M. (2016). Macrophage Migration Inhibitory Factor Secretion Is Induced by Ionizing Radiation and Oxidative Stress in Cancer Cells. PLoS One *11*, e0146482.

Haan, C., and Behrmann, I. (2007). A cost effective non-commercial ECL-solution for Western blot detections yielding strong signals and low background. J. Immunol. Methods *318*, 11–19.

Hall, A. (1998). Rho GTPases and the actin cytoskeleton. Science *279*, 509–514.

Hanahan, D. (1983). Studies on transformation of Escherichia coli with plasmids. J. Mol. Biol. *166*, 557–580.

Harris, E. S., and Higgs, H. N. (2006). Biochemical analysis of mammalian formin effects on actin dynamics. Methods Enzymol. *406*, 190–214.

Heasman, S. J., and Ridley, A. J. (2008). Mammalian Rho GTPases: new insights into their functions from in vivo studies. Nat. Rev. Mol. Cell Biol. *9*, 690–701.

Heng, Y.-W., and Koh, C.-G. (2010). Actin cytoskeleton dynamics and the cell division cycle. Int. J. Biochem. Cell Biol. *42*, 1622–1633.

Hermanowski-Vosatka, A., Mundt, S. S., Ayala, J. M., Goyal, S., Hanlon, W. A., Czerwinski, R. M., Wright, S. D., and Whitman, C. P. (1999). Enzymatically inactive macrophage migration inhibitory factor inhibits monocyte chemotaxis and random migration. Biochemistry *38*, 12841–12849.

Hong, M.-Y., Tseng, C.-C., Chuang, C.-C., Chen, C.-L., Lin, S.-H., and Lin, C.-F. (2012). Urinary macrophage migration inhibitory factor serves as a potential biomarker for acute kidney injury in patients with acute pyelonephritis. Mediators Inflamm. *2012*, 381358.

Hsieh, C.-Y., Chen, C.-L., Lin, Y.-S., Yeh, T.-M., Tsai, T.-T., Hong, M.-Y., and Lin, C.-F. (2014). Macrophage migration inhibitory factor triggers chemotaxis of CD74+CXCR2+ NKT cells in chemically induced IFN-γ-mediated skin inflammation. J. Immunol. *193*, 3693–3703.

Hu, C. *et al.* (2015). MIF, secreted by human hepatic sinusoidal endothelial cells, promotes chemotaxis and outgrowth of colorectal cancer in liver prometastasis. Oncotarget *6*, 22410–22423.

Israelson, A. *et al.* (2015). Macrophage Migration Inhibitory Factor as a Chaperone Inhibiting Accumulation

of Misfolded SOD1. Neuron, 1–15.

Ito, A., Mimae, T., Yamamoto, Y.-S.-Z., Hagiyama, M., Nakanishi, J., Ito, M., Hosokawa, Y., Okada, M., Murakami, Y., and Kondo, T. (2012). Novel application for pseudopodia proteomics using excimer laser ablation and two-dimensional difference gel electrophoresis. Lab. Investig. *92*, 1374–1385.

Ivanov, A. I. (2008). Endocytosis and Exocytosis. In: Methods in Molecular Biology, 15–33.

Jin, Y., and Dai, Z. (2016). USO1 promotes tumor progression via activating Erk pathway in multiple myeloma cells. Biomed. Pharmacother. *78*, 264–271.

Johannes, L., Parton, R. G., Bassereau, P., and Mayor, S. (2015). Building endocytic pits without clathrin. Nat. Rev. Mol. Cell Biol. *16*, 311–321.

Jung, H., Seong, H. a., and Ha, H. (2008). Direct interaction between NM23-H1 and macrophage migration inhibitory factor (MIF) is critical for alleviation of MIF-mediated suppression of p53 activity. J. Biol. Chem. *283*, 32669–32679.

Kalluri, R., and Zeisberg, M. (2006). Fibroblasts in cancer. Nat. Rev. Cancer *6*, 392–401.

Kamir, D. *et al.* (2008). A Leishmania ortholog of macrophage migration inhibitory factor modulates host macrophage responses. J. Immunol. *180*, 8250–8261.

Kerschbaumer, R. J. *et al.* (2012). Neutralization of macrophage migration inhibitory factor (MIF) by fully human antibodies correlates with their specificity for the β-sheet structure of MIF. J. Biol. Chem. *287*, 7446–7455.

Kirchhausen, T., Macia, E., and Pelish, H. E. (2008). Use of Dynasore, the Small Molecule Inhibitor of Dynamin, in the Regulation of Endocytosis. Methods Enzymol. *438*, 77–93.

Kitamura, T., Qian, B.-Z., and Pollard, J. W. (2015). Immune cell promotion of metastasis. Nat. Rev. Immunol. *15*, 73–86.

Klasen, C. *et al.* (2014). MIF promotes B cell chemotaxis through the receptors CXCR4 and CD74 and ZAP-70 signaling. J. Immunol. *192*, 5273–5284.

Kleemann, R. *et al.* (2000a). Intracellular action of the cytokine MIF to modulate AP-1 activity and the cell cycle through Jab1. Nature *408*, 211–216.

Kleemann, R., Kapurniotu, A., Frank, R. W., Gessner, A., Mischke, R., Flieger, O., Jüttner, S., Brunner, H., and Bernhagen, J. (1998). Disulfide analysis reveals a role for macrophage migration inhibitory factor (MIF) as thiol-protein oxidoreductase. J. Mol. Biol. *280*, 85–102.

Kleemann, R., Kapurniotu, A., Mischke, R., Held, J., and Bernhagen, J. (1999). Characterization of catalytic centre mutants of macrophage migration inhibitory factor (MIF) and comparison to Cys81Ser MIF. Eur. J. Biochem. *261*, 753–766.

Kleemann, R., Rorsman, H., Rosengren, E., Mischke, R., Mai, N. T., and Bernhagen, J. (2000b). Dissection of the enzymatic and immunologic functions of macrophage migration inhibitory factor: Full immunologic activity of N-terminally truncated mutants. Eur. J. Biochem. *267*, 7183–7192.

von Kleist, L., and Haucke, V. (2012). At the Crossroads of Chemistry and Cell Biology: Inhibiting Membrane Traffic by Small Molecules. Traffic *13*, 495–504.

Knapek, K., Frondorf, K., Post, J., Short, S., Cox, D., and Gomez-Cambronero, J. (2010). The molecular basis of phospholipase D2-induced chemotaxis: elucidation of differential pathways in macrophages and fibroblasts. Mol. Cell. Biol. *30*, 4492–4506.

Koga, K., Kenessey, A., Powell, S. R., Sison, C. P., Miller, E. J., and Ojamaa, K. (2011). Macrophage migration inhibitory factor provides cardioprotection during ischemia/reperfusion by reducing oxidative stress. Antioxid. Redox Signal. *14*, 1191–1202.

Kozak, S. L., Heard, J. M., and Kabat, D. (2002). Segregation of CD4 and CXCR4 into distinct lipid microdomains in T lymphocytes suggests a mechanism for membrane destabilization by human immunodeficiency virus. J. Virol. *76*, 1802–1815.

Krause, M., Dent, E. W., Bear, J. E., Loureiro, J. J., and Gertler, F. B. (2003). Ena/VASP proteins: regulators of the actin cytoskeleton and cell migration. Annu. Rev. Cell Dev. Biol. *19*, 541–564.

Kudrin, A., Scott, M., Martin, S., Chung, C.-W., Donn, R., McMaster, A., Ellison, S., Ray, D., Ray, K., and Binks, M. (2006). Human macrophage migration inhibitory factor: a proven immunomodulatory cytokine? J. Biol. Chem. *281*, 29641–29651.

Kuo, J.-C., Han, X., Hsiao, C.-T., Yates, J. R., and Waterman, C. M. (2011). Analysis of the myosin-II-responsive focal adhesion proteome reveals a role for β-Pix in negative regulation of focal adhesion maturation. Nat. Cell Biol. *13*, 383–393.

Kuriyama, S., Theveneau, E., Benedetto, A., Parsons, M., Tanaka, M., Charras, G., Kabla, A., and Mayor, R. (2014). In vivo collective cell migration requires an LPAR2-dependent increase in tissue fluidity. J. Cell Biol. *206*, 113–127.

Lai, K. N., Leung, J. C. K., Metz, C. N., Lai, F. M., Bucala, R., and Lan, H. Y. (2003). Role for macrophage migration inhibitory factor in acute respiratory distress syndrome. J. Pathol. *199*, 496–508.

Lan, H. Y., Yang, N., Nikolic-Paterson, D. J., Yu, X. Q., Mu, W., Isbel, N. M., Metz, C. N., Bucala, R., and Atkins, R. C. (2000). Expression of macrophage migration inhibitory factor in human glomerulonephritis. Kidney Int. *57*, 499–509.

Larson, D. F., and Horak, K. (2006). Macrophage migration inhibitory factor: controller of systemic inflammation. Crit. Care *10*, 138.

Laudanna, C., and Alon, R. (2006). Right on the spot. Chemokine triggering of integrin-mediated arrest of rolling leukocytes. Thromb. Haemost. *95*, 5–11.

Lawson, C. D., and Burridge, K. (2014). The on-off relationship of Rho and Rac during integrin-mediated adhesion and cell migration. Small GTPases *5*, 37–41.

Lee, C.-Y., Su, M.-J., Huang, C.-Y., Chen, M.-Y., Hsu, H.-C., Lin, C.-Y., and Tang, C.-H. (2011). Macrophage migration inhibitory factor increases cell motility and up-regulates αvβ3 integrin in human chondrosarcoma cells. J. Cell. Biochem. *113*, n/a – n/a.

Leng, L., Metz, C. N., Fang, Y., Xu, J., Donnelly, S., Baugh, J., Delohery, T., Chen, Y., Mitchell, R. A., and Bucala, R. (2003). MIF signal transduction initiated by binding to CD74. J. Exp. Med. *197*, 1467–1476.

Li, M., Tao, Y., Shu, Y., LaRochelle, J. R., Steinauer, A., Thompson, D., Schepartz, A., Chen, Z. Y., and Liu, D. R. (2015). Discovery and Characterization of a Peptide That Enhances Endosomal Escape of Delivered Proteins in Vitro and in Vivo. J. Am. Chem. Soc. *137*, 14084–14093.

Li, Z., Ren, Y., Wu, Q., Lin, S., Liang, Y., and Liang, H. (2004). Macrophage migration inhibitory factor enhances neoplastic cell invasion by inducing the expression of matrix metalloproteinase 9 and interleukin-8 in nasopharyngeal carcinoma cell lines. Chin. Med. J. (Engl). *117*, 107–114.

Liang, C.-C., Park, A. Y., and Guan, J.-L. (2007). In vitro scratch assay: a convenient and inexpensive method for analysis of cell migration in vitro. Nat. Protoc. *2*, 329–333.

Liao, H., Bucala, R., and Mitchell, R. A. (2003). Adhesion-dependent signaling by macrophage migration inhibitory factor (MIF). J. Biol. Chem. *278*, 76–81.

Lin, Y. H., Park, Z. Y., Lin, D., Brahmbhatt, A. a., Rio, M. C., Yates, J. R., and Klemke, R. L. (2004). Regulation of cell migration and survival by focal adhesion targeting of Lasp-1. J. Cell Biol. *165*, 421–432.

Lind, M., Trindade, M. C. D., Nakashima, Y., Schurman, D. J., Goodman, S. B., and Smith, R. L. (1999). Chemotaxis and activation of particle-challenged human monocytes in response to monocyte migration

inhibitory factor and C-C chemokines. J. Biomed. Mater. Res. *48*, 246–250.

Lourenco, S., Teixeira, V. H., Kalber, T., Jose, R. J., Floto, R. a., and Janes, S. M. (2015). Macrophage Migration Inhibitory Factor-CXCR4 Is the Dominant Chemotactic Axis in Human Mesenchymal Stem Cell Recruitment to Tumors. J. Immunol. *194*, 3463–3474.

Lubetsky, J. B., Swope, M., Dealwis, C., Blake, P., and Lolis, E. (1999). Pro-1 of macrophage migration inhibitory factor functions as a catalytic base in the phenylpyruvate tautomerase activity. Biochemistry *38*, 7346–7354.

Lue, H., Kapurniotu, A., Fingerle-Rowson, G., Roger, T., Leng, L., Thiele, M., Calandra, T., Bucala, R., and Bernhagen, J. (2006). Rapid and transient activation of the ERK MAPK signalling pathway by macrophage migration inhibitory factor (MIF) and dependence on JAB1/CSN5 and Src kinase activity. Cell. Signal. *18*, 688–703.

Lue, H., Thiele, M., Franz, J., Dahl, E., Speckgens, S., Leng, L., Fingerle-Rowson, G., Bucala, R., Lüscher, B., and Bernhagen, J. (2007). Macrophage migration inhibitory factor (MIF) promotes cell survival by activation of the Akt pathway and role for CSN5/JAB1 in the control of autocrine MIF activity. Oncogene *26*, 5046–5059.

Luedike, P. *et al.* (2012). Cardioprotection Through S-Nitros(yl)ation of Macrophage Migration Inhibitory Factor. Circulation *125*, 1880–1889.

Lv, J., Huang, X. R., Klug, J., Frohlich, S., Lacher, P., Xu, A., Meinhardt, A., and Lan, H. Y. (2013). Ribosomal protein S19 is a novel therapeutic agent in inflammatory kidney disease. Clin. Sci. (London, Engl. 1979) *124*, 627–637.

Lv, W., Chen, N., Lin, Y., Ma, H., Ruan, Y., Li, Z., Li, X., Pan, X., and Tian, X. (2016). Macrophage migration inhibitory factor promotes breast cancer metastasis via activation of HMGB1/TLR4/NF kappa B axis. Cancer Lett. *375*, 245–255.

Macia, E., Ehrlich, M., Massol, R., Boucrot, E., Brunner, C., and Kirchhausen, T. (2006). Dynasore, a Cell-Permeable Inhibitor of Dynamin. Dev. Cell *10*, 839–850.

McCarthy, P. L., Shaw, J. E., and Remold, H. G. (1979). The role of microtubules in the response of macrophages to MIF. Cell. Immunol. *46*, 409–415.

Meinhardt, A., Bacher, M., McFarlane, J. R., Metz, C. N., Seitz, J., Hedger, M. P., De Kretser, D. M., and Bucala, R. (1996). Macrophage migration inhibitory factor production by Leydig cells: Evidence for a role in the regulation of testicular function. Endocrinology *137*, 5090–5095.

Meinhardt, A., Bacher, M., Metz, C., Bucala, R., Wreford, N., Lan, H., Atkins, R., and Hedger, M. (1998). Local regulation of macrophage subsets in the adult rat testis: examination of the roles of the seminiferous tubules, testosterone, and macrophage-migration inhibitory factor. Biol. Reprod. *59*, 371–378.

Meinhardt, A., Bacher, M., Wennemuth, G., Eickhoff, R., and Hedger, M. (2000). Macrophage migration inhibitory factor (MIF) as a paracrine mediator in the interaction of testicular somatic cells. Andrologia *32*, 46–48.

Mejillano, M. R., Kojima, S. I., Applewhite, D. A., Gertler, F. B., Svitkina, T. M., and Borisy, G. G. (2004). Lamellipodial versus filopodial mode of the actin nanomachinery: Pivotal role of the filament barbed end. Cell *118*, 363–373.

de Mendonça-Filho, H. T. F., Pereira, K. C., Fontes, M., Vieira, D. A. D. S. A., de Mendonça, M. L. a F., Campos, L. A. D. A., and Castro-Faria-Neto, H. C. (2006). Circulating inflammatory mediators and organ dysfunction after cardiovascular surgery with cardiopulmonary bypass: a prospective observational study. Crit. Care *10*, R46.

Merk, M. *et al.* (2009). The Golgi-associated protein p115 mediates the secretion of macrophage migration inhibitory factor. J. Immunol. *182*, 6896–6906.

Merk, M. *et al.* (2011). The D-dopachrome tautomerase (DDT) gene product is a cytokine and functional homolog of macrophage migration inhibitory factor (MIF). Proc. Natl. Acad. Sci. U. S. A. *108*, E577–E585.

Merk, M., Mitchell, R. A., Endres, S., and Bucala, R. (2012). D-dopachrome tautomerase (D-DT or MIF-2): Doubling the MIF cytokine family. Cytokine *59*, 10–17.

Mitchell, R. A. (2004). Mechanisms and effectors of MIF-dependent promotion of tumourigenesis. Cell. Signal. *16*, 13–19.

Mitchell, R. A., Liao, H., Chesney, J., Fingerle-Rowson, G., Baugh, J., David, J., and Bucala, R. (2002). Macrophage migration inhibitory factor (MIF) sustains macrophage proinflammatory function by inhibiting p53: regulatory role in the innate immune response. Proc. Natl. Acad. Sci. U. S. A. *99*, 345–350.

Mitchell, R. A., Metz, C. N., Peng, T., and Bucala, R. (1999). Sustained mitogen-activated protein kinase (MAPK) and cytoplasmic phospholipase A2 activation by macrophage migration inhibitory factor (MIF). Regulatory role in cell proliferation and glucocorticoid action. J. Biol. Chem. *274*, 18100–18106.

Mostowy, S., and Cossart, P. (2012). Septins: the fourth component of the cytoskeleton. Nat. Rev. Mol. Cell Biol. *13*, 183–194.

Mueller, M. *et al.* (2015). The coordinated action of the MVB pathway and autophagy ensures cell survival during starvation. Elife *2015*, 1–25.

Nguyen, M. T., Beck, J., Lue, H., Fünfzig, H., Kleemann, R., Koolwijk, P., Kapurniotu, A., and Bernhagen, J. (2003). A 16-Residue Peptide Fragment of Macrophage Migration Inhibitory Factor, MIF-(50-65), Exhibits Redox Activity and Has MIF-like Biological Functions. J. Biol. Chem. *278*, 33654–33671.

Nishihira, J., Fujinaga, M., Kuriyama, T., Suzuki, M., Sugimoto, H., Nakagawa, A., Tanaka, I., and Sakai, M. (1998). Molecular cloning of human D-dopachrome tautomerase cDNA: N-terminal proline is essential for enzyme activation. Biochem. Biophys. Res. Commun. *243*, 538–544.

No, Y. R., Lee, S.-J., Kumar, A., and Yun, C. C. (2015). HIF1α-Induced by Lysophosphatidic Acid Is Stabilized via Interaction with MIF and CSN5. PLoS One *10*, e0137513.

O'Reilly, C., Doroudian, M., Mawhinney, L., and Donnelly, S. C. (2016). Targeting MIF in Cancer: Therapeutic Strategies, Current Developments, and Future Opportunities. Med. Res. Rev. *36*, 440–460.

Ohta, S., Misawa, A., Fukaya, R., Inoue, S., Kanemura, Y., Okano, H., Kawakami, Y., and Toda, M. (2012). Macrophage migration inhibitory factor (MIF) promotes cell survival and proliferation of neural stem/progenitor cells. J. Cell Sci. *125*, 3210–3220.

Okabe, S., Fukuda, S., Kim, Y., Niki, M., Pelus, L. M., Ohyashiki, K., Pandolfi, P. P., and Broxmeyer, H. E. (2005). Stromal cell-derived factor-1alpha/CXCL12-induced chemotaxis of T cells involves activation of the RasGAP-associated docking protein p62Dok-1. Blood *105*, 474–480.

Onodera, S., Ohshima, S., Tohyama, H., Yasuda, K., Nishihira, J., Iwakura, Y., Matsuda, I., Minami, A., and Koyama, Y. (2007). A novel DNA vaccine targeting macrophage migration inhibitory factor protects joints from inflammation and destruction in murine models of arthritis. Arthritis Rheum. *56*, 521–530.

Onodera, S., Tanji, H., Suzuki, K., Kaneda, K., Mizue, Y., Sagawa, A., and Nishihira, J. (1999). High expression of macrophage migration inhibitory factor in the synovial tissues of rheumatoid joints. Cytokine *11*, 163–167.

Ouertatani-Sakouhi, H. *et al.* (2010). Identification and characterization of novel classes of macrophage migration inhibitory factor (MIF) inhibitors with distinct mechanisms of action. J. Biol. Chem. *285*, 26581–26598.

Pakozdi, A., Amin, M. a, Haas, C. S., Martinez, R. J., Haines, G. K., Santos, L. L., Morand, E. F., David, J. R., and Koch, A. E. (2006). Macrophage migration inhibitory factor: a mediator of matrix metalloproteinase-2 production in rheumatoid arthritis. Arthritis Res. Ther. *8*, R132.

Pankov, R., Endo, Y., Even-Ram, S., Araki, M., Clark, K., Cukierman, E., Matsumoto, K., and Yamada, K. M. (2005). A Rac switch regulates random versus directionally persistent cell migration. J. Cell Biol. *170*, 793–802.

Panopoulos, A., Howell, M., Fotedar, R., and Margolis, R. L. (2011). Glioblastoma motility occurs in the absence of actin polymer. Mol. Biol. Cell *22*, 2212–2220.

Panstruga, R., Baumgarten, K., and Bernhagen, J. (2015). Phylogeny and evolution of plant macrophage migration inhibitory factor/D-dopachrome tautomerase-like proteins. BMC Evol. Biol. *15*, 64.

Pantouris, G., Syed, M. A., Fan, C., Rajasekaran, D., Cho, T. Y., Rosenberg, E. M., Bucala, R., Bhandari, V., and Lolis, E. J. (2015). An Analysis of MIF Structural Features that Control Functional Activation of CD74. Chem. Biol. *22*, 1197–1205.

Park, R. J., Shen, H., Liu, L., Liu, X., Ferguson, S. M., and De Camilli, P. (2013). Dynamin triple knockout cells reveal off target effects of commonly used dynamin inhibitors. J. Cell Sci. *126*, 5305–5312.

Pasqualon, T., Lue, H., Groening, S., Pruessmeyer, J., Jahr, H., Denecke, B., Bernhagen, J., and Ludwig, A. (2016). Cell surface syndecan-1 contributes to binding and function of macrophage migration inhibitory factor (MIF) on epithelial tumor cells. Biochim. Biophys. Acta - Mol. Cell Res. *1863*, 717–726.

Pasupuleti, V., Du, W., Gupta, Y., Yeh, I. J., Montano, M., Magi-Galuzzi, C., and Welford, S. M. (2014). Dysregulated D-dopachrome Tautomerase, a Hypoxiainducible Factor-dependent Gene, cooperates with Macrophage migration inhibitory factor in Renal Tumorigenesis. J. Biol. Chem. *289*, 3713–3723.

Pelkmans, L. (2005). Secrets of caveolae- and lipid raft-mediated endocytosis revealed by mammalian viruses. Biochim. Biophys. Acta - Mol. Cell Res. *1746*, 295–304.

Peng, C., Dong, C., Hou, Q., Xu, C., and Zhao, J. (2005). The hydrophobic surface of PaAMP from pokeweed seeds is essential to its interaction with fungal membrane lipids and the antifungal activity. FEBS Lett. *579*, 2445–2450.

Perrin, B. J., and Ervasti, J. M. (2010). The actin gene family: Function follows isoform. Cytoskeleton *67*, 630–634.

Piette, C., Deprez, M., Roger, T., Noël, A., Foidart, J. M., and Munaut, C. (2009). The dexamethasone-induced inhibition of proliferation, migration, and invasion in glioma cell lines is antagonized by macrophage migration inhibitory factor (MIF) and can be enhanced by specific MIF inhibitors. J. Biol. Chem. *284*, 32483–32492.

Põlajeva, J. *et al.* (2014). Glioma-derived macrophage migration inhibitory factor (MIF) promotes mast cell recruitment in a STAT5-dependent manner. Mol. Oncol. *8*, 50–58.

Preau, S., Montaigne, D., Modine, T., Fayad, G., Koussa, M., Tardivel, M., Durocher, A., Saulnier, F., Marechal, X., and Neviere, R. (2013). Macrophage migration inhibitory factor induces contractile and mitochondria dysfunction by altering cytoskeleton network in the human heart. Crit Care Med *41*, e125–e133.

Premzl, M. (2015). Initial description of primate-specific cystine-knot Prometheus genes and differential gene expansions of D-dopachrome tautomerase genes. Meta Gene *4*, 118–128.

Pyle, M. (2003). Macrophage migration inhibitory factor expression is increased in pituitary adenoma cell nuclei. J. Endocrinol. *176*, 103–110.

Qi, D. *et al.* (2014). The vestigial enzyme D-dopachrome tautomerase protects the heart against ischemic injury. J. Clin. Invest. *124*, 3540–3550.

Qu, G., Fetterer, R., Leng, L., Du, X., Zarlenga, D., Shen, Z., Han, W., Bucala, R., and Tuo, W. (2014). Ostertagia ostertagi macrophage migration inhibitory factor is present in all developmental stages and may cross-regulate host functions through interaction with the host receptor. Int. J. Parasitol. *44*, 355–367.

Rajasekaran, D., Zierow, S., Syed, M., Bucala, R., Bhandari, V., and Lolis, E. J. (2014). Targeting distinct tautomerase sites of D-DT and MIF with a single molecule for inhibition of neutrophil lung recruitment. FASEB J. *28*, 4961–4971.

Rakhila, H., Girard, K., Leboeuf, M., Lemyre, M., and Akoum, A. (2014). Macrophage Migration Inhibitory Factor Is Involved in Ectopic Endometrial Tissue Growth and Peritoneal-Endometrial Tissue Interaction In Vivo: A Plausible Link to Endometriosis Development. PLoS One *9*, e110434.

Reidy, T., Rittenberg, A., Dwyer, M., D'Ortona, S., Pier, G., and Gadjeva, M. (2013). Homotrimeric macrophage migration inhibitory factor (MIF) drives inflammatory responses in the corneal epithelium by promoting caveolin-rich platform assembly in response to infection. J. Biol. Chem. *288*, 8269–8278.

Ren, Y. *et al.* (2003). Macrophage migration inhibitory factor: Roles in regulating tumor cell migration and expression of angiogenic factors in hepatocellular carcinoma. Int. J. Cancer *107*, 22–29.

Ren, Y., Chan, H. M., Fan, J., Xie, Y., Chen, Y. X., Li, W., Jiang, G. P., Liu, Q., Meinhardt, A., and Tam, P. K. H. (2006). Inhibition of tumor growth and metastasis in vitro and in vivo by targeting macrophage migration inhibitory factor in human neuroblastoma. Oncogene *25*, 3501–3508.

Rendon, B. E., Roger, T., Teneng, I., Zhao, M., Al-Abed, Y., Calandra, T., and Mitchell, R. A. (2007). Regulation of human lung adenocarcinoma cell migration and invasion by macrophage migration inhibitory factor. J. Biol. Chem. *282*, 29910–29918.

Riberdy, J. M., Newcomb, J. R., Surman, M. J., Barbosa, J. a, and Cresswell, P. (1992). HLA-DR molecules from an antigen-processing mutant cell line are associated with invariant chain peptides. Nature *360*, 474–477.

Rice, E. K., Tesch, G. H., Cao, Z., Cooper, M. E., Metz, C. N., Bucala, R., Atkins, R. C., and Nikolic-Paterson, D. J. (2003). Induction of MIF synthesis and secretion by tubular epithelial cells: A novel action of angiotensin II. Kidney Int. *63*, 1265–1275.

Ridley, A. J., and Hall, A. (1992). The Small GTP-Binding Protein rho Regulates the Assembly of Focal Adhesions and Actin Stress Fibers in Response to Growth Factors. Cell *70*, 389–399.

Ridley, A. J., Paterson, H. F., Johnston, C. L., Diekmann, D., and Hall, A. (1992). The Small GTP-Binding Protein rac Regulates Growth Factor-Induced Membrane Ruffling. Cell *70*, 401–410.

Ridley, A. J., Schwartz, M. a, Burridge, K., Firtel, R. a, Ginsberg, M. H., Borisy, G., Parsons, J. T., and Horwitz, A. R. (2003). Cell migration: integrating signals from front to back. Science *302*, 1704–1709.

Robinson, R. C., Turbedsky, K., Kaiser, D. a, Marchand, J. B., Higgs, H. N., Choe, S., and Pollard, T. D. (2001). Crystal structure of Arp2/3 complex. Science *294*, 1679–1684.

Rocklin, R. E., MacDermott, R. P., Chess, L., Schlossman, S. F., and David, J. R. (1974). Studies on mediator production by highly purified human T and B lymphocytes. J. Exp. Med. *140*, 1303–1316.

Roger, T., Chanson, A.-L., Knaup-Reymond, M., and Calandra, T. (2005). Macrophage migration inhibitory factor promotes innate immune responses by suppressing glucocorticoid-induced expression of mitogen-activated protein kinase phosphatase-1. Eur. J. Immunol. *35*, 3405–3413.

Roger, T., Schneider, A., Weier, M., Sweep, F. C. G. J., Le Roy, D., Bernhagen, J., Calandra, T., and Giannoni, E. (2016). High expression levels of macrophage migration inhibitory factor sustain the innate immune responses of neonates. Proc. Natl. Acad. Sci., 201514018.

Rosengren, E., Bucala, R., Aman, P., Jacobsson, L., Odh, G., Metz, C. N., and Rorsman, H. (1996). The immunoregulatory mediator macrophage migration inhibitory factor (MIF) catalyzes a tautomerization reaction. Mol. Med. *2*, 143–149.

Rossi, A. G., Haslett, C., Hirani, N., Greening, A. P., Rahman, I., Metz, C. N., Bucala, R., and Donnelly, S. C. (1998). Human circulating eosinophils secrete macrophage migration inhibitory factor (MIF): Potential role in asthma. J. Clin. Invest. *101*, 2869–2874.

Rottner, K., and Stradal, T. E. B. (2011). Actin dynamics and turnover in cell motility. Curr. Opin. Cell Biol. *23*, 569–578.

Rotty, J. D., Wu, C., and Bear, J. E. (2013). New insights into the regulation and cellular functions of the ARP2/3 complex. Nat. Rev. Mol. Cell Biol. *14*, 7–12.

Rotty, J. D., Wu, C., Haynes, E. M., Suarez, C., Winkelman, J. D., Johnson, H. E., Haugh, J. M., Kovar, D. R., and Bear, J. E. (2015). Profilin-1 Serves as a Gatekeeper for Actin Assembly by Arp2/3-Dependent and -Independent Pathways. Dev. Cell *32*, 54–67.

Roussos, E. T., Condeelis, J. S., and Patsialou, A. (2011). Chemotaxis in cancer. Nat. Rev. Cancer *11*, 573–587.

Russell, R. C., Yuan, H.-X., and Guan, K.-L. (2014). Autophagy regulation by nutrient signaling. Cell Res. *24*, 42–57.

Sánchez-Madrid, F., and Serrador, J. M. (2009). Bringing up the rear: defining the roles of the uropod. Nat. Rev. Mol. Cell Biol. *10*, 353–359.

Schoenfeld, J., Jinushi, M., Nakazaki, Y., Wiener, D., Park, J., Soiffer, R., Neuberg, D., Mihm, M., Hodi, F. S., and Dranoff, G. (2010). Active immunotherapy induces antibody responses that target tumor angiogenesis. Cancer Res. *70*, 10150–10160.

Schrans-Stassen, B. H. G. J., Lue, H., Sonnemans, D. G. P., Bernhagen, J., and Post, M. J. (2005). Stimulation of vascular smooth muscle cell migration by macrophage migration inhibitory factor. Antioxid. Redox Signal. *7*, 1211–1216.

Schulte, W. K. (2011). D -Dopachrome Tautomerase (D-DT) – Functional Homologue or Cross-Regulator of Macrophage Migration Inhibitory Factor (MIF)? Thesis (MD). RWTH Aachen Univ.

Schultheiss, G., Hennig, B., and Diener, M. (2008). Sites of action of hydrogen peroxide on ion transport across rat distal colon. Br. J. Pharmacol. *154*, 991–1000.

Schulz, R., Marchenko, N. D., Holembowski, L., Fingerle-Rowson, G., Pesic, M., Zender, L., Dobbelstein, M., and Mol, U. M. (2012). Inhibiting the HSP90 chaperone destabilizes macrophage migration inhibitory factor and thereby inhibits breast tumor progression. J. Exp. Med. *209*, 640–640.

Schulz, R., and Moll, U. M. (2014). Targeting the heat shock protein 90: a rational way to inhibit macrophage migration inhibitory factor function in cancer. Curr. Opin. Oncol. *26*, 108–113.

Schwartz, V., Krüttgen, A., Weis, J., Weber, C., Ostendorf, T., Lue, H., and Bernhagen, J. (2012). Role for CD74 and CXCR4 in clathrin-dependent endocytosis of the cytokine MIF. Eur. J. Cell Biol. *91*, 435–449.

Schwartz, V., Lue, H., Kraemer, S., Korbiel, J., Krohn, R., Ohl, K., Bucala, R., Weber, C., and Bernhagen, J. (2009). A functional heteromeric MIF receptor formed by CD74 and CXCR4. FEBS Lett. *583*, 2749–2757.

Sedmak, J. J., and Grossberg, S. E. (1977). A rapid, sensitive, and versatile assay for protein using Coomassie brilliant blue G250. Anal. Biochem. *79*, 544–552.

Selvi, E. *et al.* (2003). Expression of macrophage migration inhibitory factor in diffuse systemic sclerosis. Ann. Rheum. Dis. *62*, 460–464.

Shahinian, H., Loessner, D., Biniossek, M. L., Kizhakkedathu, J. N., Clements, J. a., Magdolen, V., and Schilling, O. (2014). Secretome and degradome profiling shows that Kallikrein-related peptidases 4, 5, 6, and 7 induce TGFβ-1 signaling in ovarian cancer cells. Mol. Oncol. *8*, 68–82.

Shen, Y. C., Thompson, D. L., Kuah, M. K., Wong, K. L., Wu, K. L., Linn, S. a., Jewett, E. M., Shu-Chien, A. C., and Barald, K. F. (2012). The cytokine macrophage migration inhibitory factor (MIF) acts as a neurotrophin in the developing inner ear of the zebrafish, Danio rerio. Dev. Biol. *363*, 84–94.

Sherma, N. D., Borges, C. R., Trenchevska, O., Jarvis, J. W., Rehder, D. S., Oran, P. E., Nelson, R. W., and Nedelkov, D. (2014). Mass Spectrometric Immunoassay for the qualitative and quantitative analysis of the

cytokine Macrophage Migration Inhibitory Factor (MIF). Proteome Sci. *12*, 52.

Shi, X. *et al.* (2006). CD44 Is the Signaling Component of the Macrophage Migration Inhibitory Factor-CD74 Receptor Complex. Immunity *25*, 595–606.

Shin, H. N., Moon, H. H., and Ku, J. L. (2012). Stromal cell-derived factor-1α and macrophage migration-inhibitory factor induce metastatic behavior in CXCR4-expressing colon cancer cells. Int. J. Mol. Med. *30*, 1537–1543.

Shindo, A., and Wallingford, J. B. (2014). PCP and septins compartmentalize cortical actomyosin to direct collective cell movement. Science *343*, 649–652.

Simons, K., and Toomre, D. (2000). Lipid rafts and signal transduction. Nat. Rev. Mol. Cell Biol. *1*, 31–39.

Simpson, K. D., and Cross, J. V (2013). MIF: metastasis/MDSC-inducing factor? Oncoimmunology *2*, e23337.

Simpson, K. D., Templeton, D. J., and Cross, J. V (2012). Macrophage migration inhibitory factor promotes tumor growth and metastasis by inducing myeloid-derived suppressor cells in the tumor microenvironment. J. Immunol. *189*, 5533–5540.

Snider, N. T., Altshuler, P. J., and Omary, M. B. (2015). Modulation of cytoskeletal dynamics by mammalian nucleoside diphosphate kinase (NDPK) proteins. Naunyn. Schmiedebergs. Arch. Pharmacol. *388*, 189–197.

Sobierajski, J. *et al.* (2013). Assessment of macrophage migration inhibitory factor in humans: Protocol for accurate and reproducible levels. Free Radic. Biol. Med. *63*, 236–242.

Son, A., Kato, N., Horibe, T., Matsuo, Y., Mochizuki, M., Mitsui, A., Kawakami, K., Nakamura, H., and Yodoi, J. (2009). Direct association of thioredoxin-1 (TRX) with macrophage migration inhibitory factor (MIF): regulatory role of TRX on MIF internalization and signaling. Antioxid. Redox Signal. *11*, 2595–2605.

de Souza, H. S. *et al.* (2015). Macrophage migration inhibitory factor promotes eosinophil accumulation and tissue remodeling in eosinophilic esophagitis. Mucosal Immunol. *8*, 1154–1165.

de Souza, M., Curioni, O., Kanda, J., and De Carvalho, M. (2014). Serum and salivary macrophage migration inhibitory factor in patients with oral squamous cell carcinoma. Oncol. Lett., 2267–2275.

Stamps, S. L., Taylor, A. B., Wang, S. C., Hackert, M. L., and Whitman, C. P. (2000). Mechanism of the Phenylpyruvate Tautomerase Activity of Macrophage Migration Inhibitory Factor: Properties of the P1G, P1A, Y95F, and N97A Mutants. Biochemistry *39*, 9671–9678.

Stark, K. *et al.* (2013). Capillary and arteriolar pericytes attract innate leukocytes exiting through venules and “instruct” them with pattern-recognition and motility programs. Nat. Immunol. *14*, 41–51.

Strüßmann, T., Tillmann, S., Wirtz, T., Bucala, R., von Hundelshausen, P., and Bernhagen, J. (2013). Platelets are a previously unrecognised source of MIF. Thromb. Haemost. *110*, 1004–1013.

Subbannayya, T. *et al.* (2015). Macrophage migration inhibitory factor - a therapeutic target in gallbladder cancer. BMC Cancer *15*, 843.

Sugimoto, H., Taniguchi, M., Nakagawa, A., Tanaka, I., Suzuki, M., and Nishihira, J. (1999). Crystal structure of human D-Dopachrome tautomerase, a homologue of macrophage migration inhibitory factor, at 1.54 Å resolution. Biochemistry *38*, 3268–3279.

Sun, H. W., Bernhagen, J., Bucala, R., and Lolis, E. (1996). Crystal structure at 2.6-A resolution of human macrophage migration inhibitory factor. Proc. Natl. Acad. Sci. U. S. A. *93*, 5191–5196.

Swant, J. D., Rendon, B. E., Symons, M., and Mitchell, R. A. (2005). Rho GTPase-dependent signaling is required for macrophage migration inhibitory factor-mediated expression of cyclin D1. J. Biol. Chem. *280*, 23066–23072.

Tarasuk, M., Poungpair, O., Ungsupravate, D., Bangphoomi, K., Chaicumpa, W., and Yenchitsomanus, P. T. (2014). Human single-chain variable fragment antibody inhibits macrophage migration inhibitory factor

tautomerase activity. Int. J. Mol. Med. *33*, 515–522.

Tarnowski, M., Grymula, K., Liu, R., Tarnowska, J., Drukala, J., Ratajczak, J., Mitchell, R. A., Ratajczak, M. Z., and Kucia, M. (2010). Macrophage migration inhibitory factor is secreted by rhabdomyosarcoma cells, modulates tumor metastasis by binding to CXCR4 and CXCR7 receptors and inhibits recruitment of cancer-associated fibroblasts. Mol. Cancer Res. *8*, 1328–1343.

Thelen, M., and Stein, J. V (2008). How chemokines invite leukocytes to dance. Nat. Immunol. *9*, 953–959.

Thiele, M. *et al.* (2015a). Selective Targeting of a Disease-Related Conformational Isoform of Macrophage Migration Inhibitory Factor Ameliorates Inflammatory Conditions. J. Immunol. *195*, 2343–2352.

Thiele, M., Schinagl, A., Douillard, P., Barak, H., Adib, D., Yazji, S., Scheiflinger, F., and Kerschbaumer, R. (2015b). P1.10 * A fully human anti-oxMIF antibody penetrates colorectal cancer metastases and accumulates in cancer tissue. Ann. Oncol. *26*, ii18–ii18.

Tillmann, S., Bernhagen, J., and Noels, H. (2013). Arrest functions of the MIF ligand/receptor axes in atherogenesis. Front. Immunol. *4*, 1–20.

Triantafilou, M., Miyake, K., Golenbock, D. T., and Triantafilou, K. (2002). Mediators of innate immune recognition of bacteria concentrate in lipid rafts and facilitate lipopolysaccharide-induced cell activation. J Cell Sci *115*, 2603–2611.

Tzircotis, G., Thorne, R. F., and Isacke, C. M. (2006). Directional sensing of a phorbol ester gradient requires CD44 and is regulated by CD44 phosphorylation. Oncogene *25*, 7401–7410.

Varinelli, L. *et al.* (2015). 4-IPP, a selective MIF inhibitor, causes mitotic catastrophe in thyroid carcinomas. Endocr. Relat. Cancer *22*, 759–775.

Vartiainen, M. K., Guettler, S., Larijani, B., and Treisman, R. (2007). Nuclear actin regulates dynamic subcellular localization and activity of the SRF cofactor MAL. Science *316*, 1749–1752.

Venkiteswaran, G., Lewellis, S. W., Wang, J., Reynolds, E., Nicholson, C., and Knaut, H. (2013). Generation and dynamics of an endogenous, self-generated signaling gradient across a migrating tissue. Cell *155*, 674–687.

Vicente-Manzanares, M., and Sánchez-Madrid, F. (2004). Role of the cytoskeleton during leukocyte responses. Nat. Rev. Immunol. *4*, 110–122.

Wada, S., Kudo, T., Kudo, M., Sakuragi, N., Hareyama, H., Nishihira, J., and Fujimoto, S. (1999). Induction of macrophage migration inhibitory factor in human ovary by human chorionic gonadotrophin. Hum. Reprod. *14*, 395–399.

Wadgaonkar, R., Dudek, S. M., Zaiman, A. L., Linz-McGillem, L., Verin, A. D., Nurmukhambetova, S., Romer, L. H., and Garcia, J. G. N. (2005). Intracellular interaction of myosin light chain kinase with macrophage migration inhibition factor (MIF) in endothelium. J. Cell. Biochem. *95*, 849–858.

Wang, X. *et al.* (2012). MIF produced by bone marrow-derived macrophages contributes to teratoma progression after embryonic stem cell transplantation. Cancer Res. *72*, 2867–2878.

Waterman-Storer, C. M., Worthylake, R. A., Liu, B. P., Burridge, K., and Salmon, E. D. (1999). Microtubule growth activates Rac1 to promote lamellipodial protrusion in fibroblasts. Nat. Cell Biol. *1*, 45–50.

Weber, C., Kraemer, S., Drechsler, M., Lue, H., Koenen, R. R., Kapurniotu, A., Zernecke, A., and Bernhagen, J. (2008). Structural determinants of MIF functions in CXCR2-mediated inflammatory and atherogenic leukocyte recruitment. Proc. Natl. Acad. Sci. U. S. A. *105*, 16278–16283.

Welch, M. D. (2015). Cell Migration, Freshly Squeezed. Cell *160*, 581–582.

Wieffer, M., Maritzen, T., and Haucke, V. (2009). SnapShot: Endocytic Trafficking. Cell *137*, 17–19.

Winner, M. *et al.* (2008). A novel, macrophage migration inhibitory factor suicide substrate inhibits motility

and growth of lung cancer cells. Cancer Res. *68*, 7253–7257.

Wittmann, T., Bokoch, G. M., and Waterman-Storer, C. M. (2003). Regulation of leading edge microtubule and actin dynamics downstream of Rac1. J. Cell Biol. *161*, 845–851.

Wong, D., Kandagatla, P., Korz, W., and Chinni, S. R. (2014). Targeting CXCR4 with CTCE-9908 inhibits prostate tumor metastasis. BMC Urol. *14*, 12.

Wu, J., Xie, N., Zhao, X., Nice, E. C., and Huang, C. (2012). Dissection of aberrant GPCR signaling in tumorigenesis - a systems biology approach. Cancer Genomics Proteomics *9*, 37–50.

Xie, L., Qiao, X., Wu, Y., and Tang, J. (2011). β-Arrestin1 mediates the endocytosis and functions of macrophage migration inhibitory factor. PLoS One *6*, e16428.

Xin, D., Rendon, B. E., Zhao, M., Winner, M., McGhee Coleman, A., and Mitchell, R. A. (2010). The MIF homologue D-dopachrome tautomerase promotes COX-2 expression through β-catenin-dependent and -independent mechanisms. Mol. Cancer Res. *8*, 1601–1609.

Xu, L., Li, Y., Sun, H., Zhen, X., Qiao, C., Tian, S., and Hou, T. (2013). Current developments of macrophage migration inhibitory factor (MIF) inhibitors. Drug Discov. Today *18*, 592–600.

Yamada, Y., Hashida, M., and Harashima, H. (2015). Hyaluronic acid controls the uptake pathway and intracellular trafficking of an octaarginine-modified gene vector in CD44 positive- and CD44 negative-cells. Biomaterials *52*, 189–198.

Yamaguchi, N., Mizutani, T., Kawabata, K., and Haga, H. (2015). Leader cells regulate collective cell migration via Rac activation in the downstream signaling of integrin β1 and PI3K. Sci. Rep. *5*, 7656.

Zhang, Y., Shen, W., Zhang, L., Pan, Z., Long, C., Cui, W., Zhang, Y., and Wang, H. (2014). Proteomics reveals potential non-neuronal cholinergic receptor-effectors in endothelial cells. Acta Pharmacol Sin *35*, 1137–1149.

Zhang, Z. (2015). Uropathogenic Escherichia coli cause resistance to apoptotic cell death of infected cells by epigenetically suppressing BIM expression. Thesis (PhD). Justus-Liebig Univ. Giessen.

Zheng, Y., Li, X., Qian, X., Wang, Y., Lee, J.-H., Xia, Y., Hawke, D. H., Zhang, G., Lyu, J., and Lu, Z. (2015). Secreted and O-GlcNAcylated MIF binds to the human EGF receptor and inhibits its activation. Nat. Cell Biol. *17*, 1348–1355.

Zhu, G. *et al.* (2014). HIF-α/MIF and NF-κB/IL-6 Axes Contribute to the Recruitment of CD11b+Gr-1+ Myeloid Cells in Hypoxic Microenvironment of HNSCC. Neoplasia *16*, 168–179.

Zöller, M. (2011). CD44: can a cancer-initiating cell profit from an abundantly expressed molecule? Nat. Rev. Cancer *11*, 254–267.